UNIVERSITY OF
BIRMINGHAM

Proton Transfer Reaction Mass Spectrometric Investigations of Compounds of Relevance to Homeland Security and Breath Analysis

by

David Olivenza-León

A thesis submitted to

The University of Birmingham

for the degree of

Doctor of Philosophy

School of Physics and Astronomy

College of Engineering and Physical Sciences

The University of Birmingham

June 2020

Abstract

The work in this thesis presents a series of investigations of ion/molecule processes taking place in the reaction region of a proton transfer reaction mass spectrometer (PTR-MS) for the analytical detection of a series of compounds of relevance to homeland security and health sciences. These compounds include for homeland security applications illicit drugs and related compounds, TNT, mono and di- nitrotoluenes, nitroanilines, and for the health sciences ketones, anaesthetics and phthalates.

The results of quantum chemical calculations are also presented, which have been used to aid in the interpretation of the experimental results. The calculations include the proton affinities and gas-phase basicities of many of the neutral molecules and the energetics of some key ion/molecule reaction pathways.

A key objective is to present work which has improved the selectivity of PTR-MS through the manipulation of the ion chemistry or through fast pre-separation techniques. These have resulted in the PTR-MS becoming a multi-dimensional analytical technique.

Details of Research Activities

The key results presented in chapters 3-8, include those that have already been published (chapters 4-7 corresponding to references [1–4]), namely:

Paper 1. González-Méndez, R., Watts, P., Olivenza-León, D., Reich, D. F., Mullock, S. J., Corlett, C. A., Cairns, S., Hickey, P., Brookes, M. & Mayhew, C. A. Enhancement of Compound Selectivity Using a Radio Frequency Ion-Funnel Proton Transfer Reaction Mass Spectrometer: Improved Specificity for Explosive Compounds. *Analytical Chemistry* **88,** 10624–10630 (2016). DOI: 10.1021/acs.analchem.6b02982.

This paper presents for the first time the novel application of a radio frequency ion funnel (RFIF) in the drift tube of a PTR-MS for manipulating the ion/molecule chemistry to enhance specificity through selective collisional induced dissociation. Previously only sensitivity had been addressed with the application of a RFIF [5]. This paper focuses on explosive compounds, and follows on from a previous paper dealing with TNT by Sulzer *et al.* [6]. We demonstrate in this paper that a RFIF-drift tube can be applied to many compounds for improved selectivity.

Paper 2. Olivenza-León, D., Mayhew, C. A. & González-Méndez, R. Selective Reagent Ion Mass Spectrometric Investigations of the Nitroanilines. *Journal of the American Society for Mass Spectrometry,* 1–8 (2019). DOI: 10.1007/s13361-019-02325-0.

The key output from this paper is that we have demonstrated how it is possible to distinguish isomers based on the manipulation of the ion/molecule chemistry and/or using different reagent ions that favour different ionisation mechanisms.

Paper 3. Malásková, M., Olivenza-León, D., Piel, F., Mochalski, P., Sulzer, P., Jürschik, S., Mayhew, C. & Maerk, T. Compendium of the reactions of H_3O^+ with selected ketones of relevance to breath analysis using proton transfer reaction mass spectrometry. *Frontiers in Chemistry* **7,** 401 (2019). DOI: 10.1021/acs.analchem.6b02982.

The measurements presented in this paper involved three early stage researchers (ESRs)

from the Ion-Molecular Processes for Analytical Chemistry Technologies (IMPACT) Innovative Training Network (ITN), who equally contributed to performing and analysing the data, and are therefore listed as joint first co-authors of the article regarding ketones. The reactions of H_3O^+ with nineteen ketones are presented under normal and humid drift tube and as a function of the reduced electric field. The key outcome from this work is an extensive database, which is not only useful for researchers in the breath analysis field, but also for monitoring ketones in the environment. A key conclusion is that the product ion distributions, often used in the PTR-MS community, should be approached with care, as they are specific not only to the humidity within the drift (reaction) tube of a PTR-MS but also to an individual PTR-MS instrument.

Paper 4. Malásková, M., Olivenza-León, D., Chellayah, P. D., Martini, J., Lederer, W., Ruzsanyi, V., Unterkofler, K., Mochalski, P., Märk, T. D., Watts, P. & Mayhew, C. A. Studies pertaining to the monitoring of volatile halogenated anaesthetics in breath by proton transfer reaction mass spectrometry. *Journal of Breath Research* **14,** 026004 (2020). DOI: 10.1088/1752-7163/ab5e30.

This paper deals with the identification of the product ions resulting from the reactions of four common volatile inhalation anaesthetics with $H_3O^+.(H_2O)_n$ ($n = 0$ and 1) under normal and humid drift tube conditions. This project involved collaboration with another ESR, Michaela Malásková, from the IMPACT network. The work presented here is prerequisite to a large clinical study we have just begun investigating the washout characteristics of inhalation anaesthetics. There is also an additional important point in the paper, in that it highlights that the constantly stated statement that the proton affinity of M must be greater than that of H_2O for proton transfer to occur is incorrect. Reactions of H_3O^+ with VOCs whose proton affinities are less than water will occur because of the translational energy gained in the electric field, but what is crucial is that these compounds can only be detected with good sensitivity if the protonated species spontaneously dissociates to product ions specific to the compound.

Pdfs of the four associated papers are included in the appendix B of this thesis. Chapter 3 and appendix A present unpublished results dealing with drugs, and chapter 8 with phthalate esters. The drug investigations, which include cocaine (and related compounds), heroin, MDMA, morphine, codeine, cannabinoids (*i.e.* CBD, CBN, delta-9-THC), considerably expand on earlier PTR-MS drug studies, by providing details on the reaction processes for a wide range of reduced

electric field and a wider range of compounds. Chapter 8 presents investigations showing how it is possible to use PTR-MS to distinguish three phthalate isomers (*i.e.* DBP, DiBP and MEHP) without the need for any pre-separation.

Detailed Declaration of Contribution

My contribution to the experimental results part (*i.e.* chapters 3-8 in Part II and appendix A) in the present thesis is described below. Parts I and II (*i.e.* chapters 1, 2 and 9) are fully written by me.

Chapter 3. My contribution to the study described in this chapter, from which a publication is planned, was performing the experiments, analysing the results and writing the script.

Chapter 4. My contribution to article [1], of which this chapter is composed, was participating in the discussion and writing of the manuscript. I also repeated the experiments later on for reproducibility purposes.

Chapter 5. My contribution to article [2], of which this chapter is composed of, was performing the experiments, analysing the results and writing the manuscript together with the coauthors.

Chapter 6. My contribution to article [3], of which this chapter is composed, was performing the experiments using a PTR-TOF 8000 at IONICON Analytik GmbH (Innsbruck, Austria) and analysing the data with Michaela Malásková and Felix Piel during several visits between 2016 and 2017. I also did the plots included and collaborated in writing the manuscript with the other coauthors.

Chapter 7. My contribution to the study that resulted in paper [4] was in undertaking confirmatory measurements, discussing the ion/molecule chemistry and aiding in writing the script.

Chapter 8. My contribution to the study described in this chapter, from which a publication is planned, was performing the experiments, analysing the results and writing the script.

Appendix A. My contribution to the study described in this chapter was performing the experiments, analysing the results and writing the script.

A mis padres, Domingo y Juana, y a mi hermano Miguel.

Acknowledgements

First and foremost I would like to thank my supervisor Professor Chris Mayhew for giving me the opportunity to be part of the successful IMPACT network. I am grateful for his support, guidance and expertise, which have been essential for accomplishing my PhD and putting together the present thesis.

I would also like to thank Dr Peter Watts for his extensive knowledge of chemistry, which has substantially improved the value of our research.

I would like to thank my colleagues from the Molecular Physics Group: Ramón González-Méndez, Raquel Fernández-del Río, Daniel Blenkhorn, Prema Chellayah, David Howse and John Thompson, for all the discussions and moments together (in the lab or/and in the pub).

I would like to thank all the IMPACT ESRs and supervisors for their dedication to the network, and in particular KORE Technology Ltd and Fraser Reich, for their support to the Molecular Physics group, and Kathleen Hynes, for her work as Project Manager.

I want to acknowledge the financial support to the Marie Skłodowska-Curie Actions Innovative Training Network: Ion/Molecule Processes for Analytical Chemistry Technologies (IMPACT), which has been funded through the European Commission's HORIZON 2020 Programme under Grant Agreement Number 674911.

Table of Contents

List of Figures

List of Tables

List of Abbreviations

amu	Atomic Mass Unit (= 1.66×10^{-27} kg).
BBP	Benzyl Butyl Phthalate.
BR	Branching Ratio.
BzAcid	Benzoic Acid.
CID	Collision-Induced Dissociation.
cps	Counts per second.
DAP	Diallyl Phthalate.
DBD	Dielectric Barrier Discharge.
DBeP	Dibenzyl Phthalate.
DBP	Dibutyl Phthalate.
DEHP	Bis(2-ethylhexyl) Phthalate (also known as Di(2-ethylhexyl) Phthalate).
DEP	Diethyl Phthalate.
DFT	Density Functional Theory.
DiBP	Diisobutyl Phthalate.
DMP	Dimethyl Phthalate.
DPP	Dipropyl Phthalate.
DSTL	Defence Science and Technology Laboratory.

DT	Drift Tube.
E	Electric field strength.
E/N	Reduced electric field.
EI	Electron Impact.
ESI	Electrospray Ionisation.
ESR	Early Stage Researcher.
EtBz	Ethyl Benzoate.
EtIsoBut	Ethyl Isobutyrate.
eV	Electron volt (= 96.487 kJ/mol).
FWHM	Full Width at Half Maximum.
G	Gibbs free energy.
GB	Gas-phase Basicity.
GC	Gas Chromatography.
GD	Glow Discharge.
H	Enthalpy.
$\mathbf{H_3O^+}$	Hydronium ion.
HCD	Higher-energy Collisional Dissociation.
IE	Ionisation Energy.
IMPACT	Ion/Molecule Processes for Analytical Chemistry Technologies.
IMS	Ion Mobility Spectrometry.
iPrBz	Isopropyl Benzoate.

$\boldsymbol{k}$	Reaction rate coefficient.
$\boldsymbol{K}$	Ion's mobility.
$\boldsymbol{K}_0$	Ion's reduced mobility.
LCU	Liquid Calibration Unit.
LoD	Limit of Detection.
$\boldsymbol{m/z}$	Mass-to-charge ratio.
MeBz	Methyl Benzoate.
MeEcg	Methyl Ecgonine.
MEHP	Monoethylhexyl Phthalate.
MeIsoBut	Methyl Isobutyrate.
MFP	Mean Free Path.
MS	Mass Spectrometer.
MW	Molecular Weight.
$\boldsymbol{N}$	Gas number density.
$\boldsymbol{N}_0$	Gas number density at standard pressure and temperature (= 2.69×10^{19} cm^{-3} = $\mathrm{N}_A/\mathrm{V}_{mol}$).
$\boldsymbol{N}_A$	Avogadro's number (= 6.022×10^{23} mol^{-1}).
NA	Nitroaniline.
ncps	Normalised counts per second.
$\boldsymbol{P}_0$	Standard pressure (= 1 atm = 1013.25 mbar).
$\boldsymbol{PA}$	Proton Affinity.
PAcid	Phthalic Acid.

PAH Polyaromatic Hydrocarbon.

PEEK Polyether Ether Ketone.

PID Product Ion Distribution.

ppbv Parts per billion by volume.

ppmv Parts per million by volume.

ppqv Parts per quadrillion by volume.

pptv Parts per trillion by volume.

PTFE Polytetrafluoroethylene.

PTR Proton Transfer Reaction.

PTR-MS Proton Transfer Reaction Mass Spectrometry.

RFIF Radio Frequency Ion Funnel.

SCI-MS Soft Chemical Ionisation Mass Spectrometry.

SD Source Drift region.

SIFDT-MS Selected Ion Flow-Drift Tube Mass Spectrometry.

SIFT-MS Selected Ion Flow Tube Mass Spectrometry.

SRI-MS Selective Reagent Ion Mass Spectrometry.

$\boldsymbol{T}_0$ Standard temperature (= 0°C = 273.15 K).

$\boldsymbol{t}_d$ Drift time.

Td Townsend (= 10^{-17} V cm^2).

TDC Time-to-Digital Converter.

TDI Tolerable Daily Intake.

TDU Thermal Desorption Unit.

ToF-MS Time-of-Flight Mass Spectrometer.

TS Transition state.

$\boldsymbol{v}_d$ Drift velocity.

$\boldsymbol{V}_d$ Drift voltage.

$\boldsymbol{V}_{mol}$ Molar volume of an ideal gas at standard pressure and temperature (= 22414 cm^3 mol^{-1}).

VOC Volatile Organic Compound.

VP Vapour Pressure.

Part I

INTRODUCTION AND METHODOLOGY

Chapter 1

Introduction and Background

This chapter presents an introduction to soft chemical ionisation mass spectrometry (SCI-MS) and the most used SCI-MS techniques, including proton transfer reaction mass spectrometry (PTR-MS), which is the main technique used for the experimental work presented in this thesis. The thesis outline and aims are given at the end of the chapter.

1.1 Background

Proton transfer reaction mass spectrometry (PTR-MS) was developed by Werner Lindinger at the University of Innsbruck (Austria) in the 1990s as the successor of the flowing afterglow and the selected ion flow drift tube techniques [7]. This technique allows the detection and monitoring of volatile organic compounds (VOCs) to the trace level (*i.e.* parts per million, ppm, and below). The detection of the suitable compounds relies on the proton transfer to these molecules from a proton donor (*i.e* reagent) ion, typically hydronium (H_3O^+), although other alternatives can be found in the literature: *e.g.* ammonium (NH_4^+), as reported by Lindinger *et al.* [7]. The main reason hydronium is commonly the reagent ion of choice is because the proton affinity (PA) of H_2O lies between that of the common constituents of air and most VOCs, therefore allowing on-line, real-time operation with little or no sample preparation required.

The main fields in which PTR-MS is used and some examples to illustrate them are: atmospheric chemistry, where it has been used to study the emission of biogenic VOCs and their effect in the environment, and to monitor pollution and urban plumes [8–11]; homeland security, where it has been applied to the detection of explosives, rape drugs, and narcotics [12–16]; in

medical sciences, for the diagnosis and monitoring of diseases through breath analysis [17–20]; and in food sciences, to study food aroma, flavour and quality control [21–23].

Although PTR-MS is the main technique of interest in this thesis, it is not, of course, the only one used for trace gas detection applications. There are many other analytical tools that are worth mentioning, each with different strengths and weaknesses, and whose election will depend on the requirements of the work to be carried out. From all these, gas chromatography (GC), often coupled to a mass spectrometry system, is probably the "gold standard" for trace gas detection [24]. However, its needs of sample pre-concentration makes it not fast enough (*i.e.* operating times of few minutes per sample), and thus unsuitable, for applications involving transient, fast-evolving systems (*e.g.* in medical or security applications). Ion mobility spectrometry (IMS) has been widely used in the last two decades in homeland security (*i.e.* detection of explosives, drugs and chemical warfare agents) [25–27]. IMS systems operate at near atmospheric pressure, which makes these devices small and cheap, as no big pumps are required. However, because of the working principle relies only on the mobility of ions through a gas, they lack the good selectivity of systems with a mass spectrometer and care must be taken with the (often likely) presence of false positives. Selected ion flow tube mass spectrometry (SIFT-MS), which is the main analytical tool applied to breath analysis, can reach detection limits of parts per billion (ppb) [28, 29]. Whilst their injection quadrupole allows for quick reagent ion selection and switching, the main disadvantage of SIFT-MS systems is their costly need for pumps to keep the needed vacuum levels at both ends of the device. Proton transfer reaction mass spectrometry (PTR-MS) often finds a compromise within these analytical methods, often presenting some advantages. For example, whilst PTR-MS and IMS can reach similar limits of detection in the detection of explosives, the former presents better selectivity and is less prone to false positives. Specific details regarding IMS, SIFT-MS and PTR-MS are further provided in the following pages.

1.2 Soft Chemical Ionisation Mass Spectrometry

Soft chemical ionisation mass spectrometry (SCI-MS) is an analytical technique used to detect trace VOCs in complex chemical environments through the use ion/molecule reactions, for which the exothermicities are kept low to limit fragmentation [30]. This results in the associated mass

spectra being less complex than those that result from electron impact (EI). EI involves the collision of 70 eV electrons with an analyte leading to excessive fragmentation and a complex mass spectrum with many product ions, making it difficult to identify the parent molecule without any pre-separation. Soft ionisation techniques generally provide product ions that allow the identification of a compound with a high level of confidence, which is vital when dealing with complex chemical environments, such as ambient air or breath samples.

The main reactions used in soft chemical ionisation techniques are listed in Table 1.1, where X^+ and XH^+ represents a reagent ion, M and MH are the targeted analyte and in the last reaction Z is a third body required to stabilise the MX^+ adduct through collisions. Proton transfer reactions from protonated water (*i.e.* hydronium, H_3O^+) and its water clusters (*i.e.* $(H_2O)_nH_3O^+$ with $n = 1, 2, ...$) are the main reagent ions used in the work presented in this thesis, although charge transfer reactions occurring between O_2^+ and nitroanilines are also presented in chapter 5 [31].

Table 1.1: Main soft chemical ionisation reactions.

Charge transfer	$X^+ + M$	$\rightarrow$	$M^+ + X$
Proton transfer	$XH^+ + M$	$\rightarrow$	$MH^+ + X$
Hydride (H^-) transfer	$X^+ + MH$	$\rightarrow$	$M^+ + XH$
Adduct formation	$X^+ + M + Z$	$\rightarrow$	$MX^+ + Z$

1.2.1 Thermodynamics of proton transfer

The protonation reaction of an analyte M from hydronium is shown in Equation 1.1. This reaction always occurs at the collisional rate if the proton affinity (PA) of the analyte is higher than that of water.

$$H_3O^+ + M \rightarrow MH^+ + H_2O \tag{1.1}$$

Furthermore, protonation is also possible from a protonated water cluster, if the proton affinity of the analyte is higher than that of the water cluster, following Equation 1.2:

$$(H_2O)_nH_3O^+ + M \rightarrow MH^+ + (H_2O)_{n+1} \tag{1.2}$$

i.e. for this to be spontaneous we require PA (M) $>$ PA ($(H_2O)_{n+1}$), with $n = 1, 2, ...$.

Table 1.2: Organic compounds usually found in air sorted by their proton affinity [32, 33].

Compound	**Formula**	***PA* (kJ mol^{-1})**
Oxygen	O_2	421
Hydrogen	H_2	422
Nitrogen	N_2	465
Nitrogen oxide	NO	532
Carbon dioxide	CO_2	541
Nitrogen dioxide	NO_2	591
Water	H_2O	691
Formaldehyde	CH_2O	713
Benzene	C_6H_6	750
Methanol	CH_4O	754
Acetic acid	$C_2H_4O_2$	784
Acetone	C_3H_6O	812
Water dimer	$(H_2O)_2$	808
Ammonia	NH_3	854

To provide an idea of the changes in energy involved in a proton transfer reaction, the proton affinity of water compared to the proton affinities of the major constituents of air and some major VOCs in breath are provided in Table 1.2. From this table, it can be seen that one of the main advantages of using H_3O^+ as a reagent ion is that ambient air can be directly sampled as its main constituents have lower proton affinities than water. The proton affinities of the water clusters are higher than that of the monomer, because of the added stability achieved by sharing the proton with additional water molecules (see Table 3.3 for the calculated proton affinities of $(H_2O)_n$, with n = 1, 2, 3, and 4). This translates into a softer protonation process compared to the protonated monomer if an analyte can react with these protonated water clusters via proton transfer. When analytes have a proton affinity close to that of water, for example formaldehyde (712.9 kJ mol^{-1}), then providing the protonated parent does not instantaneously fragment, a back reaction will occur with the much higher concentrations of water in the reaction region, a deprotonation reaction (Equation 1.3), leading to a reduction in detection sensitivity:

$$MH^+ + H_2O \rightarrow (H_2O)H_3O^+ + M \tag{1.3}$$

The tendency of a compound M to act as proton acceptor is called gas-phase basicity (GB) and it is equal to the negative Gibbs energy (G) change of the reaction in Equation 1.4: GB(M)

= -ΔG^0, where the superscript ^{0} denotes the standard state*. Similarly, the proton affinity (PA) of a molecule is the negative of the enthalpy (H) change in Equation 1.4: PA(M) = -ΔH^0.

$$\mathrm{M} + \mathrm{H}^+ \rightarrow \mathrm{MH}^+ \tag{1.4}$$

The Gibbs free energy and the enthalpy fulfil Equation 1.5, and, likewise, the proton affinity and gas-phase basicity are related through Equation 1.6,

$$\Delta G^0 = \Delta H^0 - T\Delta S^0 \tag{1.5}$$

$$PA = GB - T\Delta S^0 \tag{1.6}$$

where T is the absolute temperature and ΔS^0 is the entropy difference between reactants and products in the protonation reaction at standard conditions of pressure and temperature. This term is usually negligible for proton transfer reactions, and hence $\Delta H^0 \sim \Delta G^0$ and $PA \sim GB$. Therefore the proton affinity of a compound is often used in SCI-MS research as a measure of the spontaneity of a protonation reaction.

For Equation 1.1, $\Delta H^0 = PA(\mathrm{H_2O})$ - PA(M) and $\Delta G^0 = GB(\mathrm{H_2O})$ - GB(M). Proton transfer following Equation 1.1 is thermodynamically allowed and will occur spontaneously when $\Delta G < 0$ (exergonic reaction) and, following the assumption made above, $\Delta H < 0$ (exothermic reaction). Thus, protonation of the analyte M will occur when $GB(\mathrm{M}) > GB(\mathrm{H_2O})$ and $PA(\mathrm{M}) > PA(\mathrm{H_2O})$.

1.2.2 Other reagent ions

Besides hydronium, other reagent ions are used in SCI-MS. These are generated by introducing different gases into the ion source, whose working principle is explained in the following chapter. After H_3O^+, NO^+ and O_2^+ are the most commonly used reagent ions, although these are also unwanted impurity ions when using H_3O^+ as the dominant reagent ion, resulting from air back-streaming from the drift tube into the ion source. However, through pressure and ion lens adjustments these impurity ion intensities can be kept to less than 3% of the total reagent ion signal, and hence their effects in the measurements using H_3O^+ can often be ignored.

*Note that, according to the IUPAC, the standard state for a gas includes a reference value for pressure but not for temperature [34].

Table 1.3: Predominant reactions of an analyte M with O_2^+ and NO^+.

Charge transfer from O_2^+	$O_2^+ + M$	$\rightarrow$	$M^+ + O_2$
Charge transfer from NO^+	$NO^+ + M$	$\rightarrow$	$M^+ + NO$
Hydride abstraction with NO^+	$NO^+ + M$	$\rightarrow$	$[M\text{-}H]^+ + HNO$
Adduct formation with NO^+	$NO^+ + M + Z$	$\rightarrow$	$M.NO^+ + Z$

NO^+ and O_2^+ may react with an analyte via a charge transfer process (Table 1.3). NO and O_2 have first ionisation energies of 9.26 eV and 12.1 eV, respectively [35]. This means that NO^+ and O_2^+ can undergo charge transfer reactions with molecules whose ionisation energies are below 9.26 eV and 12.1 eV, respectively. Owing to the low recombination energy of NO^+, charge transfer is not a common reaction mechanism. NO^+ may also react with an analyte via a hydride (H^-) abstraction or through three-body association. Note that for adduct formation a third body Z is required to stabilise the product ion. In contrast, the main reaction mechanism in the case of O_2^+ is charge transfer, as organic molecules' ionisation energies are generally in the range of 8 to 11 eV, which results in a considerable amount of energy (*e.g.* up to 3 eV) deposited into the molecule, often resulting in more fragmentation than occurs from proton transfer reactions with $(H_2O)_nH_3O^+$ (with n = 0, 1 , ...).

Ammonium (*i.e.* NH_4^+) is another impurity ion in the drift tube. It can be generated after the dissociation of N_2 and H_2 and the following reaction of N and H on the walls of the ion source that leads to formation of NH_3, which then undergoes proton transfer with H_3O^+ to produce NH_4^+ [36]. The proton affinity of ammonia is 854 kJ mol^{-1}, so proton transfer from ammonium to a volatile whose proton affinity is greater than this is obviously softer than that from hydronium, being energetically closer to that of proton transfer from $(H_2O)H_3O^+$ ($PA((H_2O)_2)$ = 842 kJ mol^{-1}) [32]. The presence of trace amounts of ammonium does not represent a problem as the main product ion arising from its reaction with the analyte will be the protonated parent molecule (if thermodynamically allowed) or an adduct ion. Müller *et al.* have demonstrated that NH_4^+ ions can be produced with high intensities, and hence become the major reagent ion, without using ammonia or ammonium-containing chemicals, through a suitable pressure, flow and electrical potential adjustments [37]. Furthermore, they demonstrated that it is possible to rapidly switch ($\sim$ 10 s) between the H_3O^+ and NH_4^+ operation modes.

1.2.3 SCI-MS techniques

A brief description of three of the most widely used SCI-MS techniques is provided below.

1.2.3.1 Ion Mobility Spectrometry

In ion mobility spectrometry (IMS) ions are separated according to their mobilities through a buffer gas. An IMS device consists of three main parts: an ion source/reaction region, where the reagent ions are generated and the reactions occur; a drift tube, where an electric field transports the ions as they are being separated across a counter-flow of buffer gas; and a detector (typically a Faraday plate) that detects the ions. The ion source/reaction region and drift tube are separated by a pulsing gate and, unlike in PTR-MS, in the drift tube of IMS systems there is no reaction, just ion separation.

Radioactive material, predominantly ^{63}Ni, was often used as the ion source, but recently, owing to the concern of radiation sources, other ionisation techniques such as corona discharge, dielectric barrier discharge (DBD), electrospray ionisation (ESI) and photoionisation, are becoming more popular [26, 38–40]. The reagent ions (*i.e.* hydronium water clusters when operating in positive ion mode) are continuously produced in the ion source and enter the drift tube when an electrical gate that separates the ion source and the drift tube is pulsed open, typically at a frequency of tens of Hz with pulse widths ranging from tens to hundreds of microseconds. The most common design of drift tube consists of a series of metallic rings electrically connected via a resistor chain, so that each one is at a different electric potential in order to create a uniform electric field (E) along the axis of the drift tube. Ions migrate under the influence of the electric field down the drift tube, suffering collisions with the background gas. The ions reach the so-called mean drift velocity (v_d), which does not represent the velocity of an individual ion but an average over the ion swarm when the acceleration due to the electric field and deceleration due to collisions with the buffer gas have balanced out:

$$v_d = K \cdot E, \tag{1.7}$$

where K is the ion mobility and E the electric field in the drift tube. The mobility can be calculated from Equation 1.7 by substituting $v_d = L/t_d$ and $E = V_d/L$ (Equation 1.8). Given that K is specific to the instrument and operational conditions, it is common to use the reduced

ion mobility (K_0), which can be calculated from K using Equation 1.9. Note that P_0 and T_0 denote the standard pressure and temperature, P and T refer to the pressure and temperature in the drift tube, L is the length of the drift tube, t_d is the drift time and V_d is the drift voltage.

$$K = \frac{L^2}{t_d V_d} \tag{1.8}$$

$$K_0 = K \frac{P}{P_0} \frac{T_0}{T} \tag{1.9}$$

The ions (reagent and product) are detected by a Faraday plate to build an ion current versus drift time plot. Peaks in this plot can be assigned to targeted compounds if their mobilities are known. As a general rule, the lighter the ion, the higher its mobility, although other characteristics, such as the ion's structure, can affect the mobility as it influences how the ion interacts with the buffer gas [41, 42].

Some of the advantages of IMS devices are that they are relatively cheap and small, as no vacuum pumps are required because they operate at atmospheric pressure. Owing to its simplicity, real-time capabilities, cheapness, robustness, high sensitivity (parts per billion by volume (ppbv)) and good selectivity IMS is widely used in security and military applications, such as the security checks in airports [26]. However, the selectivity of IMS, resulting from the temporal separation of ions, cannot compete with those analytical techniques that use mass spectrometers. But these come at a price of being more expensive and complex. Two key SCI-MS instruments have been developed over the last twenty-five years, SIFT-MS and PTR-MS, which will be described below.

1.2.3.2 Selected Ion Flow Tube Mass Spectrometry

Unlike IMS (and PTR-MS), selected ion flow tube mass spectrometry (SIFT-MS) does not use a drift tube, but a flow tube, to convect the ions downstream. A SIFT-MS instrument consists of an ion source, an injection quadrupole mass filter, a flow tube and a detection quadrupole mass analyser. The need for two mass filters adds to the cost of the instrument.

Reagent ions (*e.g.* H_3O^+, NO^+ and O_2^+) are created in the ion source, which is typically a microwave resonator [28]. Then, a quadrupole mass filter selects the reagent ion by its m/z–value. This piece of equipment also allows fast switching (tens of milliseconds) between the

reagent ion species, which can be used to extract more information of the analyte during transient experiments. After the quadrupole mass filter, the ions are injected into the flow tube. Here helium is used as a carrier gas, to which the gas sample is introduced. Reactions of the reagent ions lead to the formation of product ions. These ions together with the reagent ions are sampled into the detection mass, separated according to their m/z–values and detected using an ion detector. Scanning the quadrupole mass spectrometer results in a mass spectrum. Alternatively, selected m/z–values can be recorded, if the product ions are well known.

The presence of helium in the flow tube makes it possible to explore ion/molecule reactions at thermal energies. One of the main applications of SIFT-MS is the ability to measure absolute reaction rate coefficients. This has allowed SIFT-MS to become a valuable tool in areas for investigating the ion/molecule reactions occurring in the upper atmospheric and in interstellar space. More recently it has been developed into an analytical tool for many fields of application fields, including breath analysis [43].

1.2.3.3 Proton Transfer Reaction Mass Spectrometry

Proton transfer reaction mass spectrometry (PTR-MS) is the main analytical tool used for the experimental work presented in this thesis. It has both similarities and differences with IMS and SIFT-MS techniques. The main components of a PTR-MS instrument are the ion source, the drift tube and the mass spectrometer. Hydronium ions (and its water clusters) are generated in the ion source, typically a hollow cathode, from the water injected from the water reservoir. The reagent ions are then introduced into the drift tube (DT). It is at this stage where they meet the analyte and proton transfer takes place. Reagent and product ions are transferred into the mass analyser region, typically containing a time-of-flight or quadrupole mass spectrometer, for separation according to their time-of-flight or m/z, respectively. Further details of the working procedure of a PTR-MS instrument are given in the following chapter.

PTR-MS has many advantages as analytical technique, with most of them also shared with other SCI-MS techniques. To begin with, it can detect a significant number of VOCs such as aldehydes, ketones, aromatic compounds, alcohols, nitriles and esters [31]. Owing to its high sensitivity, PTR-MS can reach limits of detection of parts per quadrillion by volume (ppqv). An important advantage is that H_3O^+ does not react with the main constituents of air allowing the direct sampling air for online, real-time operation. Furthermore, the ion/molecule chemistry can

be manipulated by changing the conditions in the reactor to enhance selectivity. The reduced electric field can be manipulated to improve selectivity by further fragmenting the product ions through field-activated collision-induced dissociation (CID) processes, where the kinetic energy that ions have gained from the electric field is converted, through collisions with the neutral molecules, into internal energy that leads to fragmentation of the ion [34]. Two recent instrumental developments that yield selectivity enhancements, an RF ion funnel drift tube and the use of a fast switching of the reduced electric field, are discussed in this thesis [1, 5, 14].

PTR-MS also has some disadvantages. Often it is not possible to distinguish isomeric compounds, although this can be mitigated to some extent by using pre-separation techniques such as fastGC techniques. Also, for low mass resolution quadrupole mass spectrometers, product ions cannot be uniquely identified. For example, the ^{18}O isotope of the first water cluster ion (*i.e.* $(H_2O)H_3O^+$) and the ion $C_3H_3^+$ will be both found at the same nominal m/z 39. However, this issue can be resolved with the use of a high-resolution mass spectrometer and proper data analysis (*e.g.* using multi-peak fitting techniques and taking into account the isotopic distribution of the ions). Moreover, there exist compounds whose proton affinity lies between that of H_2O and $(H_2O)_2$, such as benzene (750 kJ mol^{-1}) and toluene (784 kJ mol^{-1}) [32]. The detection of these substances can yield misleading results if the abundance of water cluster ions is comparable to that of hydronium. Finally, not all VOCs can be detected in PTR-MS. There exist important VOCs that cannot react with H_3O^+, including some alkanes, which have proton affinities below that of H_2O.

1.3 Thesis outline

This thesis consists of three main parts: Part I provides an introduction and methodology of the work presented (chapters 1-2). Part II presents the experimental results (chapters 3-8). Part III deals with conclusions and further remarks (chapter 9). In chapter 2, the PTR-MS technique and relevant experimental aspects are explained in detail. The first chapter dealing with results is chapter 3, where studies of cocaine and related compounds of interest are presented, including density functional theory calculations. Chapter 4 is an adapted version of my paper regarding the enhancement of selectivity in the detection of nitro-, dinitro- and trinitrotoluenes through the implementation of an RF ion funnel in the reactor of a PTR-ToF-MS (reference [1]). Chapter

5 contains a reformatted version of my paper summarising the use of selective reagent ion mass spectrometry for the detection of nitroanilines isomers (reference [2]). Chapter 6 is a rewritten version of my paper of relevance to breath analysis dealing with nineteen ketones using a fastGC-PTR-ToF-MS instrument in dry and humid drift tube conditions (reference [3]). Chapter 7 provides a detailed PTR-MS and DFT study of anaesthetic compounds based on my fourth published paper (reference [4]). Chapter 8 presents an unpublished investigation of phthalates in PTR-MS using direct headspace sampling. The final chapter, chapter 9, summarises the key research findings and provides some closing remarks. Supplementary material is provided in the appendices: appendix A presents PTR-MS investigations of illicit drugs, including reduced electric field fast switching results; and appendix B contains copies of my four published peer-reviewed articles.

1.4 Aim of the research programmes presented in this thesis

The main goal of the work presented in this thesis is to broaden our current knowledge of ion/molecule processes occurring in PTR-MS by investigating the dependence of the different reactions on the collisional energy with the objective of enhancing selectivity.

A list of compounds of relevance to homeland security (*e.g.* phthalates, nitrotoluenes, drugs) and medicine (*e.g.* ketones, anaesthetics) have been investigated and, whilst it is common in PTR-MS to only use one fixed E/N–value (typically between 120-140 Td), the experimental results reported in this thesis are given over a wide range of reduced electric field values (typically 80-220 Td). The results present the ion signal intensities or product ion distributions arising from the reactions of the neutral compounds with the reagent ions. For some of the studies, the experimental results are complemented by density functional theory quantum chemical calculations to help interpret the results. These calculations were conducted by Dr Peter Watts using Gaussian09W and GaussView05 for Windows using the B3LYP hybrid functional and the 6-31+G(d,p) basis set.

Chapter 2

Proton Transfer Reaction Mass Spectrometry

Of the SCI-MS techniques introduced in the first chapter, PTR-MS was the main analytical tool used for the work in this thesis and hence in this chapter proton transfer reaction mass spectrometry, its underlying chemistry and relevant experimental aspects, are explained in more detail.

2.1 The PTR-ToF-MS

As stated in the introduction, PTR-MS is a sensitive technique for the real-time monitoring of VOCs in air with a minimal sample preparation. PTR-MS uses hydronium as reagent ions to donate protons to the trace compounds present in the analyte gas. A schematic of a KORE Technology Ltd (Ely, UK) RFIF Mk I PTR-ToF-MS, used for many measurements presented in this thesis, is shown in Figure 2.1. Independent of the manufacturer, the main components of a PTR-MS instrument are:

1. Ion source: production of reagent ions.
2. Drift tube: the reaction region.
3. Mass spectrometer and ion detector: separation and detection of the reagent and product ions.

These regions are explained in detail in the following sections.

(a)

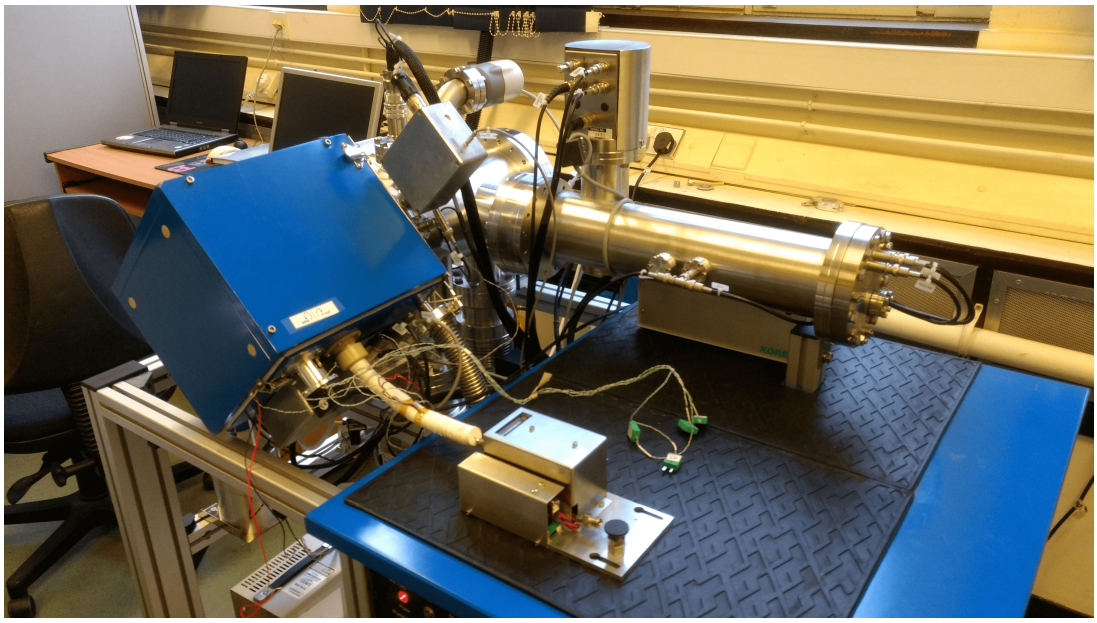

(b)

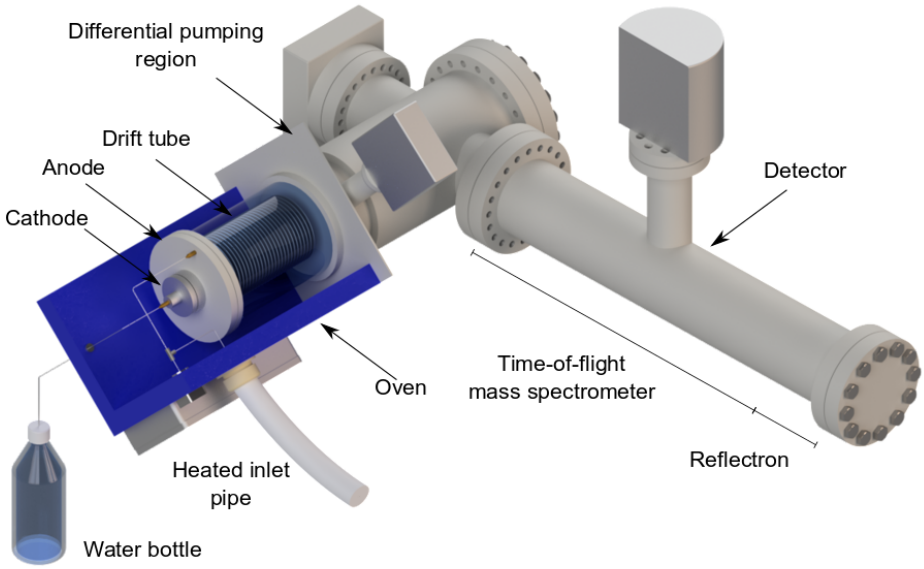

Figure 2.1: (a) Photograph of the KORE Technology Ltd RFIF Mk I PTR-ToF-MS with a thermal desorption unit attached to the drift tube inlet. (b) Schematic of the instrument with the key regions labelled.

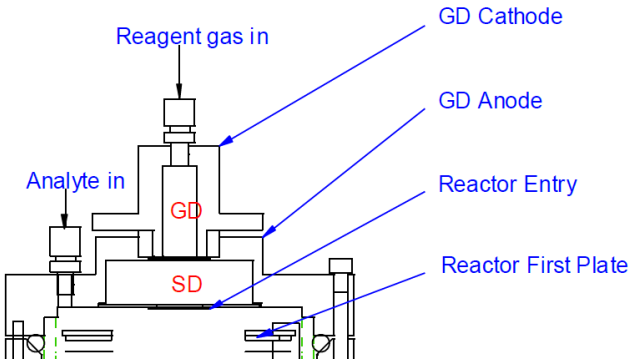

Figure 2.2: Diagram of the hollow cathode of the PTR-MS apparatus manufactured by KORE Technology Ltd. including the glow discharge (GD) and the source drift (SD) regions.

2.1.1 Ion source

The reagent ions that will ionise the sample are generated in the glow discharge (GD) in the ion source. Most PTR-MS instruments use a hollow cathode discharge ion source, to which a voltage is applied to ionise the gas that flows through it and create the plasma in which the reagent ions are being produced. The cathode in our PTR-MS instrument, which is formed of two aluminium electrodes, is schematically shown in Figure 2.2. There are alternatives available such as the triple off-axis cathode recently developed by IONICON Analytik GmbH (Austria), which allows the operator to quickly switch between reagent ion species [44].

2.1.1.1 The glow discharge: production of reagent ions

A glow discharge is a type of electrical discharge that occurs at low pressures (mbar range) and is characterised by a maintained constant current, ranging from 1 uA up to 1 A, between the cathode and the anode. It receives this name because the ionised gas produces a shining glow, whose characteristics depends on the nature of the gas, its pressure and the voltage applied.

For PTR-MS, water vapour is supplied from a water reservoir through a needle valve or mass flow controller into the cathode. A series of ion/molecule reactions occurring in the ion source lead to the production of H_3O^+ (see Table 2.1). It starts when H_2O^+ has been produced through the ionisation of H_2O. However, other water fragment ions can also undergo reactions that ultimately generate hydronium (see Table 2.1). The rates at which these reactions happen are at or very close to the collisional value. Hydronium ions can cluster to water molecules via hydrogen bonds to form the so-called water cluster ions, *i.e.* $(H_2O)_nH_3O^+$ with $n = 1, 2, 3...$

Table 2.1: Chemical reactions through which hydronium can be produced starting from products of EI of water vapour and their rate coefficients at 300 K [45].

$H_2O^+ + H_2O$	$\rightarrow$	$H_3O^+ + OH$	$k = 1.8\times10^{-9}$ cm^3s^{-1}
$OH^+ + H_2O$	$\rightarrow$	$H_3O^+ + O$	$k = 1.3\times10^{-9}$ cm^3s^{-1}
	$\rightarrow$	$H_3O^+ + OH$	$k = 1.8\times10^{-9}$ cm^3s^{-1}
$O^+ + H_2O$	$\rightarrow$	$H_2O^+ + O$	$k = 2.6\times10^{-9}$ cm^3s^{-1}
$H_2^+ + H_2O$	$\rightarrow$	$H_3O^+ + H$	$k = 3.4\times10^{-9}$ cm^3s^{-1}
	$\rightarrow$	$H_2O^+ + H_2$	$k = 3.7\times10^{-9}$ cm^3s^{-1}
$H^+ + H_2O$	$\rightarrow$	$H_2O^+ + H$	$k = 8.2\times10^{-9}$ cm^3s^{-1}

Ideally, the formation of these clusters should be avoided so that pure hydronium is injected into the drift tube. Air from the analyte gas can enter the cathode and produce other ions such as N_2^+, NO^+ and O_2^+. N_2^+ undergoes charge-transfer reaction with water to generate H_2O^+ and eventually H_3O^+:

$$N_2^+ + H_2O \quad \rightarrow \quad H_2O^+ + N_2 \qquad k = 2.8 \times 10^{-9}\,cm^3s^{-1} \tag{2.1}$$

On the other hand, the ionisation energies of NO and and O_2 are lower than that of H_2O, and thus neither NO^+ (which is formed following Equation 2.2) nor O_2^+ can undergo charge transfer with water, and hence remain as impurity reagent ions.

$$N^+ + O_2 \quad \rightarrow \quad NO^+ + O \qquad k = 2.6 \times 10^{-10}\,cm^3s^{-1} \tag{2.2}$$

However, it is possible to reduce the abundance of O_2^+ and NO^+ to a marginal percentage of that of hydronium by setting the glow discharge and drift tube to operate under suitable conditions.

The breakdown voltage, which is the voltage difference needed between cathode and anode to start the plasma, is approximately 750 V for the cathode with the geometry described in Figure 2.2. However, after the plasma has started, the voltage difference to maintain the discharge goes down to approximately 350 - 400 V. The anode voltage floats with the voltage of the first plate of the drift tube electrodes, which can be adjusted by the user to set the drift voltage, as will be discussed in the next section. After the glow discharge switch is turned on, it can take the plasma up to a couple of minutes to start. Once the voltage is applied, the glow discharge is

initiated, the stability of which will depend on the cleanliness of the cathode and the pressure and temperature. In our instrument, the ion source pressure is usually set between 1 and 1.4 mbar. The plasma struggling to get started or maintained at a pressure within the common operating range indicates that the hollow cathode is dirty: aluminium is chosen for the cathode because it is a material whose secondary electron coefficient is very high, which favours the generation of a plasma. However, when it is constantly exposed to water, a layer of aluminium oxide (Al_2O_3, white colour) can be formed. This oxide layer must be removed to achieve the correct operation of the cathode. Another factor that affects the stability of the glow is the temperature of the oven that contains the ion source and the drift tube: the higher the temperature of the oven is, the higher the cathode pressure must be for the glow to be maintained.

Downstream from the ion source, the ions reach the so-called source drift (SD) region (shown in Figure 2.2), whose goal is to break protonated water clusters apart before they enter the drift tube. High reduced electric fields ($>$ 100 Td) in the drift tube result in further fragmentation of the protonated water clusters, leading to a high concentration of H_3O^+ reagent ions in the drift tube.

2.1.2 Drift tube

The drift tube (DT) is the region of a PTR-MS instrument where the ion/molecule processes take place. It is therefore also often referred to as the reaction region. A picture of the DT taken out of the front-end of the KORE Technology Ltd PTR-ToF-MS is shown in Figure 2.3.

The drift tube of the KORE Technology Ltd RFIF Series 1 PTR-ToF-MS, whose schematic layout is shown in Figure 2.4, consists of 29 stainless-steel ring electrodes of 0.2 mm of thickness with a spacing of 3.2 mm per plate inside a cylinder of glass. The inner diameter of these electrodes is 40 mm in the first half of the stack and it gradually decreases in the second half down to 6 mm. The electrodes are connected to each other by means of 1 MΩ resistors, which generates a linearly decreasing potential in the drift tube (see Figure 2.5) when a voltage difference is applied between the first and the last plates, generating an electric field. When the instrument is operating under these conditions (*i.e.* without the RF field explained later in section 2.1.2.3), we refer to it as working in DC mode or DC-only mode.

The DC electric field causes the ions to migrate down the reactor towards the transfer lenses, where a fraction will get transmitted into the mass spectrometer. As they are drawn through

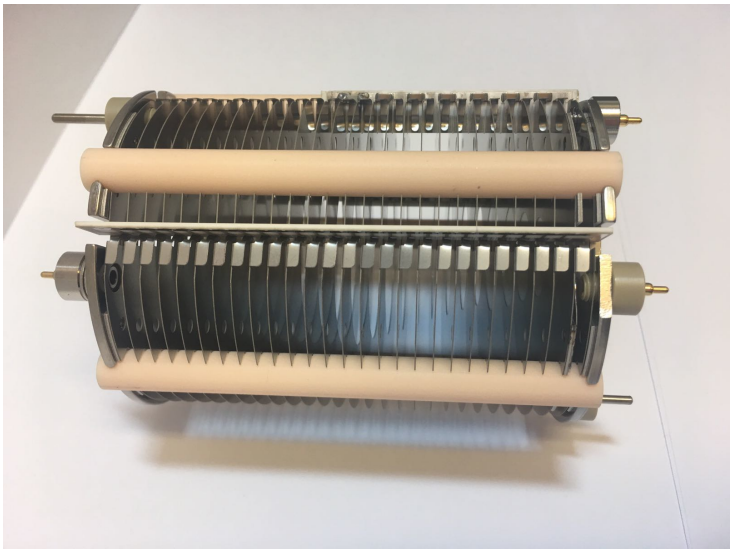

Figure 2.3: Picture of the drift tube. Note that in this model the diameter of the electrodes steadily decreases in the second half of the stack.

the reactor, ions collide with the neutral molecules of the background and analyte gases, which can result in protonation and possible subsequent fragmentation. The collisional energy can be manipulated by changing the voltage gradient across the drift tube and/or changing the drift tube's pressure and temperature, whose standard operating values are around 1 mbar and between 100 and 150 °C, respectively, although our oven can reach up to 200 °C.

2.1.2.1 Reduced electric field

As the collisional energy depends not only on the electric field strength (E) but also on the pressure and temperature of the buffer gas in the reactor, it is convenient to use the reduced electric field (E/N) as a measure of the collisional energy delivered to the ions. First, the electric field strength is defined by the potential difference V_d between the first and the last plate in the reactor divided by its length L:

$$E = \frac{V_d}{L} \tag{2.3}$$

The potentials on the first and the last plates of the reactor are known as the PTR Entry and PTR Exit voltages, respectively, and can be adjusted by the user. L is 9.36 cm in our Kore instrument. For example, a voltage difference of 250 V between the first and last plates corresponds to an electric field of 26.71 V/cm.

Similarly, the gas number density (N) is defined as the number of gas molecules per unit

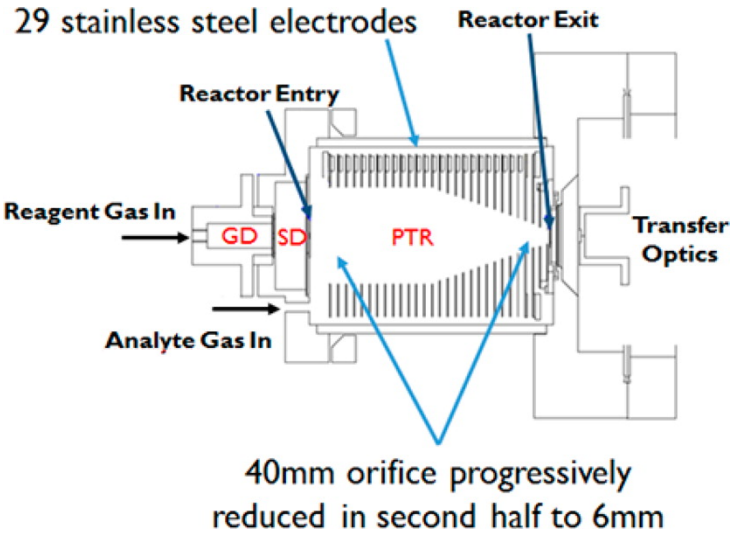

Figure 2.4: Schematic diagram of the KORE Technology Ltd RFIF Series 1 PTR-ToF-MS drift tube, together with the glow discharge (GD) and the source drift (SD) regions.

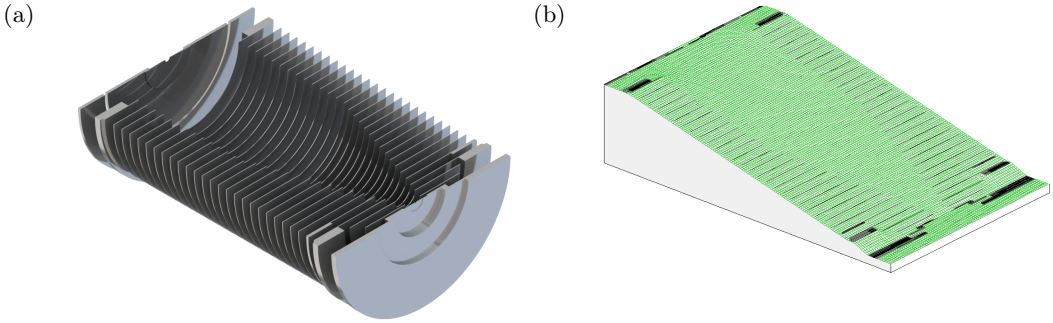

Figure 2.5: (a) Half section view of the reactor. (b) Potential energy surface of the cross section of the reactor in DC mode calculated in SIMION® for a random drift voltage.

volume and can be calculated from the ideal gas equation to be:

$$N = \frac{N_A}{V_{mol}} \frac{P_d}{P_0} \frac{T_0}{T_d} \tag{2.4}$$

where N_A is the Avogadro's number (6.022×10^{23} mol^{-1}), V_{mol} (22414 cm^3 mol^{-1}) is the molar volume of an ideal gas at standard temperature and pressure conditions P_0 and T_0, T_d is the temperature of the drift tube in Kelvin and P_d is the gas pressure in the drift tube in mbar. For the standard operating conditions of 1 mbar and 100 °C, N is 1.94×10^{16} cm^{-3}. The ratio E/N in this case would be 26.71 V cm^{-1}/1.94×10^{16} cm^{-3} $\simeq$ 1.38×10^{-15} V cm^2. However, it is usual to express the reduced electric field in a different unit called the townsend (Td), which corresponds

to 10^{-17} V cm^2. Thus, 1.38×10^{-15} V cm^2 corresponds to a value of 138 Td. Typically, a PTR-MS instrument is operated between 120 and 140 Td but going as low as 80 Td or as high as 240 Td is sometimes crucial in order to get a good picture of the dependence of the ion/molecule reactions on the collisional energy. Besides the E/N, other less used definitions of the reduced electric field can be found in the literature. For instance, Price *et al.* use the ratio E/P, with units of V/cm Torr, where E is the electric field and P is the neutral gas pressure in the drift tube [46, 47]. It is worth noting that the reagent ion percentages as a function of the E/P reported by Price *et al.* in Figure 4 of reference [46] are qualitatively comparable to the reagent ion intensities as a function of the E/N in Figure 3.2(b), with a higher abundance of clustering at lower reduced electric fields but with said clusters breaking apart as the reduced electric field increases.

As mentioned in the introduction, the ions inside the drift tube reach a steady velocity, the so-called drift velocity, $v_d = K \cdot E$, which can be also expressed in terms of the reduced mobility K_0, the gas number density at standard pressure and temperature N_0, and the reduced electric field E/N:

$$v_d = K_0 N_0 \frac{E}{N} \tag{2.5}$$

Both reagent and product ions will predominantly collide with buffer gas molecules. Equation 2.6 gives the expression for the kinetic mean free path (MFP, λ) defined as the average distance travelled between collisions, if the colliding particles are considered hard-spheres [48]:

$$\lambda = \frac{1}{\sqrt{2} N \pi d^2} \tag{2.6}$$

with d, the so-called kinetic diameter, being 3.64×10^{-10} m for N_2 and $N = 2.41\times10^{22}$ m^{-3} at 1 mbar and 300 K the mean free path is around 70 µm in the reactor, which corresponds to a "viscous" flow [49]. In contrast, in the mass spectrometer, where the pressure is around 10^{-8} mbar, $N \simeq 10^{15}$ m^{-3}: the mean free path grows up to the km order of magnitude, becoming much greater than the dimensions of the chamber. In this case the flow is "molecular" and the predominant collisions are no longer with other particles but with the walls of the chamber. The transition from the viscous to the molecular regime occurs in the differential pumping region (see Figure 2.1(b)).

2.1.2.2 Presence of water cluster ions in the drift tube

PTR-MS instruments from two different manufacturers have been employed to carry out different parts of the experimental work in this thesis. Because of the way the so-called *normal* and *humid* operating conditions were achieved was different which each instrument, it is key to explain each of the procedures. For KORE Technology Ltd instruments (Figure 2.1 and results chapters 3–5 and 8, and appendix A) the difference between the operating conditions is generated by setting the pressure in the cathode to different values. As mentioned in section 2.1.1.1, not only H_3O^+ but also $(H_2O)_nH_3O^+$ (n = 1, 2, ...) ions can be generated in the ion source and be injected into the drift tube. It has been experimentally observed that higher ion source pressures yield a higher amount of water cluster ions, which obviously affect the ion/molecule reactions taking place in the drift tube, as shown by Warneke *et al.* [50]. The normal and humid operating conditions are, in this case, differentiated because of the cathode pressure. This corresponds to a pressure of *ca.* 1.15 and 1.3-1.4 mbar for the normal and for the humid case, respectively. IONICON Analytik GmbH instruments (*i.e.* PTR-TOF 8000) were used for the work in chapters 6 and 7. For normal operating conditions, dry N_2 was used in this case as the carrier gas, and humid measurements were performed by increasing the humidity of the carrier gas. In other words, the gas containing the analyte was humidified, as opposed to generate more water cluster ions in the cathode and injecting them into the drift tube. In chapter 6 this was achieved by diluting the ketones samples in water and generating a gas stream of analyte using a liquid calibration unit (LCU, section 2.3.3), while in chapter 7 the carrier gas was humidified by making it pass through a vial containing water at room temperature. These different procedures explain the differences between the reagent ion plots provided to illustrate each set of measurements within chapters 3-8. These plots are Figures 3.2, 4.1, 5.2, 6.1, 7.1 and 8.1. It must also be noted that in Figure 8.1 the reagent ion signals are plotted as percentages and not in counts per second.

2.1.2.3 Radio frequency ion funnel

The Radio Frequency Ion Funnel (RFIF) in the reactor of our instrument is a novel piece of equipment that delivers both extra collisional energy and focuses the ions towards the exit aperture of the drift tube, enhancing both sensitivity and selectivity of the PTR-MS instrument [1, 5].

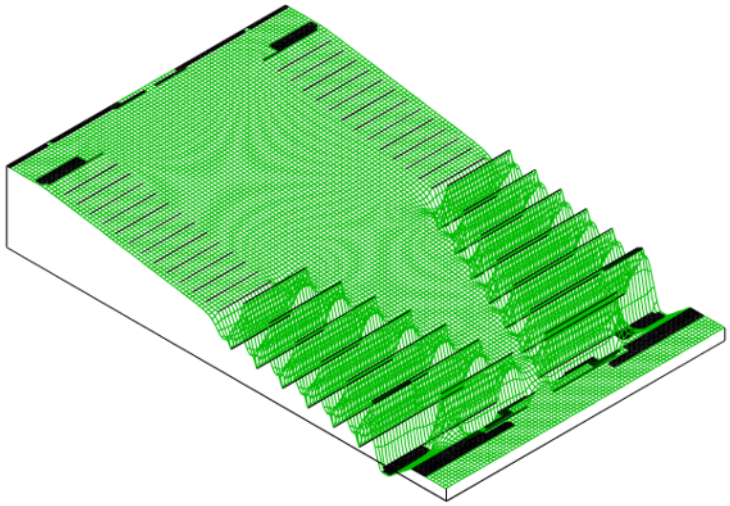

Figure 2.6: Snapshot of the potential energy view of the cross section of the reactor in RF mode superimposed to a random DC field modelled in SIMION®.

As mentioned earlier, in the second half of the drift tube stack the electrode's diameter gradually decreases from 40 mm to 6 mm in a funnel-like configuration. The suitable electronics to provide these funnel electrodes with an RF field are mounted in the instrument. These electronics provide the second half of the drift tube's electrodes with a signal of approximately 760 kHz and 200 V peak-to-peak in resonance that we will refer to as RF field (see Figure 2.6). At any given time, adjacent funnel plates are supplied with an RF field of opposite polarity. Also, this RF field can be turned on and off on the front panel of the instrument and when it is superimposed on the DC field, which is always on, the instrument is referred to as operating in the RF mode. Furthermore, in the RF mode the reduced electric field, E/N, cannot be used to refer to the collisional energy as in this mode the electric field in the drift tube is no longer uniform. A comparison of the ion trajectories in the second half of the drift tube in the DC and RF modes that I simulated using SIMION® (version 8.1, Scientific Instrument Services Inc., NJ, USA) is shown in Figure 2.7 for ions of m/z 19 at a drift voltage of 200 V, which corresponds to around 120 Td in the DC mode. The funnel effect can be observed on Figure 2.7(b), which reveals a higher ion density near the exit of the reactor than that in DC mode, even though fewer ions were flown in the RF mode simulations because this mode is computationally more demanding than in the DC mode.

The ion funnel configuration described in this section is not the only one used in PTR-MS.

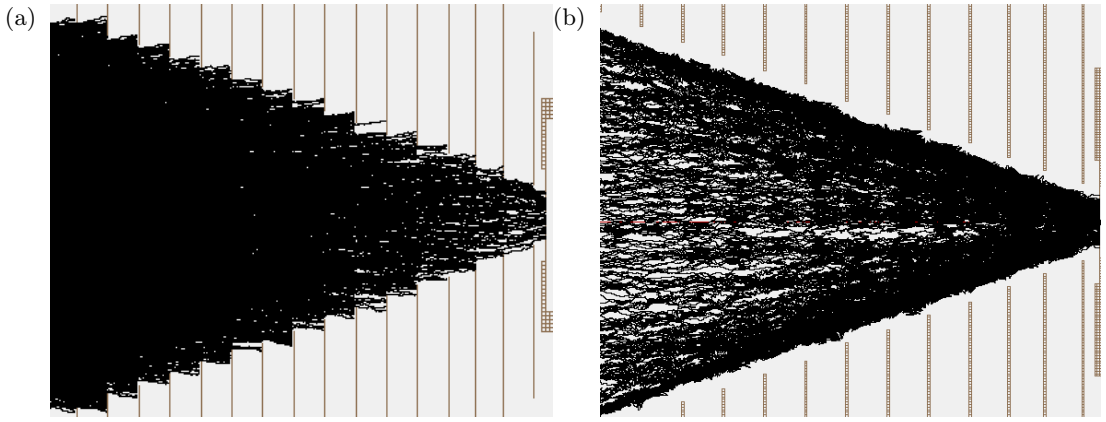

Figure 2.7: SIMION® simulation of ion trajectories in (a) DC mode and (b) RF mode in the second half of the drift tube for ions of m/z 19 at a drift voltage of 200 V (ca. 110 Td in DC mode).

Others include a short, funnel-like stack of electrodes at the end of the drift tube, and the use of quadrupole mounted on the outside of the drift tube [10, 51].

2.1.2.4 Fast reduced electric field switching

Besides the RFIF, another one of the recent hardware developments is the fast reduced electric field switching, or just fast switching. It consists of a programmable 500 V power supply unit that can quickly switch the PTR Entry voltage between two preselected values in the range from 50 V to 450 V, which corresponds to roughly the interval from 10 Td to 250 Td, at a chosen frequency. This unit can be retrofitted into any other PTR-ToF-MS from the same manufacturer. This development has been applied to the detection of different explosives by González-Méndez *et al.* [14].

An E/N study of the analyte of interest is needed to identify the characteristic product ions before using the switching device. Then the two relevant PTR Entry voltage (*i.e.* E/N) values and the switching frequency are selected. The lower limit of the switching frequency, while still achieving optimal analytical results, is around 1 Hz. This limit is a consequence of the RC time constant of the electronic circuit, which is around 150-200 ms. The rise and fall times of the voltages given by the power supply unit are not symmetrical, but as these are tens of milliseconds, they are negligible in comparison with the RC constant. A temporal resolution of 25 ms has been found to be the optimum value and also proper data analysis is needed in order to discard

the data acquired during the voltage changes. This is done by means of a script described in detail in section 2.2.3.

2.1.3 Differential pumping region and transfer lenses

When the ions leave the drift tube through the exit plate's orifice, which has a diameter of 400 µm, they enter the differential pumping region, where the transfer lenses are. There is a pressure drop from the 1 mbar range in the drift tube to the 10^{-4} mbar range in the differential pumping stage. This translates into a change in the type of flow, from viscous flow in the drift tube to a molecular flow in the transfer lenses region and further downstream in the mass analyser, with the mean free path of the ions being larger than the dimensions of the chamber, and thus ion-wall collisions are predominant over ion-neutral ones.

The role of the transfer lenses is to focus the ion beam and transport it to the mass spectrometer as effectively and efficiently as possible. For this purpose, the ion beam is driven through a set of ring electrodes at different voltages. These ion optics focus the ions in the centre of a pinhole in the same way optical lenses do with light. The pinhole helps to "clean" the beam from chromatic aberrations, which translates into narrower peaks in the mass spectra because the ion beam that reaches the mass analyser is less spatially spread out. This is qualitatively illustrated in Figure 2.8. Also, two pairs of deflectors (not included in Figure 2.8) can be tuned to steer the beam to maximise the transmission into the mass spectrometer region.

A high potential gradient between the exit plate and the first transfer optics electrode can help to increase the transmission but can create a "hard extraction" of ions (*i.e.* uncontrollably increasing ions fragmentation beyond the exit plate in the early stages of the transfer optics). This undesired fragmentation can be avoided by setting the electric field between the exit plate and the first electrode in the transfer optics to no more than a few V/cm. This phenomenon was investigated by Renaud R. Dassonville (Kore Technology Ltd.) and myself in a series of experiments not included in this thesis, that consisted of monitoring the product ions from n-butylbenzene at different extraction and transfer lenses voltages.

2.1.4 Mass spectrometer

The ion beam is transferred from the drift tube to the mass spectrometer (MS) via the transfer optics. The MS separates the ions according to their mass-to-charge ratio which are then detected

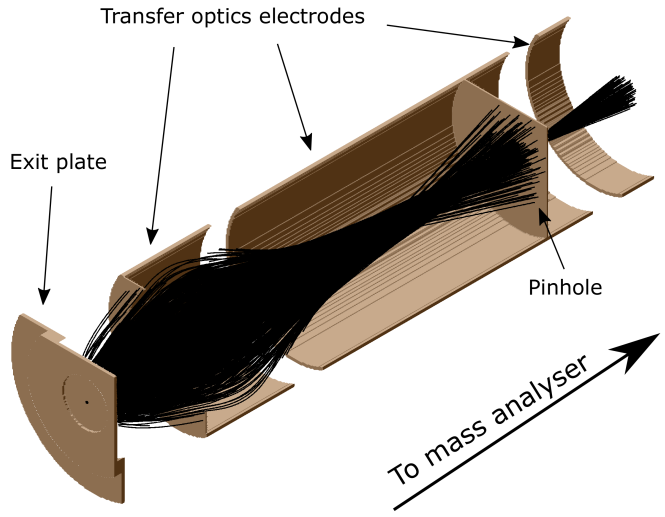

Figure 2.8: Simulation of the ion trajectories in the transfer lens region using SIMION®. 1000 ions of m/z 100 with kinetic energies uniformly distributed between 0 and 1 eV were flown.

to produce a mass spectrum. The terms mass spectrometer and mass analyser will be used here interchangeably. A mass spectrum corresponds to the intensity of the ion signal as a function of the mass-to-charge ratio m/z. There are two commonly used definitions of the m/z–value of an ion: (i) the nominal m/z, which is calculated rounding up to the nearest integer the masses of the most abundant isotope of each element, and (ii) the monoisotopic m/z, which is calculated using the exact masses (*i.e.* accounting for the mass defect) of the most abundant isotope of each element. The first is commonly used in low mass resolution mass spectrometers (*e.g.* quadrupole mass spectrometers) and the latter is used with higher resolution ones (*e.g.* time-of-flight mass spectrometers). The m/z–value is dimensionless, although the "unofficial unit" of thomson (Th) is used by some authors.

2.1.4.1 Time-of-flight mass spectrometer

Time-of-flight mass spectrometers (ToF-MS, Figure 2.9) are widely used in PTR-MS.

A ToF-MS works as follows: when ions reach the entrance of the MS (pulser region), a pulsed (tens of kHz) high voltage V of some kilovolts repels them orthogonally to their incoming direction and steers them towards the other end of the flight tube. Having left the pulser region with the same kinetic energies, the lighter ions will have a higher speed than the heavier ions, which means that they will reach the detector faster. The time it takes for an ion to reach the detector and its m/z are related through Equation 2.8, which comes from the energy balance in

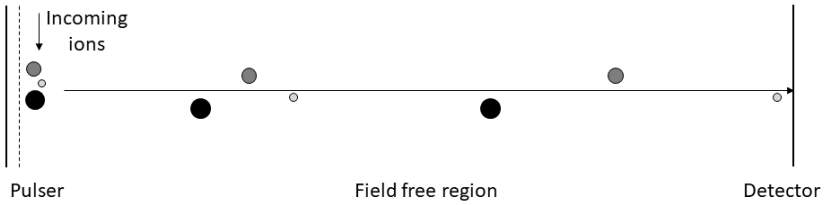

Figure 2.9: Diagram of a linear time-of-flight mass spectrometer. Circles represent ions, their diameter being proportional to their mass-to-charge ratio. The direction of the incoming ions before they are repelled by the pulser is indicated in the diagram. Note that this geometry serves purely illustrative purposes and it does not correspond to any of the ToF-MS systems employed throughout this thesis.

Equation 2.7:

$$qV = \frac{1}{2}m\left(\frac{l}{t}\right)^2 \tag{2.7}$$

$$t = \sqrt{\frac{m}{z}\frac{l^2}{2eV}} \tag{2.8}$$

where m/z is the mass-to-charge ratio of the ion, l is the length of the flight tube, t is the flight time and $q = ez$ is the ion's charge. This allows the m/z–value of the ions to be determined as they are being collected at the detector and hence a mass spectrum can be built-up by measuring the ions' times of flight.

2.1.4.2 Reflectron

A spatially spread distribution of ions of the same m/z in the pulser region can result in different ion velocities, and hence being detected at different times, broadening the mass spectrum peaks. To overcome this a reflectron can be implemented in the flight tube of a ToF-MS.

A diagram showing how a reflectron works is provided in Figure 2.10. It basically consists of a series of electrodes with increasing voltage that will reverse the trajectory of the ions. When a cloud of ions reaches the reflectron, ions of the same m/z–value but going faster go deeper in it, having a longer flight distance than slower ions. This way, slow and fast ions of the same m/z will reach the detector at the same time, having travelled different distances, yielding narrower peaks and improved mass resolution.

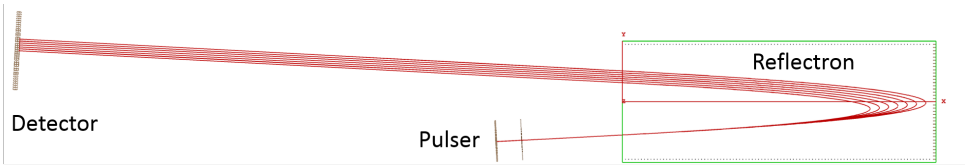

Figure 2.10: Schematic diagram of a flight tube with a reflectron showing the different trajectories of seven ions of the same m/z with different initial velocities simulated in SIMION®. Note that this geometry serves purely illustrative purposes and it does not correspond to any of the ToF-MS systems employed throughout this thesis.

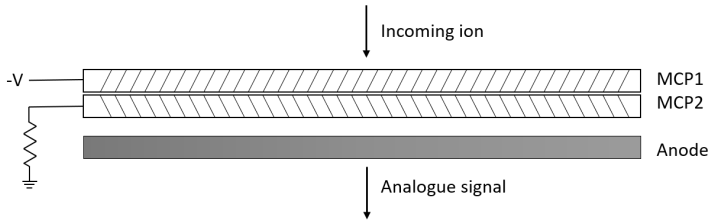

Figure 2.11: Schematic diagram of a MCP detector.

2.1.4.3 Detector

Prior to detection, an individual ion needs to be amplified to a detectable level. A common pre-amplification setup consists of two microchannel plates (MCPs), which are circular plates of a few millimetre of thickness with an array of tubes that go from one face to the other. These tubes form an angle with the ion trajectory and the second MCP is rotated 180° from the first one as shown in Figure 2.11 so ions cannot go through without hitting the plates.

Incoming ions are accelerated to ∼2 kV before they hit the MCP surface. MCPs are made of a high resistive material with a secondary electron emission factor greater than one, so that when the incoming ion hits it, one or more electrons are emitted per collision, generating an avalanche that can amplify a single event by up to a factor of 10^8. The cascade electron signal will then reach the anode, where the time-to-digital converter (TDC) will process the analogue signal and convert it into digital.

The ion detection system in the KORE Technology Ltd PTR-MS instrument (shown in Figure 2.1) has the following characteristics: a dead-time between the arrival of consecutive ions of <10 ns, a high time resolution of <1 ns, and a maximum sustained count rate of >17,000,000 counts/s (theoretical) and >4,000,000 counts/s (measured) [52].

2.1.4.4 Mass Calibration

As with any other scientific instrument, the PTR-ToF-MS must be calibrated before performing any experiment. Note that this section refers to calibration as the method to calculate the mass conversion parameters, not the calibration to calculate a concentration from an ion signal. The mass conversions parameters can be calculated by selecting some reference peaks and assigning them their exact m/z. Some peaks that can be used to calibrate the instruments are the ^{18}O isotope of hydronium ($H_3^{18}O^+$, m/z 21.023), NO^+ (m/z 29.998) and NO_2^+ (m/z 45.993). It is also useful to include peaks from the higher end of the mass spectrum (*i.e.* m/z >200). If a single analyte is being studied (*i.e.* not a mixture), its protonated parent ion can be used. The TDC uses Equation 2.9 for this task doing a least squares fitting:

$$m/z = \left(\frac{t - t_0}{C_b}\right)^2 \tag{2.9}$$

where m/z is the mass-to-charge ratio, t is the ion's time-of-flight, and t_0 and C_b are parameters that depend on the mass range the instrument will measure and in some experimental quantities like the length of the flight tube. Note that this equation is the same as Equation 2.8 for $t_0 = 0$ and $C_b = l/\sqrt{2eV}$.

2.2 Data post-processing and computational methods

2.2.1 Data acquisition, visualisation and treatment

The analogue data acquired by the PTR-ToF-MS is translated into digital files by the TDC to be visualised and analysed with the proper software. An experiment can consist of either a static measurement, yielding a stable signal throughout the experiment, or a transient measurement, where the ion signals are time-dependent. These different types of experiments are usually acquired as a mass spectrum in the form of a Galactic .spc file from Thermo Fisher Scientific® (Cheshire, UK), or as a temporal evolution of the mass spectrum, in the form of a binary .lst file, respectively.

A mass spectrum is the plot of the counts of detected ions as a function of their m/z which, in our case, is stored in .spc files. Figure 2.12(a) shows an example of a mass spectrum visualised with the Thermo Fisher Scientific® GRAMS/AI™ Spectroscopy Software, which has been

adapted by KORE Technology Ltd to be used with their equipment. The software does the time to m/z conversion utilising Equation 2.9.

Transient experiments are stored in .lst files. These files record the timestamp in microseconds of each event in three consecutive bytes in hexadecimal notation, with the most significant byte first, and they are accompanied by a text (.ini) file containing information about the experiment. An event can be either the start of a cycle in the detector (*i.e.* when the pulser repels the ion in the mass spectrometer), always indicated by 0x000000 (*i.e.* $t = 0$ µs), or a detected ion (for instance, an ion detected at $t = 12500$ µs would be recorded as 0x0030D4). Therefore an .lst file holds all the information about the experiment and can be plotted as either a cumulative mass spectrum as a function of the m/z or as a transient of selected ion signals as a function of the experiment time. The software GRAMS/AI^{TM} allows one to open the .lst files as a mass spectrum, like that in Figure 2.12(a), or as the time-evolution of some particular m/z, as shown in Figure 2.12(b). For the latter plot, the so-called regions of interest must be selected before starting the experiment to display targeted ion signals.

Additionally, the Matlab® (Natick, MA, USA) command *tgspcread()* is compatible with Galactic .spc files from Thermo Fisher Scientific® (Cheshire, UK). This command imports all the fields in the data file into an object-oriented data type called *struct*, which allows quick and easy extraction and manipulation of large amounts of data. In the case of the .lst files, the extraction of the data has to be done without any help from a library. It is rather more tedious, as it requires reading the hexadecimal file, building the mass spectra using the parameters stored in the .ini file, do the time-mass conversion and extract the m/z of interest for transient experiments.

2.2.2 Calculation of ion intensities

Once the data are acquired and stored in the files as explained in the previous section, they can be analysed and plotted for interpretation, although there are some concerns to take into account when doing this.

The counting electronics in the PTR-ToF-MS assumes that each pulse measured at the MCP corresponds to one ion. This can be not true if two or more ions arrive at the detector very close together and their analogue signals overlap so that the TDC translates it as a single event. This phenomenon is known as saturation and happens more often when a high concentration of a compound is being measured. At a given m/z, the maximum number of counts per second the

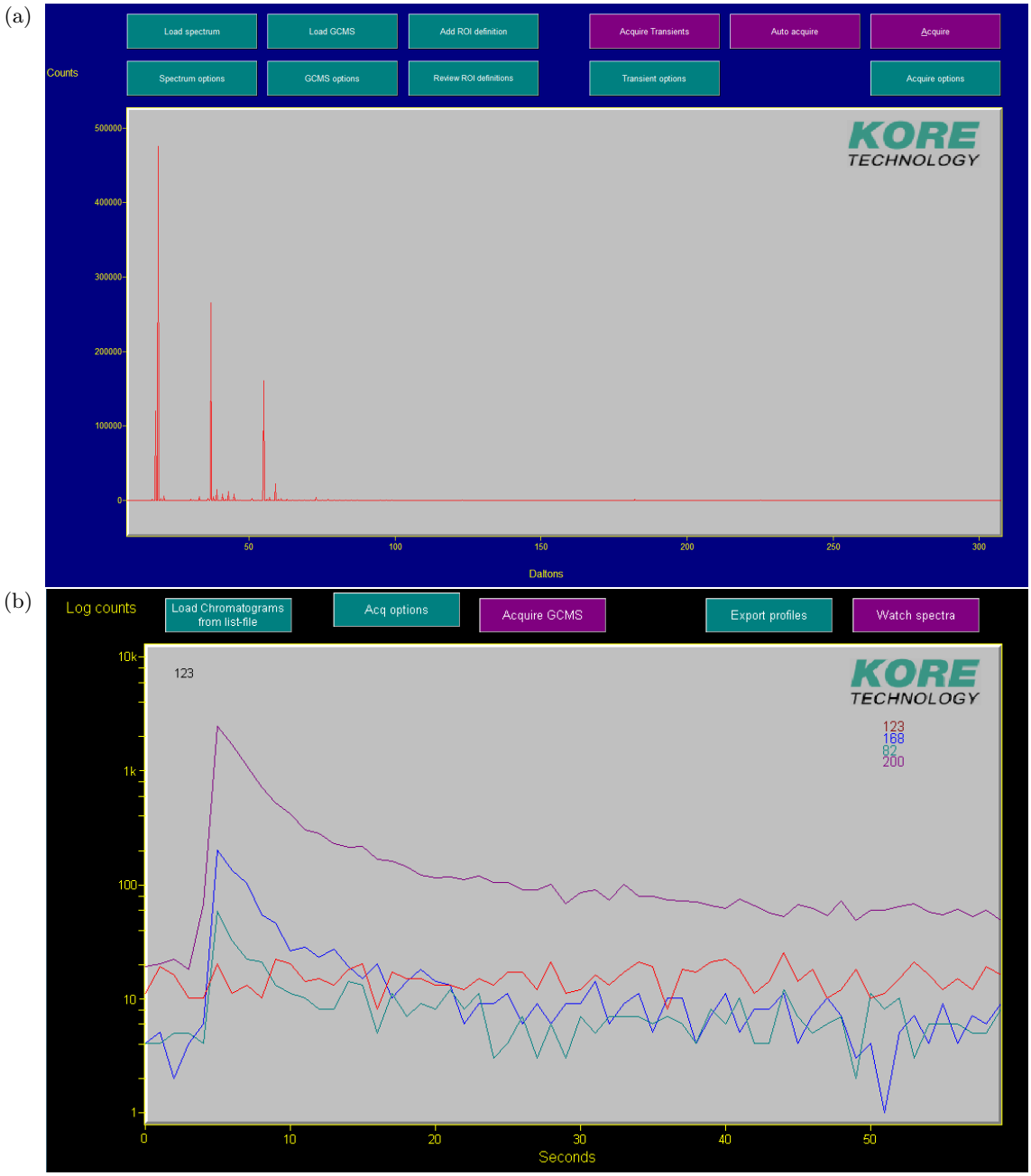

Figure 2.12: Screenshot of the GRAMS/AI^{TM} user interface for the PTR-ToF-MS instrument manufactured by KORE Technology Ltd showing (a) an example of mass spectrum, and (b) an example of transient experiment data.

instrument can measure corresponds to the number of cycles per second of the mass spectrometer, which is the number of times the ions are pulsed each second. In other words, at a certain m/z only one ion per cycle can be measured. Therefore, a compromise must be found when the experiment is being designed to avoid situations of saturation while getting a suitable signal. In our experimental setup, this is given by the rule of thumb that says that saturation occurs when the ion count at a peak corresponding to a certain m/z–value is higher than 60% of the cycles per second in the time of flight. This means that a peak can present saturation effects even before showing a distorted shape. For instance, for a cycle length of 36 µs, the mass spectrometer will be pulsing at a rate of ∼27777 cycles per second. In this case, the 60% saturation limit would be at an ion signal of ∼16666 cps.

Peak saturation situations should be avoided when they occur at product ion peaks, as thus can result in wrong estimations of the analyte concentration. However, saturation is commonly observed for the reagent ion peaks, whose intensities can be calculated using the suitable isotopes in each case. The ^{18}O isotope peak is used to calculate the reagent ion intensities of H_3O^+ or O_2^+ as their more abundant ^{16}O peak is often saturated. The natural composition of oxygen is ^{16}O (99.76%), ^{17}O (0.03%) and ^{18}O (0.21%) [53]. The ^{18}O isotope is found at m/z 21.023 for H_3O^+ and at m/z 33.994 for O_2^+. However, for NO^+ it is better to use the $^{15}NO^+$ at m/z 30.995 rather than the $N^{18}O^+$ at m/z 32.002 for two reasons: the $^{15}NO^+$ isotope is more abundant and it does not interfere with the signal of the isobaric compound O_2^+ at m/z 32.

The ^{13}C isotope is often used to calculate product ion intensities in saturated peaks and to verify composition assignments if the mass resolution is not enough to distinguish between isobaric compounds. It is the second most abundant isotope (1.07%) compared to ^{12}C (98.93%), with ^{14}C being only present at 1 ppt [54]. ^{13}C is obviously more useful with bigger molecules because normally the bigger the molecule, the more carbons it will have, yielding a peak intensity of more than 10% at $m/z + 1$ of that at m/z for molecules with ten or more carbon atoms. Of special interest are as well the halogenated compounds containing Cl or Br, which show very characteristic isotopic peaks. ^{35}Cl and ^{37}Cl are naturally present at abundances of 75.76% and 24.24%, while for ^{79}Br and ^{81}Br these are 50.69% and 49.31%, respectively [55, 56]. Thus, molecules containing a single Cl atom show a pattern of peaks whose intensity is ca. 3:1 at m/z and $m/z + 2$, while for molecules with two Cl atoms this is 9:6:1 at m/z, $m/z + 2$ and $m/z + 4$. For molecules with a single Br this is approximately 1:1 at m/z and $m/z + 2$ while for two

Br atoms it is 1:2:1 at m/z, $m/z + 2$ and $m/z + 4$.

With these considerations in mind, for the rest of this thesis when an ion's m/z is given with a chemical composition, it will refer to the most abundant isotopologue. In this thesis, the data are either given in branching percentages (also referred to as branching ratios, BR, or product ion distributions, PID) or in raw counts per second, after being replicated two or three times, averaged and background–subtracted.

2.2.3 Fast switching software

Analysing data from fast switching experiments can be tedious if needed to be done manually file by file. For this purpose, it was useful to write a script in Matlab® including a graphical user interface to analyse the data in a quicker way. This interface is shown in Figure 2.13. It basically imports the suitable files, opens the cumulative mass spectrum to select the regions of interest, calculates and plots the ion intensities splitting the data in frames (*i.e.* each of the time intervals in which the drift tube is kept at the same E/N), and exports the data to an excel file in both counts per second and branching ratios together with the experiment time and the E/N. Note that different colours are used in the raw and averaged data to ease the visualisation.

The files that this script imports are the .lst ones and their accompanying .ini files, which contain the information on the fast switching experiment that is necessary to work with the data. This comprises, among other parameters, the number of phases, the number of cycles per phase, the total number of cycles, the cycle period, the number of frames and the dead time of the switching. The number of phases refers to the number of different values that the E/N takes during a single experiment. This value is two for the fast switching experiments, which we will refer to as E/N low and E/N high. The fast switching frequency is not explicitly recorded but it is given by the inverse of multiplying the cycle period by the number of cycles per phase. For instance, for a cycle period of 40 µs and 25000 cycles per phase, the switching frequency is 1 Hz. The total length of the experiment is not recorded either but, similarly to the switching frequency, it can be calculated by multiplying the cycle period by the total number of cycles. For example, a cycle period of 40 µs and 1.5×10^6 total cycles corresponds to a 1–minute experiment. In a measurement lasting 60 seconds at a fast switching frequency of 1 Hz there are 60 total frames and 30 frames per phase. The dead time recorded in the .ini file in this case refers to that given by the delay in the electronics to supply the right voltage to the drift tube (*i.e.* the rise and

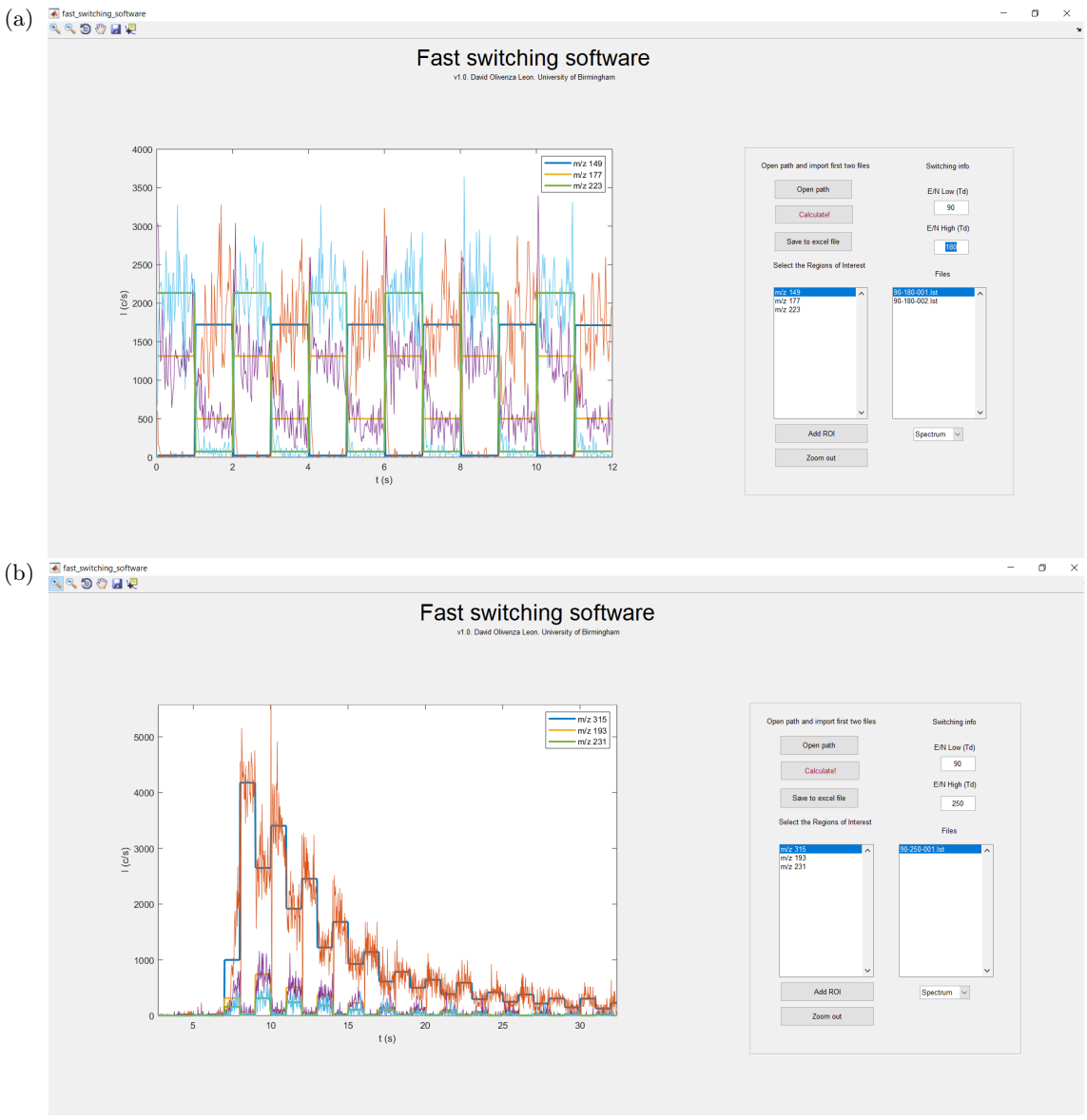

Figure 2.13: Screenshot of the graphical user interface for the script that analyses fast-switching data for: (a) a steady signal, and (b) a transient experiment.

fall times) and it is around 70 ms. The software automatically ignores the interval three times bigger than this dead time to account for the capacitance of the reactor, which was explained in section 2.1.2.4.

If the files are saved with the name format [*low E/N*]-[*high E/N*]-[*file number*], the script automatically reads and writes in the output file the values of the low and high *E/N*. If not, they must be manually added. The data inside each frame can be exported in raw format or averaged. For steady experiments like the one shown in Figure 2.13(a), the data from all the frames from a phase (*i.e.* high or low *E/N*) can also be averaged as is shown in this figure. Obviously, this does not make sense for transient measurements like that in Figure 2.13(b). Once the data analysis is finished, the results can be exported. The format in which these files are saved allows easy double-y axis plot of the ion intensities and *E/N* as a function of the experiment time, as it is shown in Figure 2.14, for a (a,c) steady-state and (b,d) transient measurement.

2.2.4 Density functional theory

Experimental data in this thesis are in some cases accompanied by theoretical values of the proton affinities, gas-phase basicities and energetics of the protonation and/or fragmentation reactions. These density functional theory (DFT) results were computed by Dr Peter Watts using Gaussian09W and GaussView05 for Windows and the B3LYP functional with the 6-31+G(d,p) basis set [57].

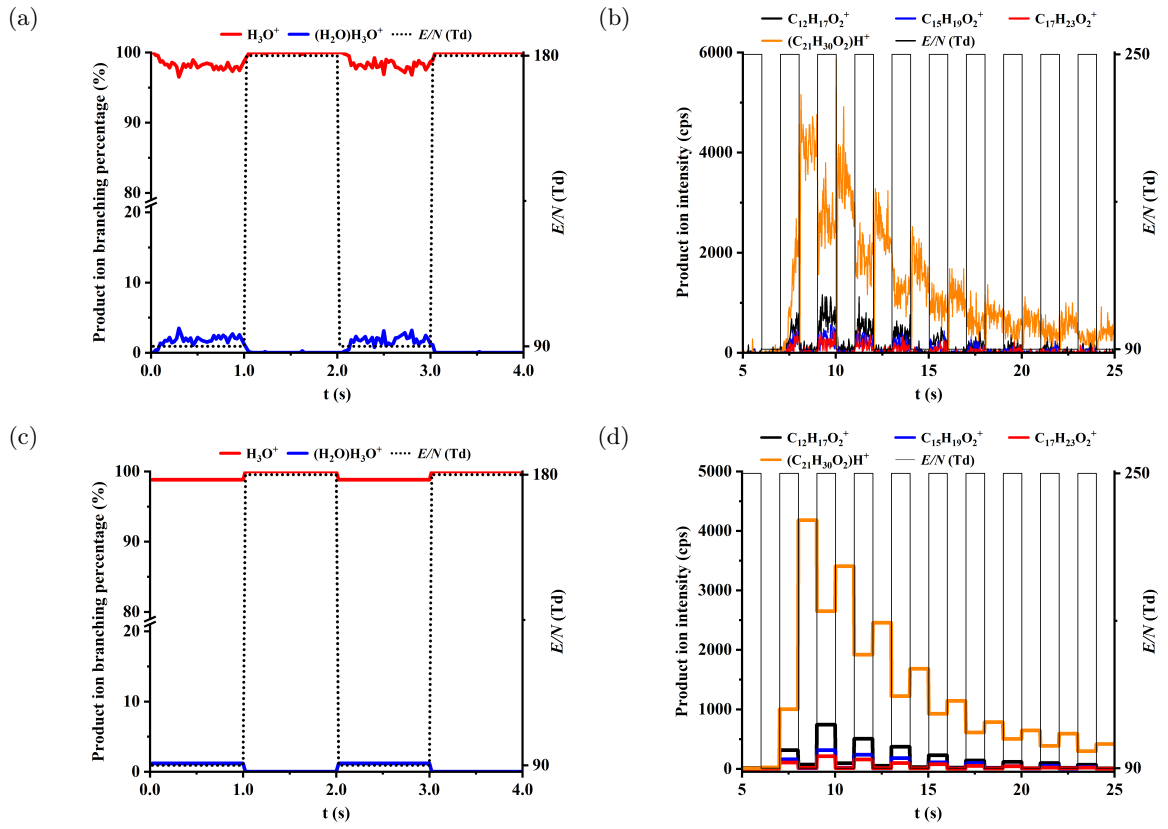

Figure 2.14: Example plots of data analysed with the fast-switching software. Left: (a) raw and (c) averaged plots of H_3O^+ and $(H_2O)H_3O^+$ for the fast switching between 90 and 180 Td. Right: (b) raw and (d) averaged plots of the signal obtained from the desorption of trace amounts of cannabidiol while fast switching the reduced electric field between 90 and 250 Td.

2.3 PTR-MS Add-ons

Besides the essential components described earlier in this chapter, there are some accessories that can be coupled to a PTR-MS instrument for different purposes. These include devices like the CHARON real-time aerosol inlet or the PREFICS pre–concentrator with chromatographic separation [10, 58, 59]. The ones included in this section are those used at some point in the experimental work in this thesis.

2.3.1 Thermal Desorption Unit

For many applications, PTR-MS has been demonstrated to be a sensitive analytical tool, yet the primary analytical device used for homeland security applications is IMS. Most substances of relevance in this sector, including drugs and explosives, as well as in other fields, have very

low vapour pressures at room temperature, which challenges the detection capabilities of the instruments without pre-concentration or thermal desorption.

This issue has been approached in many interesting ways. These include the patents for hand-held suction systems capable of identifying small quantities of explosives that were granted to Conrad and to Carroll *et al.* [60, 61]. Jjunju *et al.* also created a portable tool to detect nitroaromatic explosives on-site via atmospheric pressure chemical ionisation that can operate for 12 h in one charge [62]. Additionally, the development of a biomimetic electronic dog nose by Staymates *et al.* is an exciting new development [63].

Swab desorptions are commonly used in IMS, and the same approach has been used here for PTR-MS. A thermal desorption unit (TDU) such as the one designed, developed and engineered by KORE Technology Ltd is used to study low vapour pressure compounds when coupled to a PTR-MS device (Figure 2.15). This was applied by González-Méndez *et al.* to the detection of explosives and by Blenkhorn to the detection polyaromatic hydrocarbons [12, 64]. This TDU works with polytetrafluoroethylene (PTFE) swabs (ThermoFisher Scientific, Cheshire, UK) mounted in a cardboard frame (shown in Figure 2.15(a)) onto which the targeted compounds are deposited. Then, the swab is inserted in the TDU, whose plates come together clamping the swab and creating a high-quality circular seal. The metal plates are kept at high temperature (150 °C) and a carrier gas is flown through their holes, pulling the analyte towards the inlet pipe, whose surfaces are passivated (treated with SilcoNert® 2000) to minimise adsorption. This creates a desorption profile like the one in Figure 2.16, where the two main fragment ions from trace amounts of the desorption of heroin are shown. The duration of the desorption depends on many factors, some of which are the volatility of the analyte, the temperature of the inlet and TDU and the carrier gas flow. The ion signal goes down to 10% of the peak maximum in between 10 to 20 seconds, although it usually takes between 60 and 120 seconds for a sample to be completely desorbed into the instrument (*i.e.* to reach baseline) after the swab has been inserted in the TDU and its jaws have clamped together. After the measurement is finished, the TDU can be opened to extract the swab, which can be reused.

2.3.2 FastGC and Multicapillary Column (MCC)

The fastGC (IONICON Analytik GmbH, Austria) is an add-on that aids in the product ion identification process by separating the analyte molecule from possible contaminants and impurities.

(a)

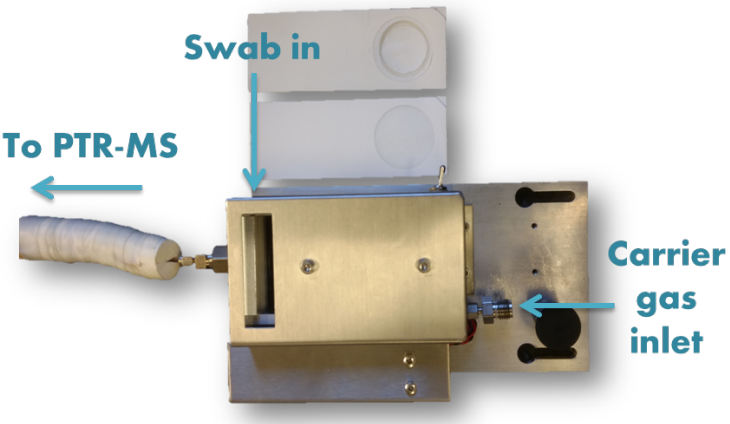

(b)

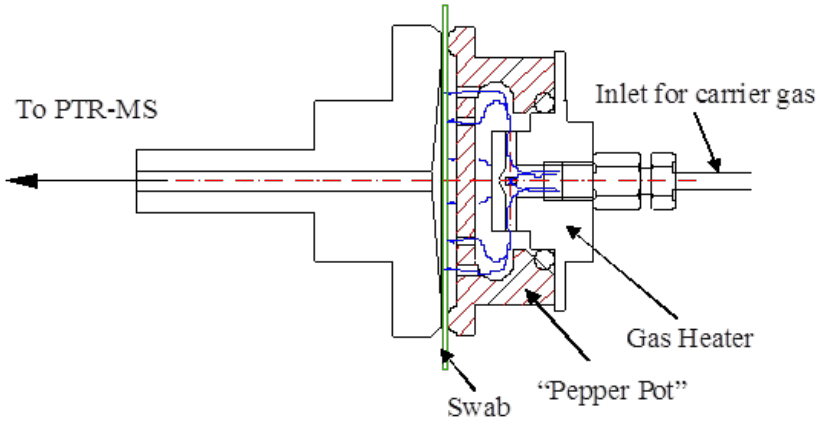

Figure 2.15: (a) Picture of the TDU near to (top) used and (bottom) new PTFE swabs. (b) Schematic diagram of the TDU [12].

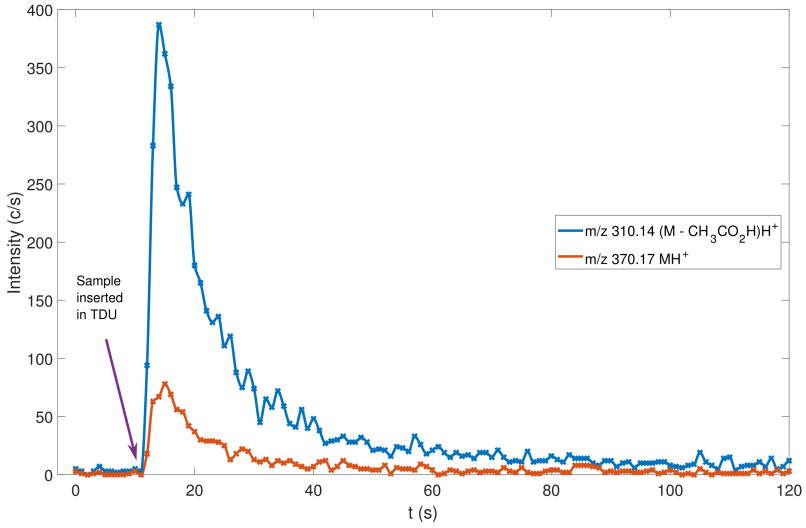

Figure 2.16: Time profiles of the count rates of two characteristic product ions at m/z 310 and m/z 370 during the thermal desorption of trace amounts of heroin at 120 Td using the TDU in PTR-MS.

The working principle of the fastGC is the same as that of gas chromatography (GC) systems, where the components of a gas mixture (mobile phase) present different retention times when flowing through a liquid or solid (stationary phase) packed inside a capillary column, which separates them temporally. This separated mixture can be then injected into an analytical instrument for compound identification, where ion peaks occurring at the same retention time as the parent ion correspond to product ions. The main differences between GC and fastGC are that GC columns are tens of meters long, while fastGC ones are 10 meters long or less, and also that the heating ramp in fastGC is up to forty times faster than in conventional GC systems. These characteristics make possible to perform a fastGC analysis in few minutes.

The fastGC was used in conjunction with a PTR-ToF 8000 (IONICON Analytik GmbH, Austria) to study the reactions of several ketones with H_3O^+ [3]. This add-on was used to facilitate the ion identification as the purity of the ketones was in the range 97 - 99% and also decomposition of the sample could have occurred during storage. This fastGC is a modification of that used by Ruzsanyi *et al.* and Romano *et al.* [65, 66]. Therefore, only the differences from those will be briefly described here. The stationary phase in our system was a MXT-1 column (10 m × 0.53 mm, film thickness 0.25 µm, dimethyl polysiloxane phase, Restek, USA), which was heated from room temperature up to 240 °C in 2 minutes and 40 seconds. Also, a

10-port passivated valve (VICI AG, Switzerland) and a three-way gas valve made from polyether ether ketone (PEEK) replaced the four three-way valves and needle valve in the previous design. All sections of the inlet system are mounted in the oven which houses the drift tube to avoid cold spots. This updated configuration allowed the sample loop to be constantly filled and the capillary column to be constantly back-flushing with the carrier gas. The carrier gas and make-up gas flows used were 8 ml min^{-1} and 20 ml min^{-1} of 6.0 N_2. Furthermore, the multicapillary column (MCC) used for the investigations described in chapter 7 has similar characteristics to those of the fastGC as it is, in fact, a previous version of the fastGC with some modifications. For instance, the MCC works at constant temperature, while the fastGC heats up following a ramp.

2.3.3 Liquid Calibration Unit

The liquid calibration unit (LCU, IONICON Analytik GmbH, Austria) is a standalone device that can be coupled to trace gas analysers for calibration purposes where liquid standards are evaporated into a gas stream to yield known trace concentrations.

The working principle of the LCU has been explained in detail by Fischer *et al.* [67]. The liquid sample is pumped from its container by a liquid flow controller into the nebuliser (X175, Burgener Research®), where it mixes with the carrier gas (N_2 or zero air). The nebulisation process creates a stream of micro-droplets that is then injected into the evaporation chamber. This chamber is held at 100 °C to continue the process of evaporation, leading in a continuous flow of a known trace gas dilution that is then injected through a heated sampling line into the analytical instrument.

The LCU was used in the study of the reactions of several ketones with H_3O^+ in humid conditions [3]. This add-on was not used to calibrate the instrument but to create a steady signal of ketones samples in known concentrations under humid conditions. The sampling vials, kept at 30 °C, contained trace quantities of ketones diluted in 100 ml of purified water and were connected to the liquid inlet of the LCU. The liquid sample flow was of 35 µl/min, which with the carrier gas (N_2) flow of 950 ml/min gave an absolute humidity of 5%*.

*The ketones-containing *liquid* sample (which is >99% water) flow of 35 µl/min corresponds to a H_2O *gas* flow of 47.44 ml/min, assuming that all the liquid water is converted into gas. This gas flow is calculated by dividing the liquid flow by the liquid molar volume $V_{l,mol}$ ($= M/\rho$ = 18.02 g/mol /0.998 g/ml = 18.05 ml/mol, with M the molar mass and ρ the density of water) and multiplying it by the gas molar volume $V_{g,mol}$ (which is approximated to the value at standard conditions, *i.e.* $V_{g,mol} \sim$ 24414 ml/mol). Then the absolute humidity is

given by the ratios:

$$AH = \frac{\dot{V}_{H_2O}}{\dot{V}_{H_2O} + \dot{V}_{N_2}}$$

with $\dot{V}_{H_2O} = 47.44$ ml/min, $\dot{V}_{N_2} = 950$ ml/min and $AH = 4.76\%$.

Part II

EXPERIMENTAL RESULTS

Chapter 3

Theoretical and experimental investigations of cocaine and related compounds in PTR-MS

In this chapter a PTR-MS study of cocaine and associated compounds (*e.g.* cocaethylene, methyl ecgonine, ethyl ecgonine and benzoate esters) is presented, together with the proton affinities, gas phase basicities and energetics corresponding to the structures and transition states arising from reaction of these compounds with $(H_2O)_nH_3O^+$ (n = 0, 1, ...), which were computed using density functional theory by Dr Peter Watts.

3.1 Introduction

Cocaine is one of the most consumed illicit drugs worldwide. For instance, Mastroianni *et al.* found that only the use of cannabis is higher than that of cocaine in the surroundings of Barcelona (Spain) [68]. According to the *World Drug Report 2019* from the *United Nations Office on Drugs and Crime*, the global produced and seized quantities of cocaine have increased three-fold in the period 1998 - 2018, with a nearly two-fold raise in the seized amount in the period 2014 - 2017 from 652 to 1275 metric tonnes (Figure 3.1) [69]. The consumption of illicit drugs involves drug trafficking from the manufacturing countries in South America to the consumers (*e.g.* North America and Europe). Because of this, law enforcement agencies need to detect cocaine and similar compounds rapidly and with a high level of confidence in locations where outstanding

amounts of goods are exchanged, such as at airports and seaports. One real–time analytical technique that can provide this is PTR-MS. To be able to use this instrument in the field, we first need to determine and understand the protonation and fragmentation processes that cocaine and related compounds undergo as a function of the key operational parameter, namely the reduced electric field.

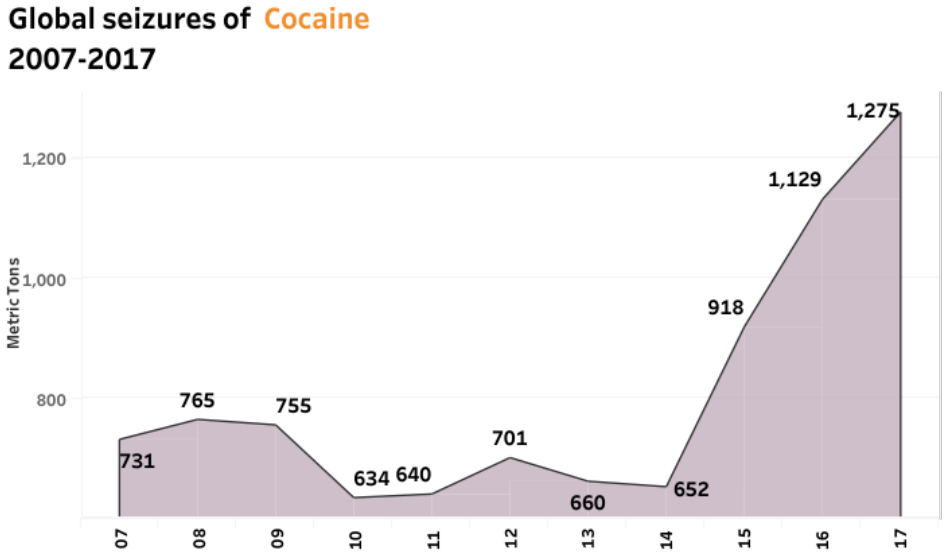

Figure 3.1: Metric tons of worldwide seized cocaine per year in the 2007 - 2017 period [69].

PTR-MS has already been proved to be a useful tool for the detection of drugs: e. g. Jürschik *et al.* successfully used PTR-MS to detect rape drugs mixed with drinks and Lanza *et al.* proved that ion/molecule processes can be manipulated to differentiate between mephedrone isomers without initial pre-separation [15, 70]. Nevertheless, the PTR-MS studies of cocaine in the literature are limited. For example, Agarwal *et al.* only reported the product ions obtained from the analysis of several drugs at a reduced electric field of 120 Td, which is useful information at the standard conditions a PTR-MS is often used at, but at the same time these data lack the spread in collisional energy that the PTR-MS instruments can be operated to improve selectivity [16].

Only around 1% of the consumed cocaine is retrieved through excretion in the few hours after intake. The rest of it is converted into metabolites, which can be detected in urine up to 24 - 36 hours after consuming the drug or in hair samples potentially up to several weeks later [71]. The main metabolites arising from cocaine consumption are: benzoylecgonine, ecgonine methyl ester, ecgonine ethyl ester, cocaethylene, norcocaine, methylecgonidine and hydroxycocaines. Hence

we have included these to the study (see Table 3.1).

Benzoylecgonine and ecgonine methyl ester (also known as methyl ecgonine) are the main metabolites of cocaine, which are formed when cocaine undergoes deesterification through hydrolysis in the liver [72]. As for most cocaine metabolites, benzoylecgonine and methyl ecgonine are inactive and hence do not induce any toxicity effects when present in the human body. These two are the metabolites that are normally screened in urine tests, for whose analysis GC-MS is commonly used. This technique requires a derivatisation process of the samples prior the chemical analysis, which can be done using different compounds but it is time-consuming. For instance, Ambre *et al.* performed methylation of benzoylecgonine to transform it back to cocaine while Fleming *et al.* detected benzoylecgonine and methylecgonidine as pentafluoropropionyl derivatives [73, 74]. On the contrary, techniques that do not require derivatisation are, for example, that developed by Hezinová *et al.* and HPLC [75, 76].

Cocaine users are often heavy drinkers of alcohol. When both cocaine and ethanol are present in the bloodstream, the active metabolite cocaethylene is produced in the body, which in itself is a recreational drug with similar (*i.e.* euphoria and increased heart rate) but stronger effects than those of cocaine [77, 78]. Cocaethylene is formed in the liver through the transesterification of around 15 - 20% of the consumed cocaine, which occurs 3.5 times faster than deesterification to benzoylecgonine [79–81]. The toxicity effects of cocaethylene are not only stronger and longer-lasting than those of cocaine: the amount of cocaine found in dead bodies when alcohol was also found was lower than in cases where only cocaine was present, indicating that cocaethylene is also a deadlier substance [82]. Furthermore, ecgonine ethyl ester (also known as ethyl ecgonine) is produced from cocaethylene through deesterification in a similar way ecgonine methyl ester is produced from cocaine.

Another active metabolite of cocaine is norcocaine. This metabolite is found in low amounts compared to benzoylecgonine and ecgonine methyl ester, but its presence in blood increases when alcohol is consumed at the same time [83]. It is formed through the demethylation of the pyrolidine nitrogen in cocaine and, like cocaethylene, norcocaine has been also found in hair samples from cocaine users [71].

Hydroxycocaines form a group of lesser-known cocaine metabolites because of their low abundance relative to that of other metabolites. This family consists of different isomeric compounds whose structural difference only resides on the carbon atom of the benzene ring the

hydroxy group is attached to, yielding three structures: o-, m- and p-hydroxycocaine. These metabolites have been detected using different analytical techniques in human hair, blood and urine [71, 84–87].

Besides the above mentioned metabolites, cocaine also decays to other compounds. One of the degradation products of cocaine is methyl benzoate, whose production is enhanced at higher humidities. Furton *et al.* linked the reaction of canine units to solid-phase microextraction gas chromatography stating that dogs react more to methyl benzoate than to cocaine itself, while Waggoner *et al.* also proved that the canine units react to both methyl benzoate and cocaine samples, but with inconclusive results of whether it is methyl benzoate the compound dogs are reacting to [88, 89].

A brief introduction of the main metabolites of cocaine was presented above to provide context for this chapter. However, PTR-MS will never be used as an analytical tool for the screening of these substances because other techniques (*e.g.* GC-MS or HPLC) are the standard tools already established in each field. Therefore the reason some cocaine metabolites were included in this study was to shed some light on the PTR-MS and DFT results from other compounds and, at the same time, potentially be the basis for future research involving other analytical techniques.

3.2 Methodology

3.2.1 Experimental details

The KORE Technology Ltd (Ely, UK) PTR-ToF-MS instrument described in chapter 2 was used for this study. The reactor was kept at a pressure of 1 mbar and at 150 °C throughout all the experiments, while the pressure in the hollow cathode was set at 1.1 mbar for normal measurements and 1.4 mbar for humid ones. More details of this are given in subsection 3.3.1.

3.2.2 Chemicals

All the substances used in this study were acquired from Sigma Aldrich (Gillingham, United Kingdom). Some of the samples were sourced as solids diluted in organic solvents: cocaine (1 mg/mL in acetonitrile, certified reference material), methyl ecgonine (1 mg/mL in acetonitrile, certified reference material), cocaethylene (1 mg/mL in acetonitrile, certified reference material), ethyl ecgonine (1 mg/mL in acetonitrile, certified reference material), norcocaine hydrochlor-

ide (1 mg/mL in acetonitrile (as free base), certified reference material), o-hydroxycocaine (1 mg/mL in acetonitrile, certified reference material) and methyl ecgonidine (1 mg/mL in acetonitrile, certified reference material). These were further diluted using HPLC grade solvents to give a concentration of 100 µg/mL. Although cocaine is a schedule 2 drug, no license is required for research purposes given that minimal quantities (*i.e.* mg level or less) are used. The benzoates (*i.e.* methyl, ethyl and isopropyl benzoate) and the isobutyrates (*i.e.* methyl and ethyl isobutyrate) esters are colourless liquids. Benzoic acid is a white crystalline powder. These liquid substances and benzoic acid were acquired with a purity of at least 99% and were used without further purification.

3.2.3 Sampling methods

Cocaine is a white solid with a vapour pressure of 2.5×10^{-7} mbar at 25 °C, which makes it challenging to detect it without any pre-separation system [90]. González-Méndez *et al.* successfully implemented a thermal desorption unit developed by KORE Technology Ltd to tackle this low vapour pressure issue for explosives, and Blenkhorn applied it to the detection of polyaromatic hydrocarbons [12, 64]. The same thermal desorption unit was used for this study to desorb compounds into the PTR-MS instrument. Typically, a volume of 1 - 5 µL of a solvent containing a trace sample was spotted onto the PTFE swab, which was inserted into the TDU after waiting approximately 1 minute for the solvent to evaporate. The carrier gas, was oxygen-free nitrogen (99.998% purity, BOC Gases, Manchester, UK), which drags the analyte through the heated inlet pipe and into the drift tube, creating a desorption "pulse" of 10 - 20 seconds depending on the analyte (see Figure 2.16).

Liquid samples and benzoic acid are more volatile and were studied by means of headspace analysis. Oxygen-free nitrogen was used as carrier gas to drag the headspace of 22 mL vials containing trace amounts (<1 mL) of the samples, which were also connected to the inlet line of the instrument.

3.3 DFT and PTR-MS results

The PTR-MS results and associated DFT calculations are presented in this section. The PTR-MS results are provided over a broad E/N range: approximately 20 - 255 Td, which corresponds

to a drift voltage from 35 up to 410 V (*i.e.* the whole voltage range that the instrument can supply). Reagent ion counts are found to be low at low *E/N*, this is simply a result of the low abundance of reagent ions present in the drift tube (see Figure 3.2). At the same time, the residence time, which is proportional to $1/(E/N)$, is much higher at low *E/N* and the ions spend longer in the drift tube than at high *E/N*, which results in more collisions with the buffer gas and a higher chance of proton transfer from the reagent ions to analyte molecules.

Key details on the compounds investigated in this study are summarised in Table 3.1 and Table 3.2, including their nominal molecular weight, vapour pressure, chemical formula and structure. The vapour pressure values in these tables have been taken from the United States Environmental Protection Agency Chemistry Dashboard [91]. These are experimental values except for that of methyl ecgonine, ethyl ecgonine, cocaethylene and methyl ecgonidine, in which case the predicted values are presented. In the further tables included in this chapter, which provide the energetics relative to the protonation reaction or further fragmentation, the given *m/z* refers to the detected ion, *i.e.* where the charge remains, and the neutrals H_2O or $(H_2O)_2$ have been omitted in all the cases.

3.3.1 Reagent ions

For many of the compounds discussed in this chapter, "normal" and "humid" *E/N* studies were done. The reagent ion signal for hydronium and the corresponding protonated water clusters are shown in Figure 3.2. The calculated *PA* and *GB* of $(H_2O)_n$ (n = 1, 2, 3, and 4) are given in Table 3.3. From now on, the energetics given refer to the calculated ones using DFT, unless otherwise stated. The abundance of protonated water and the different protonated water cluster species (*i.e.* $(H_2O)_nH_3O^+$, n = 1, 2 and 3) as a function of the reduced electric field that is observed in these figures are in agreement with those reported by Price *et al.* as a function of the reactor pressure, temperature and the *E/P* ratio [46].

A higher humidity in the drift tube can be achieved by increasing the humidity of the buffer gas (see Malásková *et al.* [3]). However, the measurements at higher humidity were unintended in this study, as the standard parameters setting (*i.e.* drift tube at 1 mbar and hollow cathode at 1.3 - 1.4 mbar) resulted in significant protonated water cluster intensities. It was only by operating the drift tube at 150 Td that H_3O^+ became more abundant than $(H_2O)H_3O^+$ (Figure 3.2(b)). This was only discovered after doing a whole set of experiments under these humid conditions.

Table 3.1: Nominal molecular weight, vapour pressure at 25 °C, formula and structure of cocaine, methyl ecgonine, cocaethylene, ethyl ecgonine, norcocaine, methyl ecgonidine and o-hydroxycocaine. The numbers are used to indicate the main protonation sites in the molecules.

Compound	**MW (g mol^{-1})**	**VP (mbar)**	**Formula**	**Structure**
Cocaine	303	2.5×10^{-7}	$C_{17}H_{21}NO_4$	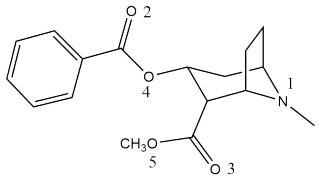
Methyl ecgonine	199	4.9×10^{-5}	$C_{10}H_{17}NO_3$	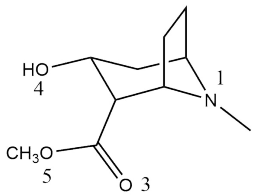
Cocaethylene	317	1.0×10^{-6}	$C_{18}H_{23}NO_4$	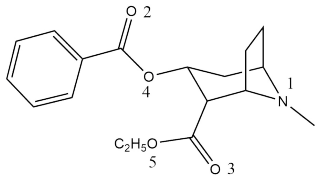
Ethyl ecgonine	213	7.8×10^{-6}	$C_{11}H_{19}NO_3$	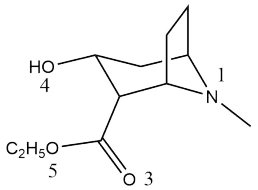
Norcocaine	289	-	$C_{16}H_{19}NO_4$	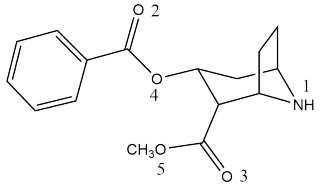
Methyl ecgonidine	181	1.3×10^{-2}	$C_{10}H_{15}NO_2$	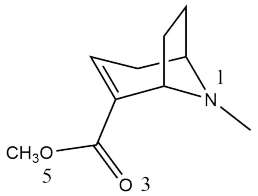
o-Hydroxycocaine	319	-	$C_{17}H_{21}NO_5$	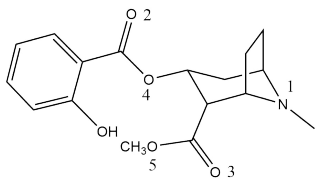

Table 3.2: Nominal molecular weight, vapour pressure at 25 °C, formula and structure of benzoic acid, methyl benzoate, ethyl benzoate, isopropyl benzoate, methyl isobutyrate and ethyl isobutyrate. The numbers are used to indicate the main protonation sites in the molecules.

Compound	**MW (g mol^{-1})**	**VP (mbar)**	**Formula**	**Structure**
Benzoic acid	122	9.3×10^{-4}	$C_7H_6O_2$	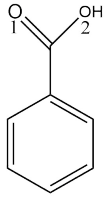
Methyl benzoate	136	0.51	$C_8H_8O_2$	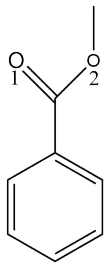
Ethyl benzoate	150	0.36	$C_9H_{10}O_2$	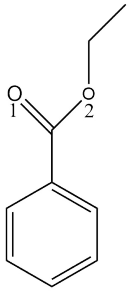
Isopropyl benzoate	164	4.6×10^{-4}	$C_{10}H_{12}O_2$	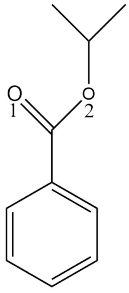
Methyl isobutyrate	102	65.7	$C_5H_{10}O_2$	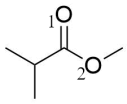
Ethyl isobutyrate	116	33.9	$C_6H_{12}O_2$	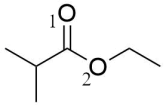

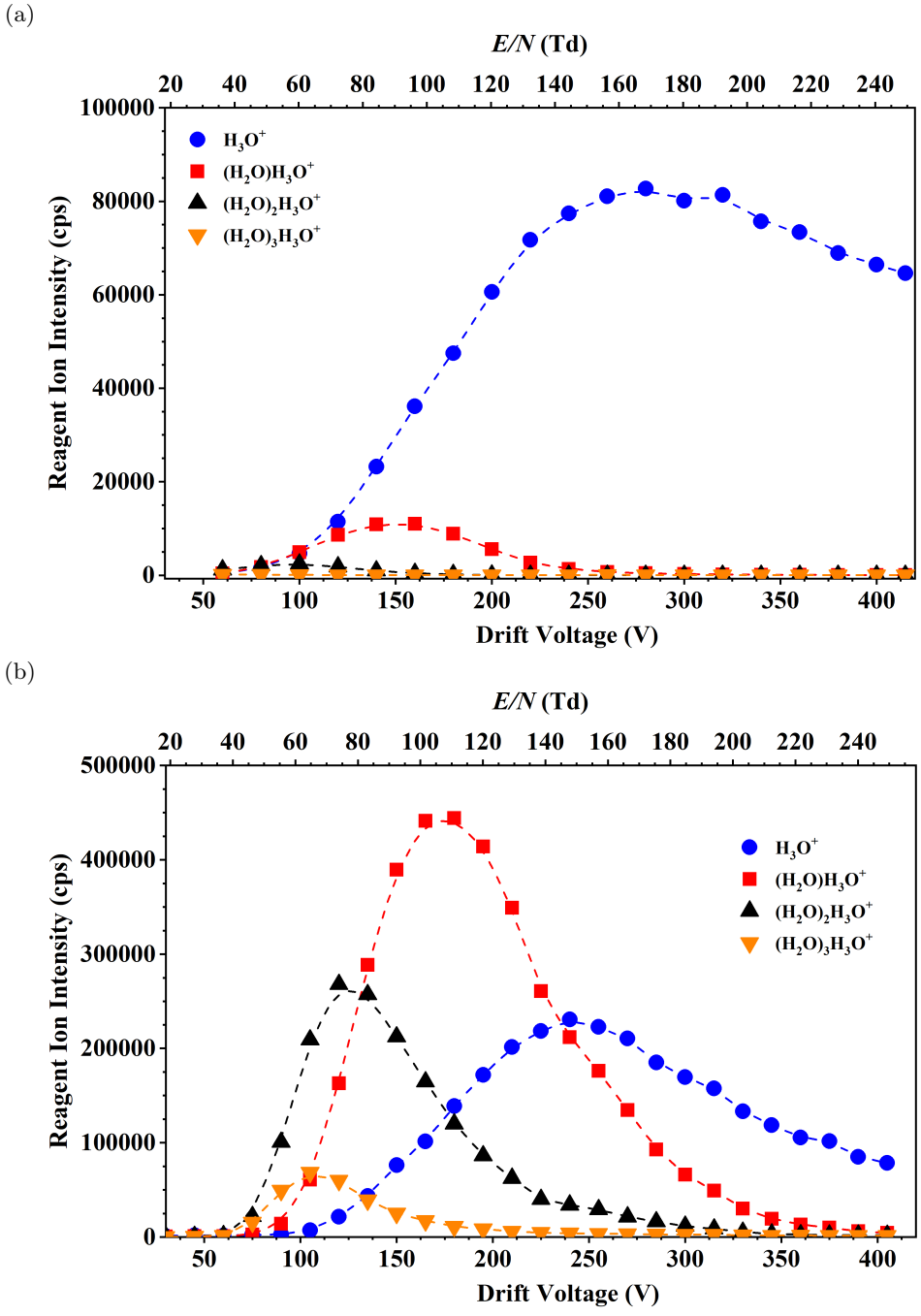

Figure 3.2: Reagent ion intensities in counts per second as a function of the drift voltage and the reduced electric field in (a) normal and (b) humid drift tube conditions.

Table 3.3: DFT calculations of the proton affinity and gas phase basicity of water and its clusters.

Molecule	***PA*** **(kJ mol^{-1})**	***GB*** **(kJ mol^{-1})**
H_2O	684	653
$(H_2O)_2$	842	777
$(H_2O)_3$	937	841
$(H_2O)_4$	1013	886

Nevertheless, with the proton transfer from $(H_2O)H_3O^+$ being softer than that from H_3O^+, it was also interesting to acquire data in the driest conditions that the instrument could achieve to compare with the humid data set. The main consequence of a high abundance of water cluster ions at low E/N is that it gets more complicated to ascertain whether the formation of a product ion at high E/N is due to the higher collisional energy supplied by the electric field or is a consequence of the remaining energy after a harder proton transfer as the proton donating species is different from that at low E/N.

The hollow cathode pressure can be reduced to minimise the clustering of reagent ions. However, there are two limitations when reducing the hollow cathode pressure: (i) lower pressure difference between cathode and drift tube increases the back-streaming of buffer gas into the hollow cathode, generating undesirable reagent ions, and also (ii) at lower cathode pressures the power supply unit struggles to maintain the glow (*i.e.* the glow discharge indicator is flickering). A compromise was found at a hollow cathode pressure of 1.1 mbar and this drier configuration, whose reagent ion signal is shown in Figure 3.2(a), is referred to as "normal" conditions in this chapter.

The total reagent ion signal for "normal" and "humid" operating conditions (see Figure 3.2) present a maximum at different values of the reduced electric field (*i.e.* around 170 Td for "normal" and 120 Td for "humid"). The product ion plots presented in this chapter are also given in raw counts per second to avoid the possible misleading effects created by normalising to the reagent ion signal and are used to calculate the product ion distributions. However, the raw cps do not give a true measure on the abundance of ion channels either, as the transmission of the ions along the different stages of the instrument depends on both the E/N and the m/z–value.

3.3.2 Cocaine

The structure of cocaine is given in Table 3.1 and in 3D in Figure 3.3. The main protonation sites are the pyrolidine nitrogen N1*, the benzoyl oxygen O2, the carbonyl oxygen O3, and the ester oxygen atoms O4 and O5. DFT calculations show that the most basic site is N1 and the most stable structure of the protonated cocaine molecule is with the proton on N1 hydrogen bonded to O3. This structure is designated cocaine1H$^+$. Likewise, when the proton is on O2 or O3 the structure is named cocaine2H$^+$ or cocaine3H$^+$. Direct protonation of the ester sites O4 and O5 is also possible. The proton was found to be able to move between the studied basic sites and hence it will reside in the most basic site (N1). In other words, MH$^+$ will predominantly be cocaine1H$^+$. The migration of the proton from N1 to other sites will result in fragmentation. The *PA* and *GB* for the two most stable protonation sites of cocaine, N1 and O2, are given in Table 3.4 and these indicate that cocaine can be protonated from $(H_2O)_nH_3O^+$ up to $n = 3$. Proton transfer from $(H_2O)_3H_3O^+$ would be thermoneutral as PA($(H_2O)_4$) = 1013 kJ mol^{-1}.

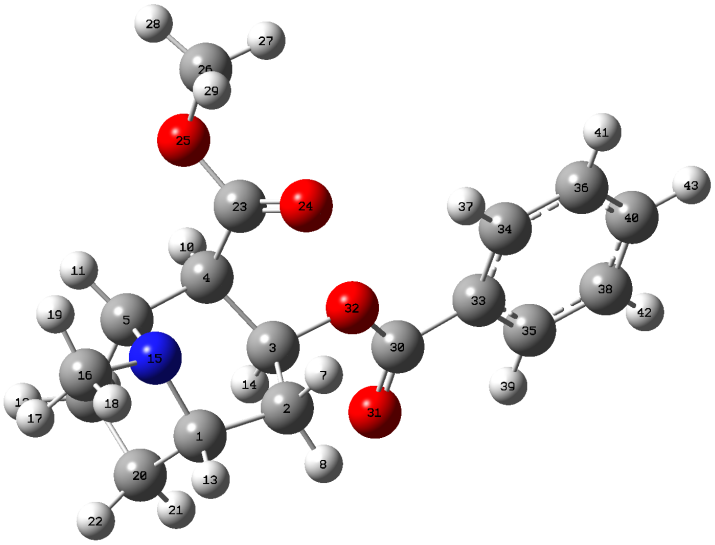

Figure 3.3: Ball-and-stick representation of the molecule of cocaine. The colour code of the atoms is blue: N, red: O, grey: C and white: H). Note that the main text refers to the numbers of the figure in Table 3.1 and numbers in this figure can be ignored.

The product ion intensities in cps for the reaction of $(H_2O)_nH_3O^+$ ($n = 0, 1, 2, 3$) with cocaine are plotted in Figure 3.4. These agree with the product ions reported in the literature [16, 92].

*Note that the atom numbers in this chapter refer to the numbers provided in the structures shown in Table 3.1 and 3.2.

Table 3.4: Proton affinity and gas phase basicity of the two most stable protonation sites of cocaine (*i.e.* Cocaine1 and Cocaine2) to yield the structures cocaine1H^+ and cocaine2H^+.

Final Structure	***PA*** **(kJ mol^{-1})**	***GB*** **(kJ mol^{-1})**
Cocaine1H^+	1013	980
Cocaine2H^+	933	895

The dominant product ion in both the normal and humid measurements is the protonated parent molecule MH^+ (*i.e.* $(C_{17}H_{21}NO_4)H^+$). There are other product ions resulting from dissociative proton transfer that are observed with less abundance. The ion at *m/z* 182 (*i.e.* $C_{10}H_{16}NO_2^+$) is a carbocation resulting from the loss of benzoic acid from MH^+, while the one at *m/z* 272 (*i.e.* $C_{16}H_{18}NO_3^+$) is an acyl following the loss of methanol (MeOH) from MH^+. At high *E/N*, $C_5H_8N^+$ is found at *m/z* 82. In humid conditions two other ions are also observed: benzoyl$^+$ at *m/z* 105 and protonated benzoic acid at *m/z* 123.

The energetics associated to the formation of the observed product ions are given in Table 3.5. These are only compared to H_3O^+ and $(H_2O)H_3O^+$ because these are the most relevant reagent ions: they are the most abundant in the 100 - 200 Td range and also proton transfer to the analyte from $(H_2O)_2H_3O^+$ or $(H_2O)_3H_3O^+$ would be energetically similar to that from $(H_2O)H_3O^+$ but slightly softer. Given that all the fragmentation pathways are thermodynamically allowed, it is surprising that MH^+ is the dominant product ion for all the *E/N* range. One could think that in the humid results most of the MH^+ ion comes from the reaction with the water clusters (*i.e.* $(H_2O)H_3O^+$ and $(H_2O)_2H_3O^+$), but as similar proportions of product ions are observed in the normal case, this cannot be the reason. It is more likely that the proton stays in the most basic site (*i.e.* N1) and it transfers to other sites, which is thermodynamically allowed and needed for fragmentation to occur, but it does not occur rapidly.

The formation of the ion at *m/z* 272 is the result of the loss of MeOH in the methyl ester moiety of the protonated cocaine molecule. This happens through a barrierless dissociation when the proton is on O5. The migration from the protonation site to O5 occurs through a transition state. Two transition states were found, named TS2 and TS2A. TS2 refers to the transfer of the proton from the more basic carbonyl oxygen O3 to the less basic ester oxygen O5 followed by the split up of the C–O5 bond. TS2A is similar to TS2 with the proton migrating from the benzoyl oxygen O2 instead. TS2 is marginally exergonic (*i.e.* -9 kJ mol^{-1} for the reaction with

(a)

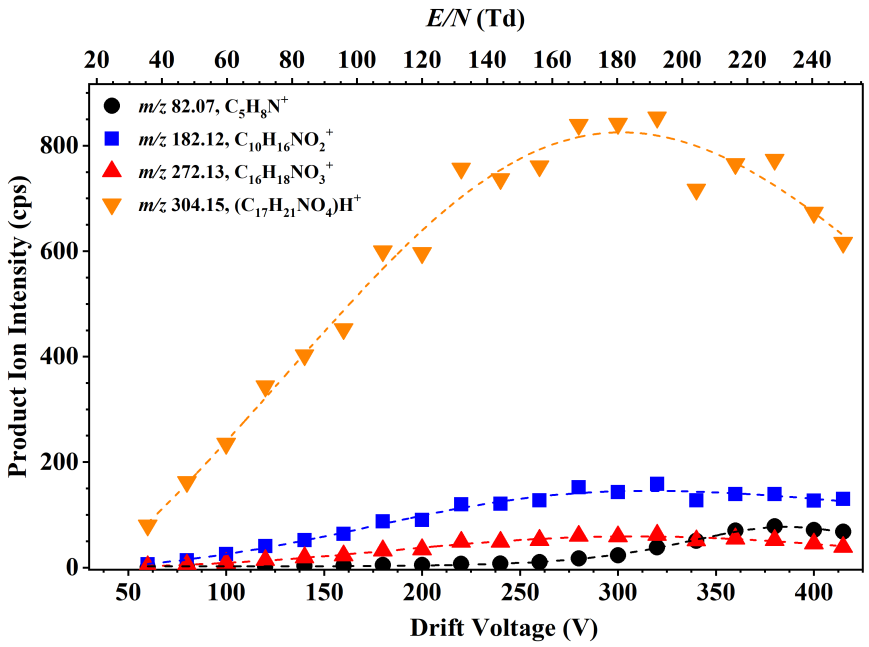

(b)

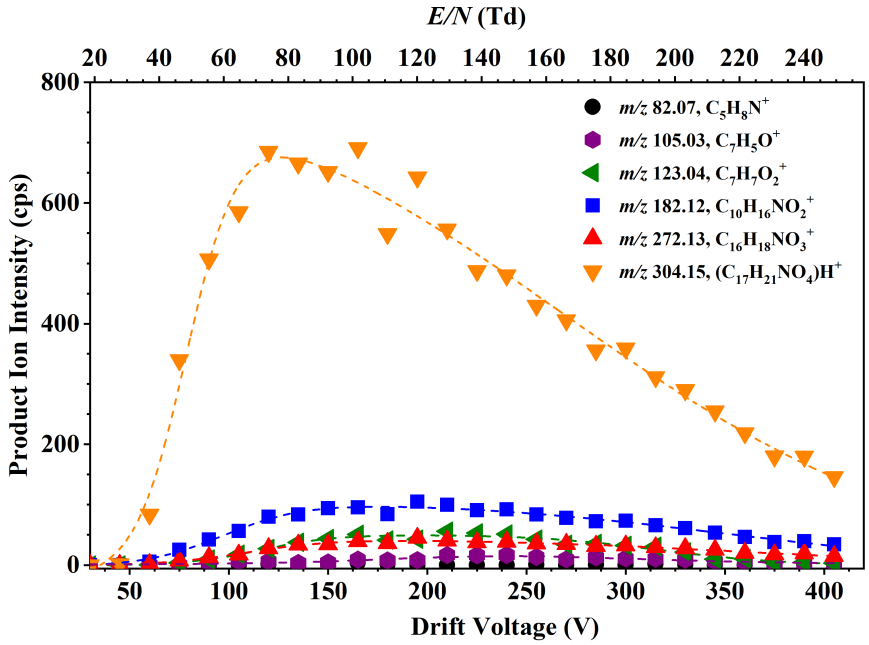

Figure 3.4: Product ion signal intensities in counts per second of the product ions resulting from reactions of $H_3O^+.(H_2O)_n$ (n = 0, 1, 2, 3) with cocaine as a function of the drift voltage and the reduced electric field in (a) normal and (b) humid conditions.

H_3O^+) while TS2A has much lower energy requirements (*i.e.* -111 kJ mol^{-1} for the reaction with H_3O^+). Furthermore, the abundance of the ion at *m/z* 272 is comparable to other fragment ions, which hints that the formation of this ion is carried out through the transition state TS2A.

Table 3.5: Energetics of the reaction of cocaine with $(H_2O)_nH_3O^+$ (n = 0, 1) yielding the respective structure or transition state. ΔH_{298} and ΔG_{298} are relative to cocaine and H_3O^+ and, in brackets, to cocaine and $(H_2O)H_3O^+$.

Structure	***m/z***	ΔH_{298} **(kJ mol^{-1})**	ΔG_{298} **(kJ mol^{-1})**
Cocaine1H$^+$	304	-328 (-170)	-326 (-202)
(CocaineH$^+$ - MeOH) + MeOH	272	-138 (+20)	-186 (-62)
(CocaineH - benzoic acid)$^+$ + benzoic acid	182	-272 (-114)	-336 (-212)
(CocaineH - benzoyl) + benzoyl$^+$	105	-54 (+104)	-104 (+20)
(Cocaine - benzoic acid) + benzoic acidH$^+$	123	-88 (+70)	-144 (-20)
Transition state	***m/z***	ΔH_{298} **(kJ mol^{-1})**	ΔG_{298} **(kJ mol^{-1})**
MeOH loss: TS2 for H migration O3 to O5	272	-8 (+150)	-9 (+115)
MeOH loss: TS2A for H migration O2 to O5	272	-119 (+39)	-111 (+13)

Possible structures for the $C_5H_8N^+$ product ion at *m/z* 82 are provided in Figure 3.5. The nitrogen atom N1 is the most basic site of the cocaine molecule, and hence the first structure was thought to be the correct one. However, experiments from Wang and Bartlett using deuterated precursor ions in a triple quadruple system also yield the product ion at *m/z* 82, which proves that the deuterium (or proton in our case) is not part of this ion and therefore the right structure must be the second or the third of those in Figure 3.5, with the third structure being 16 kJ mol^{-1} more stable than the second one Wang and Bartlett. Furthermore, these authors reported this ion in higher abundance than it was found in PTR-MS, and they also found the ion at *m/z* 182 to be the dominant ion, rather than MH$^+$ as it is observed in PTR-MS. These differences can be explained in terms of the collisional energy. The range of energies used by Wang *et al.* was in the range 17 - 23 eV, while in PTR-MS the collisional energies are calculated to be ca. 1 eV (= 96.48 kJ mol^{-1}) and below. $C_5H_8N^+$ is also found in methyl ecgonine, cocaethylene and ethyl ecgonine but its formation will not be considered for now because it is only found at a low abundance at high reduced electric fields and it is a product of field-activated collision-induced

dissociation.

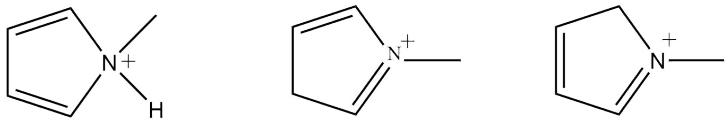

Figure 3.5: Possible structures of the fragment ion at m/z 82 from the reaction of cocaine with $(H_2O)_nH_3O^+$.

The formation of $C_{10}H_{16}NO_2^+$ at m/z 182 requires the elimination of benzoic acid from the protonated parent molecule. This needs the proton to be on O2 or O4 during the transition state, after which the benzoic acid is removed (*i.e.* the C–O4 bond breaks), yielding protonated methyl ecgonidine (see Figure 3.6). However, the fact that the transition state was not found and that two other ions coming from the benzoate moiety (*i.e.* m/z 105 and m/z 123) were seen only in the humid conditions drove this research to the examination of a cocaine homologue, methyl ecgonine, and a series of benzoate esters.

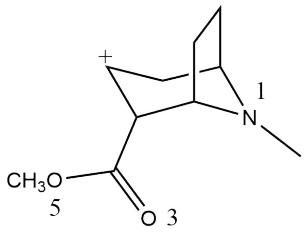

Figure 3.6: Structure of the fragment ion at m/z 182 from the reaction of cocaine with $(H_2O)_nH_3O^+$.

3.3.3 Methyl ecgonine

The protonation sites for methyl ecgonine (MeEcg) are numbered in the same way as those for cocaine (see structure in Table 3.1). The *PA* and *GB* of the protonation sites that give the two most stable structures of protonated methyl ecgonine are given in Table 3.6. MeEcg can undergo proton transfer from $(H_2O)_nH_3O^+$ for $n = 0$, 1, 2, as $PA((H_2O)_3) = 937$ kJ mol^{-1}. The structure MeEcg1H$^+$ is with the proton on the pyrolidine nitrogen (N1) hydrogen bonded to O3. MeEcg3H$^+$ is with the proton hydrogen between and hydrogen bonded to O3 and O4. Similarly to cocaine, the proton can move between the protonation sites although it will reside mainly on N1.

Table 3.6: Proton affinity and gas phase basicity of the two most stable protonation sites of methyl ecgonine (*i.e.* MeEcg1 and MeEcg3) that yield the structures MeEcg1H$^+$ and MeEcg3H$^+$.

Final Structure	***PA*** **(kJ mol^{-1})**	***GB*** **(kJ mol^{-1})**
MeEcg1H$^+$	996	965
MeEcg3H$^+$	906	873

Figure 3.7 shows the product ion intensities for the reaction of $(H_2O)_nH_3O^+$ (n = 0, 1, 2) with methyl ecgonine as a function of the drift voltage and reduced electric field. The difference in ion intensities between the normal and humid case can be explained in terms of the reagent ion intensities for each case (see Figure 3.2). The observed product ions follow similar fragmentation pathways as those found for cocaine. The dominant ion in both the normal and humid case is MH$^+$. Other product ions found are $C_9H_{14}NO_2^+$ at m/z 168 or $C_{10}H_{16}NO_2^+$ at m/z 182, resulting from the loss of MeOH or H_2O from the protonated parent molecule in each case. Traces of $C_5H_8N^+$ at m/z 82 are also found at high E/N (>140 Td) but, as mentioned in the cocaine section, this will not be further investigated.

Table 3.7 gives the energetics of the main structures and transition states compared to those of MeEcg and H_3O^+ or $(H_2O)H_3O^+$. All the structures are exergonic with H_3O^+, with the energetics for the transition state for the loss of MeOH being similar to the transition state TS2 for cocaine. This transition state consists of the barrierless loss of MeOH after the proton has migrated from O3 to O5 to yield $C_9H_{14}NO_2^+$ at m/z 168. However, direct protonation of O5 can also take place. The formation of $C_{10}H_{16}NO_2^+$ at m/z 182 needs the proton to be on O4. Then the barrierless loss of H_2O takes place, with further rearrangements and bond breaking to yield the structure in Figure 3.8.

3.3.4 Benzoate esters and benzoic acid

Benzoate esters are chemical substances with a benzene ring bonded to the carbon atom of a carboxylate ester. The benzoate moiety in cocaine has the structure of isopropyl benzoate.

Protonated methyl ecgonidine at m/z 182 is a carbocation resulting from the loss of benzoic acid from the protonated cocaine molecule. The proton needs to be on O2 or O4 of the cocaine molecule for this fragmentation pathway to take place but a transition state yielding such con-

(a)

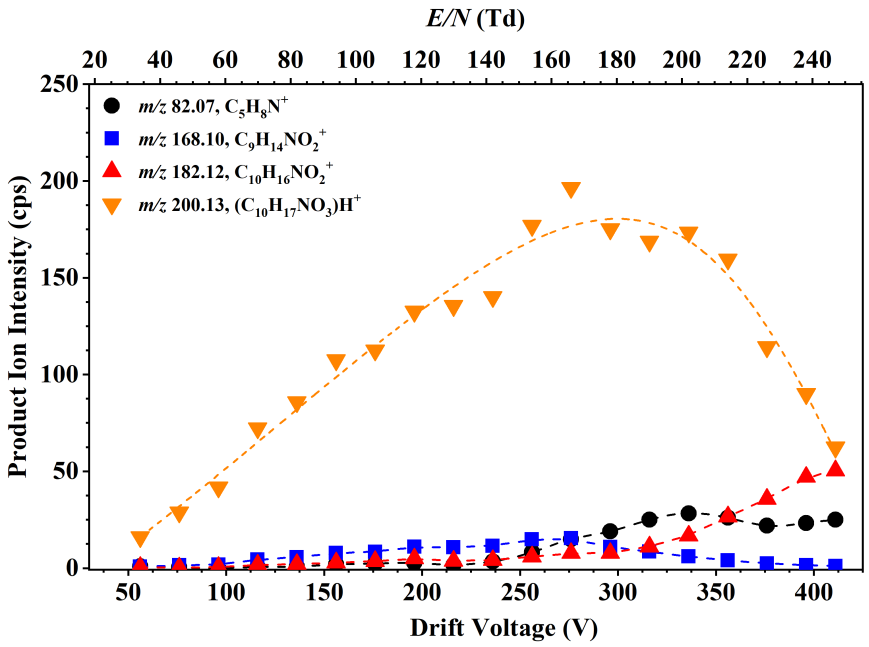

(b)

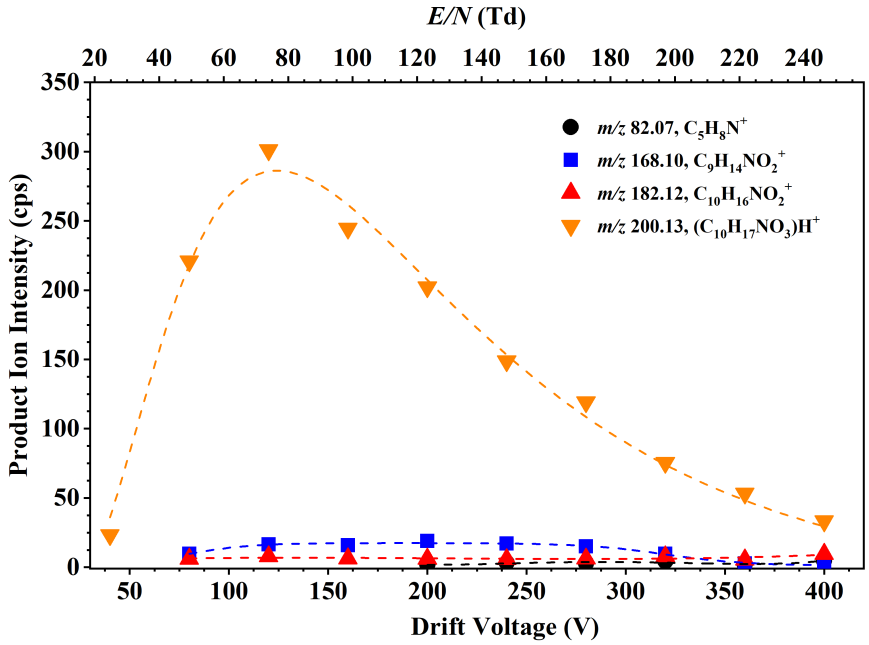

Figure 3.7: Product ion signal intensities in counts per second of the product ions resulting from reactions of $H_3O^+.(H_2O)_n$ (n = 0, 1, 2) with methyl ecgonine as a function of the drift voltage and the reduced electric field in (a) normal and (b) humid conditions.

Table 3.7: Energetics of the reaction of methyl ecgonine with $(H_2O)_nH_3O^+$ (n = 0, 1) yielding the respective structure or transition state. ΔH_{298} and ΔG_{298} are relative to methyl ecgonine and H_3O^+ and, in brackets, to methyl ecgonine and $(H_2O)H_3O^+$.

Structure	***m/z***	ΔH_{298} **(kJ mol^{-1})**	ΔG_{298} **(kJ mol^{-1})**
MeEcg1H$^+$	200	-312 (-154)	-312 (-188)
(MeEcgH - MeOH)$^+$ + MeOH	168	-118 (+40)	-171 (-47)
(MeEcgH - H_2O)$^+$ + H_2O	182	-62 (+96)	-120 (+4)
Transition state	***m/z***	ΔH_{298} **(kJ mol^{-1})**	ΔG_{298} **(kJ mol^{-1})**
TS for loss of MeOH	168	+4 (+162)	0 (+124)

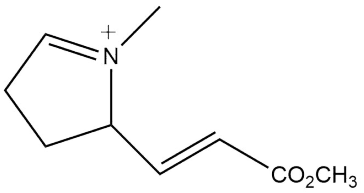

Figure 3.8: Rearrangement of the product ion at m/z 182 from protonated methyl ecgonine.

figuration was not found as the proton migrated to O3 instead. For this reason benzoic acid (BzAcid) and some benzoate esters, namely ethyl benzoate (EtBz), methyl benzoate (MeBz) and isopropyl benzoate (iPrBz) were included in the study. Benzoic anhydride was also tested but with benzoic acid being a decomposition product of benzoic anhydride with lower vapour pressure, the results could be misleading and hence this compound was finally discarded.

Table 3.8 presents the calculated proton affinity and gas phase basicity of the protonation sites that yield the two most stable structures of protonated benzoic acid and methyl, ethyl and isopropyl benzoate. The suffix 1H$^+$ is used here to name protonated molecules with the proton on O1 (*i.e.* the carbonyl oxygen) while 2H$^+$ refers to the proton is in O2 (*i.e.* the alkoxy oxygen). These protonation sites are indicated in Table 3.2.

3.3.4.1 Methyl benzoate

The most stable structure of protonated MeBz is that with the proton on the carbonyl oxygen O1 (*i.e.* MeBz1H$^+$), whose proton affinity and gas phase basicity are 839 and 808 kJ mol^{-1}, respectively. Thus MeBz can undergo proton transfer from H_3O^+ and $(H_2O)H_3O^+$ only and

Table 3.8: Proton affinity and gas phase basicity of the main protonation sites of benzoic acid, methyl benzoate, ethyl benzoate and isopropyl benzoate to yield the indicated structures.

Final Structure	***PA*** **(kJ mol^{-1})**	***GB*** **(kJ mol^{-1})**
BzAcid1H$^+$	812	783
BzAcid2H$^+$	724	741
MeBz1H$^+$	839	808
MeBz2H$^+$	764	741
EtBz1H$^+$	859	831
EtBz2H$^+$	779	750
iPrBz1H$^+$	861	831
iPrBz2H$^+$	786	760

not from the higher order water cluster ions. Proton transfer from $(H_2O)H_3O^+$ to MeBz yields MeBz1H$^+$, while proton transfer from H_3O^+ can result in either MeBz1H$^+$ or MeBz2H$^+$.

The product ion intensities as a function of the drift voltage and the reduced electric field for the reaction of MeBz with $(H_2O)_nH_3O^+$ (n = 0, 1) are given in Figure 3.9 and the energetics for the formation of the main product ions resulting from this reaction are provided in Table 3.9. The most abundant ion for most of the studied E/N range is the protonated parent molecule. Only at more 230 Td in the normal conditions measurement are other product ions signals detected at significantly higher counts than the protonated parent molecule: m/z 77 and m/z 91. Also, clustering of MH$^+$ with H_2O at m/z 155 is observed at low E/N in the humid case.

Table 3.9: Energetics of the reaction of methyl benzoate with $(H_2O)_nH_3O^+$ (n = 0, 1) yielding the respective structure or transition state. ΔH_{298} and ΔG_{298} are relative to methyl benzoate and H_3O^+ and, in brackets, to methyl benzoate and $(H_2O)H_3O^+$.

Structure	***m/z***	$\Delta \boldsymbol{H}_{298}$ **(kJ mol^{-1})**	$\Delta \boldsymbol{G}_{298}$ **(kJ mol^{-1})**
MeBz1H$^+$	137	-155 (+3)	-155 (-31)
MeBz2H$^+$	137	-80 (+78)	-88 (+36)
Benzoyl$^+$ + MeOH	105	-29 (+134)	-82 (+42)
$C_7H_9^+$ + CO_2	93	-188 (-20)	-228 (-104)
Transition state	***m/z***	$\Delta \boldsymbol{H}_{298}$ **(kJ mol^{-1})**	$\Delta \boldsymbol{G}_{298}$ **(kJ mol^{-1})**
TS 1H$^+$ to 2H$^+$	137	+15 (+173)	+14 (+138)

(a)

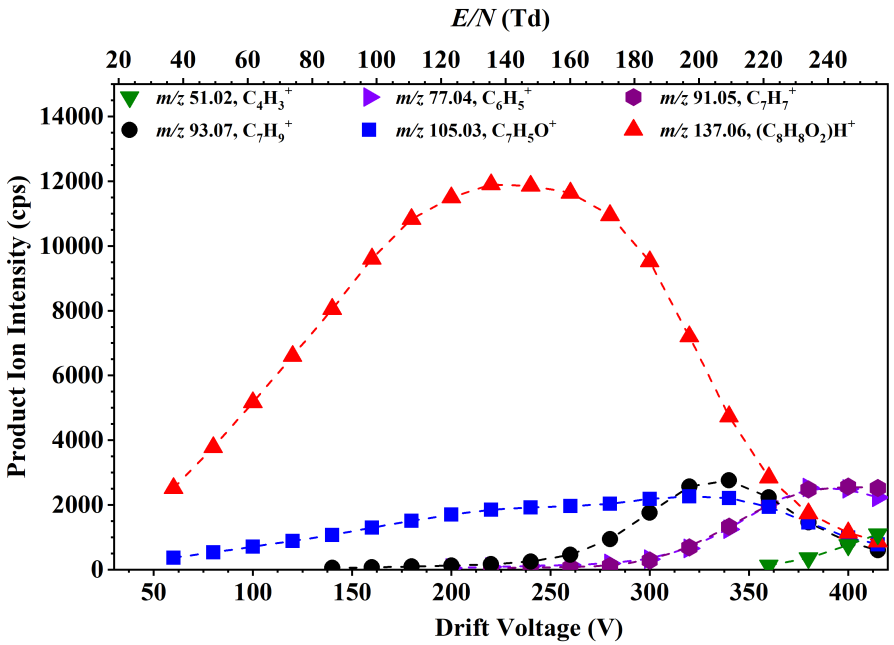

(b)

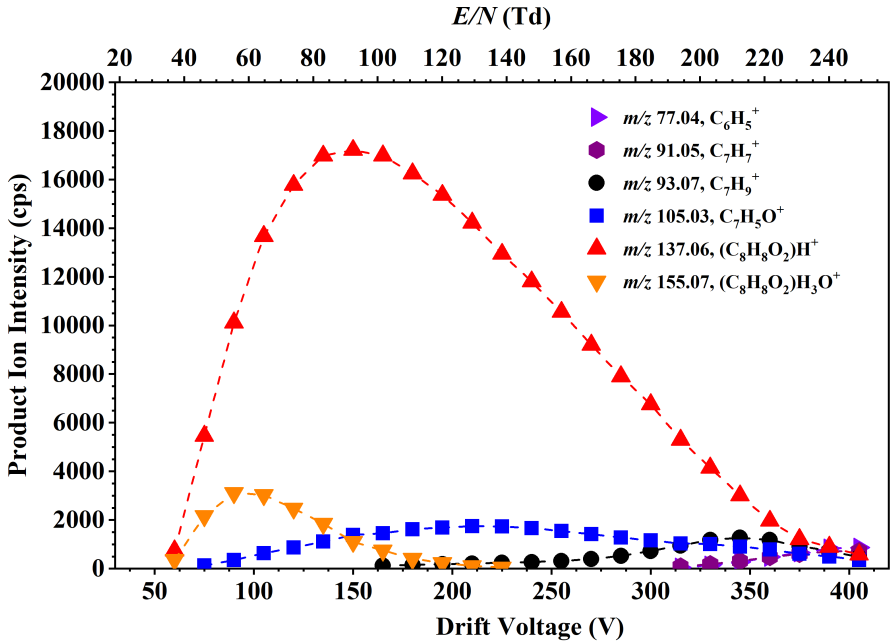

Figure 3.9: Product ion signal intensities in counts per second of the product ions resulting from reactions of $H_3O^+.(H_2O)_n$ ($n = 0, 1$) with methyl benzoate as a function of the drift voltage and the reduced electric field in (a) normal and (b) humid conditions..

Benzoyl$^+$ ($C_7H_5O^+$) at m/z 105 comes from the barrierless loss of MeOH from MeBz2H$^+$. This needs the proton to be on O2, which can occur following two different pathways: (i) direct protonation of O2 from H_3O^+ resulting in MeBz2H$^+$, or (ii) migration of the proton from O1 to O2. When the proton is on O2 (*i.e.* MeBz2H$^+$) loss of MeOH occurs through the barrierless breaking of the C–O bond. The difference between the two pathways lies in the energetics. Direct protonation of O2 is exergonic, while for the migration of the proton following protonation of O1 an endergonic transition state was found and hence the loss of MeOH following this pathway will only occur at collisional energies that are high enough to overcome the transition state TS (see Table 3.9). It is not possible to directly distinguish which of the pathways (if not both) is operating but it was found that direct protonation of O2 in EtBz occurs, which suggests that the same happens with MeBz (see section 3.3.4.2).

The other observed product ions are fragments generated through field-activated collision-induced dissociation. Protonated toluene ($C_7H_9^+$) is found at m/z 93 resulting from the loss of CO_2 from MeBz1H$^+$. Although the formation of this ion is exergonic (see Table 3.9), it is only observed at high reduced electric fields, which indicates that there must be a transition state with high requirements in terms of energy. This ion will not be considered further, neither will those resulting from its fragmentation at higher E/N: $C_7H_7^+$ at m/z 91 (loss of H_2 from m/z 93), $C_6H_5^+$ at m/z 77 (loss of CH_4 from m/z 93), and $C_4H_3^+$ at m/z 51 (loss of CH_2 from m/z 77, only observed in the normal conditions experiment at very high E/N).

3.3.4.2 Ethyl benzoate

Similarly to MeBz, EtBz can undergo proton transfer from $(H_2O)_nH_3O^+$ for $n = 0$ and 1. The product ion intensities as a function of the drift voltage and the reduced electric field for the reaction of EtBz with $(H_2O)_nH_3O^+$ ($n = 0$, 1) are given in Figure 3.10 and the energetics for the formation of the main product ions resulting from this reaction are provided in Table 3.10.

The dominant ion at low E/N (*i.e.* up to ca. 170 Td under normal conditions and ca. 180 Td in humid conditions) is the protonated parent EtBzH$^+$. As the first experiment that was done was that in humid conditions, it was initially thought that the large amounts of EtBzH$^+$ (presumably with the structure EtBz1H$^+$) that were observed were the result of proton transfer from $(H_2O)H_3O^+$ and that proton transfer from H_3O^+ would always result in loss of ethene (C_2H_4), yielding BzAcidH$^+$ at m/z 123. The energetics in Table 3.10 support this argument

(a)

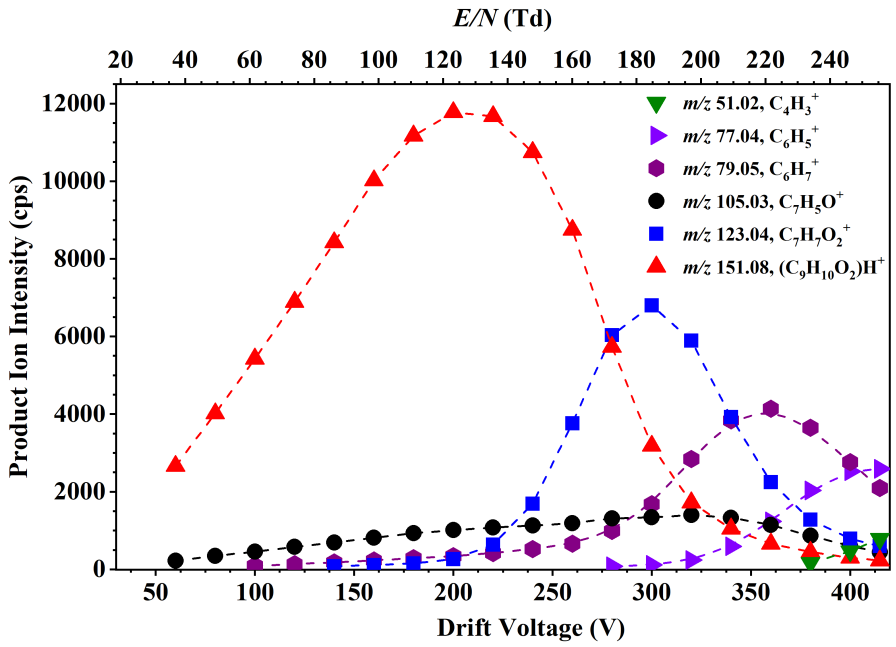

(b)

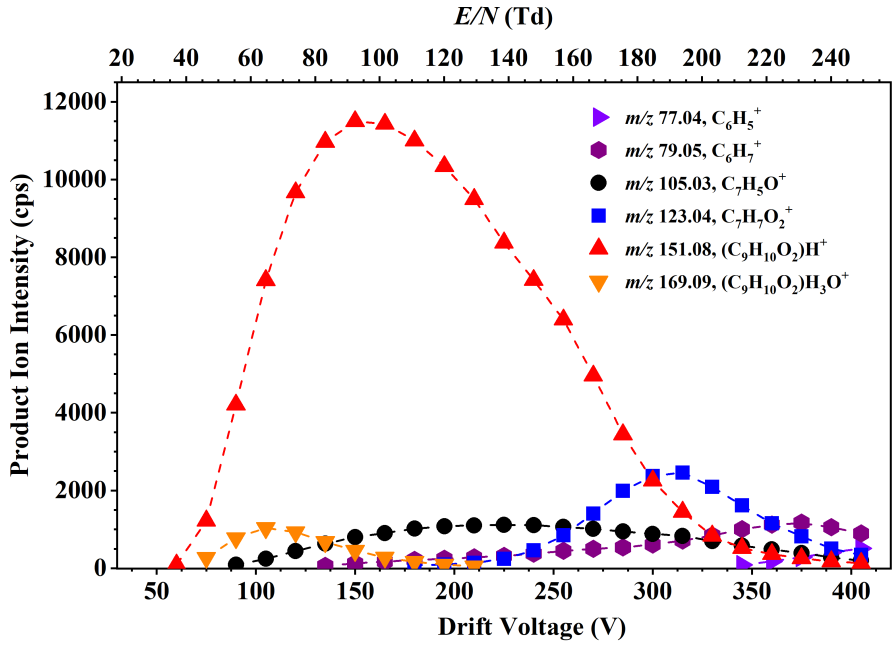

Figure 3.10: Product ion signal intensities in counts per second of the product ions resulting from reactions of $H_3O^+.(H_2O)_n$ (n = 0, 1) with ethyl benzoate as a function of the drift voltage and the reduced electric field in (a) normal and (b) humid conditions.

Table 3.10: Energetics of the reaction of ethyl benzoate with $(H_2O)_nH_3O^+$ (n = 0, 1) yielding the respective structure or transition state. ΔH_{298} and ΔG_{298} are relative to ethyl benzoate and H_3O^+ and, in brackets, to ethyl benzoate and $(H_2O)H_3O^+$.

Structure	***m/z***	$\Delta \boldsymbol{H}_{298}$ **(kJ mol^{-1})**	$\Delta \boldsymbol{G}_{298}$ **(kJ mol^{-1})**
EtBz1H$^+$	151	-180 (-22)	-178 (-54)
EtBz2H$^+$	151	-95 (+63)	-97 (+27)
Benzoyl$^+$ + EtOH	105	-36 (+122)	-83 (+41)
BzAcidH$^+$ + C_2H_4	123	-74 (+84)	-120 (+4)
Benzoyl$^+$ + C_2H_4 + H_2O	105	+15 (+173)	-77 (+47)
BenzeneH$^+$ + C_2H_4 + CO_2	79	+34 (+192)	-132 (-8)
Transition state	***m/z***	$\Delta \boldsymbol{H}_{298}$ **(kJ mol^{-1})**	$\Delta \boldsymbol{G}_{298}$ **(kJ mol^{-1})**
TS 1H$^+$ to 2H$^+$	151	-3 (+155)	+2 (+126)
TS1 for loss of ethene from 1H$^+$	123	-36 (+122)	-41 (+83)
TS2 for loss of ethene from 2H$^+$	123	-15 (+143)	-14 (+110)
TS3 for loss of H_2O from BzAcidH$^+$	105	+98 (+256)	+52 (+176)

because the two transition states for the loss of ethene from EtBz1H$^+$ and EtBz2H$^+$(*i.e.* TS1 and TS2) are exergonic upon proton transfer from H_3O^+. But the experiment in normal conditions in Figure 3.10(a) (with substantially less $(H_2O)H_3O^+$ reagent ions, as Figure 3.2(a) shows) demonstrates that this argument is not correct because the crossover point of *m/z* 123 and *m/z* 151 for normal and humid conditions occurs at a similar reduced electric field, with a shift of only 5 - 10 Td, and hence the loss of ethene from EtBzH$^+$ to yield BzAcidH$^+$ is the result of field-activated collision-induced dissociation. In other words, loss of ethene from the protonated parent is kinetically rather than thermodynamically driven.

The benzoyl$^+$ cation at *m/z* 105, which was observed at all *E/N* values, can be formed through two different pathways: (i) loss of ethanol from EtBzH$^+$, or (ii) loss of ethene from BzAcidH$^+$. The second fragmentation needs to overcome the endergonic transition state TS3 (+52 kJ mol^{-1} relative to H_3O^+), which could be achieved through CID at high *E/N*, but, since *m/z* 105 is observed for the whole *E/N* range, it must be formed through the loss of ethanol from protonated ethyl benzoate. This requires direct protonation of O2 to give the structure EtBz2H$^+$, because the transition state TS 1H$^+$ to 2H$^+$ is slightly endergonic.

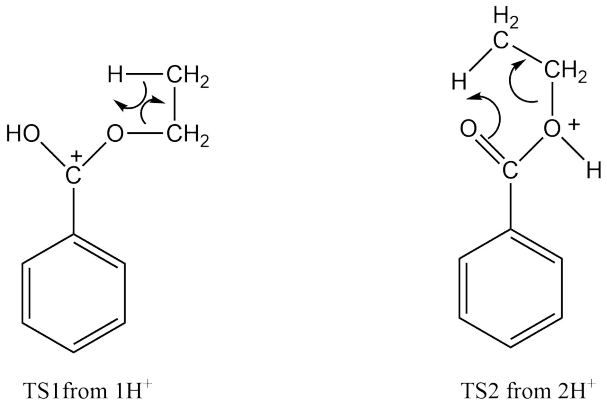

TS1from $1H^+$ TS2 from $2H^+$

Figure 3.11: Structure of the two transition states for the loss of ethene from protonated ethyl benzoate.

The two transitions TS1 and TS2 for the loss of ethene from $EtBz1H^+$ and $EtBz2H^+$ are given in Figure 3.11. Although TS2 is thermodynamically feasible, it needs direct protonation of O2 to yield $EtBz2H^+$ because the transition state $EtBz1H^+$ to $EtBz2H^+$ is endergonic. $EtBz2H^+$ then fragments to $benzoyl^+$ through the barrierless loss of ethanol, rather than to $BzAcidH^+$ through TS2, as the former process has lower energy requirements. The presence of m/z 105 means that direct protonation of O2 to give $EtBz2H^+$ happens. Likewise, the loss of ethanol to yield m/z 105 from $EtBz1H^+$ could happen through the transition state TS $EtBz1H^+$ to $EtBz2H^+$ (see Table 3.10), but the loss of ethene through TS1 is more energetically favourable. The loss of ethene to $BzAcidH^+$ is thus concluded to happen through TS1.

The question that arises now is why the ion with m/z 105 (*i.e.* the loss of ethanol from $EtBz2H^+$) is found at low E/N while the ion with m/z 123 is only found at high E/N. This can be better understood with the ΔG plot as a function of the reaction coordinate in Figure 3.12. $EtBz1H^+$ and $EtBz2H^+$ are promptly formed. However, while the loss of ethanol occurs readily, the loss of ethene from $EtBz1H^+$ needs to go through the transition state TS1. This is still energetically allowed but the data shows that it is slower than the loss of ethanol. Therefore at low E/N the loss of ethanol is kinetically dominant over the loss of ethene. In contrast, ethene elimination is the dominant ion at high E/N because $EtBz1H^+$ formed via proton transfer from both $(H_2O)H_3O^+$ and H_3O^+ fragments through TS1. A hypothesis is that at low E/N the molecules loss energy through collisions with the buffer gas and hence the fragmentation to $BzAcidH^+$ only occurs when the collisional energy from the field is enough to overcome the 137

kJ mol^{-1} difference between EtBz1H$^+$ and TS1.

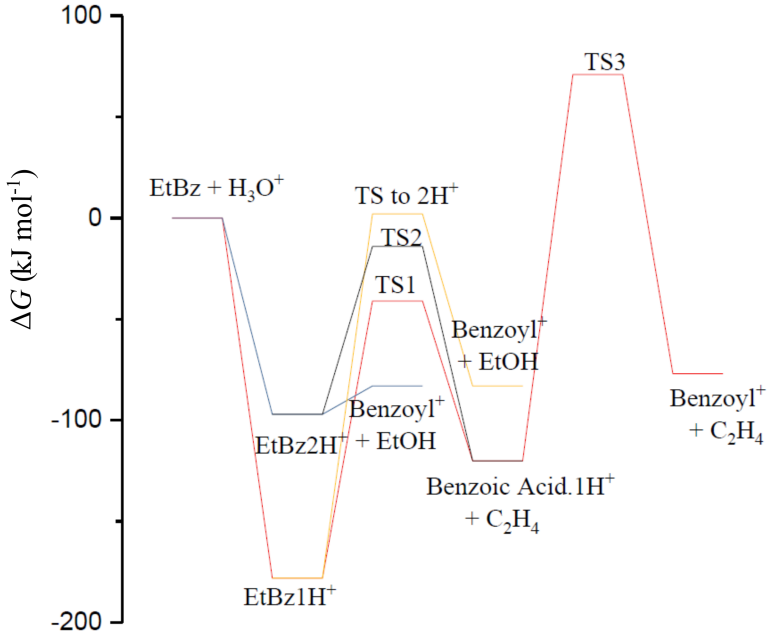

Figure 3.12: ΔG for the various reactions of H_3O^+ with EtBz. Note that the neutral water has been omitted from the labels.

Similarly to the MeBz case, other fragment ions are found at high E/N, such as protonated benzene ($C_6H_7^+$) at m/z 79 resulting from the loss of CO_2 from BzAcidH$^+$. Although its formation is exergonic, it is thought to have a transition state similar to that in MeBzH$^+$ which can only be exceeded through collision-induced processes. $C_6H_5^+$ at m/z 77 (loss of H_2 from protonated benzene), $C_4H_3^+$ at m/z 51 (loss of CH_2 from m/z 77) in normal conditions and the cluster of protonated ethyl benzoate with water at m/z 169, this one in humid conditions, at low E/N were also observed.

3.3.4.3 Isopropyl benzoate

Isopropyl benzoate is a key molecule to investigate in this study, because it resembles the benzoate moiety in the cocaine molecule, which is attached to two carbons. Similarly to MeBz and EtBz, iPrBz can undergo proton transfer from H_3O^+ and $(H_2O)H_3O^+$ but not from higher order water cluster ions, with iPrBzH$^+$ being the result of proton transfer from $(H_2O)H_3O^+$ because, as it is explained later on, proton transfer from H_3O^+ results in fragmentation. The product ion intensities as a function of the drift voltage and the reduced electric field for the reaction of iPrBz

with $(H_2O)_nH_3O^+$ (n = 0, 1) are given in Figure 3.13 and the energetics for the formation of the main product ions resulting from this reaction are provided in Table 3.11.

Table 3.11: Energetics of the reaction of isopropyl benzoate with $(H_2O)_nH_3O^+$ (n = 0, 1) yielding the respective structure or transition state. ΔH_{298} and ΔG_{298} are relative to isopropyl benzoate and H_3O^+ and, in brackets, to isopropyl benzoate and $(H_2O)H_3O^+$.

Structure	***m/z***	$\Delta \boldsymbol{H}_{298}$ **(kJ mol^{-1})**	$\Delta \boldsymbol{G}_{298}$ **(kJ mol^{-1})**
iPrBz1H$^+$	165	-176 (-18)	-177 (-53)
iPrBz2H$^+$	165	-102 (+56)	-107 (+17)
Benzoyl$^+$ + iPrOH	105	-45 (+113)	-99 (+25)
Benzoic acid + iPr$^+$	43	-35 (+123)	-91 (+33)
Benzoic acidH$^+$ + C_3H_6	123	-84 (+74)	-137 (-13)
BenzeneH$^+$ + C_3H_6 + CO_2	79	-52 (+106)	-151 (-27)
Transition state	***m/z***	$\Delta \boldsymbol{H}_{298}$ **(kJ mol^{-1})**	$\Delta \boldsymbol{G}_{298}$ **(kJ mol^{-1})**
TS 1H$^+$ to 2H$^+$	165	-24 (+134)	-25 (+99)
TS1 for loss of propene from 1H$^+$	123	-105 (+53)	-115 (+9)

The product ion counts may indicate that the fragmentation pathways of iPrBz are similar to those of EtBz, but the energetics show that these are actually quite different. BzAcidH$^+$ is still the major fragment ion, in this case becoming dominant at a lower E/N compared to EtBz (*i.e.* at ca. 100 Td for both the normal and humid experiments), although protonated benzene at m/z 79 is the dominant ion at the higher end of the E/N range. Benzoyl$^+$ at m/z 105 is found over the same range it was found for EtBz. Furthermore, a new ion at m/z 43, tentatively assigned to isopropyl radical (iPr$^+$, $C_3H_7^+$), is also found with a comparable abundance of that of benzoyl$^+$ in humid conditions but only traces were observed in the measurements in normal conditions. Other product ions that were observed are, at low E/N, the cluster with water of protonated benzoic acid and protonated isopropyl benzoate at m/z 141 and m/z 183, respectively; and at high E/N, $C_6H_5^+$ at m/z 77 (loss of H_2 from protonated benzene) and $C_4H_3^+$ at m/z 51 (loss of CH_2 from m/z 77).

As for MeBz and EtBz, the loss of an alcohol needs the proton to be on O2. For iPrBz, loss of isopropyl alcohol (iPrOH) from iPrBz2H$^+$ yields benzoyl$^+$, but fragmentation of iPrBz2H$^+$ can also result in iPr$^+$. This can be illustrated with the structures in Figure 3.14. The length

(a)

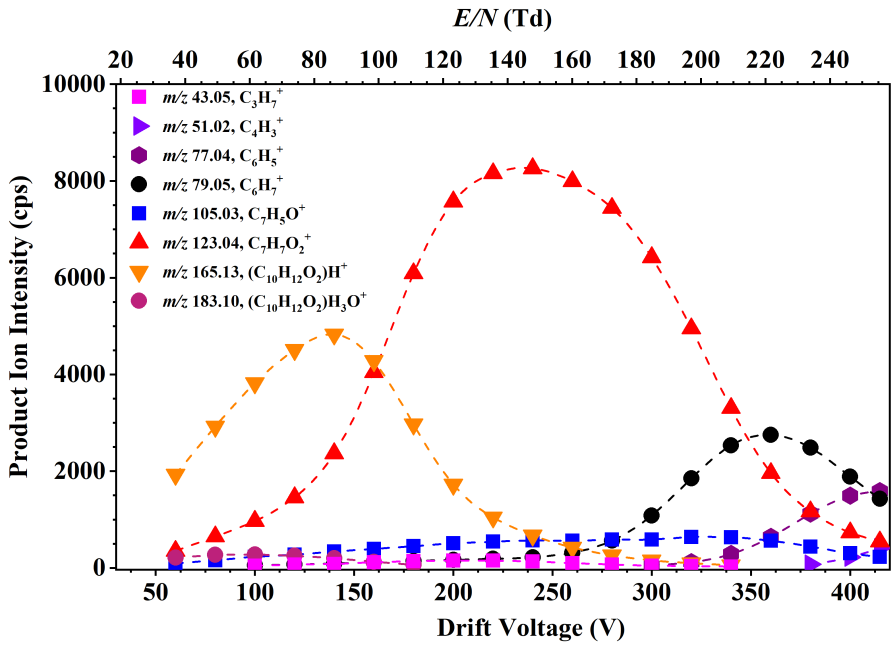

(b)

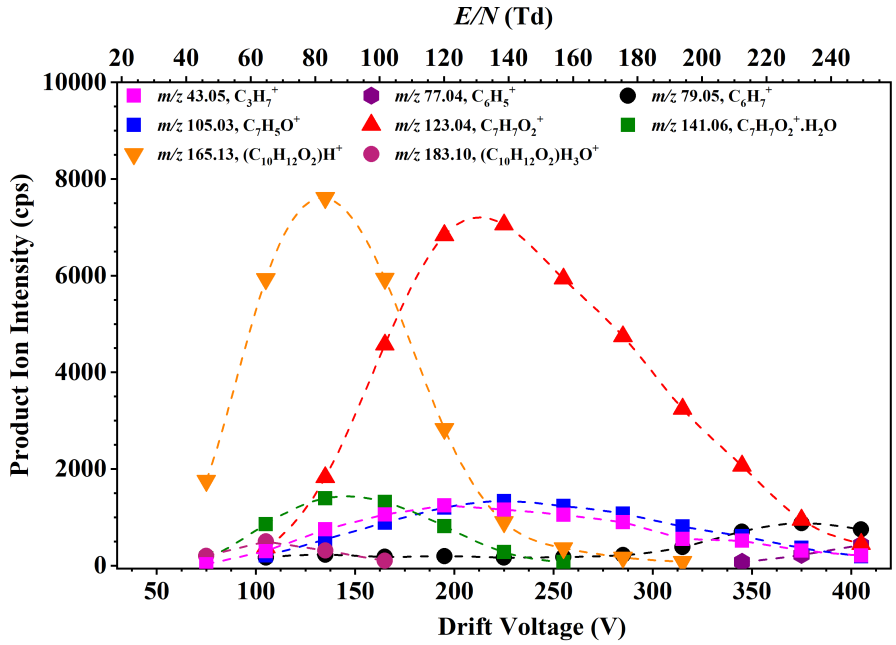

Figure 3.13: Product ion signal intensities in counts per second of the product ions resulting from reactions of $H_3O^+.(H_2O)_n$ (n = 0, 1) with isopropyl benzoate as a function of the drift voltage and the reduced electric field in (a) normal and (b) humid conditions.

of the C1-O and C2-O bonds in EtBz2H$^+$ are 1.74 and 1.50 Å, respectively. The length of these for iPrBz2H$^+$ are 1.62 and 1.57 Å. The C1-O bond in iPrBz2H$^+$ is longer that the equivalent in the iPrOH molecule, which is 1.44 Å. This longer bond allows the iPr$^+$ ion to be formed. The formation of both fragment ions of iPrBz2H$^+$ (*i.e.* iPr$^+$ and benzoyl$^+$ from the loss of iPrOH) have similar energetics and both are barrierless (as shown in Figure 3.15). There are however two questions that can be asked at this point: (i) why are there such differences in the ion signals of *m/z* 43 and *m/z* 105 in normal conditions when they have similar intensities (as expected) in the humid measurements? And, considering that iPr$^+$ resembles the fragment with *m/z* 182 in the benzoate moiety, (ii) why is iPr$^+$ so low compared to *m/z* 182 in the cocaine measurements? While the first question remains unanswered for now, there are two possible explanations for the second one. In first place, ions with greater *m/z* are transported more efficiently through the different stages of the PTR-ToF-MS. This is the reason transmission coefficients are often used to account for ion losses of lower *m/z* ions. The other reason could be related to the fact that iPrBz was measured through headspace analysis while the TDU was used for studying cocaine, potentially decomposing some of the sample which then gets ionised in the drift tube. However it is unlikely that the latter is the reason because the product ion with *m/z* 182 in cocaine presents a comparable branching percentage to that reported by Agarwal *et al.* (*i.e.* ca. 15% of the total product ion counts at 120 Td), whose measurements were doing through headspace analysis [16].

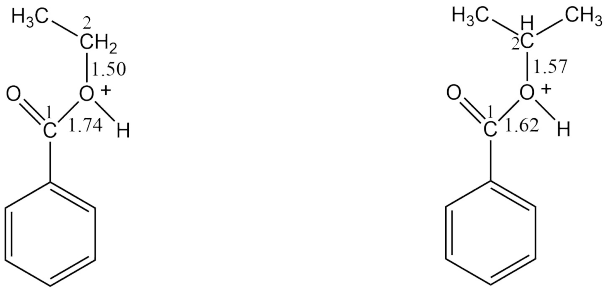

Figure 3.14: Structure of EtBz2H$^+$ and iPrBz2H$^+$.

The plot of ΔG as a function of the reaction coordinate in Figure 3.15 indicates that proton transfer from H_3O^+ will readily result in fragmentation and hence any observed protonated iPrBz will come from the reaction with $(H_2O)H_3O^+$ having the structure iPrBz1H$^+$. That the dominant product is BzAcidH$^+$ indicates that whilst direct protonation of O2 can occur, protonation or the more basic O1 is more likely, probably influenced by dipolar attraction. The difference in

energy between iPrBz1H$^+$ and TS1 is only of 62 kJ mol^{-1}, while for EtBz this is 137 kJ mol^{-1}, which explains why BzAcidH$^+$ is observed at lower E/N in iPrBz compared to EtBz.

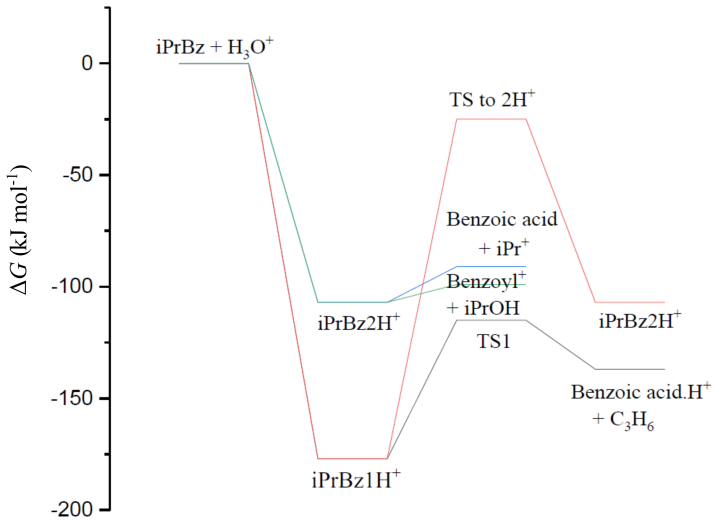

Figure 3.15: ΔG as a function of the reaction coordinate for the various reactions of H_3O^+ with iPrBz. Note that the neutral water has been omitted from the labels.

3.3.4.4 Benzoic acid

Protonated cocaine loses benzoic acid resulting in a dominant fragment product ion at m/z 182. For this reason, benzoic acid was included in this study. Similarly to the benzoate esters, BzAcid can undergo proton transfer from $(H_2O)H_3O^+$, to give BzAcid1H$^+$, and H_3O^+, to give either BzAcid1H$^+$ or BzAcid2H$^+$, although the latter readily fragments to benzoyl$^+$ + H_2O. The product ion intensities as a function of the drift voltage and the reduced electric field for the reaction of BzAcid with $(H_2O)_nH_3O^+$ (n = 0, 1) are given in Figure 3.16 and the energetics for the formation of the main product ions resulting from this reaction are provided in Table 3.12.

For this compound, the protonated parent molecule at m/z 123 is the dominant ion for most of the E/N range, with protonated benzene and the subsequent loss of H_2 (*i.e.* m/z 79 and m/z 77) appearing at high E/N, and the cluster of protonated BzAcid with water being observed at low E/N (with higher intensities under humid conditions, as would be expected). As observed for the previous compounds, the formation of benzoyl$^+$ at m/z 105 requires the proton to be on O2, to yield BzAcid2H$^+$ in this case, followed by the barrierless loss of water (see Figure 3.17). Benzoyl$^+$ ions being produced at all reduced electric fields proves again that direct protonation

(a)

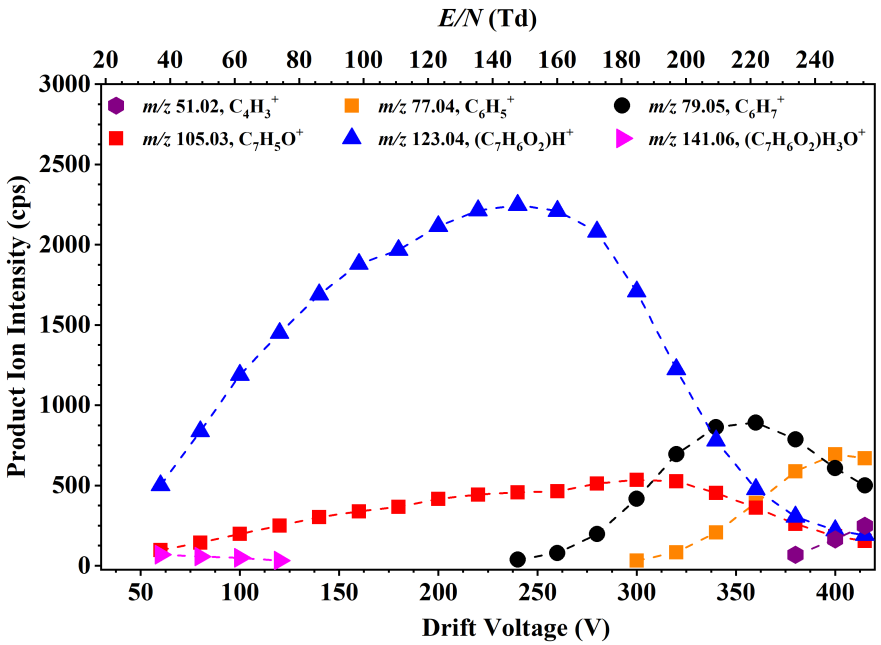

(b)

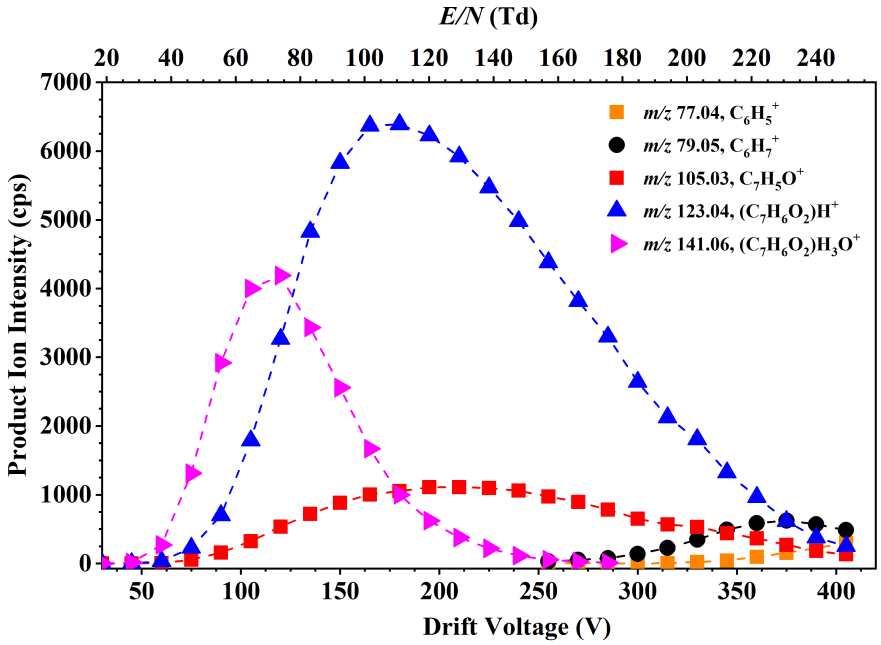

Figure 3.16: Product ion signal intensities in counts per second of the product ions resulting from reactions of $H_3O^+.(H_2O)_n$ (n = 0, 1) with benzoic acid as a function of the drift voltage and the reduced electric field in (a) normal and (b) humid conditions.

Table 3.12: Energetics of the reaction of benzoic acid with $(H_2O)_nH_3O^+$ (n = 0, 1) yielding the respective structure or transition state. ΔH_{298} and ΔG_{298} are relative to benzoic acid and H_3O^+ and, in brackets, to benzoic acid and $(H_2O)H_3O^+$.

Structure	***m/z***	$\Delta \boldsymbol{H}_{298}$ **(kJ mol^{-1})**	$\Delta \boldsymbol{G}_{298}$ **(kJ mol^{-1})**
BzAcid1H$^+$	123	-128 (+30)	-130 (-6)
BzAcid2H$^+$	123	-40 (+118)	-88 (+36)
Benzoyl$^+$ + H_2O	105	-83 (+75)	-100 (+24)
BenzeneH$^+$ + CO_2	79	-97 (-61)	-143 (-19)
Transition state	***m/z***	$\Delta \boldsymbol{H}_{298}$ **(kJ mol^{-1})**	$\Delta \boldsymbol{G}_{298}$ **(kJ mol^{-1})**
TS 1H$^+$ to 2H$^+$	123	+44 (+202)	+45 (+169)

of O2 occurs, because the TS 1H$^+$ to 2H$^+$ is endergonic and hence benzoyl$^+$ is not a product of the structure BzAcid1H$^+$. When the PTR-MS results for BzAcid are compared to those from MeBz, EtBz and iPrBz at low E/N, it can be concluded that the formation of benzoyl$^+$ does not occur from fragmentation of protonated benzoic acid, but by direct protonation of the alkoxy oxygen O2 for each molecule. Furthermore, Figure 3.16 also confirms that protonated benzene and its loss of H_2 are formed from protonated benzoic acid through collision-induced dissociation at high E/N.

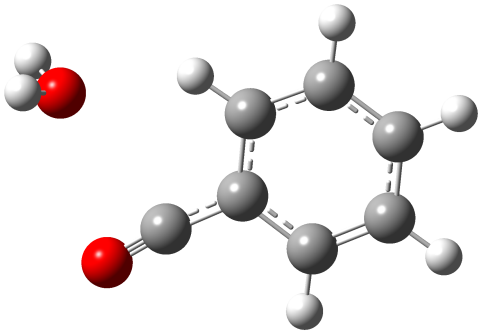

Figure 3.17: Ball-and-stick representation of the BzAcid2H$^+$ structure. Note that this essentially corresponds to benzoyl$^+$ + H_2O, as BzAcid2H$^+$ undergoes the barrierless loss of water.

3.3.5 Isobutyrate esters

Methyl and ethyl isobutyrates (MeIsoBut and EtIsoBut) are of relevance for this study because of their similarity with the carboxylic acid ester moiety in cocaine and its analogues (see structure in Table 3.2). The PTR-MS data for these two compounds were only acquired under normal drift tube operating conditions (*i.e.* no humid PTR-MS data is provided for either MeIsoBut or EtIsoBut).

3.3.5.1 Methyl isobutyrate

The *PA* and *GB* of methyl isobutyrate leading to the most stable structure of $MeIsoButH^+$ are 815 and 786 kJ mol^{-1}, respectively, and thus it can receive a proton from H_3O^+ and $(H_2O)H_3O^+$ because $GB(\text{MeIsoBut}) > GB((H_2O)_2) = 777$ kJ mol^{-1} although $PA(\text{MeIsoBut}) < PA((H_2O)_2) = 842$ kJ mol^{-1}. The product ion signal in counts per second from the reaction of MeIsoBut with $(H_2O)_nH_3O^+$ ($n = 0, 1$) are shown in Figure 3.19. $MeIsoButH^+$ is the dominant ion through the whole range of E/N values and fragmentation only occurs at high E/N.

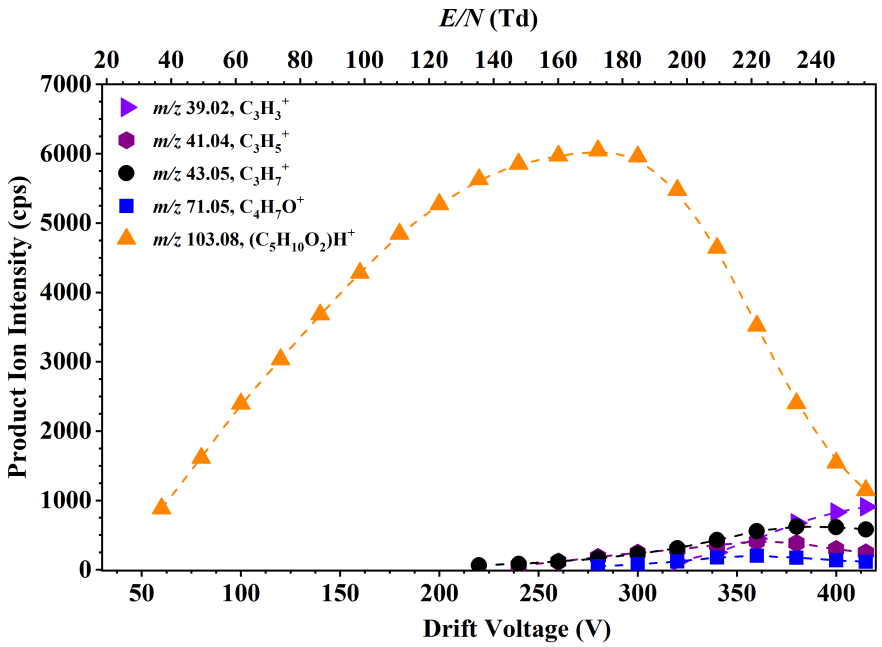

Figure 3.18: Product ion signal intensities in counts per second of the product ions resulting from reactions of $H_3O^+.(H_2O)_n$ ($n = 0, 1$) with methyl isobutyrate as a function of the drift voltage and the reduced electric field.

As the loss of MeOH from $MeBzH^+$ is observed, the loss of MeOH from $MeIsoButH^+$ was

expected as well because of the structural similarities between the benzoates and isobutyrates, but this ion (m/z 71) is only observed with low intensities at high E/N, which is surprising. The ΔG for the transition state $1H^+$ to $2H^+$ for $MeIsoButH^+$ is 34 kJ mol^{-1}, while for $MeBzH^+$ this is 14 kJ mol^{-1}. This could mislead one to think that the loss of MeOH occurs through a transition state which MeBz can overcome with the energy gained from the electric field while MeIsoBut cannot. However, this cannot be the reason because EtIsoBut has similar energetics to those of MeBz for the loss of MeOH, but the loss of EtOH is only observed at high E/N (see subsection 3.3.5.2). At present we have no explanation for this discrepancy.

3.3.5.2 Ethyl isobutyrate

Similarly to MeIsoBut, EtIsoBut can undergo proton transfer from $(H_2O)_nH_3O^+$ for $n = 0$ and 1, but not from higher order protonated water clusters. The energetics for the structures arising from the reaction of ethyl isobutyrate and $(H_2O)_nH_3O^+$ ($n = 0$, 1) are provided in Table 3.13 and the product ion signal in cps as a function of the drift voltage and the reduced electric field for the same reaction are given in Figure 3.19.

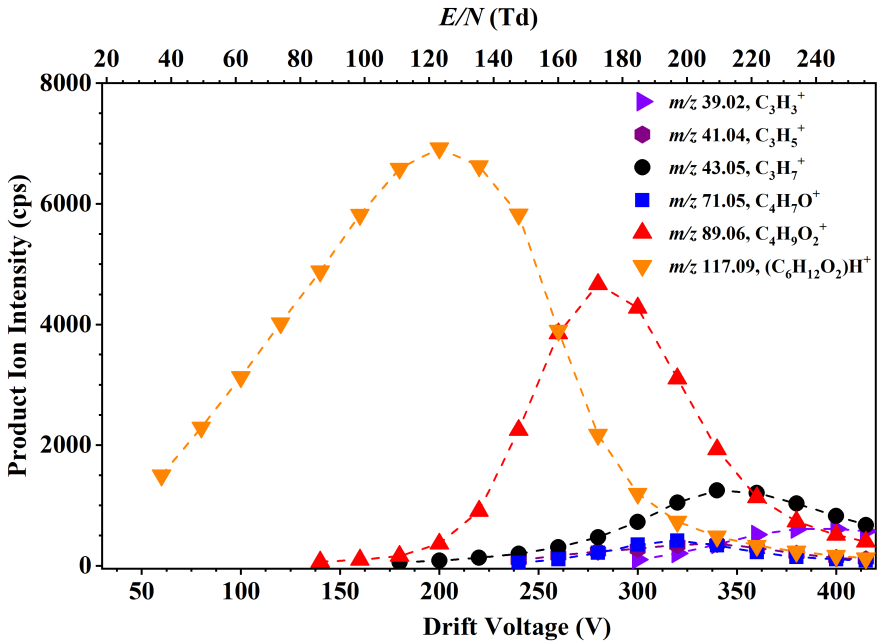

Figure 3.19: Product ion signal intensities in counts per second of the product ions resulting from reactions of $H_3O^+.(H_2O)_n$ ($n = 0$, 1) with ethyl isobutyrate as a function of the drift voltage and the reduced electric field.

Table 3.13: Energetics of the reaction of ethyl isobutyrate with $(H_2O)_nH_3O^+$ (n = 0, 1) yielding the respective structure or transition state. ΔH_{298} and ΔG_{298} are relative to ethyl isobutyrate and H_3O^+ and, in brackets, to ethyl isobutyrate and $(H_2O)H_3O^+$.

Structure	***m/z***	$\Delta \boldsymbol{H}_{298}$ **(kJ mol^{-1})**	$\Delta \boldsymbol{G}_{298}$ **(kJ mol^{-1})**
EtIsoBut1H$^+$	117	-145 (+13)	-146 (-22)
EtIsoBut2H$^+$	117	-81 (+77)	-86 (+38)
IsoButyryl$^+$ + EtOH	71	-9 (+149)	-59 (+65)
IsoButyric acidH$^+$ + C_2H_4	89	-38 (+120)	-85 (+39)
Transition state	***m/z***	$\Delta \boldsymbol{H}_{298}$ **(kJ mol^{-1})**	$\Delta \boldsymbol{G}_{298}$ **(kJ mol^{-1})**
TS 1H$^+$ to 2H$^+$		+18 (+176)	+17 (+141)
TS1 loss of ethene		-28 (+130)	-34 (+90)
TS2 loss of ethene		-6 (+152)	-11 (+113)

The main fragment ion at m/z 89 results from the loss of ethene to yield (isobutyric acid)H$^+$. This fragmentation pathway resembles the one for EtBz to yield BzAcidH$^+$. Furthermore, the energetics for the transition states TS1 and TS2 are comparable to those of EtBz and hence the loss of ethene must be the result of collision-induced dissociation for EtIsoBut as it was concluded for EtBz.

The interesting finding in Table 3.13 is that the energetics of the transition state 1H$^+$ to 2H$^+$ are comparable to those of MeBz, so loss of EtOH from EtIsoBut was expected as loss of MeOH from MeBz was observed. However, this was not found in the PTR-MS data. Therefore, the loss of MeOH or EtOH does not occur through the transition state, but via direct protonation of the alkoxy oxygen O2, as stated in the benzoate esters section.

3.3.6 Cocaethylene

Cocaethylene was included in this study because it is structurally similar to cocaine, but it has an ethyl group attached to the ester oxygen O5 instead of a methyl group. The product ion signal intensities of the product ions resulting from the reaction of cocaethylene with $(H_2O)_nH_3O^+$ as a function of the drift voltage and the reduced electric field are given in Figure 3.20. The product ions shown in this plot are analogous to those found with cocaine, which indicates that the

fragmentation pathways and energetics are very similar for these two molecules. The dominant ion for the whole E/N range in both normal and humid conditions is the protonated parent. Some minor product ions are those resulting from the loss of benzoic acid at m/z 196 and the loss of EtOH at m/z 272. As found for cocaine, the product ion $C_5H_8N^+$ at m/z 82 is observed with low intensities in the normal operating drift tube conditions at high E/N (*i.e.* $>$ 200 Td).

3.3.7 Ethyl ecgonine

Ethyl ecgonine was included in this study because it has a similar structure as methyl ecgonine, but with an ethyl instead of a methyl group attached to the ester oxygen O5. The product ion signal intensities of the product ions resulting from the reaction of ethyl ecgonine with hydronium and protonated water clusters as a function of the drift voltage and the reduced electric field are given in Figure 3.21. Note that this compound was only studied under the so-called normal drift tube operating conditions. In other words, no humid conditions data of ethyl ecgonine were acquired, although it would be expected to be similar to that from methyl ecgonine exchanging the methyl group for an ethyl group where needed. The ion-chemistry is similar to that found for methyl ecgonine. The most abundant ion through the whole E/N range is the protonated parent molecule at m/z 214. The three observed fragment ions correspond to the loss of benzoic acid from the protonated parent ($C_{11}H_{18}NO_2^+$ at m/z 196), the loss of EtOH from the protonated parent ($C_9H_{14}NO_2^+$ at m/z 168), and $C_5H_8N^+$ at m/z 82.

3.3.8 Norcocaine

The product ion signal intensities as a function of the drift voltage and the reduced electric field for the reaction of norcocaine with $(H_2O)_nH_3O^+$ are provided in Figure 3.22. As for ethyl ecgonine, only normal drift tube condition data are provided. The plot in Figure 3.22 illustrates two similarities with cocaine: (i) the protonated parent molecule is the most abundant ion and (ii) the loss of benzoic acid, resulting in $C_9H_{14}NO_2^+$ at m/z 168, is the main fragmentation pathway. It is surprising that that the loss of MeOH alone (m/z 258) does not occur, but rather the combined loss of MeOH and benzoic acid producing $C_8H_{10}NO^+$ at m/z 136 is observed. The ion at m/z 68 is analogous to that found in cocaine, cocaethylene, methyl ecgonine and ethyl ecgonine at m/z 82 replacing the CH_3 group at the pyrolidine nitrogen with a hydrogen atom.

The product ions at m/z 290, m/z 168 and m/z 136 are the ones used by Moore *et al.* to

(a)

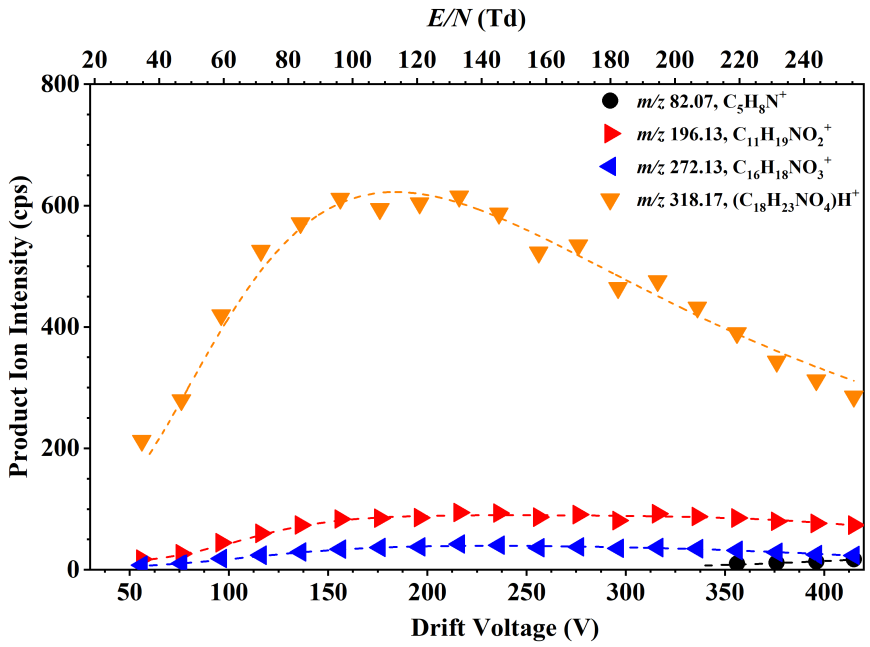

(b)

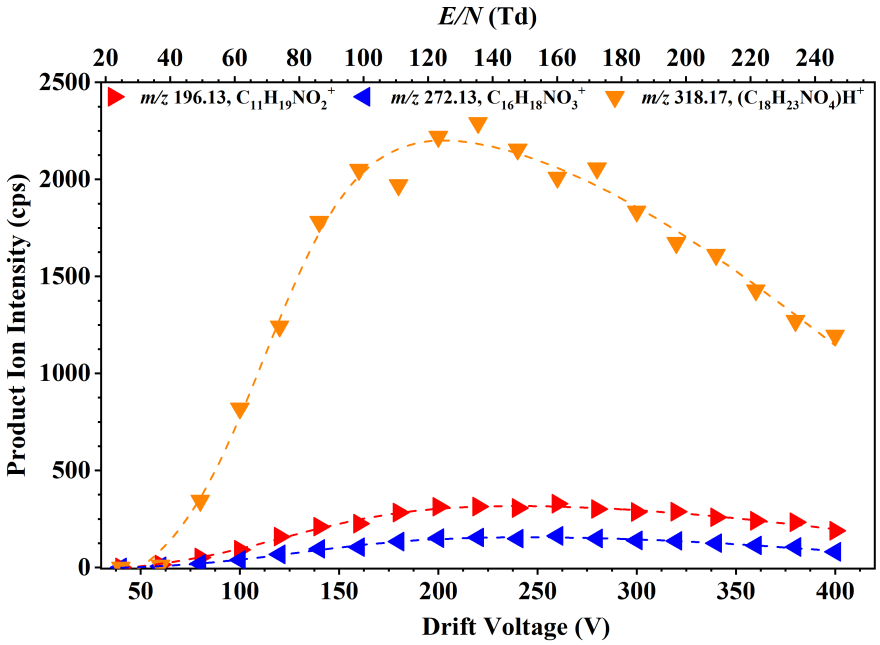

Figure 3.20: Product ion signal intensities in counts per second of the product ions resulting from reactions of $H_3O^+.(H_2O)_n$ (n = 0, 1, 2) with cocaethylene as a function of the drift voltage and the reduced electric field in (a) normal and (b) humid conditions.

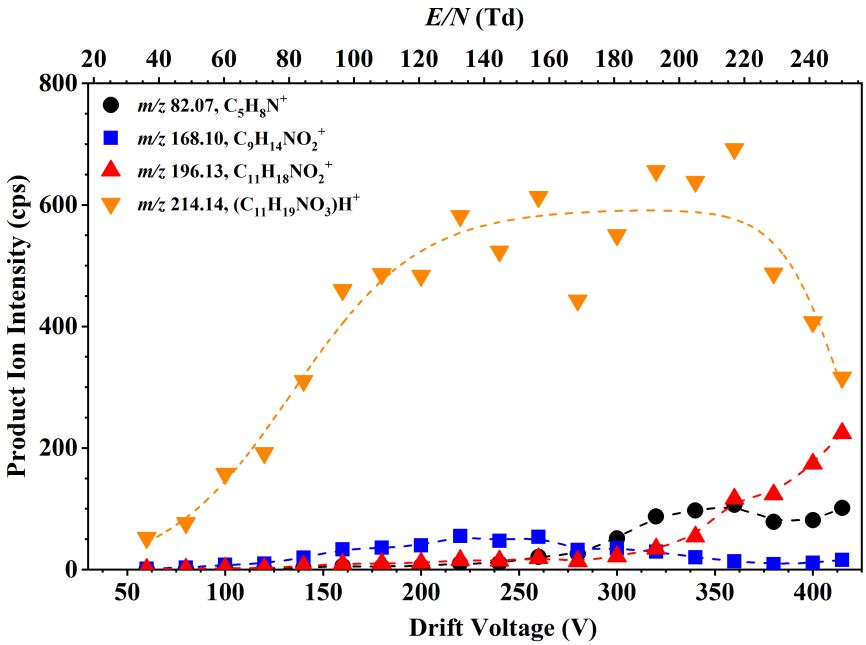

Figure 3.21: Product ion signal intensities in counts per second of the product ions resulting from reactions of $H_3O^+.(H_2O)_n$ (n = 0, 1, 2) with ethyl ecgonine as a function of the drift voltage and the reduced electric field. Note that the data shown in this plot are atypically scattered. This is being currently investigated and therefore these data should only be considered preliminary.

quantify the amount of norcocaine in human hair using a positive atmospheric pressure chemical ionization LC/MS/MS [93]. Furthermore, these ions are also reported in the mzCloud database [94].

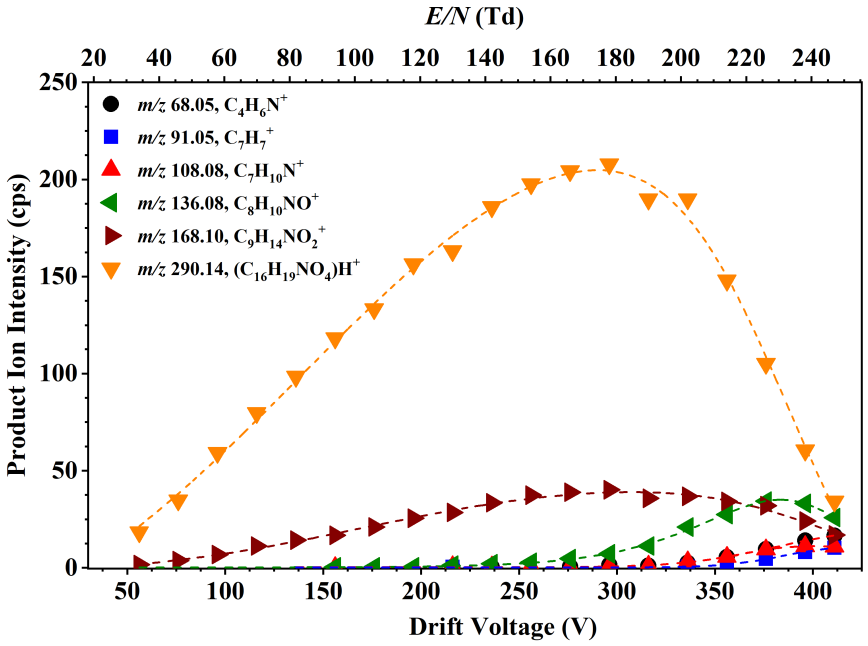

Figure 3.22: Product ion signal intensities in counts per second of the product ions resulting from reactions of $H_3O^+.(H_2O)_n$ (n = 0, 1, 2) with norcocaine as a function of the drift voltage and the reduced electric field.

3.3.9 Methyl ecgonidine

Figure 3.23 gives the signal intensities of the product ions obtained from the reaction of methyl ecgonidine with $H_3O^+.(H_2O)_n$ as a function of the drift voltage and the reduced electric field under normal drift tube conditions. Little fragmentation is observed as only low signals are associated with fragment product ions. The protonated parent is found to be the dominant species for the whole E/N range. This is considered to be a consequence of the rigidity of the molecule, resulting from the double bond between the carbon atoms (see Table 3.1), with the proton having reduced mobility between the protonation sites. This explains the low abundance of m/z 150, because loss of MeOH needs direct protonation of the O5 ester oxygen. Also, the absence of the ion at m/z 82 is remarkable, as it was thought that such a rigid molecule would fragment at high collisional energies. The ion at m/z 152, from which only low intensities

were observed in PTR-MS, is tentatively assigned to $C_9H_{12}O_2^+$. This is controversial, due to the rearrangements required for its formation, but the fact that it was also found with other analytical techniques supports this assignment [85].

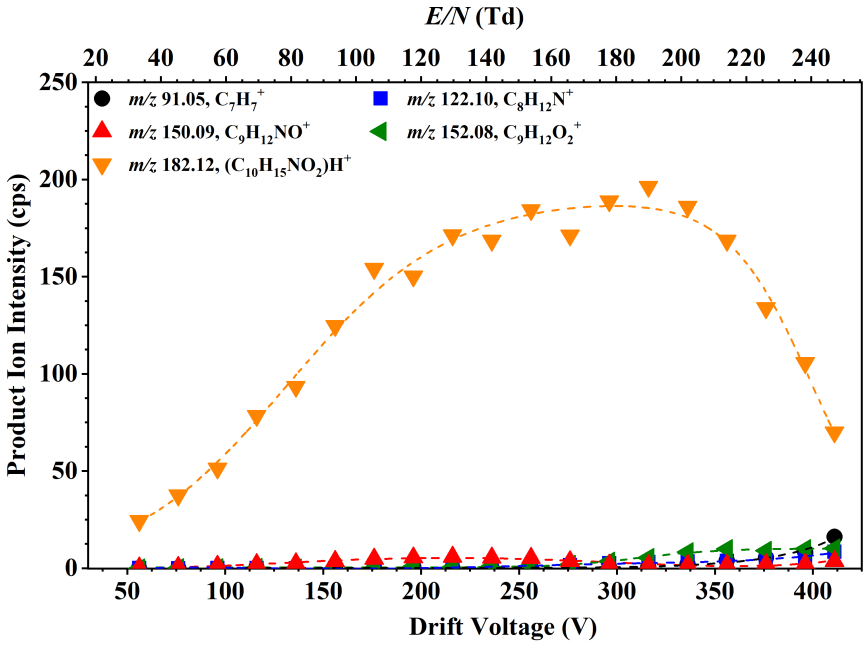

Figure 3.23: Product ion signal intensities in counts per second of the product ions resulting from reactions of $H_3O^+.(H_2O)_n$ (n = 0, 1, 2) with methyl ecgonidine as a function of the drift voltage and the reduced electric field.

3.3.10 o-Hydroxycocaine

Figure 3.24 shows the product ion signal intensities from the reaction of o-hydroxycocaine with $H_3O^+.(H_2O)_n$ (n = 0, 1, 2) as a function of the drift tube voltage and the reduced electric field in both normal and humid conditions. The dominant ion for all the E/N range is the protonated parent ion at m/z 320 as it is commonly found in the cocaine metabolites we have studied. The main fragment ion is $C_{10}H_{16}NO_2^+$ at m/z 182, resulting from the loss of 2-hydroxybenzoic acid. These two ions have been reported in the literature. Schaffer *et al.* used the fragmentation of the protonated parent to m/z 182 in hydroxycocaine isomers to quantify cocaine ingestion using a LC/MS/MS system to analyse hair samples [84].

A very low signal associated with the product ion $C_{10}H_{18}NO_3^+$ at m/z 200 was found under both normal and humid drift tube conditions in PTR-MS. This is controversial because it has not

(a)

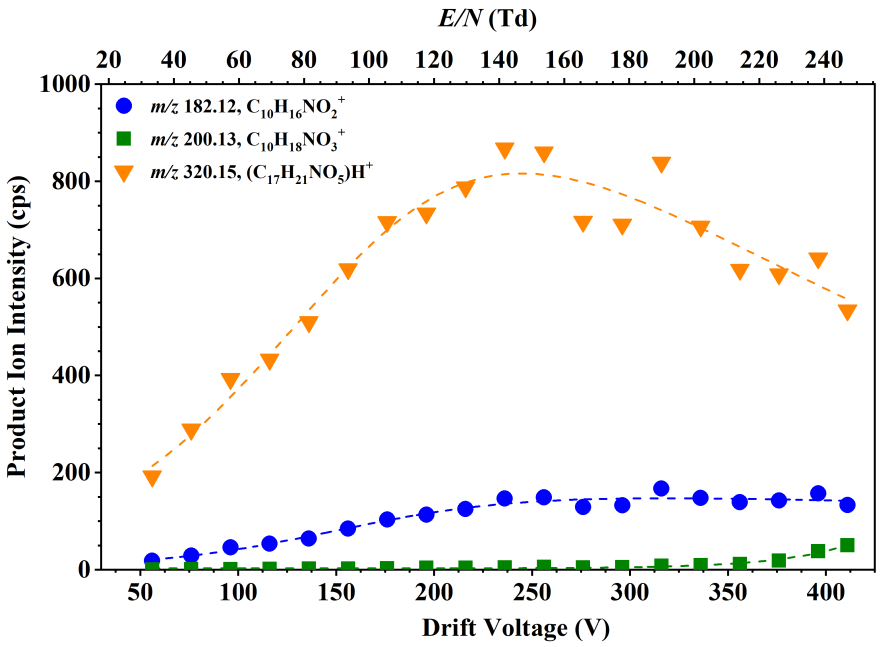

(b)

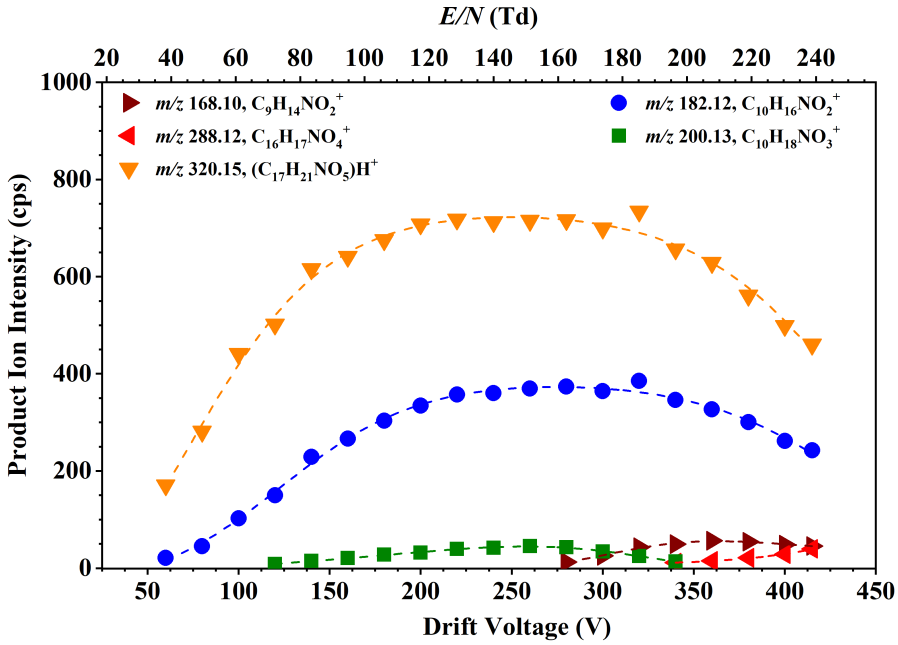

Figure 3.24: Product ion signal intensities in counts per second of the product ions resulting from reactions of $H_3O^+.(H_2O)_n$ (n = 0, 1, 2) with o-hydroxycocaine as a function of the drift voltage and the reduced electric field in (a) normal and (b) humid conditions.

been found for any other cocaine metabolite, although it has been discussed in the literature. Musshoff *et al.* claim that the ion at m/z 200 has the same structure as protonated methyl ecgonine and it is formed through the loss of the hydroxy-benzoyl moiety [95]. Furthermore, Minoli *et al.* used $C_{10}H_{18}NO_3^+$, as well as the protonated parent molecule and other ions, to quantify cocaine consumption by monitoring the m-hydroxycocaine isomer in hair samples using UHPLC-MS/MS [96].

3.3.11 Concerns regarding benzoylecgonine

Benzoylecgonine ($C_{16}H_{19}NO_4$, Figure 3.25) is the main metabolite of cocaine. PTR-MS investigations of benzoylecgonine have been carried out with inconclusive results. This led to an attempt of measuring ecgonine ($C_9H_{15}NO_3$) and ecgonidine ($C_9H_{13}NO_2$) in PTR-MS, which were similarly unsuccessful.

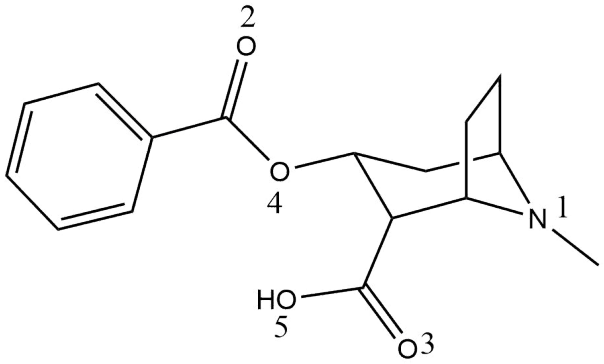

Figure 3.25: Structure of benzoylecgonine.

Preliminary PTR-MS measurements (not included in this thesis) show that the reaction of benzoylecgonine with hydronium and its water clusters yield mostly protonated benzoic acid, with traces of the MH^+ ion at m/z 290. This is surprising since the energetics calculated through DFT (not included in this thesis either) predict similar product ions to those observed from the reaction of cocaine with $H_3O^+.(H_2O)_n$ (n = 0, 1, 2, 3). At present we have no explanation for this. An answer for this issue could lie in the fact that benzoylecgonine, ecgonine and ecgonidine have a carboxylic acid group instead of the methyl ester group in cocaine, methyl ecgonine, norcocaine, methyl ecgonidine and o-hydroxycocaine, or the ethyl ester group in cocaethylene and ethyl ecgonine.

A remaining question is why it was possible to measure methyl ecgonine, when this compound

is also derivatised for GC-MS analysis? An answer to this question might be in the differences in the value of the melting points, which is 98 °C for cocaine and 80.6 °C for methyl ecgonine, but more than 100 °C higher for benzoylecgonine, ecgonine and ecgonidine, having values of 195 °C, 205 °C and 228 °C, respectively. These values were obtained from Haynes for cocaine, benzoylecgonine, ecgonine and ecgonidine, while the melting point of methyl ecgonine was the predicted one from the U.S. Environmental Protection Agency [91, 97]. As indicated in subsection 3.2.1, the TDU was set at 150 °C. This temperature was enough to desorb most compounds into the PTR-MS instrument, but not benzoylecgonine, ecgonine and ecgonidine. Further measurements of benzoylecgonine at the highest achievable TDU temperature were performed (*i.e.* front plate at 223 °C, back plate at 195 °C) where the protonated parent ion was not observed even at low *E/N*. There is however the risk that the sample is being thermally decomposed at such high temperatures, so it is concluded that proper analysis was not possible with the present TDU and PTR-MS instrument. Therefore, all the results related to benzoylecgonine are considered preliminary at the present time and further investigations are needed.

3.4 Conclusions and further remarks

PTR-MS and theoretical (DFT) studies of the reactions of cocaine and related compounds with $(H_2O)_nH_3O^+$ have been presented. Volatile compounds (*i.e.* benzoates and isobutyrates) were studied through headspace analysis, while the TDU was used for the thermal desorption of solid samples into the PTR-MS instrument. Experiments were performed under two different humidities in the drift tube: the so-called "normal" and "humid" conditions, although for some compounds only the normal conditions data were acquired. The product ion signal intensities were given in counts per second as a function of the drift voltage and the reduced electric field. The data were acquired across the broadest range of drift tube voltages that the PTR-MS instrument could provide, resulting in a wide range of *E/N* values investigated. This is in contrast to the narrow 120 - 140 Td *E/N* values reported in the literature. The fuller *E/N* study has helped to elucidate the fragmentation pathways.

The loss of an alcohol moiety (*i.e.* MeOH, EtOH or iPrOH in each case) is a common fragmentation pathway observed for all of the substances studied, except the isobutyrate esters. This is supported by the DFT calculations, which reveal that this loss is a barrierless process once

the proton is attached to the ester oxygen. In contrast, DFT reveals that the formation of some of the fragment ions is not thermodynamically allowed and therefore they are formed through electric field-activated collision-induced dissociation, *e.g.* resulting in protonated benzene and other fragment ions.

There is some disagreement between the DFT and the experimental results for the loss of C_2H_4 from ethyl benzoate and ethyl isobutyrate, and the loss of C_3H_6 from isopropyl benzoate. Whilst these reactions are exergonic, they are only observed at certain values of the reduced electric field. These fragmentation pathways must therefore be kinetically rather than thermodynamically driven. The same argument is considered valid to justify the little observed fragmentation with other compounds. The energetics for cocaine and methyl ecgonine predicted a higher abundance of fragment ions than was observed, because the proton is mobile between the protonation sites and the formation of the most fragment ions is exergonic. But PTR-MS results show that the dominant ion is the protonated parent across the whole E/N range, which suggests that the proton goes to the most basic site (*i.e.* the pyrolidine nitrogen N1) and stays sequestered there. Furthermore, using quantum mechanical calculations the transition state for the loss of benzoic acid to yield the ion at m/z 182 has not been found yet. Although it is not observed with the range of collisional energies available in PTR-MS, this ion becomes more abundant than the protonated parent at high enough collisional energies as reported in the mzCloud database for electrospray ionisation measurements of cocaine [98], which confirms the hypothesis of the fragmentation being kinetically rather than thermodynamically driven. The dominant reaction channel was also found to be non-dissociative proton transfer for cocaethylene, ethyl ecgonine, norcocaine, methyl ecgonidine, o-hydroxycocaine and methyl isobutyrate for the whole studied E/N range, although there are no DFT calculations available with which to compare these observations.

Chapter 4

Enhancement of Compound Selectivity Using a Radio Frequency Ion Funnel Proton Transfer Reaction Mass Spectrometer: Improved Specificity for Explosive Compounds

This chapter is a reformatted copy of my published article (reference [1]):

González-Méndez, R., Watts, P., Olivenza-León, D., Reich, D. F., Mullock, S. J., Corlett, C. A., Cairns, S., Hickey, P., Brookes, M. & Mayhew, C. A. Enhancement of Compound Selectivity Using a Radio Frequency Ion-Funnel Proton Transfer Reaction Mass Spectrometer: Improved Specificity for Explosive Compounds. *Analytical Chemistry* **88,** 10624–10630 (2016). DOI: `10.1021/acs.analchem.6b02982`.

4.1 Abstract

A key issue with any analytical system based on mass spectrometry with no initial separation of compounds is to have a high level of confidence in chemical assignment. This is particularly true for areas of security, such as airports, and recent terrorist attacks have highlighted the need

for reliable analytical instrumentation. Proton transfer reaction mass spectrometry is a useful technology for these purposes because the chances of false positives are small owing to the use of a mass spectrometric analysis. However, the detection of an ion at a given m/z for an explosive does not guarantee that that explosive is present. There is still some ambiguity associated with any chemical assignment owing to the presence of isobaric compounds and, depending on mass resolution, ions with the same nominal m/z. In this article we describe how for the first time the use of a radio frequency ion-funnel (RFIF) in the reaction region (drift tube) of a proton transfer reaction – time-of-flight – mass spectrometer (PTR-ToF-MS) can be used to enhance specificity by manipulating the ion/molecule chemistry through collisional–induced processes. Results for trinitrotoluene, dinitrotoluenes, and nitrotoluenes are presented to demonstrate the advantages of this new RFIF-PTR-ToF-MS for analytical chemical purposes.

4.2 Introduction

Ion funnels (IF) have been used since the late 1990s in conjunction with several ionisation and mass spectrometric techniques with a key purpose of increasing ion transmission efficiency and hence instrumental sensitivity and dynamic range [99, 100]. Of relevance to our study, Shaffer *et al.* developed a radio-frequency (RF) IF for focusing and transmitting ions from relatively high pressure ($>$ 1 Torr) ion sources to mass spectrometers [99]. Given that the typical operating pressure of a drift tube used in proton transfer reaction mass spectrometry (PTR- MS) is close to the optimum pressure for the operation of a RFIF, Kore Technology Ltd. designed and developed a RFIF to be incorporated into drift tubes in order to increase the instruments sensitivity [5]. This compact drift tube can simultaneously operate as an ion funnel and a reaction region with a controllable reaction time (dependent on the voltage supplied across the tube). The funnel design and the supplied RF and DC fields act in such a way as to channel reagent and product ions towards the exit orifice of the drift tube so that more ions leave the reaction region into the much lower pressure mass spectrometric region, thereby decreasing the loss of ions that occurs at the end of the drift tube. The proof-of-principle study reported increases in sensitivity of this RFIF-PTR-ToF-MS system that were found to be dependent on the m/z–value of the product ions, but were typically between 1 and 2 orders of magnitude. For example enhancement factors of 45 and 200 were reported for protonated acetaldehyde and protonated acetone, respectively,

at a reduced electric field of 120 Td (where this field refers to the DC voltage applied across the drift tube) [5].

Given that the RFIF forms part of the drift tube, we asked the question whether the high RF fields involved in the operation of an IF could be used to enhance collisions of the reagent and product ions with the buffer gas in the DT and hence change either the nature of the initial chemical ionisation process or induce collisional-induced dissociation, respectively, occurring within the DT? We hypothesised that changes would result from raising the internal energy of the product ions and the energy of the reactions between reagent ions and neutral species through collisional processes as a result of the applied RF field. The real question is whether the RF collisional–induced dissociation would lead to substantial fragmentation, or be more selective resulting in unique product ions that could be used to identify a chemical compound of interest with a higher specificity than that achievable just by using a standard drift tube at a given reduced electric field. Here we report details on a collaborative project involving KORE Technology Ltd. and the University of Birmingham which investigated the application of a RFIF drift tube of a PTR-ToF-MS for improved selectivity using several explosives as illustrative compounds, namely 2,4,6-trinitrotoluene (TNT), 2,4-, 2,6- and 3,4- dinitrotoluene (DNT) and 2-, 3- and 4-nitrotoluene (NT). We will show how the application of a RFIF leads to a higher confidence in compound identification. We thus demonstrate for the first time that the addition of a RFIF to a PTR-ToF-MS results in a more multi- dimensional analytical instrument that improves the selectivity that can be achieved by operating a drift tube of a PTR-MS in DC mode only.

4.3 Methodology

4.3.1 Experimental details

A KORE Technology Ltd. RFIF Series I PTR-ToF-MS was used. Details of KORE's PTR-ToF-MS system with no IF has been described in detail elsewhere [12, 101, 102]. Hence only the salient points of this instrument are provided here. Using a needle valve, water vapour is introduced into a hollow cathode discharge where, after ionisation via electron impact and subsequent ion/molecule processes, the terminal reagent ion is H_3O^+ [31]. These ions are transferred from the ion source into the drift tube (the reaction region) of the PTR-ToF-MS, which is typically at a pressure of 1 mbar and temperature 100 °C, where they encounter the analyte. H_3O^+ ions

react with the analyte M by donating their protons at the collisional rate, providing M has a proton affinity greater than that of water ($PA(H_2O)$ = 691 kJ mol^{-1}). This process can be non-dissociative (resulting in the protonated molecule MH^+) and/or dissociative. Dissociative proton transfer results in product ions which may be useful in the identification of a compound. Fragmentation may be spontaneous upon proton transfer or may require additional energy which is supplied through collisions with the analyte gas occurring during the migration of ions under the influence of the electric field, E. The ratio of E to the buffer gas number density, N, is an important parameter (known as reduced electric field) which determines the mean collisional energy of ions with the neutral buffer gas. Hence it is the parameter often referred to and changed for investigating product ion branching ratios [6, 15, 103–108].

The IF (schematically shown in Figure 2.4) consists of 29 stainless steel plates of 0.2 mm thickness, mounted on precision-machined ceramic rods at an even spacing of 3.2 mm per plate. Tabs on the electrodes permit a resistor chain on a ceramic strip to be connected in addition to two capacitor stacks which allow the RF to be applied to the second half of the reactor. The orifice diameters of the plates through the first half of the stack are 40 mm, as used in the standard drift tube reactor. In the second half of the drift tube the orifice diameter steadily decreases to 6 mm at the final plate before the exit orifice. Across the complete ion- funnel a DC voltage is applied driving ions axially. When just operating with this voltage we shall refer to the instrument as operating in DC-only mode. In addition to this, to the second part of the drift tube a RF field can be applied. Although the RF field frequency and amplitude are two extra parameters that can be manipulated, they are kept fixed unless otherwise stated at a frequency of ∼760 kHz, which corresponds to the resonance frequency of the electronic circuitry involved, and a peak-to-peak amplitude of 200 V. The RF field is superimposed on the DC voltage gradient across the drift tube.

The main purpose of the RF field is to focus ions radially by creating repulsive effective potentials at the edges of the electrodes. However, in addition to this intended purpose, the RF results in ions oscillating between electrodes as they drift down the reactor. This gives ions higher collisional energies than those in the first half of the drift tube. We shall refer to operating the instrument with the RF on as RF-mode. At the end of the drift tube is a 400 µm orifice, through which ions enter the ion transfer region for ToF-MS.

The use of specifying a reduced electric field, E/N, is an appropriate parameter to use in the

DC-only mode, because it is well defined. In the RF-mode (ion funnel on) the presence of DC and RF electric fields complicates the situation, because the electric field strength varies with distance from the RF electrodes, so that specifying a reduced electric field is not appropriate. Barber *et al.* simply adopted an empirical effective reduced electric field by finding operating conditions for the ion-funnel drift tube that matched the performance of the same drift tube when operated under DC-only mode [5]. However, given that it is uncertain what the effective reduced electric field means, in this paper we use the DC voltage (V_{drift}) applied across the drift tube as the independent variable.

A thermal desorption unit (TDU) connected to the inlet of the drift tube was used to introduce the explosive samples, details of which have been given elsewhere [12]. The TDU, connecting lines and drift tube were operated at a temperature of 150 °C. PTFE swabs (ThermoFisher Scientific), onto which known quantities of explosives were deposited, were placed into the TDU. The swabs came prepared from the manufacturer mounted on rectangular cardboard for easy insertion into the TDU. Once a seal was created, a carrier gas (in this study laboratory air) is heated to the temperature of the TDU before it flows through a series of holes in a heated metal plate. This heated air then passes through the swab and into the inlet system driving any desorbed material through to the drift tube creating a temporal concentration "pulse" of typically between 10 – 20 seconds of an explosive in the drift tube [12]. Each swab provided one measurement, which was replicated three times and then the results were averaged and any background signals were subtracted.

Explosive standards were purchased from AccuStandard Inc., New Haven, CT. Typically these standards contained 0.1 mg of the explosive compound in 1 ml of solvent. For TNT, 2,4- and 2,6-DNT, and the NTs this involved an acetonitrile:methanol (1:1) mix. 3,4- DNT was just mixed with methanol. These samples were diluted in the appropriate solvent(s) (HPLC grade) to provide the required quantity of an explosive. Typically 1 µl of a solvent containing the required mass of an explosive was spotted onto a PTFE swab.

4.3.2 Electronic structure calculations

To aid in the interpretation of the experimental results a series of electronic structure calculations have been undertaken at 298 K. These involve density functional theory calculations using the GAUSSIAN09 PROGRAM with the GaussView 5 interface [57]. The B3LYP functional with

the 6-31+G(d,p) basis set was used throughout. Although it is appreciated that the drift tube temperature and the effective ion temperature are greater than 298 K, with the effective ion temperature being uncertain, the thermochemical calculations simply provide us with an indicator as to whether a reaction pathway is energetically possible or not.

4.4 Results and discussion

4.4.1 Reagent ions

Before we begin discussing the results of the explosives, it is informative to present details on the reagent ion signal as a function of drift tube voltage, comparing intensities for DC-only mode (Figure 4.1(a)) and RF-mode (funnel-on) (Figure 4.1(b)) under identical operating conditions of hollow cathode and drift tube pressures and temperature. The observed decrease of H_3O^+ reagent ion signal with decreasing drift tube voltage is predominantly a result of the clustering with water molecules in the drift tube, which are not broken-up through collisions at lower drift tube voltages. The marked decrease in total reagent ion signal below about 50 Td is considered to be a result of the low source drift (SD) potential, which scales with the DC drift tube potential. As the SD voltage decreases we can expect that fewer reagent ions reach the reactor entry.

Figure 4.1(a) shows that by 100 Td the H_3O^+ reagent ion signal has reduced significantly and that the protonated water clusters start to dominate at the lowest reduced electric field corresponding to a voltage drop across the drift tube of about 200 V under the operational temperature and pressure values used. (The actual percentage of protonated water clusters for fixed E/N is also strongly dependent on the humidity of the buffer gas in the drift tube, which is dependent on the amount of forward flow of H_2O from the ion source into the drift tube and the humidity of the laboratory air.) In RF-mode no protonated water clusters are observed, because they are broken-up through collisions in the RFIF region of the drift tube. Furthermore, at about 120 V the H_3O^+ intensity is approximately at its maximum value. As the drift voltage decreases, the reagent ion signal decreases. However, even at a drift tube voltage of only 20 V (which in DC-only mode would correspond to a reduced electric field of only about 10 Td) there is still a significant reagent ion count. This enhancement of reagent ion signal at low drift tube voltages can only be a result of the trapping that the RF field provides thereby reducing the diffusional loss that occurs in DC-only mode under low drift tube voltages.

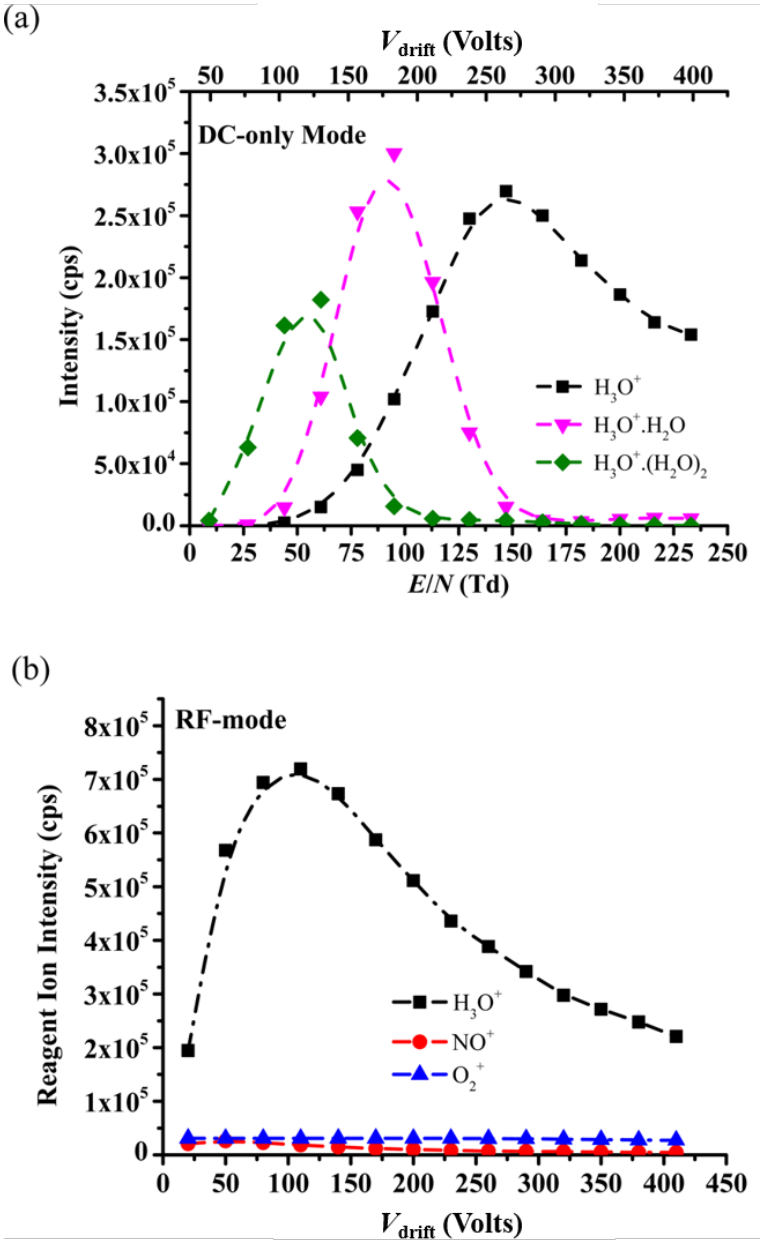

Figure 4.1: Ion intensities in counts per second (cps) of the water reagent ions present in the drift tube as a function of drift tube voltage (a) in DC-only mode and (b) in RF-mode (ion funnel on). For (b) the ion signals at m/z 30 (NO^+) and 32 (O_2^+) are presented because although low intensity they are still significant and are observed as a result of the improved ion transmission in RF-mode. In the DC-mode the signal intensities of these ions are negligible and are therefore not presented. The RF field in the RF-mode has a frequency of ∼760 kHz and a peak-to-peak amplitude of 200 V.

4.4.2 2,4,6-trinitrotoluene (TNT)

Using both PTR-ToF-MS and PTR-Quad-MS systems Sulzer *et al.* have previously shown that there is an unusual dependence of the intensity of protonated TNT on the reduced electric field in that there is an increase in the sensitivity of detection with increasing *E/N* [6, 109]. This increase continues until a maximum is reached at about 180 Td, after which the signal intensity shows the more usual behaviour of decreasing with increasing *E/N*. This is opposite to what is commonly found in PTR-MS studies because, with reduced reaction times, fragmentation to non-specific product ions, and reduction in ion transmission the protonated molecule intensity reduces with increasing *E/N*. The explanation of this unusual intensity dependence for $TNTH^+$ has been described in detail [6]. In brief, it is a result of a secondary reaction of $TNTH^+.H_2O$ (which is readily formed at low *E/N*) with H_2O leading to a terminal ion which does not contain TNT, namely $H_3O^+.H_2O$.

In the DC-only mode and when a product ion signal is detected, for all *E/N* values investigated only one product ion is observed that contains the explosive, namely protonated TNT at *m/z* 228. However, in the RF mode, another fragment ion is found at *m/z* 210, the intensity of which increases with decreasing drift tube voltage (*i.e.* decreasing *E/N* in the DC mode) down to values under which the PTR-ToF-MS does not perform in the DC mode owing to a lack of sufficient transmission of ions to the mass spectrometer (Figure 4.1(a)). Typical results obtained for TNT are shown in Figure 4.2. That the fragment ion *m/z* 210 intensity increases with decreasing drift tube voltage (Figure 4.2) is perhaps not what is expected given that decreasing DC voltage means lower collisional energies. However, that only applies in the first half of the drift tube. As the drift tube voltage is reduced more collisions in the RFIF region of the drift tube occur, which in turn enhances collisional–induced dissociation. Following proton transfer the protonated molecule gains sufficient internal energy through collisions in the RFIF section of the drift tube to eliminate H_2O (Equations 4.1–4.2):

$$H_3O^+ + TNT \rightarrow (TNTH^+)^* + H_2O \tag{4.1}$$

$$(TNTH^+)^* + M \rightarrow [TNT\text{-}H_2O]H^+ + H_2O + M \tag{4.2}$$

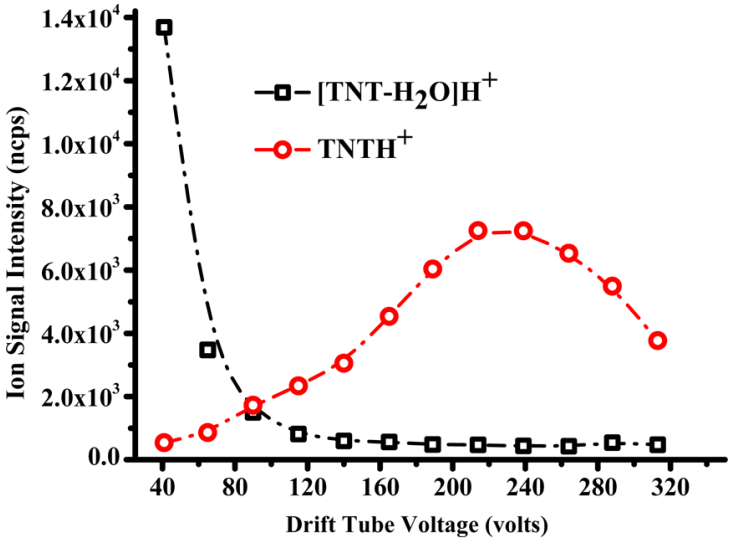

Figure 4.2: Product ion intensities as a function of drift tube voltage in RF mode. The data have been taken using 100 ng of TNT. The ion signals have been normalized to 10^6 H_3O^+ reagent ions and drift times. (The lines used in all graphs are just a guide to the eye.)

where M is a buffer gas molecule. Thus specificity can be increased by either switching off and on the RFIF at a specific drift tube voltage or by switching the drift tube voltage. Note that a minor percentage of the observed m/z 210 results from the reaction of the O_2^+ (always present in low concentrations in the drift tube as an impurity ion) with TNT via a dissociative charge transfer process leading to the loss of OH from TNT^+ [105].

That the reaction pathway leading to the elimination of H_2O is overall energetically favourable (Table 4.2) but is only observed in RF mode, is an indication that there must be an energy barrier for the pathway in Equation 4.2. Evidence of this is provided from the results obtained when investigating the effects of changing the RF amplitude at fixed drift tube voltages and fixed frequency: Figure 4.3 provides a summary of these measurements, which shows that as the RF peak-to-peak voltage is decreased the intensity of the m/z 210 decreases for all drift tube voltages.

The initial step leading to m/z 228 is the transfer of a proton from H_3O^+ to TNT. Protonation of TNT can occur on the nitro groups at the 2- and 4- positions, both having similar proton affinities, although as elimination of water from $TNTH^+$ will presumably involve the methyl group, only protonation of the nitro group in the 2- position is of relevance. However, protonation on the 4 nitro will occur (the *PA* and *GB* are slightly greater than the 2 nitro) and this will reduce

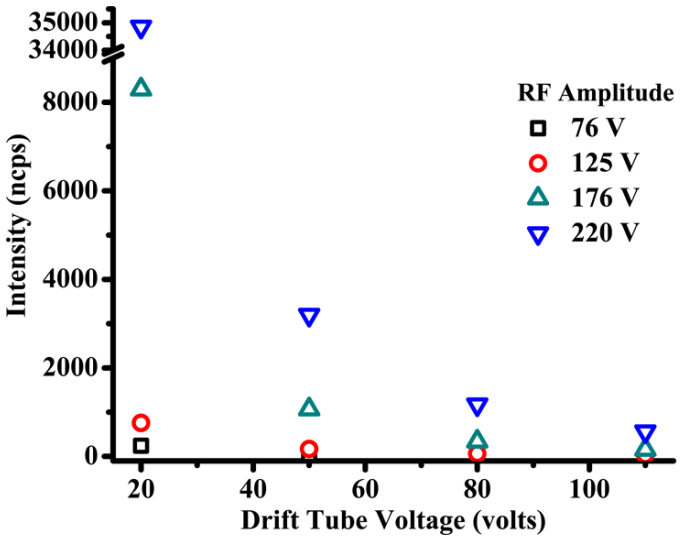

Figure 4.3: Intensities in ncps of the product ion [TNT - H_2O]H^+ as a function of drift tube voltage and RF amplitude (volts) with the frequency kept at 760 kHz (±3%).

Table 4.1: Energetics for the proton transfer from H_3O^+ to TNT calculated using the B3LYP functional and the 6-31+G(d,p) basis set. The structures *syn* and *anti*, corresponding to protonation in the 2- position to yield $TNTH^+(2NO_2syn)$ and $TNTH^+(2NO_2anti)$ in this table, are shown in Figure 4.4. TS syn/anti refers to the transition of state between these structures. $TNTH^+(4NO_2)$ corresponds to protonation of TNT in the 4- position.

Products	ΔH_{298} **(kJ mol^{-1})**	ΔG_{298} **(kJ mol^{-1})**
$TNTH^+(2NO_2syn)$ + H_2O	-46	-47
$TNTH^+(2NO_2anti)$ + H_2O	-55	-55
$TNTH^+(4NO_2)$ + H_2O	-68	-60
TS syn/anti + H_2O	-9	-5

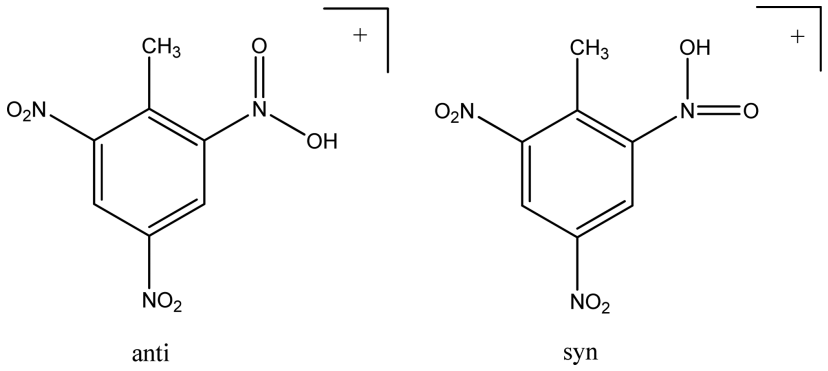

Figure 4.4: Two possible configurations resulting from protonation of TNT in the 2- position.

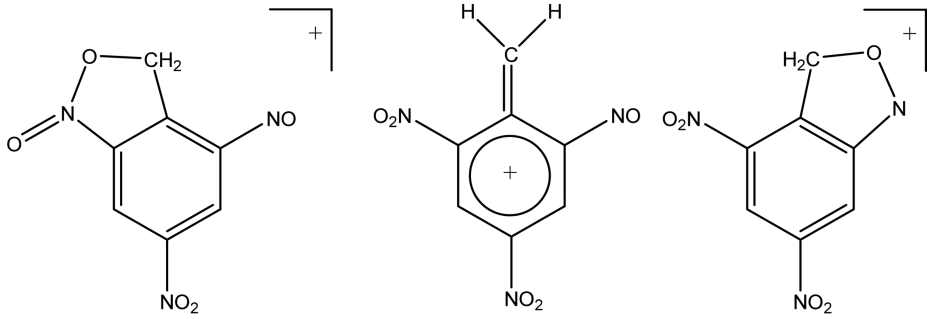

TNTH$^+$- H_2O (a) TNTH$^+$- H_2O (b) TNTH$^+$- H_2O (c)

Figure 4.5: Stable structures of the [TNT - H_2O]H^+ ion.

Table 4.2: Energetics for the elimination of water from TNT following proton transfer from H_3O^+ for the three stable structures shown in Figure 4.5.

Products	ΔH_{298} **(kJ mol^{-1})**	ΔG_{298} **(kJ mol^{-1})**
TNTH$^+$ - H_2O (a) + $2H_2O$	-104	-145
TNTH$^+$ - H_2O (b) + $2H_2O$	+47	-7
TNTH$^+$ - H_2O (c) + $2H_2O$	-128	-168

the amount of TNTH$^+$ available to lose water. Two configurations are possible for protonation in the 2 position as illustrated in Figure 4.4, with the anti being slightly more stable by ca. 8 kJ mol^{-1}. The transition state energetics for interconversion are ΔH_{298} = +46 kJ mol^{-1} and ΔG_{298} = +51 kJ mol^{-1} above the anti-conformation, but whichever is formed there is sufficient energy in the initial protonation to allow rapid interconversion (Table 4.1).

There are three stable structures for the ion remaining after the elimination of water from TNTH$^+$ (Figure 4.5). A fourth structure, similar to [TNTH$^+$ - H_2O (b)] with the hydrogens of the methylene group orthogonal to the ring, proved to be unstable and rearranged to [TNTH$^+$ - H_2O (a)] . The energetics for the transformation of TNTH$^+$ to [TNTH$^+$ - H_2O (a-c) + H_2O] are given in Table 4.2.

Various attempts were made to find transition states for these possible reactions but all led to [TNTH$^+$ - H_2O (c)], though interestingly the transition state had a close resemblance to [TNTH$^+$ - H_2O (b)]. The transition state was characterised by one imaginary frequency and the internal reaction coordinate leading to [TNTH$^+$ - H_2O (c)] in the forward direction and TNTH$^+$ with the proton on the 2-nitro group in the syn conformation in the reverse direction. The activation energies relative to [TNT + H_3O^+] are ΔH_{298} = +158 kJ mol^{-1} and ΔG_{298} = +162 kJ mol^{-1}.

The presumption that the elimination of water from protonated TNT can only occur when

the methyl and nitro groups are adjacent to each other was readily tested by investigating isomers of DNT and NT. For those isomers that satisfy the condition of an adjacent nitro and methyl group, then [DNT - H_2O]H^+ and [NT - H_2O]H^+ fragment ions should be observed, otherwise not. Thus we predicted to observe elimination of water from the 2,6-DNT, 2,4-DNT and 2-NT but not from 3,4-DNT, 3-NT or 4-NT following proton transfer in RF mode.

4.4.3 Dinitrotoluenes

In both the RF-mode and DC-only modes for 3,4-DNT the only primary product ion that is observed with any significant intensity for all drift tube voltages is the protonated molecule. That no m/z 165 is observed, which would correspond to the elimination of water from the protonated molecule, is in agreement with our prediction, because neither nitro group are adjacent to the methyl group. With decreasing drift tube voltage the protonated 3,4-DNT clusters with H_2O, leading to a reduction in the $DNTH^+$ signal. Whilst this is particularly significant in the DC-only mode, with $DNTH^+.(H_2O)_n$ (n = 1, 2 and 3) ions becoming the dominant product ions by about 100 Td, some water clustering is still observed in the RF-mode. For example at a drift tube voltage of 20 V the percentage branching ratios are approximately 70%, 20% and 10% for the production of $DNTH^+$, $DNTH^+.H_2O$, and $DNTH^+.(H_2O)_2$ ions, respectively.

For the 2,4- and 2,6-DNT isomers, at low drift tube voltages, in addition to an observed ion at m/z 201 corresponding to the $DNTH^+.H_2O$ in the RF-mode, a product ion is observed at m/z 165, which is [DNT-H_2O]H^+. Figure 4.6 illustrates this for 2,6-DNT, which shows that the probability for the elimination of water increases with decreasing drift tube voltage (the results for 2,4-DNT in RF-mode are similar, although the production for [DNT-H_2O]H^+ is less by about 10%). In the DC-only mode, m/z 165 is also observed for 2,6-DNT, but its intensity only becomes significant when a high drift tube voltage is applied (*i.e.* at reduced electric fields above about 180 Td), and even then the percentage ion product distribution is only approximately 10% (Figure 4.7). However, this can explain the slight increase in the production of m/z 165 in Figure 4.6 when the applied drift tube voltage is above about 275 V. With increasing drift tube voltage additional fragment ions are found at m/z 136 and 91, corresponding to an elimination of HONO and $2NO_2$, respectively, from the protonated molecule. These two ions are also found with significant intensities for 2,6-DNT when operating in the DC-only mode when the reduced electric fields is greater than about 160 Td. That $DNTH^+.H_2O$ is observed in the RF mode at

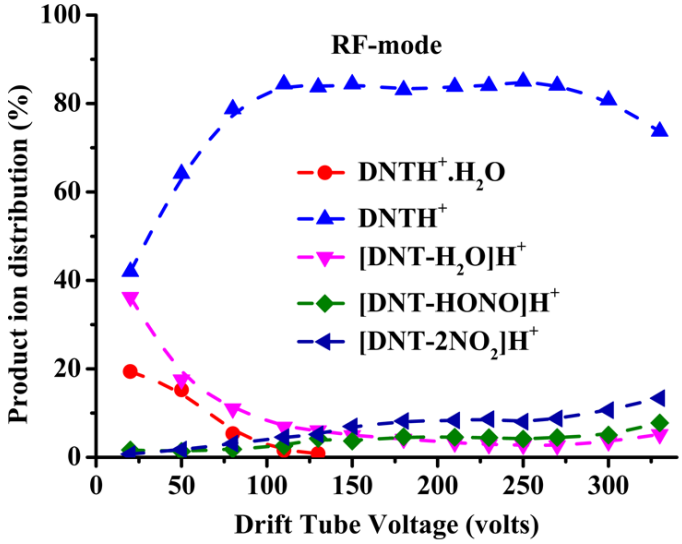

Figure 4.6: Percentage product ion distributions resulting from the reaction of H_3O^+ with 2,6-DNT in the RF-mode including the secondary process resulting in the association of the protonated molecule with water as a function of supplied drift tube voltage. The RF field has a frequency of ~760 kHz and a peak-to-peak amplitude of 200 V.

low drift tube voltages, when no protonated water clusters are observed (Figure 4.1 (b)), requires some explanation. We propose that following a collision the energy involved is distributed in more degrees of freedom for $DNTH^+.H_2O$ than for $H_3O^+.(H_2O)_n$ and hence it is less likely for energy to be concentrated into losing the water molecule.

Building on the comprehensive investigation of the TNT system we can go straight to the salient structures and energetics for the loss of water from 2,4-DNT and 2,6-DNT following proton transfer from H_3O^+. These calculations are given in Table 4.3 (a) and (b), respectively.

4.4.4 Nitrotoluenes

In order to further investigate the requirement of methyl and nitro functional groups to be adjacent in order to facilitate the elimination of water when using the RFIF, the three isomers of nitrotoluene have been investigated. We can expect in the RF-mode that only 2-NT should have a reaction pathway which would lead to the elimination of water following proton transfer from H_3O^+. For 3-NT and 4-NT no such elimination should occur. A review of the resulting mass spectra for all three isomers shows that that is the case. However, the nitrotoluenes are more complicated than TNT and the DNTs, because other product ions are observed even at the lowest

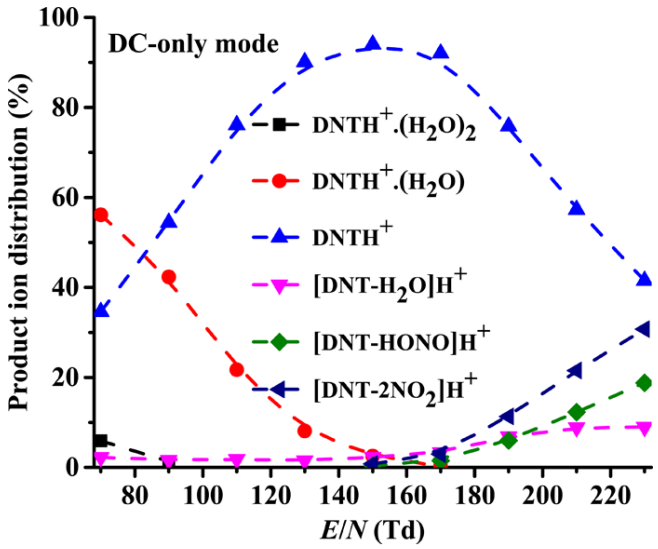

Figure 4.7: Percentage product ion distributions resulting from the reaction of H_3O^+ with 2,6-DNT in the DC-only mode, including the secondary process resulting in the association of the protonated molecule with water, as a function reduced electric field.

Table 4.3: Energetics for the elimination of water from (a) 2,4-DNT and (b) 2,6-DNT following proton transfer from H_3O^+.

(a)		
Products	ΔH_{298} **(kJ mol^{-1})**	ΔG_{298} **(kJ mol^{-1})**
2,4-DNTH$^+$(syn) + H_2O	-89	-87
2,4-DNTH$^+$(anti) + H_2O	-96	-95
TS syn/anti + H_2O	-21	-16
TS for loss of H_2O + H_2O	+126	+130
2,4-DNT-H_2O (c) + 2H_2O	-146	-187
(b)		
Products	ΔH_{298} **(kJ mol^{-1})**	ΔG_{298} **(kJ mol^{-1})**
2,6-DNTH$^+$(syn) + H_2O	-87	-88
2,6-DNTH$^+$(anti) + H_2O	-95	-95
TS syn/anti + H_2O	-42	-38
TS for loss of H_2O + H_2O	+117	+120
2,6-DNT-H_2O (c) + 2H_2O	-177	-217

Table 4.4: Energetics for the elimination of water from 2-NT following proton transfer from H_3O^+.

Products	ΔH_{298} **(kJ mol^{-1})**	ΔG_{298} **(kJ mol^{-1})**
2-NTH$^+$(syn) + H_2O	-132	-138
2-NTH$^+$(anti) + H_2O	-105	-110
TS syn/anti + H_2O	-71	-76
TS for loss of H_2O + H_2O	+82	+78
2-NT-H_2O + 2H_2O	-93	-126

drift tube voltage. The NT isomers show significant fragmentation following proton transfer. This is found to occur in not only the RF-mode but also in the DC-only mode. In addition to the elimination of water, which is not the dominant product ion, channels corresponding to the elimination of C_2H_4, NO, CH_3NO, NO_2 and HONO are observed in both modes. This is illustrated in Figure 4.8 for 2-NT when operating (a) in the RF-mode and (b) in the DC-only mode. At low drift tube voltages NTH$^+$.H_2O is observed (Figure 4.8(a)) in the RF mode, presumably for reasons described above for DNT.

Table 4.4 presents the DFT energetics calculations for the elimination of water for 2-NT following proton transfer from H_3O^+.

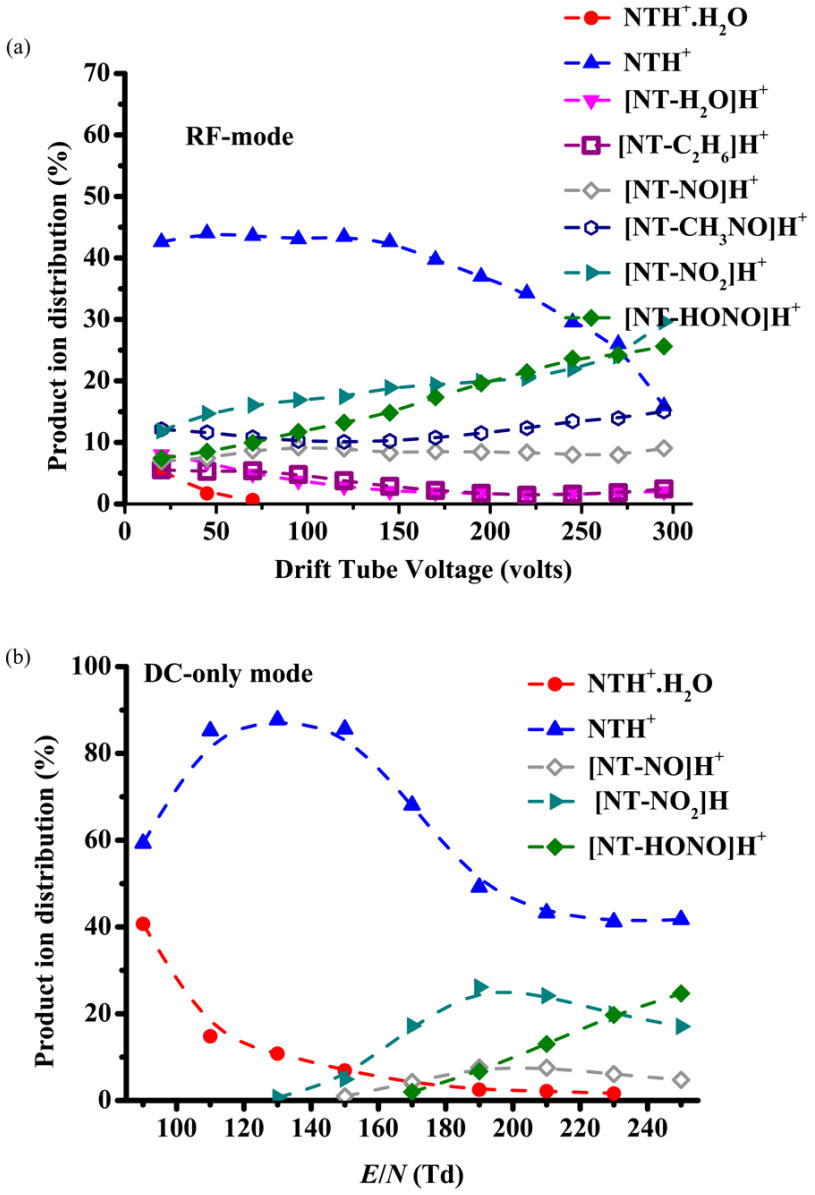

Figure 4.8: Percentage product ion distributions resulting from the reaction of H_3O^+ with 2-NT in (a) RF-mode and (b) DC-only mode as a function drift tube voltage. Included are the secondary ion/molecule processes resulting in the association of the protonated molecule with water. The RF field has a frequency of ∼760 kHz and a peak-to-peak amplitude of 200 V.

4.5 Conclusions

A PTR-ToF-MS equipped with a radio frequency ion funnel has been used in an unusual way to induce fragmentation of product ions through changes in collisional-induced dissociation. We have illustrated how this can be used to improve compound specificity by monitoring the ion signal in the RF-mode. We propose that the rapid switching between the RF and DC modes would be the best method to enhance selectivity. We are currently developing the instrument to achieve this, and this will be the subject of another paper. The key point of this work is that in place of major and costly changes in instrumental design to improve chemical specificity, such as having a high mass resolution time-of-flight mass spectrometer or adding a pre-separation technique, which also makes the instrument unacceptable for use in security areas, a new analytical method has been described which at its heart manipulates the ion chemistry.

Chapter 5

Selective Reagent Ion Mass Spectrometric Investigations of the Nitroanilines

This chapter is a reformatted copy of my published article (reference [2]):

Olivenza-León, D., Mayhew, C. A. & González-Méndez, R. Selective Reagent Ion Mass Spectrometric Investigations of the Nitroanilines. *Journal of the American Society for Mass Spectrometry,* 1–8 (2019). DOI: 10.1007/s13361-019-02325-0.

5.1 Abstract

This paper presents an investigation of proton and charge transfer reactions to 2-, 3- and 4-nitroaniline ($C_6H_6N_2O_2$) involving the reagent ions $H_3O^+.(H_2O)_n$ (n = 0, 1 and 2) and O_2^+, respectively, as a function of reduced electric field (60 - 250 Td), using Selective Reagent Ion – Time-of-Flight – Mass Spectrometry (SRI-ToF-MS). To aid in the interpretation of the $H_3O^+.(H_2O)_n$ experimental data, the proton affinities and gas-phase basicities for the three nitroaniline isomers have been determined using density functional theory. These calculations show that proton transfer from both the H_3O^+ and $H_3O^+.H_2O$ reagent ions to the nitroanilines will be exoergic and hence efficient, with the reactions proceeding at the collisional rate. For proton transfer from H_3O^+ to the NO_2 sites, the exoergicities are 171 kJ mol^{-1} (1.8 eV), 147 kJ mol^{-1} (1.5 eV), and 194 kJ mol^{-1} (2.0 eV) for 2-, 3- and 4-nitroaniline, respectively. Electron transfer from

all three of the nitroanilines is also significantly exothermic by approximately 4 eV. Although a substantial transfer of energy occurs during the ion/molecule reactions, the processes are found to proceed predominantly via non-dissociative pathways over a large reduced electric field range. Only at relatively high reduced electric fields ($>$ 180 Td) is dissociative proton and charge transfer observed. Differences in fragment product ions and their intensities provides a means to distinguish the isomers, with proton transfer distinguishing 2-NA from 3- and 4-NA, and charge transfer distinguishing 4-NA from 2- and 3-NA, thereby providing a means to enhance selectivity using SRI-ToF-MS.

5.2 Introduction

Selective Reagent Ion Mass Spectrometry (SRI-MS) is a variation of the soft chemical ionisation technique PTR-MS that uses not only H_3O^+ but also other reagent ions, like O_2^+ and NO^+, that undergo charge transfer with the analyte rather than proton transfer [31]. It has been proved to be a useful tool in several fields, like the environmental sciences, food sciences, atmospheric chemistry, health science and homeland security [6, 16, 17, 104, 108–114]. Like PTR-MS, SRI-MS is used to investigate ion/molecule reactions occurring inside a drift tube maintained at a known pressure, temperature, humidity and collisional energy. Then analyte molecules of interest are introduced through the inlet pipe (typically without pre-separation) into the drift tube, where they meet the reagent ions, and the proton or charge transfer reaction occurs. The switching between the different reagent ion species can be done quick enough ($\sim$100 ms), which makes SRI-MS a suitable tool for transient experiments.

Over the last few years, many projects have been conducted to confirm the applicability of SRI-MS to Homeland Security [1, 6, 12, 14, 104–106, 109, 115–119]. The main achieved goals are the development of instrumentation and the improvement of our understanding of the ion/molecule reactions occurring in the drift tube. The former includes the use of different reagent ions [13], new sampling methods [12], implementation of radio frequency ion funnels [1, 5] and rapid electric field switching [14]. One of the drawbacks of SRI-MS is that it is not possible to directly distinguish between isomeric compounds, although there are exceptions [70]. Here we present a study of the reactions of three nitroaniline (NA) isomers with both O_2^+ and H_3O^+ as a function of the reduced electric field. The main goal is to determine if they can be

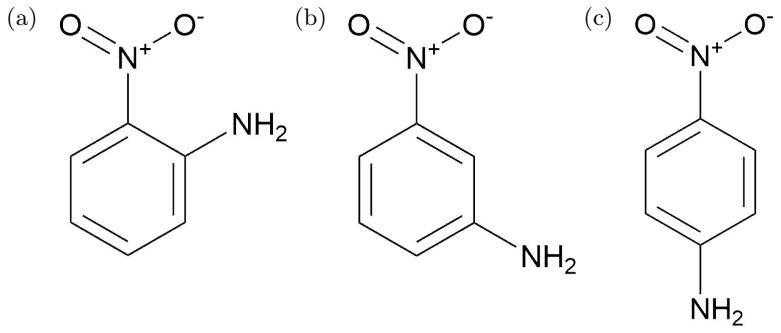

Figure 5.1: Structure of (a) 2-nitroaniline, (b) 3-nitroaniline and (c) 4-nitroaniline.

distinguished without initial pre-separation by solely enhancing the ion/molecule reactions using different reagent ions.

The structures of 2-, 3- and 4-nitroaniline are shown in Figure 5.1. Nitroanilines ($C_6H_6N_2O_2$) are chemical compounds that are a derivative of aniline, a known reactant in the polymer industry, and are present in the fabrication of dyes, pesticides and pharmaceuticals products [120, 121]. Therefore, they are widespread in the environment. Also, their aromatic ring and nitro functional group makes them show explosive behaviour and hence this study represents a continuation of PTR-MS studies in the same topic [1, 6, 12, 14, 104–106, 109, 116–119]. Furthermore, nitroanilines (specially the 4- isomer) are toxic compounds [122]. It is then key to have the analytical tools to rapidly and accurately detect and analyse them.

In the present study, the product ion distributions as a function of the reduced electric field obtained from the reactions of 2-, 3- and 4-nitroaniline with H_3O^+ and O_2^+ are presented, the role of the nitro group in these reactions is evaluated, and quantum chemical calculations are used to obtain the proton affinity and gas phase basicities, complementing the experimental work.

5.3 Experimental details

5.3.1 Selective Reagent Ion-Mass Spectrometry (SRI-MS)

The SRI-MS instrument used was a KORE Technology Ltd PTR-ToF-MS, and the different reagent ions were generated injecting different gases into its ion source. This device has been described in detail elsewhere [1, 31], so only a shallow overview will be given here.

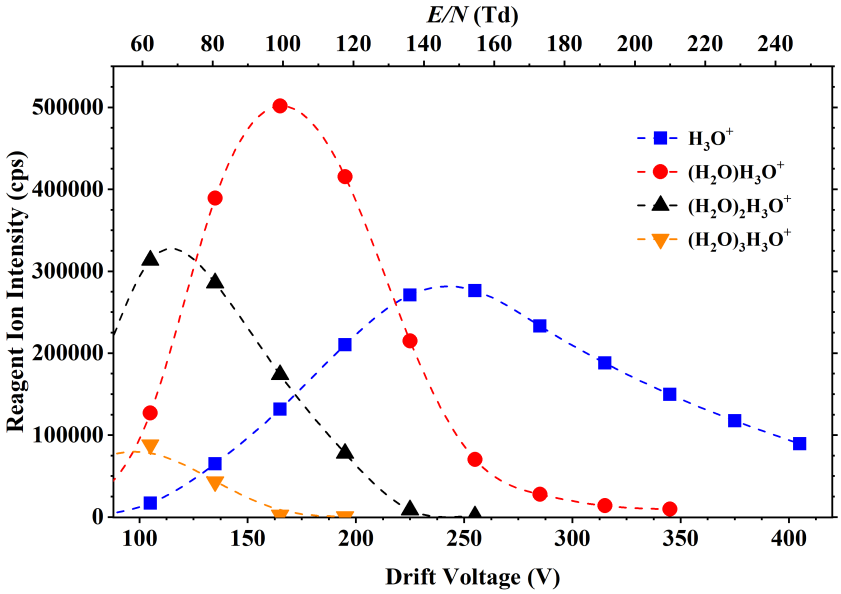

Figure 5.2: Ion intensities in counts per second of the water reagent ions ($H_3O^+.(H_2O)_n$, n = 0, 1, 2 and 3) recorded at the detector of the KORE SRI-ToF-MS as a function of reduced electric field (approximately 60 - 250 Td).

5.3.1.1 Proton Transfer Reaction Mode

This mode has been described in chapter 2 and corresponds to the regular use of the instrument, where H_3O^+ (and the relevant water cluster ions) react with the analyte through the reactions described in Equation 1.1 and Equation 1.2. It is important to note, however, that, although proton transfer can be spontaneously dissociative, the energy available upon proton transfer from a protonated water cluster is much less than that compared to proton transfer from hydronium. Nevertheless, the reduced electric field in the reactor can trigger collisional-induced dissociation when the proton transfer process has been non-dissociative, enhancing fragmentation of the protonated molecule.

The reagent ions for proton transfer mode were produced through the injection of water into the hollow cathode. These are then transferred into the drift tube. Figure 5.2 presents the reagent ion intensities (in counts per second) at the end of the drift tube as a function of the E/N and it shows that $H_3O^+(H_2O)_n$ for n = 0, 1 and 2 are the most abundant water clusters, although the one with n = 3 is also noticeable at low E/N. Only at E/N values of 130 Td of more H_3O^+ becomes the dominant ion. Other impurity or contamination ions can sometimes be

observed in the mass spectra, resulting from the back–streaming of the analyte-containing buffer gas into the hollow cathode. The most usual impurity ions are NO^+ and O_2^+, which, in this case, represented less than 0.5% of the total reagent ion signal for any reduced electric field. Also, the signal corresponding to hydronium and the water cluster ions is usually saturated and the intensity at the ^{18}O isotope was used in each case to calculate the signal of the relevant reagent ion.

5.3.1.2 Charge Transfer Reaction Mode

O_2^+ was generated by injecting pure oxygen (99.998% purity, BOC Gases, Manchester, UK) into the hollow cathode. The O_2^+ ion signal as a function of the reduced electric field is displayed in Figure 5.3. Similarly to the reagent ion in the proton transfer mode, the O_2^+ signal is too large to be directly measured and the $^{18}O^{16}O^+$ isotope at m/z 34 can be used to calculate it. When O_2^+ encounters the analyte in the drift tube, charge transfer occurs if the analyte's ionisation energy (IE) is less than 12.07 eV. However, and contrary to what happens in proton transfer, even if the analyte has an ionisation energy of less than 12.07 eV, the reaction may not be occurring at the collisional rate [123]. Like in proton transfer, charge transfer can be either non-dissociative, yielding the M^+ ion, or dissociative, and fragmentation can be enhanced upon collisionally-induced processes. Regarding contamination and unwanted ions, hydronium can be formed in the ion source if there is residual water vapour but in these experiments it was only ca. 0.1% of the O_2^+ signal.

5.3.2 Chemicals

The samples in this investigation were acquired from Sigma Aldrich (Gillingham, United Kingdom). Each of the three nitroaniline isomers (yellow granulated solids, >98% purity) came in an individual container and they were individually studied (*i.e.* they were not analysed in a mixture). Each of these substances was then used to create a solution of approximately 100 µg/mL of concentration in a mixture of methanol and acetonitrile (analytical grade). 1 µL of this diluted sample was placed on a swab, waiting one minute for the solvent to evaporate before inserting it into the TDU. The vapour pressures of 2-, 3- and 4- nitroaniline are 3.7×10^{-3}, 1.3×10^{-4}, and 4.3×10^{-6} mbar, respectively [124–126].

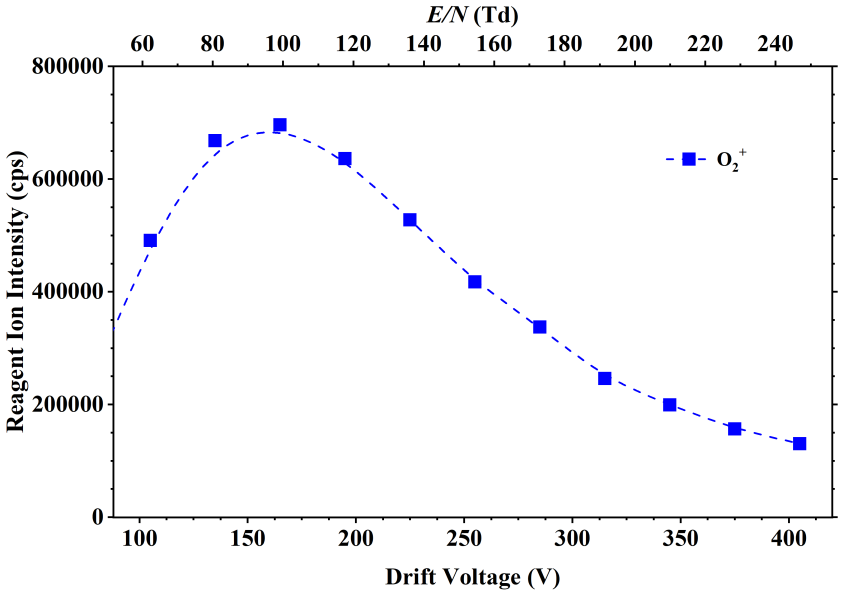

Figure 5.3: Ion intensities in counts per second of O_2^+ recorded at the detector of the KORE SRI-ToF-MS as a function of reduced electric field (approximately 60 - 250 Td).

5.3.3 Operational procedures

The thermal desorption unit, described in subsection 2.3.1 and also elsewhere [12], was used in this study to get the nitroanilines solution into gas phase. The TDU was connected to the inlet line through, which is made of stainless steel passivated with SilcoNert® 2000) (SilcoTek Coatings, PA, USA). The carrier gas flowing through the TDU was oxygen-free nitrogen (99.998% purity, BOC Gases, Manchester, UK). Three measurements were acquired for each E/N value, which were then averaged and the background–signal subtracted. The reactor, inlet line and thermal desorption unit were kept at 150 °C. The drift tube was at 1 mbar and the ion source at 1.4 mbar when generating both H_3O^+ and O_2^+. The reduced electric field was manipulated only by adjusting the drift voltage in the reactor in the range from approximately 100 to 400 V, which corresponds to a E/N range from approximately 60 to 250 Td.

5.3.4 Density Functional Theory Calculations

The proton affinities and gas-phase basicities of the three nitroaniline isomers and the water monomer, dimer and trimer were computed through DFT calculations using Gaussian09W and GaussView05 for Windows by Dr Peter Watts [57]. The functional and the basis set used for

this calculations were the B3LYP and 6-31+G(d,p), respectively, which have proved adequate in past studies [38, 127].

5.4 Results

In this section the experimental and DFT results are presented. The experimental work consists of obtaining the product ion distributions (PID) resulting from the reaction of each nitroaniline isomer with the reagent ion (*i.e.* H_3O^+ or O_2^+ in each case) as a function of the reduced electric field (top x-axis) and the drift voltage (bottom x-axis). All the isotopologues were taken into account when calculating the product ion distributions, although only the lightest one is given. The uncertainty has been estimated to be around 10% for any of the percentages provided here.

5.4.1 DFT Results

The proton affinity and gas-phase basicity for the nitroaniline isomers and the water monomer, dimer and trimer are shown in Table 5.1, which also includes the ionisation energies of O_2 and the nitroanilines [35]. Furthermore, Table 5.1 also contains the calculations for the change in the enthalpy (ΔH_{298}) and Gibbs free energy (ΔG_{298}) for the addition of H_2O to the already protonated nitroaniline molecule. The calculated thermochemical data related to the proton transfer case (*i.e.* *PA*, *GB*, ΔH_{298} and ΔG_{298}) are given independently for the amino and nitro groups for comparison. These quantities were also calculated for the aniline and nitrobenzene molecules.

It is interesting to note that the *PA* and *GB* of the amine group in the aniline molecule are higher than those of the nitro group in nitrobenzene, but when both functional groups are present in the same molecule (*i.e.* for the three nitroaniline isomers), the values of *PA* and *GB* of the amine and nitro groups are reversed. This is caused by the NH_2 group donating electrons to the benzene ring and the NO_2 group pulling electrons from the ring. The calculated basicities show that all three nitroanilines can undergo proton transfer from H_3O^+ and $H_3O^+.(H_2O)$, and that 4-nitroaniline can also do it from $H_3O^+.(H_2O)_2$ to its nitro group. As proton transfer to both groups of the nitroanilines is exoergic, $NA.H^+$ is thought to be a mixture of parent molecules protonated at the NH_2 and the NO_2 sites. However, as in 2-nitroaniline the two functional groups are very close, there the proton sits bonded to both functional groups.

Table 5.1: Proton affinities, gas phase basicities and ionisation energies for nitroaniline isomers. The *PA* and *GB* values calculated using the B3LYP functional and the 6-31+G(d,p) basis set at 298 K. ΔH_{298} and ΔG_{298} refer to the enthalpies and free energies for the addition of water to the protonated species. For convenience the ionisation energies of O_2 and the three nitroanilines are also provided.

Chemical	**Site**	***PA****	***GB****	$\Delta \boldsymbol{H}_{298}$*	$\Delta \boldsymbol{G}_{298}$*	***IE**†*
Water		684	653			
Water dimer		842	777			
Water trimer		937	841			
O_2						12.07 [128]
2-NA	NH_2	840	806	-69	-37	8.27
	NO_2	858	824	-76	-43	
3-NA	NH_2	824	796	-78	-43	8.31
	NO_2	830	800	-84	-51	
4-NA	NH_2	810	784	-78	-43	8.34
	NO_2	879	847	-73	-39	
Aniline	NH_2	874	846	-72	-40	
Nitrobenzene	NO_2	806	775	-90	-55	

*Thermochemical data expressed in kJ mol^{-1}. †Ionisation energies (in eV) have been taken from NIST database [35].

5.4.2 Fragmentation patterns and branching ratios studies in proton transfer mode

5.4.2.1 2-nitroaniline

The product ion distributions for the reaction of 2-nitroaniline with H_3O^+ and $H_3O^+.(H_2O)$ from 60 to 250 Td are shown in Figure 5.4. The most abundant ion from 60 to ca. 230 Td is the protonated parent molecule 2-NA.H^+ at *m/z* 139. The ion coming from the association of the protonated parent with a water molecule (*i.e.* 2-$NAH^+.H_2O$ at *m/z* 157) is present at low *E/N*, and it decreases with the increasing *E/N*, with a maximum contribution to the total ion signal of ∼15% at 60 Td. Additionally, further product ions are observed at high reduced electric fields. $C_6H_5N_2O^+$ at *m/z* 121, which comes from the loss of water from the protonated parent, appears at 150 Td and becomes dominant at approximately 230 Td. Likewise, $C_6H_7N^+$ at *m/z* 93 and $C_6H_5N^+$ *m/z* 91 are also observed at high *E/N*. The former results from the loss of a nitro group from 2-NA.H^+, while the latter comes from the loss of a hydrogen molecule after a loss of a nitro group from the protonated parent.

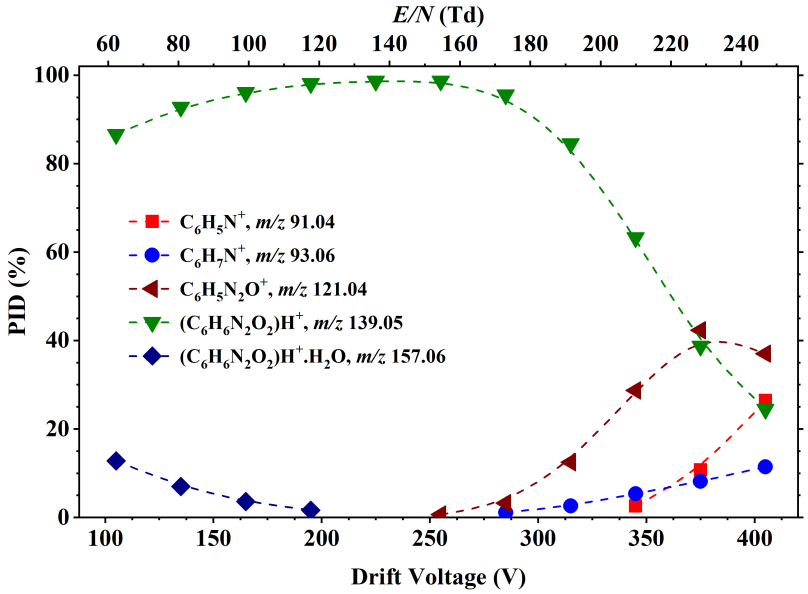

Figure 5.4: Percentage product ion distribution (PID in %) resulting from the reaction of 2-nitroaniline with $H_3O^+.(H_2O)_n$ (n = 0 and 1) as a function of the reduced electric field from 60 to 250 Td.

The mass spectra shown in Figure 5.5 are included as illustrative examples of the data acquired when performing these experiments. These two different data sets relate to measurements of 2-nitroaniline with different E/N values in the drift tube, while the rest of variables were kept constant. Comparable mass spectra were found with the rest of compounds in both proton transfer and charge transfer modes, but these are not included as those results are summarised in the PID plots, which include the product ions with a branching percentage higher than >1% for any E/N.

5.4.2.2 3-nitroaniline

The PID plot for the reaction of the 3- isomer with H_3O^+ and $H_3O^+.(H_2O)$ (Figure 5.6) shows that, like in the 2-NA case, the most abundant ion is the protonated parent, 3-NA.H^+ at m/z 139, over a large reduced electric field range. In addition to that, the three body association with water yielding 3-NA.$H^+.H_2O$ is observed at low E/N, but in the case of 3-nitroaniline the presence of this ion is much higher than that in the 2-nitroaniline experiment, reaching roughly 50% at 60 Td and having the same intensity as the protonated parent signal.

On the other side, two other product ions are observed at high reduced electric field. $C_6H_7N^+$

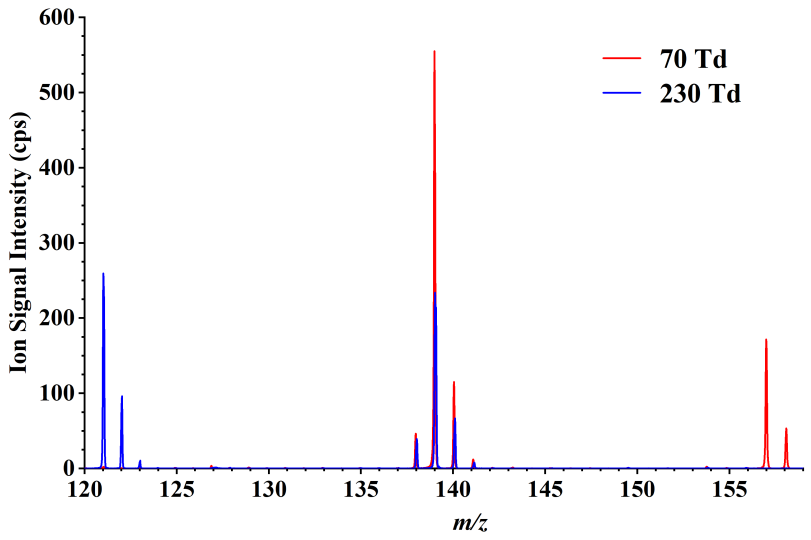

Figure 5.5: Overlaid mass spectra for 2-nitroaniline at 70 and 230 Td. This figure illustrates the clear difference in ion signal intensities for m/z 121, 139 and 157 upon the reduced electric field applied to the DT of the instrument.

at m/z 93.03 becomes the most abundant ion at around 230 Td. At the same, $C_6H_7NO^+$ at m/z 109, which was not found for 2-nitroaniline and comes from the loss of NO from the protonated parent, is observed for E/N values higher than 190 Td. Furthermore, $C_6H_5N_2O^+$ at m/z 121, which was observed with the 2- isomer, was not observed with the 3- (nor with the 4-) isomer. This can be explained with the same argument presented in chapter 4 for the loss of water from nitrotoluenes (*i.e.* elimination of water from the protonated parent molecule only occurs when the methyl and nitro groups are adjacent to each other). In the case of the nitroanilines, the elimination of water yielding $C_6H_5N_2O^+$ only occurs with the 2- isomer, which is the only one whose amine and nitro functional groups are adjacent.

5.4.2.3 4-nitroaniline

The PID for the reaction of 4-nitroaniline with H_3O^+, $H_3O^+.(H_2O)$ and potentially $H_3O^+.(H_2O)_2$ is shown in Figure 5.7. The protonated parent (4-NA.H^+ at m/z 139) is the most abundant ion across the whole reduced electric field range (>80%). The clustering with water at low E/N has an intensity comparable to that in the 2-NA case (max 5-10% at 60 Td) and the only fragment ion ($C_6H_7N^+$ at m/z 93) is found at >160 Td.

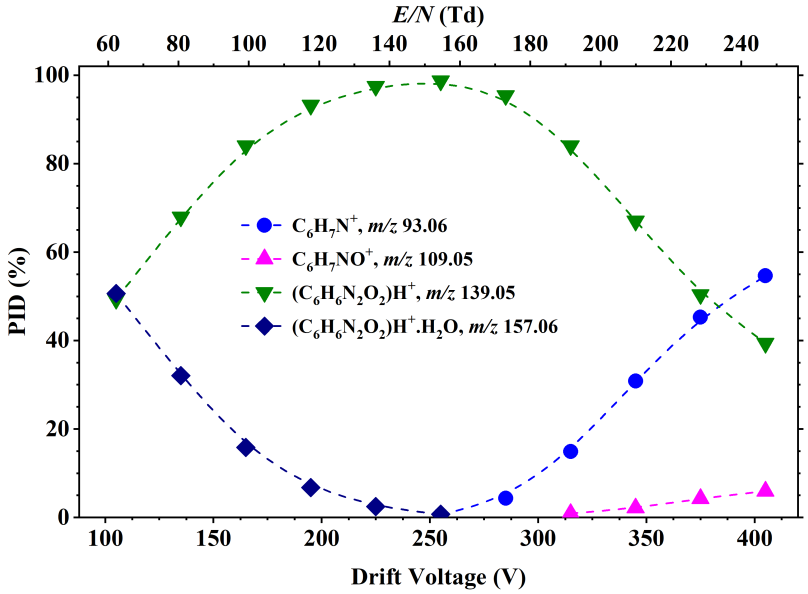

Figure 5.6: Percentage product ion distribution resulting from the reaction of 3-nitroaniline with $H_3O^+.(H_2O)_n$ (n = 0 and 1) as a function of the reduced electric field from 60 to 250 Td.

A key result of these experiments is that protonated 3-nitroaniline shows more clustering with water than the other two isomers but this can be explained in terms of the thermochemical data presented in Table 5.1. The calculated change in the Gibbs free energy, ΔG_{298}, for the clustering of 2-NA and 4-NA with water is 43 kJ mol^{-1}, while this is 51 kJ mol^{-1} for 3-NA. This 8 kJ mol^{-1} difference, translated into equilibrium constants at 298 K, indicates that the solvation reaction is 25 times more effective for 3-NA.H$^+$ than for the other isomers. Furthermore, at the temperature of the drift tube (*i.e.* 150°C, 423 K) 8 kJ mol^{-1} represents a tenfold difference for the association of water with 3-NA.H$^+$ than for that with 2-NA.H$^+$ and 4-NA.H$^+$.

In the 4-nitroaniline molecule, the nitro and amine functional groups are on opposite sites of the aromatic ring, which makes it difficult to create a transition state between the functional groups which would result in further product ions. The main consequence of this feature is that, as mentioned above, the protonated parent is the largely dominant ion, showing less fragmentation than the 2- and 3- isomers, which is in agreement with the chemical ionisation results for mononitroarenes with electron-releasing substituents [129]. This is also the reason $C_6H_5N_2O^+$ at m/z 121 is not observed with the 4- isomer either, as explained in section 5.4.2.2.

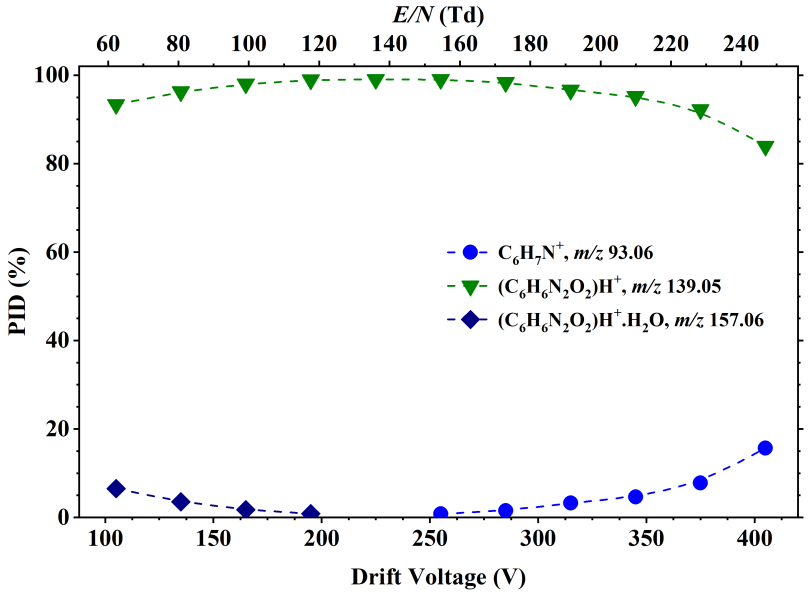

Figure 5.7: Percentage product ion distribution resulting from the reaction of 4-nitroaniline with $H_3O^+.(H_2O)_n$ (n = 0, 1, 2) as a function of the reduced electric field from 60 to 250 Td.

5.4.3 Fragmentation patterns and branching percentage studies in charge transfer mode

5.4.3.1 2-nitroaniline

The PID plot resulting from the reaction of 2-nitroaniline with O_2^+ as a function of the E/N is shown in Figure 5.8. The charge-transferred parent ion 2-NA^+ at m/z 138 is the most abundant ion below 230 Td. The branching percentage of this ion decreases with the E/N while other product ion arise, with $C_5H_6N^+$ at m/z 80 becoming dominant at 230 Td. The other observed fragment ions, in order of increasing m/z are $C_5H_5^+$ at m/z 65, the loss of the nitro group from 2-NA^+ (*i.e.* $C_6H_6N^+$) at m/z 92 and the loss of NO from 2-NA^+ (*i.e.* $C_6H_6NO^+$) at m/z 108. All these product ions have been reported by Beynon *et al.* for electron impact experiments [130].

5.4.3.2 3-nitroaniline

Figure 5.9 shows the PID plots for the reaction of 3-nitroaniline with O_2^+ as a function of the reduced electric field, which is quite similar to that of the 2- isomer in Figure 5.8. The observed product ions correspond to the same structures as indicated in the previous section, being in this case 3-NA^+ the parent ionised molecule. However, their branching percentages for a given

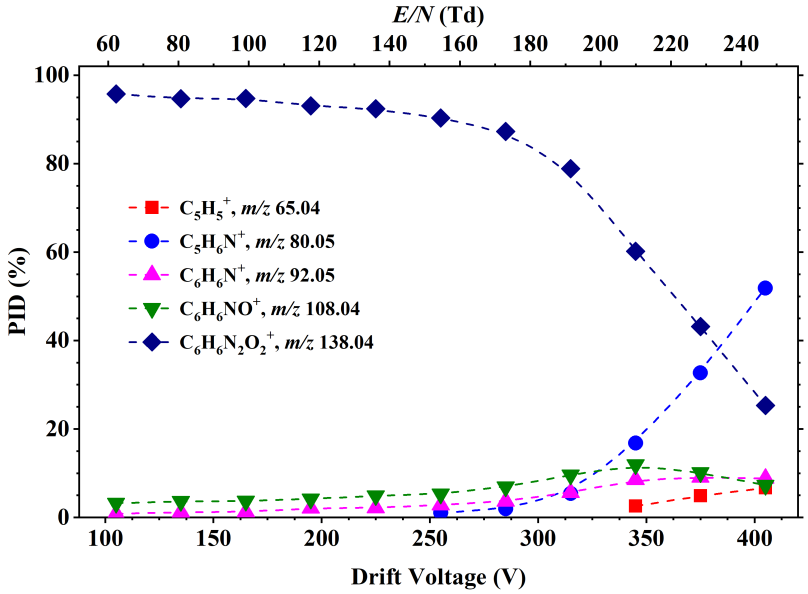

Figure 5.8: Percentage product ion distribution resulting from the reaction of 2-nitroaniline with O_2^+ as a function of the reduced electric field from 60 to 250 Td.

E/N are slightly different. For the 3- isomer, the parent ion is the most abundant over the whole reduced electric field study except for values higher than 240 Td, where $C_5H_6N^+$ at *m/z* 80 becomes dominant. Also, $C_6H_6N^+$ at *m/z* 92 reaches a maximum product ion distribution of 15% for 3-NA, while only around 5% for 2-NA, and for $C_5H_5^+$ at *m/z* 65 it is 12% for 3-NA and around 6% for 2-NA.

5.4.3.3 4-nitroaniline

The PID plot in Figure 5.10 shows that the fragmentation for 4-NA is different to that for the 3- and 2- isomers showing only three product ions. As stated in the proton transfer mode case, this is an effect coming from the *para* arrangement of the functional groups in the ring. For the 4-nitroaniline isomer, the parent ion (4-NA^+ at *m/z* 138) is the most abundant from low reduced electric field up to around 190 Td, where $C_6H_6NO^+$ at *m/z* 108 becomes dominant. Furthermore, $C_5H_6N^+$ at *m/z* 80 appears at 190 Td and increases with the *E/N*, reaching a branching percentage of around 30% at 250 Td.

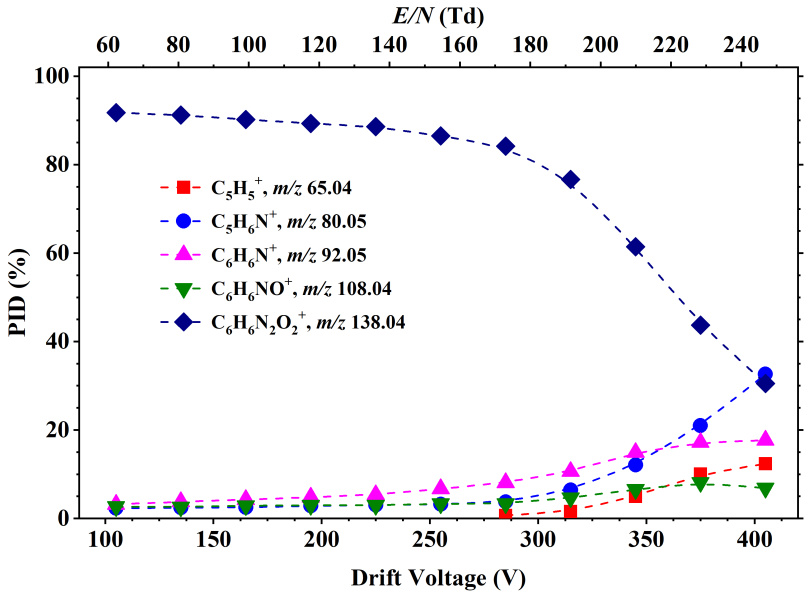

Figure 5.9: Percentage product ion distribution resulting from the reaction of 3-nitroaniline with O_2^+ as a function of the reduced electric field from 60 to 250 Td.

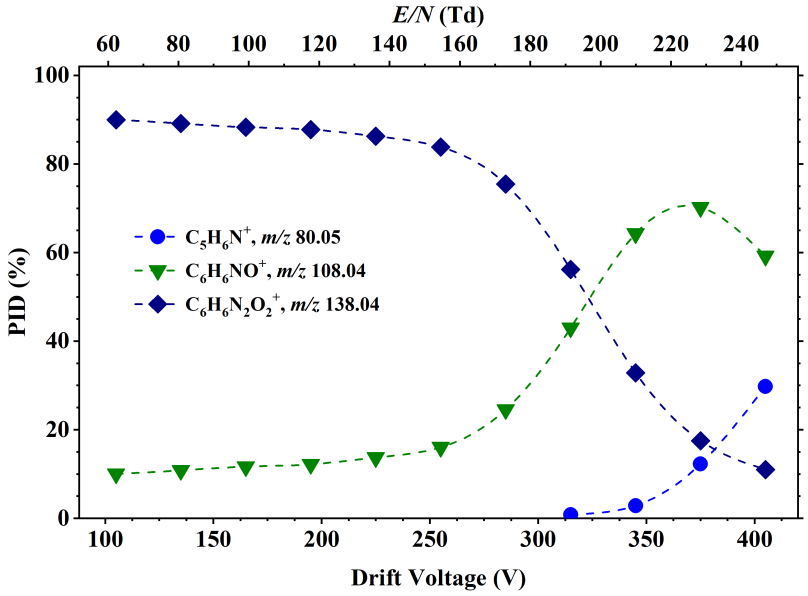

Figure 5.10: Percentage product ion distribution resulting from the reaction of 4-nitroaniline with O_2^+ as a function of the reduced electric field from 60 to 250 Td.

5.5 Conclusions

With this investigation we have shown how to separate nitroaniline isomers using the SRI-MS technique to enhance the ion/molecule reactions. This study contains the product ion distributions resulting from the reaction of the three isomers with H_3O^+ and O_2^+ as a function of the reduced electric field illustrated with quantum chemical results. We have proved that SRI-MS has good selectivity when detecting nitroanilines with H_3O^+ and O_2^+ as reagent ions.

In the proton transfer mode, the protonated parent at *m/z* 139 was the dominant ion over a wide *E/N* range for the three nitroanilines, while for the charge transfer mode the parent ion at *m/z* 138 was the most abundant for almost the whole *E/N* range. It is however the clustering with water in the proton transfer mode and the presence of the product ion at *m/z* 108 in the charge transfer mode that allows for isomer identification here. Whilst the product ion distributions of the reactions of 2- and 3-nitroaniline with O_2^+ are very similar, the 3- isomer shows higher clustering with water at low *E/N* in proton transfer mode, with the 3-NA.H^+.H_2O ion reaching ca. 50% at 60 Td (*i.e.* the lowest reduced electric field). Moreover, 4-nitroaniline shows less fragmentation than the 2- and 3- isomers in the proton transfer mode but, in the charge transfer mode, $C_6H_6NO^+$ at *m/z* 108 becomes the most abundant ion above approximately 190 Td. This ion enables the identification of the 4- isomer, as it never represents more than about 15% for 2- or 3-nitroaniline.

Chapter 6

Compendium of the Reactions of H_3O^+ With Selected Ketones of Relevance to Breath Analysis Using Proton Transfer Reaction Mass Spectrometry

This chapter is a reformatted copy of my published article (reference [3]):

Malásková, M., Olivenza-León, D., Piel, F., Mochalski, P., Sulzer, P., Jürschik, S., Mayhew, C. & Maerk, T. Compendium of the reactions of H_3O^+ with selected ketones of relevance to breath analysis using proton transfer reaction mass spectrometry. *Frontiers in Chemistry* **7,** 401 (2019). DOI: 10.1021/acs.analchem.6b02982.*

6.1 Abstract

Soft chemical ionization - mass spectrometric techniques, such as proton transfer reaction mass spectrometry (PTR-MS), are often used in breath analysis, being particularly powerful for real-time measurements. To ascertain the type and concentration of volatiles in exhaled breath clearly assignable product ions resulting from these volatiles need to be determined. This is difficult for compounds where isomers are common, and one important class of breath volatiles where this

*MM, DOL and FP are Early Stage Researchers who have contributed equally to the measurements, data analyses and contribution to the completion of this paper.

occurs are ketones. Here we present a series of extensive measurements on the reactions of H_3O^+ with a selection of ketones using PTR-MS. Of particular interest is to determine if ketone isomers can be distinguished without the need for pre-separation by manipulating the ion chemistry through changes in the reduced electric field. An additional issue for breath analysis is that the product ion distributions for these breath volatiles are usually determined from direct PTR-MS measurements of the compounds under the normal operating conditions of the instruments. Generally, no account is made for the effects on the ion/molecule reactions by the introduction of humid air samples or increased CO_2 concentrations into the drift tubes of these analytical devices resulting from breath. Therefore, another motivation of this study is to determine the effects, if any, on the product ion distributions under the humid conditions associated with breath sampling. However, the ultimate objective for this study is to provide a valuable database of use to other researchers in the field of breath analysis to aid in analysis and quantification of trace amounts of ketones in human breath. Here we present a comprehensive compendium of the product ion distributions as a function of the reduced electric field for the reactions of H_3O^+. $(H_2O)_n$ ($n = 0$ and 1) with nineteen ketones under normal and humid (100% relative humidity for 37 °C) PTR-MS conditions. The ketones selected for inclusion in this compendium are (in order of increasing molecular weight): 2-butanone, 2-pentanone, 3-pentanone, 2-hexanone, 3-hexanone, 2-heptanone, 3-heptanone, 4-heptanone, 3-octanone, 2-nonanone, 3-nonanone, 2-decanone, 3-decanone, cyclohexanone, 3-methyl-2-butanone, 3-methyl-2-pentanone, 2-methyl-3-pentanone, 2-methyl-3-hexanone, and 2-methyl-3-heptanone.

6.2 Introduction

Although high resolution PTR-MS instruments can readily separate many isobaric compounds, the main strategy being used nowadays to deal with these mixtures is the manipulation of the ion/molecule chemistry, which can be done by changing: (i) the reagent ion species or distribution, or (ii) the reduced electric field (*i.e.* E/N) in the drift tube. The former approach was applied to investigations of explosives by Sulzer *et al.* and Agarwal *et al.* [105, 106], while Lanza *et al.* and Acton *et al.* did it for psychoactive substances [107, 108]. On the other hand, changing the reduced electric field to manipulate the collisional processes has been applied to homeland security: detection of chemical warfare agents [131], explosives [6, 105, 109], and rape

drugs [15], and to the environmental sciences: identification of monoterpenes [132]. Moreover, the implementation of the radio frequency ion-funnel drift tube [1] and the computer-controlled fast switching drift tube [14] mentioned already in the chapter 2 of the present thesis are technical advances that were developed to enhance compound selectivity through changes in the reduced electric field. However, separating isomeric compounds presents a bigger challenge than isobaric ones, and in general their differentiation cannot be done without a pre-separation stage. Examples of isomeric distinction without pre-separation are the study from Lanza *et al.*, which differentiated between two isomeric drugs (4-methylethcathinone and N-ethylbuphedrone) using O_2^+ and NO^+ as reagent ions while reactions with H_3O^+ were not successful [70], and the study presented in chapter 5 of the present thesis, where 2-, 3- and 4-nitroaniline isomers can be separated because they yield different product ion distributions as a function of the reduced electric field for their reactions with H_3O^+ and O_2^+ [2]. But these are exceptions rather than the general case.

One of the best ways to investigate ketone isomers in PTR-MS is by coupling a pre-separation stage to the inlet of the instrument. The best choice for this is to use a fastGC device, as it gives a better compromise than standard GC systems to maintain the real-time advantages of PTR-MS. FastGC systems allow quick analysis (1 - 2 minutes) while still separating compounds in a fairly good way and thus enhancing specificity of PTR-MS [65, 66, 133]. In the present study we present a wide database resulting from the investigations of the reaction of a number of ketones with H_3O^+ as a function of the reduced electric field using the fastGC PTR-MS technique, where the fastGC made the product ion identification easier, helping to discard products coming from impurities or potential contamination in the samples.

Ketones can be detected in breath, blood and urine [134]. Their importance resides in the roles they play in metabolic processes in the human body and the possibility of them being detected through breath analysis for non-invasive monitoring and assessment of health processes and concerns. The main ketone found in the human body is acetone, which is linked to fat metabolism as other ketones but it is not included in the present study as it has been widely investigated in the past [133]. We have focused however on larger molecular-weight ketones, including linear, cyclic and branched ones, which are found in smaller quantities, and are not present in many PTR-MS studies, while still being of relevance.

One of the differences between the standard working conditions in PTR-MS and the human

breath is the humidity. Dry air or N_2 are typically used as carrier gas in PTR-MS, and this is not comparable to the amount of moisture present in the human breath. The implications of this humidity issue in the reaction processes happening in PTR-MS have been mentioned in the literature [50, 135, 136], and this should be accordingly accounted for. A 100% relative humidity at 34 °C, like that in breath samples, can influence the reactions in the drift tube in different ways. First of all, there is less energy available when the analyte reacts with a water cluster ion (*i.e.* $(H_2O)_nH_3O^+$ for $n>0$) instead of with H_3O^+ as the proton affinity of the water clusters is higher than that of water (see Table 1.2). Also, higher humidity translates into a higher presence of water cluster ions for a given reduced electric field in the clustering-declustering processes compared to those in drier conditions, and this is particularly noticeable at low E/N (*i.e.* less than 120 Td). For instance, for a molecule with a proton affinity between that of water and the first water cluster, this means that sensitivity can be compromised for that particular compound, yielding a misleading amount in its detected concentration. Moreover, even when the protonation is energetically allowed, other secondary ion processes can occur, like clustering of the product ions with water molecules, which can also produce confusing results. As the consequences of humid operating conditions are not often considered in the literature because the experiments are carried out in "normal" conditions, one of our goals is to study the role of humidity in ketone product ion formation.

There are several studies available on the literature about how humidity affects the detection of different families of compounds. The most remarkable one is that from Warneke *et al.* where, at a constant E/N, they demonstrate that benzene and toluene do not react with $H_3O^+.(H_2O)_n$ clusters as the product ion yield decreases with increasing humidity [50]. A work-around for this was proposed by de Gouw *et al.*, who defined a humidity factor that compensates for the unreactive behaviour of a particular compound with $H_3O^+.(H_2O)$ taking into account the $H_3O^+.(H_2O)/H_3O^+$ ratio [8]. de Gouw *et al.* successfully corrected the product ion signal for the humidity effects for methanol, acetonitrile, acetaldehyde, acetone, benzene and toluene [137]. Demarcke *et al.* studied the influence of the humidity in PTR-MS from the reactions of H_3O^+ with α-cedrene and longifolene (*i.e.* two sesquiterpenes), although in this case there was no significant variation in the product ion signal [138]. Furthermore, Trefz *et al.* found considerable differences between the dry and humid cases when studying more than 20 volatile organic compounds, including aldehydes, ketones, aromatic compounds and hydrocarbons at a

fixed E/N [111], while Kari *et al.* reported no meaningful change in the product ion signal for investigations of α-pinene, δ-limonene, and longifolene with different humidity levels [139]. It is possible to conclude then, taking into account the information available in the literature, the effects of humidity strongly vary from a compound to another.

In the present study we discuss the reactions of H_3O^+ and water cluster ions with several ketones for a broad reduced electric field range in both "normal" and "humid" operating conditions. These different operating conditions have been proved to yield different product ion distributions, which implies that humidity should be taken into account when breath analysis is being performed with a PTR-MS instrument to avoid misleading ion signal yields.

6.3 Materials and Methods

6.3.1 Sample preparation

Two different procedures were followed to prepare the samples. The measurements in normal conditions were done by first purging the headspace of the ketone-storing glass vial with dry N_2 (Alphagaz 1, Air Liquide GmbH., Austria) to remove the air and the possibly contaminated headspace, and replace it with N_2 to minimise the presence of O_2 and water vapour. The N_2 had been purified to grade 6.0 (*i.e.* N_2 purity of $> 99.9999\%$) prior the purging process using a P300-1 Filter (VICI AG, Switzerland). Some parafilm was then used to cover the vial and some headspace vapour was taken from the vial by injecting a glass syringe through the parafilm. Then, this headspace sample (containing both the ketone and N_2) was introduced into a 3-litre PTFE bag that had been previously been filled with dry 6.0 N_2 and that was connected to the inlet line of the PTR-MS instrument. Different headspace volumes, from 5 µL to 10 mL, were used for different ketones owing to their different volatilities. On the other hand, a LCU was employed to generate the humid samples. As explained in subsection 2.3.3, this device can create a defined gaseous stream of a compound using liquid samples. In the present study, the liquid samples consisted of 1 - 10 µL of liquid ketone sample diluted in 100 mL of water in a 16 mL glass vials kept at 30 °C. This mixture was injected into the LCU at a rate of 35 µL min^{-1} while diluted in a carrier gas flow (N_2) of 950 mL min^{-1} to yield a 5% absolute humidity (see footnote in section 2.3.3). This was then injected into the fastGC through the inlet of the PTR-MS instrument. A concentration of the ketones of approximately 100 ppbv was generated

and introduced in the PTR-MS instrument in both dry and humid measurements.

An automated routine was used to perform the experiments shown in this study. This routine started with a 5-minute background study, which for the dry case consisted on measuring the N_2-filled bag with no ketone traces, while for the humid case it was measuring a vial containing only purified water. Then the ketone sample was connected to the inlet pipe. This consisted on injecting the headspace sample into the N_2-filled bag for the dry case, and switching the vial with water for the one containing the diluted ketone for the humid case. A 2-minute stabilisation period followed. Then a fastGC study at 180 Td for 2 minutes 40 seconds was performed to aid in the product ions identification. The final part was a E/N study from 100 to 220 Td in steps of 10 Td at a speed of 1 minute/step, in both directions (*i.e.* from 100 to 220 Td and back), lasting 26 minutes in total. The whole study was repeated two times for each ketone for both humid and dry conditions.

6.3.2 FastGC PTR-ToF-MS

A wide description of PTR-ToF-MS operating techniques was given in chapter 2 besides being also available in the literature [31], and therefore only a short description stating the differences with the typical setup is needed here. For this piece of research, a PTR-TOF 8000 with a fastGC add-on (IONICON Analytik GmbH, Austria) was used [140, 141]. The basic working of this apparatus is similar to any PTR-MS instrument. In essence, $H_3O^+.(H_2O)_n$ (n = 0, 1, 2, ...) ions are created in the ion source through electron ionisation of water and ion/molecule reactions, and are transported to the drift tube, where they are dragged downstream by the electric field. Figure 6.1 shows the dependence of the water cluster ions signal as a function of the reduced electric field for the normal and humid case. It is important to note that these are the reagent ion intensities measured at the end of the drift tube and that the analyte molecules may have encountered a different distribution of reagent ions upstream. In other words, the analyte would encounter at the beginning of the drift tube more water cluster ions that broke up through collisions with the buffer gas and that at the end of the drift tube have already dissociated to hydronium and neutral water molecules.

If the analyte, which is fed through the inlet pipe into the drift tube, has a proton affinity higher than that of water ($PA(H_2O)$ = 691 kJ mol^{-1}), it undergoes proton transfer from hydronium (or from the relevant protonated water cluster if the analyte's proton affinity is higher

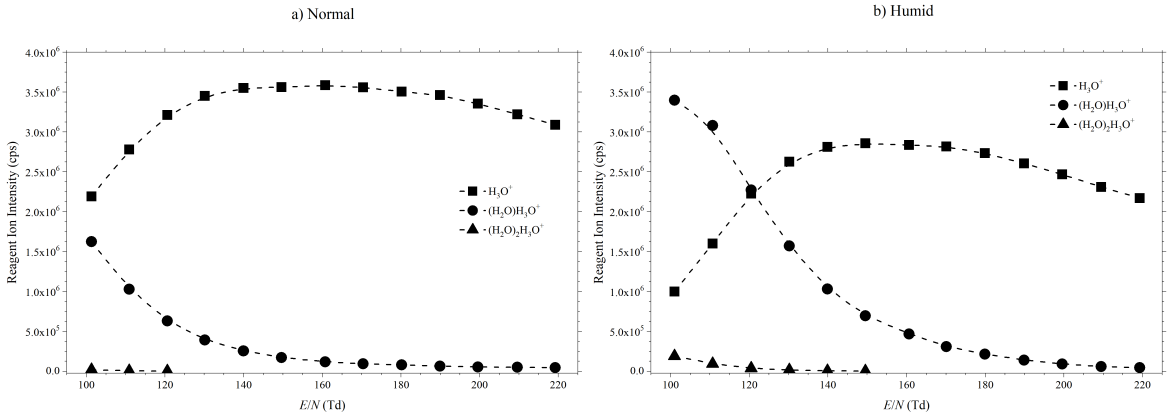

Figure 6.1: Reagent ion intensities in counts per second (cps) as a function of the reduced electric field for (a) normal (dry buffer gas) and (b) humid (5% absolute humidity buffer gas) conditions.

than that of the proper water cluster). The protonation process can be either dissociative or non-dissociative, and it is important to note that protonated molecule fragmentation can be a barrierless and spontaneous process or may be caused by the reagent ion collision with the analyte and/or charged analyte with the buffer gas.

The drift tube of the PTR-TOF 8000 was kept at 2.3 mbar and 100 °C, this also being the temperature of the inlet line. This values were the same for all the measurements, giving a constant N, and thus the reduced electric field was solely manipulated by changing the drift voltage in the range from 410 V to 890 V, which corresponds to a E/N range from 100 to 220 Td. To aid in the product ion identification a fastGC was used, which is a modified version of that from Romano *et al.* and Ruzsanyi *et al.* [65, 66]. Details of this device were already given earlier in this thesis (see subsection 2.3.2) and are also available in the literature [3].

It is worth clarifying the choice of terms for the operating conditions regarding the humidity in the drift tube. Even when the carrier gas is dry N_2, some water vapour can diffuse from the ion source into the reactor. Thus, referring to this as "dry" is not totally correct and we will refer to it as the "normal" operating condition. On the other hand, when the carrier gas is not under dry conditions because it has been moisturised in the LCU we will refer to this as "humid" conditions.

6.3.3 Chemicals

The chemicals used in this study, their purities and their respective providers are: 2-butanone (99.5%, Honeywell Austria GmbH, Vienna, Austria), 2-pentanone (98%, Sigma-Aldrich, Vienna, Austria), 3-pentanone (99%, Sigma-Aldrich), 2-hexanone (98%, Sigma-Aldrich), 3-hexanone (98%, Sigma-Aldrich), 2-heptanone (98.5%, Honeywell), 3-heptanone (analytical standard, Sigma-Aldrich), 4-heptanone (98%, Sigma-Aldrich), 3-octanone (99%, Acros Organics, Thermo Fisher Scientific, Schwerte, Germany) 2-nonanone (99%, Sigma-Aldrich), 3-nonanone (99%, Sigma-Aldrich), 2-decanone (98%, Sigma-Aldrich), 3-decanone (97%, SAFC), cyclohexanone (99.8%, Sigma-Aldrich), 3-methyl-2-pentanone (99%, Sigma-Aldrich), 2-methyl-3-pentanone (97%, Sigma-Aldrich), 2-methyl-3-hexanone (98%, Sigma-Aldrich), 2-methyl-3-heptanone (99%, Sigma-Aldrich) and 3-methyl-2-butanone (98.5%, Honeywell). No further purification process was applied to these substances.

6.3.4 Data analysis

The analysis of the data for this study was done with the "PTR-MS Viewer" (IONICON Analytik GmbH, Austria) software, which was used to extract the data from the experiment files. The multi-peak feature of this software was also useful to separate some isobaric ions, like for example $C_3H_3^+$ and the ^{18}O isotopes of $(H_2O)H_3O^+$ (*i.e.* $(H_2\,^{18}O)H_3O^+$ and $(H_2O)H_3\,^{18}O^+$), which are both found at m/z 39. For easier comparison with other instruments, the raw data were not corrected for transmission effects, although it was normalised to 10^6 reagent ion counts and the background signals were subtracted. Only the ion signal from H_3O^+ was used to normalise that from those ketones whose proton affinities are greater than that of $(H_2O)_2$ (808 kJ mol^{-1}): 2-butanone (827 kJ mol^{-1}), 2-pentanone (833 kJ mol^{-1}), 3-pentanone (837 kJ mol^{-1}), and 3-methyl-2-butanone (836 kJ mol^{-1}). For the rest of the ketones, the sum of the counts from H_3O^+ and $(H_2O)H_3O^+$ was used to normalise the ion yield.

6.4 Results and Discussion

The product ion distributions for all the compounds studied in this investigation are shown in Table 6.1 at 100, 140 and 180 Td for both normal and humid conditions. These numbers provide a fast picture of the observed product ions for each ketone and show quickly the impacts, if any,

of humidity on the distribution of product ions. The ketones presented in Table 6.1 (in increasing molecular weight) are thirteen linear, one cyclic and five branched ones. Moreover, Figure 6.2 graphically presents the product ion distributions as a function of the reduced electric field. The product ions considered in this study are those that represent at least 3% of the total product ion signal at any given E/N. Furthermore, the ^{13}C peak intensities and the exact m/z–values were used to tentatively assign the product ions to the provided chemical compositions in both Table 6.1 and Figure 6.2.

Table 6.1: Product ions identified and their associated product ion branching ratios (percentages) measured at reduced electric fields of 100, 140, and 180 Td resulting from the reactions of H_3O^+ with several ketones.

Ketone	**Product**	**Product**	**Product Ion Branching Percentages**					
Molecular Formula	**Ion m/z**	**Ion**	**Normal E/N (Td)**			**Humid E/N (Td)**		
Nominal MW		**Formula**	**100**	**140**	**180**	**100**	**140**	**180**
		Linear ketones						
2-butanone	73.07	$C_4H_8OH^+$	100	99	87	100	100	88
C_4H_8O	55.05	$C_4H_7^+$	0	1	10	0	0	10
72	39.02	$C_3H_3^+$	0	0	3	0	0	2
2-pentanone	87.08	$C_5H_{10}OH^+$	99	67	20	99	84	29
$C_5H_{10}O$	45.03	$C_2H_5O^+$	1	33	70	1	16	66
86	39.02	$C_3H_3^+$	0	0	10	0	0	5
3-pentanone	87.08	$C_5H_{10}OH^+$	98	72	23	99	91	43
$C_5H_{10}O$	69.07	$C_5H_9^+$	1	4	2	1	4	4
86	45.03	$C_2H_5O^+$	1	20	55	0	4	39
	41.04	$C_3H_5^+$	0	3	5	0	1	5
	39.02	$C_3H_3^+$	0	1	15	0	0	9
2-hexanone	101.1	$C_6H_{12}OH^+$	100	94	48	100	95	49
$C_6H_{12}O$	59.05	$C_3H_7O^+$	0	1	3	0	1	3
100	45.03	$C_2H_5O^+$	0	5	39	0	4	40
	39.02	$C_3H_3^+$	0	0	10	0	0	8
3-hexanone	101.1	$C_6H_{12}OH^+$	93	73	31	96	88	44
$C_6H_{12}O$	83.09	$C_6H_{11}^+$	1	4	4	1	4	5

(Continued)

Ketone	**Product**	**Product**	**Product Ion Branching Percentages**					
Molecular Formula	**Ion *m/z***	**Ion**	**Normal *E/N* (Td)**			**Humid *E/N* (Td)**		
Nominal MW		**Formula**	**100**	**140**	**180**	**100**	**140**	**180**
100	59.05	$C_3H_7O^+$	3	9	15	3	7	17
	55.05	$C_4H_7^+$	0	3	5	0	0	12
	45.03	$C_2H_5O^+$	2	5	15	0	0	0
	41.04	$C_3H_5^+$	0	4	6	0	1	9
	39.02	$C_3H_3^+$	1	1	18	0	0	13
	31.02	CH_3O^+	0	1	6	0	0	0
2-heptanone	115.11	$C_7H_{14}OH^+$	94	76	31	96	86	52
$C_7H_{14}O$	97.1	$C_7H_{13}^+$	4	10	7	2	7	9
114	59.05	$C_3H_7O^+$	1	2	4	2	3	6
	55.05	$C_4H_7^+$	0	9	14	0	4	20
	45.03	$C_2H_5O^+$	1	3	15	0	0	0
	39.02	$C_3H_3^+$	0	0	29	0	0	13
3-heptanone	115.11	$C_7H_{14}OH^+$	98	89	35	99	95	57
$C_7H_{14}O$	97.1	$C_7H_{13}^+$	2	5	4	1	4	5
114	59.05	$C_3H_7O^+$	0	0	0	0	1	7
	55.05	$C_4H_7^+$	0	4	8	0	0	12
	41.04	$C_3H_5^+$	0	1	7	0	0	3
	39.02	$C_3H_3^+$	0	0	27	0	0	16
	31.02	CH_3O^+	0	1	19	0	0	0
4-heptanone	115.11	$C_7H_{14}OH^+$	98	90	52	99	95	70
$C_7H_{14}O$	73.07	$C_4H_9O^+$	0	1	2	0	0	0
114	59.05	$C_3H_7O^+$	1	2	6	1	1	4
	55.05	$C_4H_7^+$	0	6	15	0	4	16
	53.04	$C_4H_5^+$	0	0	5	0	0	3
	39.02	$C_3H_3^+$	1	1	20	0	0	7
3-octanone	129.13	$C_8H_{16}OH^+$	99	96	46	100	98	73
$C_8H_{16}O$	69.07	$C_5H_9^+$	0	3	5	0	1	6
128	59.05	$C_3H_7O^+$	1	1	3	0	1	4
	41.04	$C_3H_5^+$	0	0	11	0	0	10
	39.02	$C_3H_3^+$	0	0	35	0	0	7
2-nonanone	143.14	$C_9H_{18}OH^+$	100	93	34	100	97	62

(Continued)

Ketone	**Product**	**Product**	**Product Ion Branching Percentages**					
Molecular Formula	**Ion *m/z***	**Ion**	**Normal *E/N* (Td)**			**Humid *E/N* (Td)**		
Nominal MW		**Formula**	**100**	**140**	**180**	**100**	**140**	**180**
$C_9H_{18}O$	83.09	$C_6H_{11}^+$	0	0	0	0	1	4
142	69.07	$C_5H_9^+$	0	4	4	0	2	6
	55.05	$C_4H_7^+$	0	1	4	0	0	7
	41.04	$C_3H_5^+$	0	1	10	0	0	10
	39.02	$C_3H_3^+$	0	1	48	0	0	11
3-nonanone	143.14	$C_9H_{18}OH^+$	100	87	48	100	100	79
$C_9H_{18}O$	55.05	$C_4H_7^+$	0	4	6	0	0	5
142	41.04	$C_3H_5^+$	0	8	11	0	0	6
	39.02	$C_3H_3^+$	0	1	35	0	0	10
2-decanone	157.16	$C_{10}H_{20}OH^+$	100	94	48	100	99	81
$C_{10}H_{20}O$	83.09	$C_6H_{11}^+$	0	2	3	0	1	6
156	55.05	$C_4H_7^+$	0	3	13	0	0	13
	39.02	$C_3H_3^+$	0	1	36	0	0	0
3-decanone	157.16	$C_{10}H_{20}OH^+$	99	95	48	100	100	86
$C_{10}H_{20}O$	55.05	$C_4H_7^+$	1	4	10	0	0	7
156	39.02	$C_3H_3^+$	0	1	42	0	0	7
		Cyclic ketone						
cyclohexanone	99.08	$C_6H_{10}OH^+$	99	88	30	99	93	40
$C_6H_{10}O$	81.07	$C_6H_9^+$	1	12	65	1	7	56
98	79.05	$C_6H_7^+$	0	0	5	0	0	3
	39.02	$C_3H_3^+$	0	0	0	0	0	1
		Branched ketones						
3-methyl-2-butanone	87.08	$C_5H_{10}OH^+$	100	98	63	99	96	66
$C_5H_{10}O$	69.07	$C_5H_9^+$	0	2	5	1	3	7
86	45.03	$C_2H_5O^+$	0	0	8	0	0	8
	41.04	$C_3H_5^+$	0	0	4	0	1	8
	39.02	$C_3H_3^+$	0	0	20	0	0	11
3-methyl-2-pentanone	101.1	$C_6H_{12}OH^+$	100	70	23	100	73	22
$C_6H_{12}O$	59.05	$C_3H_7O^+$	0	11	28	0	7	26
100	57.07	$C_4H_9^+$	0	4	3	0	5	4
	45.03	$C_2H_5O^+$	0	15	39	0	15	40

(Continued)

Ketone	**Product**	**Product**	**Product Ion Branching Percentages**					
Molecular Formula	**Ion *m/z***	**Ion**	**Normal *E/N* (Td)**			**Humid *E/N* (Td)**		
Nominal MW		**Formula**	**100**	**140**	**180**	**100**	**140**	**180**
	39.02	$C_3H_3^+$	0	0	7	0	0	8
2-methyl-3-pentanone	101.1	$C_6H_{12}OH^+$	98	61	17	95	74	24
$C_6H_{12}O$	59.05	$C_3H_7O^+$	1	15	29	3	9	29
100	57.07	$C_4H_9^+$	0	4	2	0	3	3
	45.03	$C_2H_5O^+$	1	20	41	2	13	40
	39.02	$C_3H_3^+$	0	0	11	0	1	4
2-methyl-3-hexanone	115.11	$C_7H_{14}OH^+$	95	66	24	96	72	24
$C_7H_{14}O$	97.1	$C_7H_{13}^+$	5	14	8	4	10	7
114	59.05	$C_3H_7O^+$	0	8	17	0	4	17
	55.05	$C_4H_7^+$	0	4	5	0	2	7
	45.03	$C_2H_5O^+$	0	5	17	0	11	27
	41.04	$C_3H_5^+$	0	3	7	0	1	6
	39.02	$C_3H_3^+$	0	0	22	0	0	12
2-methyl-3-heptanone	129.13	$C_8H_{16}OH^+$	96	76	26	97	81	28
$C_8H_{16}O$	111.12	$C_8H_{15}^+$	3	5	3	2	5	3
128	69.07	$C_5H_9^+$	0	8	5	0	4	5
	59.05	$C_3H_7O^+$	0	0	0	0	3	14
	45.03	$C_2H_5O^+$	0	2	8	0	3	10
	43.05	$C_3H_7^+$	1	2	2	1	2	3
	41.04	$C_3H_5^+$	0	6	15	0	2	15
	39.02	$C_3H_3^+$	0	1	41	0	0	22

The protonated parent molecule is the dominant ion for all ketones at low E/N values (<140 Td). This is in agreement with some studies present in the literature, like the one by Buhr *et al.*, where they demonstrated that, independently of the chain length, the main reaction channel between ketones and hydronium at approximately 140 Td is non-dissociative proton transfer [142]. SIFT-MS [143–145] and SIFDT-MS [146] investigations also agree with the observation of the protonated parent being dominant at low collisional energies.

On the other hand, other product ions rather than the protonated parent molecule are observed for high E/N values (>140 Td). This does not agree with Buhr *et al.* for 2-butanone,

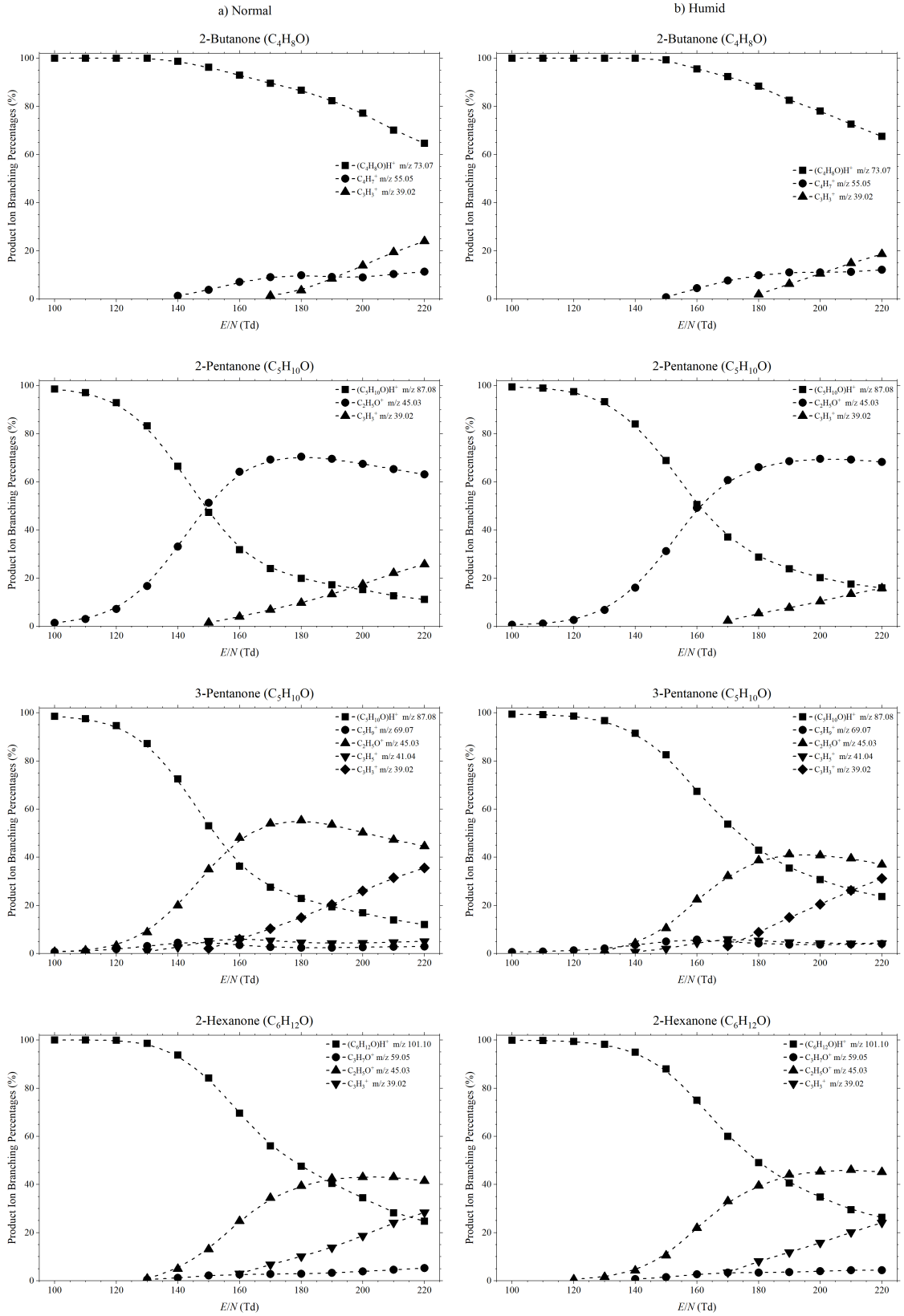

Figure 6.2: *Continued*

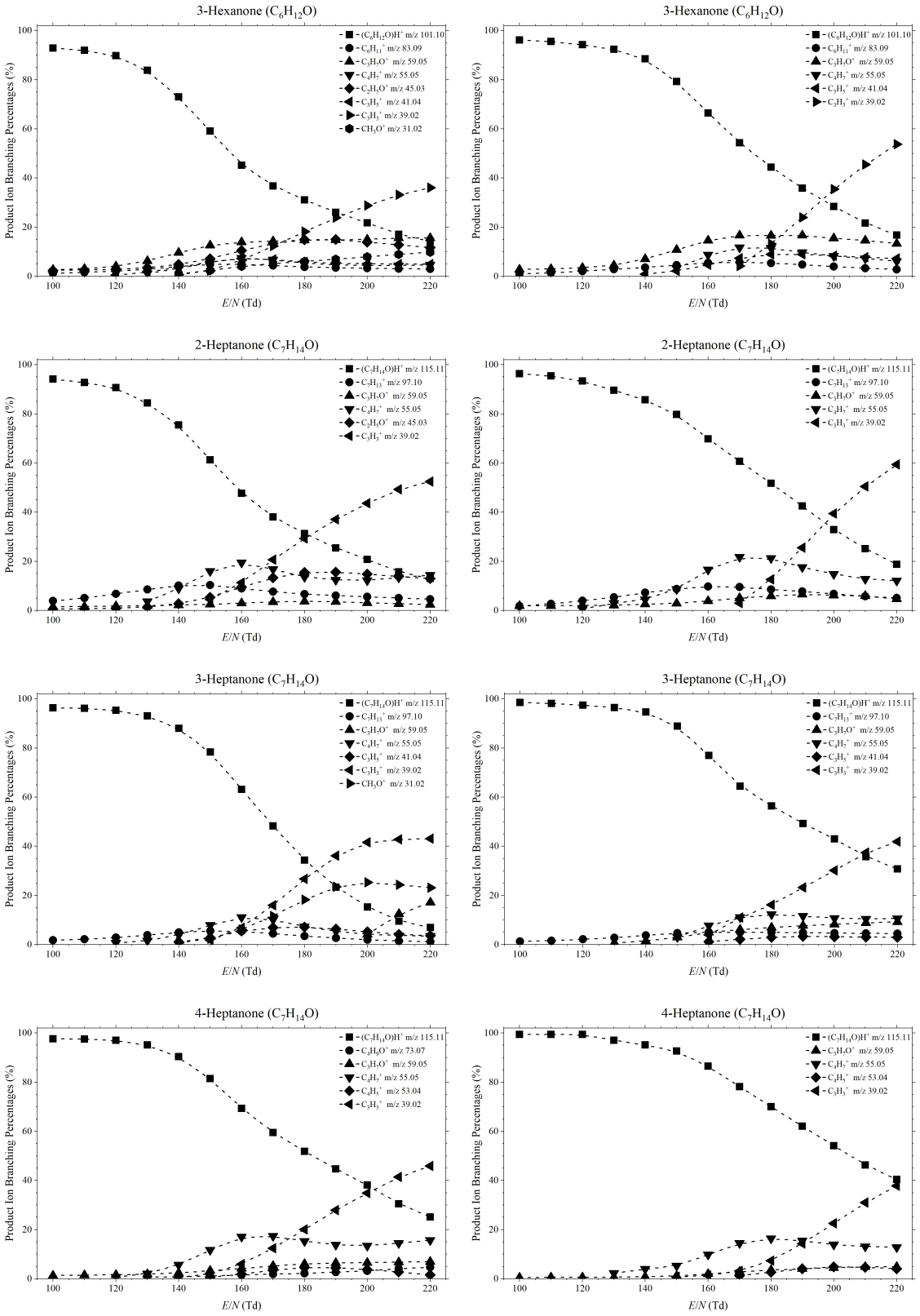

Figure 6.2: *Continued*

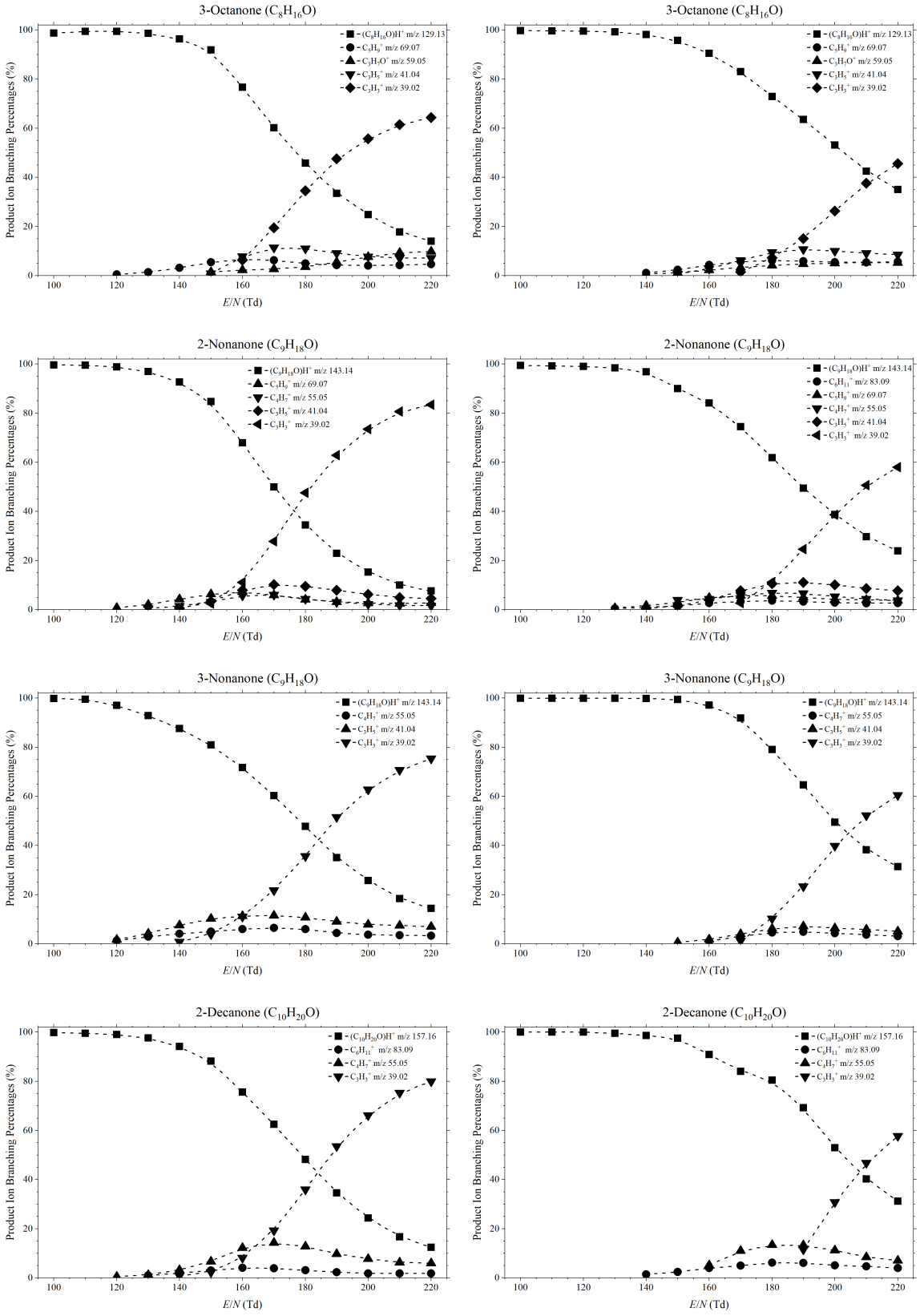

Figure 6.2: *Continued*

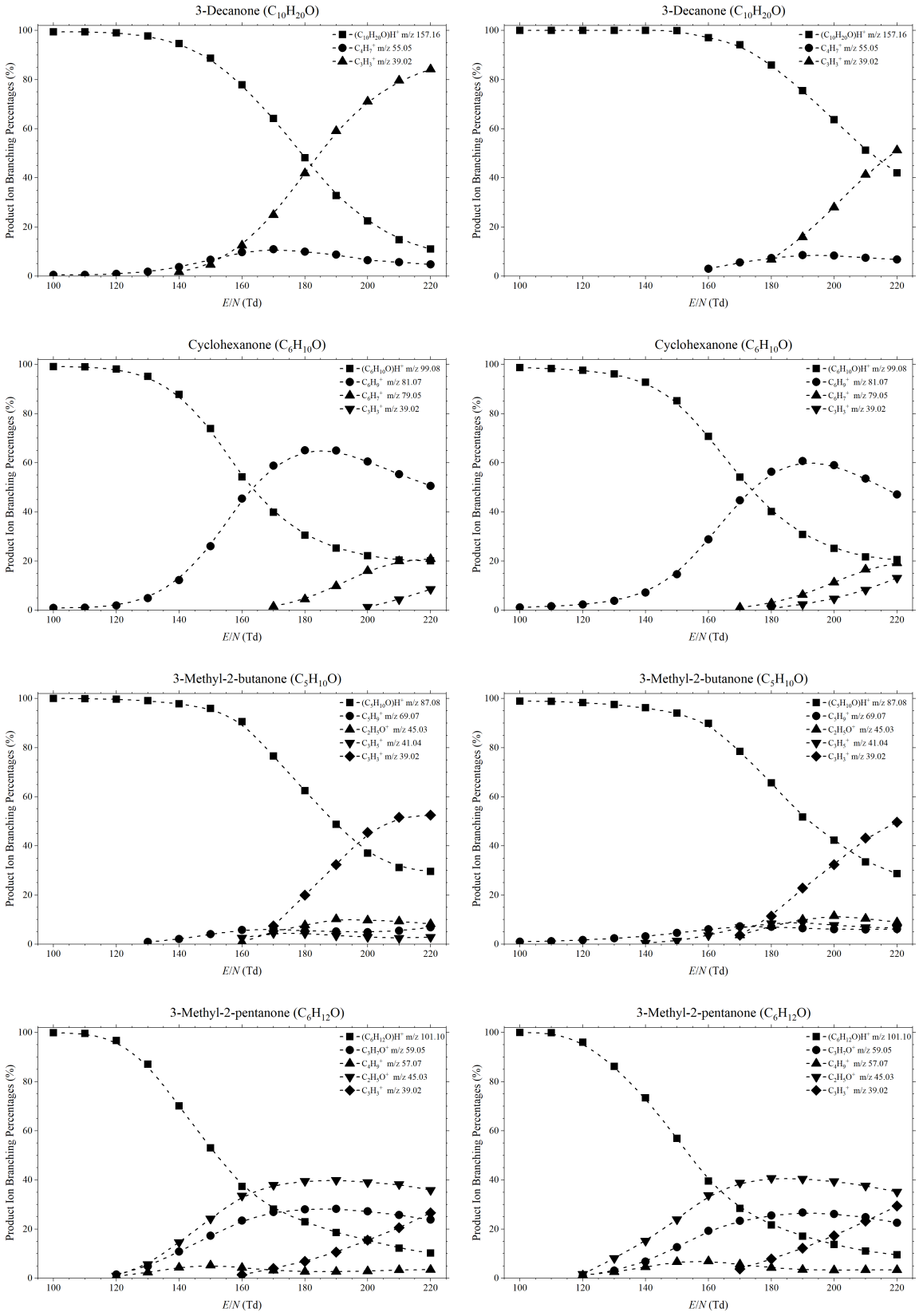

Figure 6.2: *Continued*

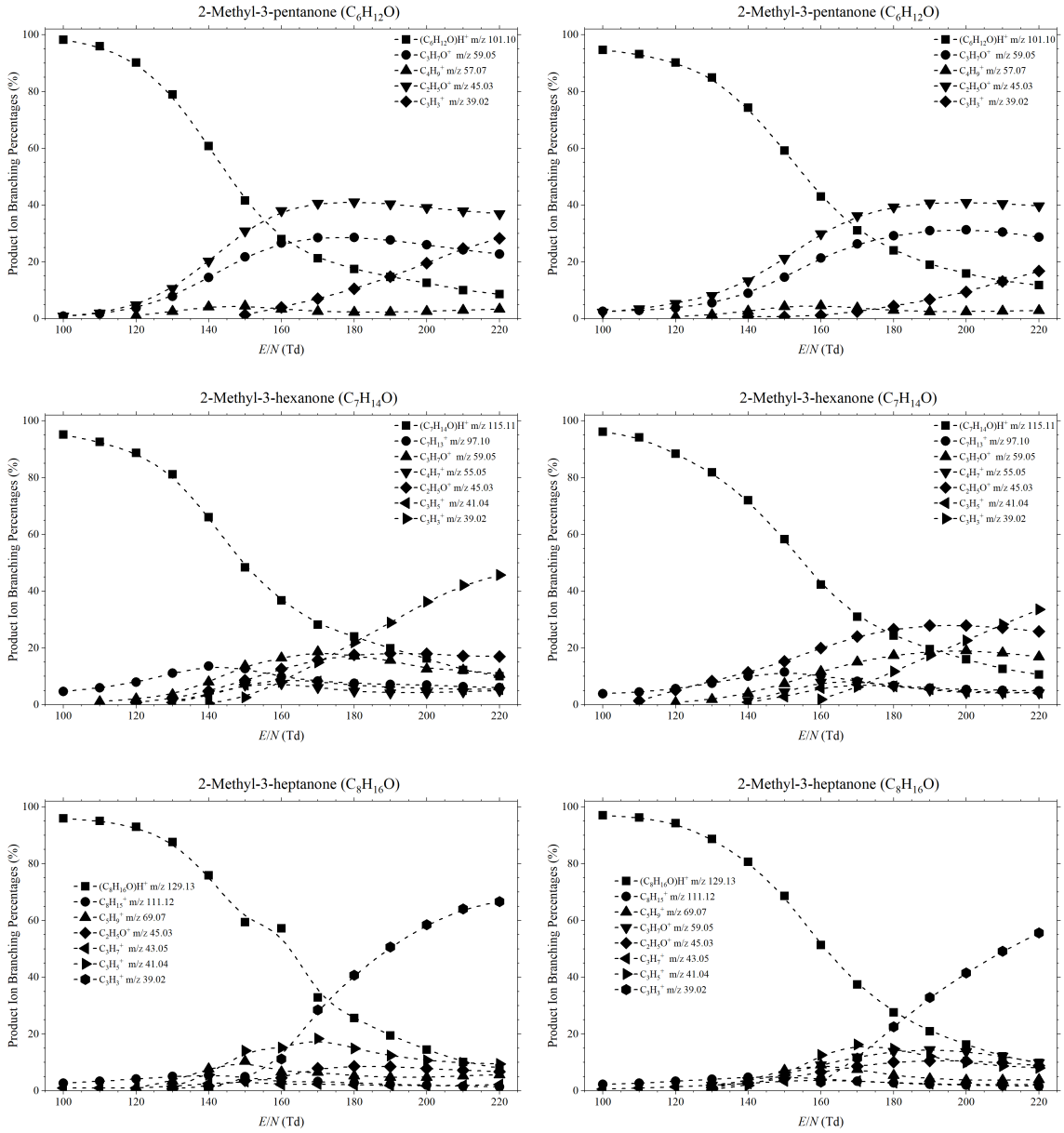

Figure 6.2: Product ion distributions (branching percentages) as a function of E/N resulting from reaction with H_3O^+ (and potentially $H_3O^+.H_2O$ as stated above) under (a) normal and (b) high humidity drift tube conditions with several ketones.

2-hexanone, 2-heptanone, 3-heptanone, 4-heptanone, 3-octanone, 2-nonanone and 2-decanone as they reported the protonated parent ion as the only product ion. However, Buhr *et al.* did observe for 2-pentanone, although at a lower percentage compared to our study, a product ion at m/z 45 tentatively assigned to protonated acetaldehyde ($C_2H_5O^+$), but these discrepancies could be explained in terms of the different equipment used in each case.

Further discrepancies are observed when comparing our product ion distributions with those from Pan *et al.*, who investigated 2-butanone, 2-pentanone, 2-hexanone, 2-heptanone and cyclohexanone using a dipolar PTR-Quad-MS (DP-PTR-MS[†]) over a range of low E/N values (50-110 Td) [147]. Pan *et al.* observed an unexpected amount of hydrocarbon ions ($C_nH_m^+$) at those collisional energies, which are also found in our investigations but only at high E/N values. This is another proof showing that the findings of various PTR-MS instruments need to be compared carefully.

In the present study, in general the protonated parent ion dominates (>80% branching percentage) up to ca. 130 Td, although 2 - 7 further product ions have been observed for each ketone. However, their contribution to the total ion signal was only noticeable at high E/N values in most cases. For example, of $C_3H_3^+$ and $C_3H_5^+$ only appear at reduced electric values of approximately 150 Td or higher. The analytes showing the highest number of fragmentation channels were 3-hexanone (7 channels), 3-heptanone (6 channels), 2-methyl-3-hexanone (6 channels) and 2-methyl-3-heptanone (7 channels). Higher molecular weight ketones were found to be more stable and show less fragmentation channels.

Additionally, the loss of H_2O was also observed for some of the analysed ketones, yielding hydrocarbons with a $C_nH_{2n-1}^+$ composition, but these represent a low percentage of the total product ion signal and also they rapidly break up at high E/N. Furthermore, it has been observed for C5 and C6 ketones that the fragmentation path resulting in $C_2H_5O^+$ very common.

The main observed result of the higher humidity conditions is that it lessens the fragmentation of the ketones, with the product ion distributions at a given E/N in normal conditions being comparable to those at a reduced electric field approximately 20 Td higher in humid conditions. This behaviour is more noticeable at mid reduced electric field values (ca. 150 Td) because of the

[†]The DP-PTR-MS technique combines both proton transfer reaction mass spectrometry (PTR-MS) and proton extraction mass spectrometry (PER-MS) to produce (in absence of fragmentation) the protonated parent ion $[M + H]^+$ at m/z m + 1 and the deprotonated parent ion $[M - H]^-$ at m/z m – 1, respectively, with M being the analyte of molecular weight m.

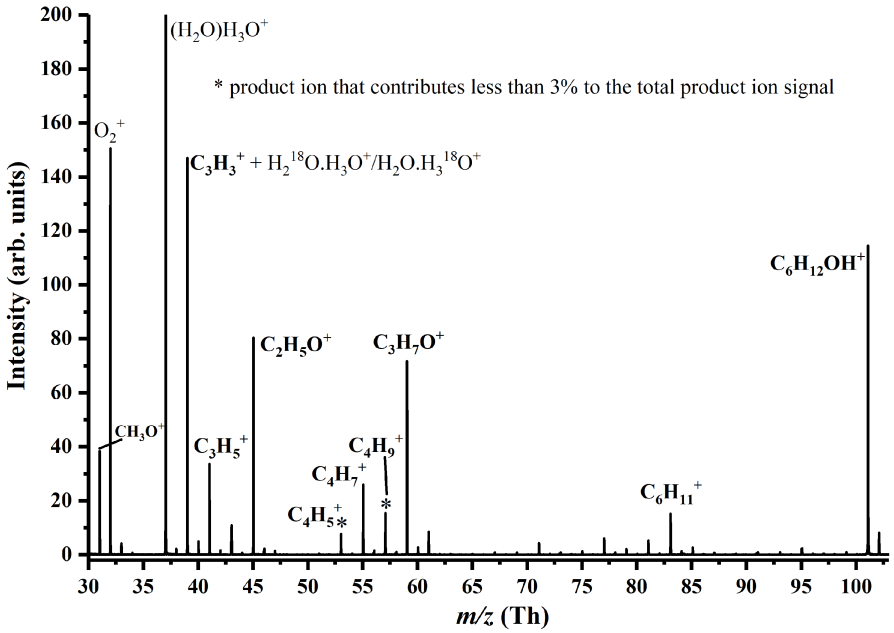

Figure 6.3: Mass spectrum for 3-hexanone recorded at 180 Td. Product ions coming from the compound are identified. The product ions $C_4H_5^+$ and $C_4H_9^+$ each contribute <3% to the total product ion percentage even at the highest reduced electric field investigated.

higher presence of protonated water clusters compared to normal conditions and the emerging fragment ions at higher collisional energies. At low E/N the higher humidity makes no difference in this ketone study because the main observed product ion is the protonated parent. Also, the three body association of the protonated parent with water was not observed in any case. On the other side, at high E/N the protonated water clusters are broken up through collisions with the buffer gas, which reduces this humidity effect. This can be illustrated by monitoring the protonated parent molecules from 2-pentanone and 3-nonanone, which, at 150 Td and normal and dry conditions, represent 47% and 69%, and 48% and 79%, respectively.

Figure 6.3 presents one of the acquired mass spectra for illustrative purposes, corresponding in this case to 3-hexanone at 180 Td. This figure shows all the detected product ions, although some of them (*i.e.* $C_4H_5^+$ and $C_4H_9^+$) are not included in Figure 6.2 or Table 6.1 because they represent less than 3% of the total product ion signal.

6.5 Conclusions

The research expounded in this chapter offers a broad database for PTR-MS users of the product ions and their relative intensities as a function of the reduced electric for the reactions of H_3O^+ and $H_3O^+.(H_2O)$ with a variety of ketones. Initially conceived because of the relevance of ketones in breath analysis, this study can however be relevant as well in the environmental sciences and atmospheric chemistry.

It is important to note that the product ion branching ratios presented here are associated to a certain PTR-MS under specific conditions (*e.g.* humidity in the drift tube), and that these may vary when using different instrumentation and configurations. Thus, these product ion branching ratios are only indicatives of the main ion/molecule reactions and fragmentation channels occurring in the drift tube. Also, no enhancement of selectivity was found for any of the ketones through manipulation of the collisional energy. This means that a pre-separation stage (*i.e.* a fastGC device) is required when analysing ketones mixtures containing isomeric compounds (*e.g.* breath samples) to distinguish between them.

A final remark is that aldehydes, which are isomers of ketones, should be accounted for when working with breath samples, as they cannot be directly separated from ketones in PTR-MS. This needs further investigation, although one of the key differences between these two families of compounds is that aldehydes fragment extensively more than ketones in PTR-MS, with the protonated parent ion usually representing less than 10% of the total product ion signal [142, 148]. Consequently, aldehydes will only represent a small portion of the protonated parent ions observed in a breath sample at low and mid reduced electric fields that could potentially be assigned to either aldehydes or ketones.

Chapter 7

Studies Pertaining to the Monitoring of Volatile Halogenated Anaesthetics in Breath by Proton Transfer Reaction Mass Spectrometry

This chapter is a reformatted copy of my published article (reference [4]):

Malásková, M., Olivenza-León, D., Chellayah, P. D., Martini, J., Lederer, W., Ruzsanyi, V., Unterkofler, K., Mochalski, P., Märk, T. D., Watts, P. & Mayhew, C. A. Studies pertaining to the monitoring of volatile halogenated anaesthetics in breath by proton transfer reaction mass spectrometry. *Journal of Breath Research* **14,** 026004 (2020). DOI: 10.1088/1752-7163/ab5e30*.

7.1 Abstract

Post-operative isoflurane has been observed to be present in the end-tidal breath of patients who had undergone major surgery for several weeks after the surgical procedures. A major new non-controlled, non-randomised, and *open–label*† approved study will recruit patients undergoing

*Ms Michaela Malásková and Mr David Olivenza-León are Early Stage Researchers attached to the IMPACT ITN. They contributed equally to the experimental investigations, and hence they should be considered as joint first authors.

†In an *open–label* study all the parts involved (*i.e.* patients, researchers and health providers) are aware of the subject of the study (*e.g.* the technique being applied or the drug being tested), unlike in a *blind* study.

various surgeries under different inhalation anaesthetics, with two key objectives, namely (1) to record the washout characteristics following surgery and (2) to investigate the influences of a patient's health and the duration and type of surgery on elimination. In preparation for this breath study using proton transfer reaction time-of-flight mass spectrometry (PTR-TOF-MS) it is important to identify first the analytical product ions needed to be monitored and under what operating conditions. In this first paper of this new research programme, we present extensive PTR-TOF-MS studies of three major anaesthetics used worldwide, desflurane ($CF_3CHFOCHF_2$), sevoflurane ($(CF_3)_2CHOCH_2F$), and isoflurane ($CF_3CHClOCHF_2$) and a fourth one, which is used less extensively, enflurane (CHF_2OCF_2CHFCl), but is of interest because it is an isomer of isoflurane. Product ions are identified as a function of reduced electric field (E/N) over the range of approximately 80 Td to 210 Td, and the effects of operating the drift tube under "normal" or "humid" conditions on the intensities of the product ions are presented. To aid in the analyses, density functional theory (DFT) calculations of the proton affinities and the gas-phase basicities of the anaesthetics have been determined. Calculated energies for the ion/molecule reaction pathways leading to key product ions, identified as ideal for monitoring the inhalation anaesthetics in breath with a high sensitivity and selectivity, are also presented.

7.2 Introduction

The monitoring of unlabelled drugs in the body in real-time offers an opportunity to determine their therapeutic effectiveness and washout characteristics in a continuous and non-invasive way. By way of illustration, several soft chemical ionisation studies have highlighted the use of breath analysis to detect intravenous anaesthetics, such as propofol during surgery [149–153], or to monitor the concentrations of inhaled anaesthetics post-surgery, either in the breath of patients or within operating and recovery rooms in hospitals [154–158]. The former has led to the development of a low cost analytical device to monitor propofol levels in the breath of patients during anaesthesia or under sedation in real-time [159]. The latter provides interesting information on the length of time these anaesthetics remain in a patient's body so that the pharmacokinetics of these anaesthetics can be better understood. Within this context, the work presented in this paper explores some potential applications of breath gas analysis in inhalation anaesthesia, which are applicable to use in a clinical setting.

In a recent proton transfer reaction – quadrupole – mass spectrometric (PTR-Quad-MS) study, involving a number of severely ill patients who had undergone major surgery, it was found that the inhalation anaesthetic used, isoflurane, took several weeks to be fully eliminated [158]. This was a very limited study, involving a small number of extremely sick people, and hence a key aim of our new research programme is to extend this pilot isoflurane study to explore the elimination characteristics for a number of inhalation anaesthetics used in surgical procedures, and investigate the dependence of the lifetime of an anaesthetic in the body on various factors that could influence the outcome, including the duration and type of surgery, the quantity of an anaesthetic inhaled, ventilation, and the health, body mass index (BMI), gender, and age of patients.

Once inhaled, an inhalation anaesthetic enters the blood stream through the alveoli where it is transported to be delivered to the brain, but on its journey to the brain some of the anaesthetic becomes stored in tissues. Of the inhalation anaesthetics being investigated, desflurane and sevoflurane have the lower tissue solubility, and therefore we can expect those two anaesthetics to be eliminated from the body in shorter timescale than that for isoflurane. Nevertheless, their lifetime in the human body may still be long given that they are primarily eliminated from the body via exhalation, and are only minimally metabolised by the liver and kidneys [160]. The low solubility of sevoflurane in blood suggests that this agent should enter and leave the body more rapidly than isoflurane. The closeness of sevoflurane and isoflurane tissue/blood partition coefficients suggests that the rates of equilibration with and elimination from tissues should be similar [161]. Yet sevoflurane is eliminated faster than isoflurane despite its greater blood/tissue partition coefficient, but slower than desflurane.

The Medical University of Innsbruck has recently granted us ethical approval to undertake a long-term respiratory gas analyses of patients following scheduled surgery. For this, the patients will be classified according to their American Society of Anaesthesiologists (ASA) physical status classification, which is used for defining the pre-operative risk assessment of the physical conditions (fitness) of patients [162]. Our study is restricted to ASA 1-3, where ASA 1 refers to normal healthy individual, ASA 2 denotes pre-operative patients who have a mild systemic disease and ASA 3 is assigned to those patients who have a severe systemic disease. It will be of considerable interest to see how the physical fitness and physical status of our volunteers will affect the retention and exhalation of an inhalation anaesthetic.

For the analyses of breath samples, we will be using mass spectrometric analytical methods, with the key instruments being proton transfer reaction mass spectrometry (PTR-MS) and ion mobility spectrometry. Proton transfer reaction mass spectrometry is a popular analytical tool used for detecting volatile compounds in complex chemical environments for a wide range of applications, ranging from food sciences through to homeland security [6, 16, 31, 104, 108, 109]. It is particularly ideal for real-time measurements, which is useful for tracking rapid changes of trace volatiles such as occurs in the atmosphere, industrial processing and in breath and for those studies for which pre-preparation and pre-concentration of the gas samples are not possible.

Before any detailed breath washout measurements on any analytical device are undertaken, it is important to ascertain how the various anaesthetics can be best detected (highest sensitivity with high selectivity) for a given analytical instrument. In the case of PTR-MS this is associated with determining the product ions (types and intensities) resulting from the reactions of reagent ions with the individual anaesthetics in the drift (reaction) tube over a range of reduced electric fields. (The reduced electric field is defined by the ratio E/N, where E is the electric field strength and N is the total molecular gas number density in the drift tube of a PTR-MS. The unit used for E/N is the townsend (Td), where 1 Td = $1{\times}10^{-17}$ V cm^2.)

In the PTR-Quad-MS study of isoflurane ($C_3H_2ClF_5O$, monoisotopic mass (lightest isotopomer) 183.97 Da) by Fernández del Río *et al.* [158], the product ion branching percentages over a small range of reduced electric fields (96-138 Td) were investigated. Prior to that study, PTR-Quad-MS studies of isoflurane were reported by Rieder *et al.* [154] at one fixed E/N to determine the air quality in a post-anaesthetic care unit. In that study they claim to have monitored protonated isoflurane, but no such product ion was observed in the study by Fernández del Río *et al.*. Only product ions resulting from dissociative proton transfer are reported in the paper by Fernández del Río *et al.* Therefore, a minor objective of the work presented in this paper is to resolve this discrepancy in the observed product ions between the two published isoflurane studies.

In addition to isoflurane, two other halogenated ether compounds are routinely used as modern inhalation anaesthetics for surgical procedures, namely desflurane ($C_3H_2F_6O$, 168.00 Da) and sevoflurane ($C_4H_3F_7O$, 200.01 Da). The choice of anaesthetic is determined by the anaesthetist depending upon its pharmacological properties, a patient's underlying diseases and use of medication, the type of breathing system being used, and duration and type of surgical procedure

[160].

The first reported PTR-MS study of sevoflurane is by Critchley *et al.* [114], using the same PTR-Quad-MS as used in the later isoflurane study of Fernández del Río *et al.*, but only at one fixed reduced electric field of approximately 140 Td. As found for isoflurane, proton transfer to sevoflurane is dissociative. Given the low mass resolution of PTR-Quad-MS systems, the reported product ions are only listed at nominal m/z–values of m/z 199, tentatively identified as $C_4F_7OH_2^+$, which would result from the elimination of H_2 from the protonated parent, m/z 181, identified as $C_4F_6H_2OH^+$, which results from the loss of HF from the protonated parent, and m/z 49, ascribed to be $CHFOH^+$. The product ion at m/z of 181 was by far the dominant product ion observed by Critchley *et al.* In agreement to this, Summer *et al.* [156], who also used a PTR-Quad-MS instrument, report using a product ion at m/z of 181 to monitor sevoflurane, although it is incorrectly identified in their work as the protonated parent. In a later study by Trefz *et al.* [157], who used a Proton Transfer Reaction - Time-of-Flight - Mass Spectrometer (PTR-ToF-MS), which has a far higher mass resolution compared to a PTR-Quad-MS, they reported sevoflurane product ions at m/z ratios of 181.007 and 198.999, with the product ion at m/z 181.007 being by far the most intense, in agreement with the study by Critchley *et al.* Given the high mass accuracy achievable with a PTR-ToF-MS, the product ion reported by Trefz *et al.* at m/z 198.999 is certainly consistent with the product ion assignment, $C_4F_7OH_2^+$, of Critchley *et al.*.

In contrast to the PTR-MS results, two investigations of the reaction of H_3O^+ with sevoflurane by Selected Ion Flow Tube-Mass Spectrometry (SIFT-MS) (Critchley *et al.* [114] and Wang *et al.* [163]) observed the same three product ions. In the study by Critchley *et al.*, the product ion at the nominal m/z value of 199 was by far the most intense of the three product ions. The earlier SIFT-MS study by Wang *et al.* found that the intensities of the product ions varied greatly with the experimental parameters and conditions, namely reaction length and the humidity in the flow tube, respectively, with the longer the reaction length resulting in $CHFOH^+$ being the dominant product ion. When using moist air in the flow tube, Wang *et al.* observed that all of the product ions, other than $CHFOH^+$, react with water and are lost.

Although enflurane is rarely used in operations, it is included in this study because it is still commercially available, and furthermore being an isomer of isoflurane it is analytically challenging to distinguish from isoflurane and provides an interesting comparison to the ion chemistry for

isoflurane. To our knowledge, there have been no other reported PTR-MS studies of desflurane and enflurane.

Details of the current PTR-ToF-MS studies of the four inhalation anaesthetics, desflurane, sevoflurane, isoflurane and enflurane as a function of reduced electric field and drift tube humidity will be presented in the following text. These provide a new or an improved understanding of the ion/molecule chemistry occurring in the drift (reaction) region of a PTR-MS for these anaesthetics. This study clearly establishes which product ions and drift tube conditions should be used in order to monitor these anaesthetics in breath following surgery with a high selectivity and sensitivity. Furthermore, and for the first time, we present in this paper density functional theory (DFT) calculations of the proton affinities, gas-phase basicities and changes in the enthalpy and free energy for the key reaction pathways leading to the product ions to be monitored for all four of the halogenated ethers. These are used in this paper to aid in the interpretation of the observed product ions.

7.3 Methods

7.3.1 Chemicals

For these present studies, surgical grade inhalation anaesthetics were obtained. Sevoflurane (CAS number: 28523-86-6) and isoflurane (CAS number: 26675-46-7) were purchased from the biopharmaceutical company AbbVie GmbH (Vienna, Austria), enflurane (CAS number: 13838-16-9) was supplied by Abbott Products Operations AG (Zwolle, Netherlands), and desflurane (CAS number: 57041-67-5) was sourced from Baxter Healthcare GmbH (Vienna, Austria). The chemicals were used directly without further purification for the PTR-MS headspace analyses reported in this paper. All of these chemicals are liquids at room temperature.

7.3.2 Proton Transfer Reaction-Time-of-Flight-Mass Spectrometry (PTR-ToF-MS)

Thorough descriptions of the instrument's operating principles and details of its applications are provided in depth by Ellis and Mayhew [31]. Hence only pertinent details will be provided here. All of the PTR-ToF-MS measurements presented in this paper were taken using an Ionicon Analytik GmbH (Innsbruck, Austria) PTR-TOF 8000, with or without the addition of a mul-

ticapillary column (MCC) for gas chromatographic pre-separation. The MCC was used under "normal" drift tube conditions to help in identifying the product ions coming from an anaesthetic of interest through limited pre-separation, thereby providing us with a higher confidence in product ion assignment to an anaesthetic. However, MCC separation capabilities are less than can be obtained with conventional (single capillary column) GC. For MCC, temporal resolution is sacrificed for smaller size and shorter cycle times, and therefore we cannot completely rule out an impurity that may be present in the sample being investigated contributing to the observed product ions.

The PTR-TOF 8000 and the MCC have been described elsewhere by Ruzsanyi *et al.* [65], and therefore only a brief overview of settings is given here. The hollow-cathode ion source was operated at a current of 3.5 mA and a voltage of 160 V, with the source-out voltage maintained at 140 V. The source valve opening was set at 40%. The drift tube's pressure and temperature were maintained at 2.3 mbar and 60°C, respectively. The voltage drop across the drift tube was varied from 365 V up to 965 V at the fixed drift tube pressure, resulting in a range of reduced electric field values from approximately 80 Td up to about 210 Td. The MCC was used at a temperature of 40°C with a N_2 (99.9999% purity) flow of 10 mL/min. For the MCC measurements, resulting products ions under three reduced electric field values of 80 Td, 140 Td and 180 Td were investigated.

The mass spectra, obtained by converting the drift times of the ions in the ToF-MS analyser, ranged from approximately m/z 3 to m/z 230, and were acquired in a time of 1 s by co-adding 25 000 single 40 μs extraction periods recorded at a sampling frequency of 10 GHz. The mass resolution in the present experiment obtained from the detected peaks was ∼2400 at m/z 100. The total duration of a complete reduced electric field experimental run was approximately 14 min, which corresponds to the acquisition of 60 mass spectra per single E/N value. The averages of the ion signal levels at each m/z–value identified to be associated with a given anaesthetic from these 60 spectra were used to calculate the intensities and branching percentages of the product ions.

Data were analysed using the PTR-MS Viewer 3.2.8, which also performed mass calibration and peak identification. Raw product ion signal intensities (counts per second) were used and, where needed for determining the sensitivity of detection, these were normalised to a constant reagent ion signal of 10^6 $H_3^{16}O^+$ ions per second for each reduced electric field measurement.

The $H_3^{16}O^+$ signal intensity cannot be measured directly, owing to its high intensity, which saturates the detector. Instead the signal intensity for the spectral line peaking at m/z 21.02, corresponding to $H_3^{18}O^+$, was recorded, from which the intensity of $H_3^{16}O^+$ was calculated.

Two humidity conditions in the drift tube were investigated, which will be referred to as "normal" or "humid", with the latter approximately corresponding to that of exhaled breath. "Normal" corresponds to the case where a dry analyte gas (absolute humidity $< 0.1\%$) is being flowed into the drift tube, but note that owing to diffusion of water vapour from the ion source into the drift tube, the buffer gas in the drift tube is not dry and hence is at a higher absolute humidity. "Humid" refers to the situation when water saturated buffer gas is used (absolute humidity 5%).

Although H_3O^+ (or the protonated water dimer – depending on the value of the reduced electric field applied) dominates the reagent ion signal, other reagent ions are always present in the drift tube, with the dominant ones being NO^+ and O_2^+, which are at levels of 1-2% and 2-6% relative to H_3O^+, respectively, with the value depending on the reduced electric field value and under "normal" operating conditions. Generally, at such low percentages they can be ignored, but care must be taken to ensure that product ions are not coming from reactions with these reagent ions if proton transfer from H_3O^+ or $H_3O^+.H_2O$ is not efficient, or at values of E/N where the reagent ion signal intensities are low.

7.3.3 Sampling Procedures

The samples were prepared as follows: A Tedlar® bag (SKC Inc., USA) of 3 L capacity was flushed with N_2 (99.9999% purity) multiple times in order reduce any possible background volatile contamination. Then the bag was filled with 2 L of dry N_2 (for the so-called "normal" measurements) or with 2 L of N_2 bubbled through water at room temperature (for the so-called "humid" measurements). Background mass spectra were recorded for each reduced electric field from approximately 80 to about 210 Td in steps of 10 Td, first ascending and then descending.

To prepare the anaesthetic samples, a 1 L gas bulb (Supelco, Canada) was maintained at 60°C while evacuating. The gas bulb was then closed, and 0.5 μL of an anaesthetic was injected into it through a septum. Dry N_2 was then introduced into the bulb to bring it to atmospheric pressure. Finally, a 5 mL sample of the gas was taken from the bulb and introduced into the bag containing either dry or humid N_2. This bag was then connected to the heated inlet of

the PTR-TOF 8000 for direct measurement. The anaesthetic concentrations entering the drift tube were in the range of approximately 400-500 parts per billion by volume (ppbv). These concentrations are sufficiently low to ensure there was not any detectable loss of the reagent ion signal, but sufficiently high to give good product ion signal intensities.

7.3.4 Density Functional Theory Calculations

Density functional theory (DFT) calculations have been undertaken to determine the proton affinities (PA) and gas-phase basicities (GB) of water, the water dimer, desflurane, sevoflurane, isoflurane and enflurane. These calculations were conducted using the Gaussian09W program with the GaussView05 for Windows interface and the B3LYP functional with 6-31+G(d,p) basis set [57] at 298 K. It should be noted that using 298 K is arbitrary as the temperature of the drift tube bath (buffer) gas is greater than this (in this study it is at 333 K) and that the translational temperature of the ions even higher due to the electric field (see later). But this is not considered too important as the energetics (particularly ΔG rather than ΔH) are being used to assist in determining the likely fragmentation pathways to the observed ions [164].

A full account of the DFT results and their interpretation for the four anaesthetics is ongoing, and are too extensive to be given with any detail in this experimentally focused paper. Furthermore, given that the main aim of this paper is to provide details on which product ion(s) should be monitored to determine the concentrations of these four volatile anaesthetics in breath with the best sensitivity, we only present sufficient DFT information to provide details on the pathways leading the key product ions that are to be recommended for monitoring purposes in the breath analysis research programme. A more detailed report on the DFT calculations will be the subject of another paper.

7.4 Results

7.4.1 PTR-ToF-MS results

7.4.1.1 $H_3O^+.(H_2O)_n$ (n = 0 and 1) reagent ions

The intensities (counts per second) of the reagent ions $H_3O^+.(H_2O)_n$ ($n = 0$ and 1) in the PTR-ToF-MS experiments, as measured at the detector as a function of reduced electric field (obtained

by changing the drift tube voltage at constant drift tube pressure) under the "normal" and the "humid" drift tube conditions already defined [20, 165] are illustrated in Figure 7.1. It can be seen that under "normal" operating conditions, H_3O^+ remains the dominant reagent ion for the complete range of the reduced electric fields investigated. This is not the case under "humid" conditions, for which the dominant reagent ion becomes $H_3O^+.(H_2O)$ for reduced electric fields below about 110 Td, and by about 80 Td it is the only reagent ion with any significant intensity.

Under both "normal" and "humid" operating conditions we find that $H_3O^+.(H_2O)_n$ (for n = 2 and 3) make negligible contributions to the total reagent ion signal at any reduced electric field. For example, at the lowest reduced electric field applied (80 Td), under "normal" and "humid" conditions, combined they contribute less than 3% and 10%, respectively, to the total reagent ion signal, with their intensities significantly declining with increasing reduced electric field, as is expected. Although it should be appreciated that these intensities correspond to those measured at the detector and hence they may not be a completely true reflection of the distributions present in the drift tube, we have found that changes in voltage supplied to the ion extraction lens, which is situated behind the skimmer cone just after the exit of orifice of the drift tube does not significantly alter the relative intensities. Therefore, we will assume that the measurements at the detector provide a reasonable indication of the protonated water and protonated water cluster distributions within the drift tube. Given their low intensities under any operating conditions, the reagent ions $H_3O^+.(H_2O)_n$ (n = 2 and 3) have been neglected in any analysis of the measurements obtained.

7.4.1.2 MCC-PTR-ToF-MS results

The m/z–values (lightest isotopomer), the molecular ion formulae (the identification of which is greatly aided by the accurate measurement of the mass spectral peak owing to the high mass resolution of the PTR-TOF 8000) and distributions of the product ions (percentages) at three E/N–values selected determined using the MCC-PTR-TOF 8000 are provided in Table 7.1. The molecular formulae of the product ions have been identified via the exact m/z (to 2 decimal places) and isotopic (^{13}C and where relevant 37Cl) intensities. This section only presents the product ions that have been identified being derived from a given anaesthetic and which result in a branching percentage of 3% or above at any given reduced electric field value investigated in this study. It should, however, be noted that there are difficulties associated with the accurate

(a)

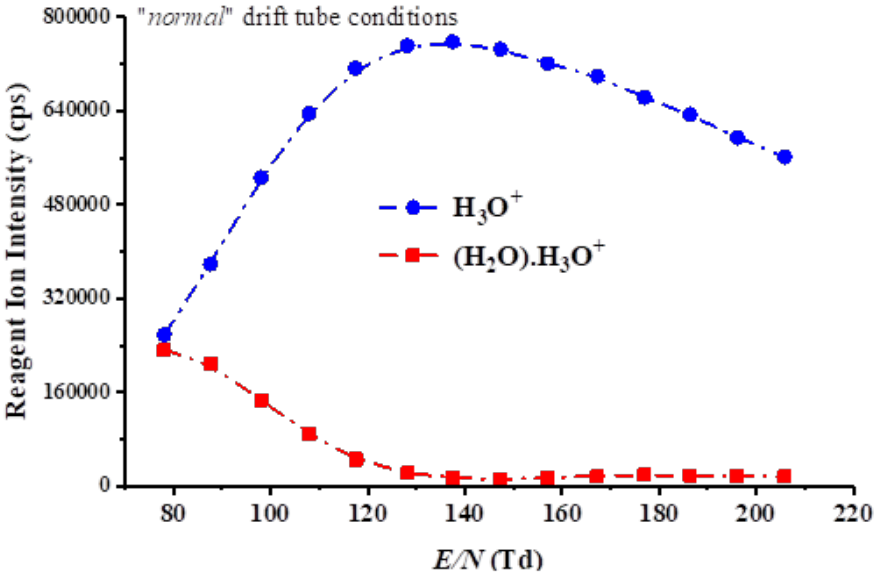

(b)

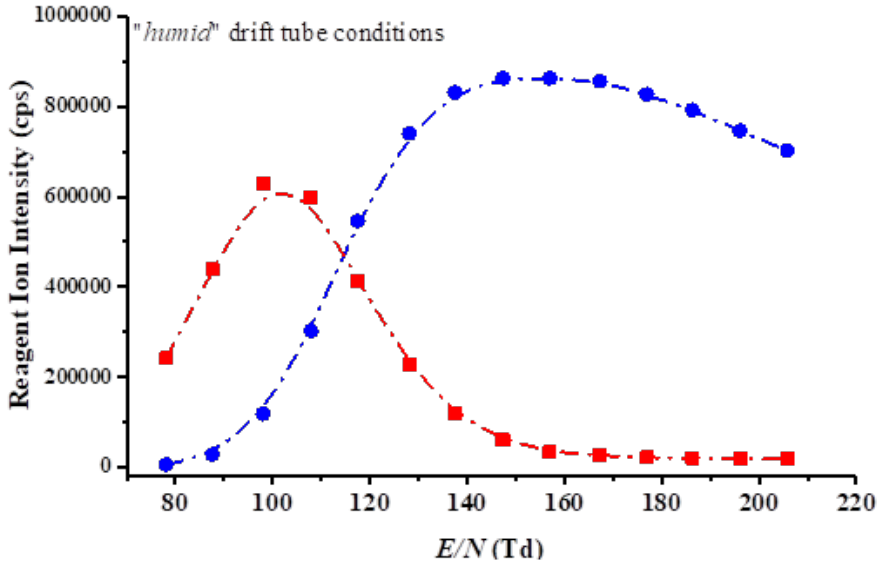

Figure 7.1: Reagent ion intensities in counts per second (cps) for $H_3O^+.(H_2O)_n$, where $n = 0$ and 1, recorded at the detector of the PTR-TOF 8000 used in this investigation under (a) "normal" and (b) "humid" operating conditions as a function of the reduced electric field (E/N).

determination of the branching percentages owing to m/z discrimination in PTR-MS. There are several factors influencing this, including diffusional and Coulombic losses of the product ions in the drift tube, and m/z discrimination in the transfer optics, mass analyser and the ion detector. Collectively, they cannot be easily quantified with a reliable accuracy over a wide range of reduced electric fields, and thus reported branching percentages are only indicative rather than quantitative, and are rather specific for the PTR-MS and its settings being used.

Details of the various product ions follow in the next section. Here we comment that the proton transfer reaction of H_3O^+ with all four anaesthetics is found to be completely dissociative, with a substantial number of product ions resulting from the reaction, and this is particularly so for isoflurane and enflurane.

7.4.1.3 Reduced electric field (E/N) investigations of the product ion intensities resulting from the individual anaesthetics

The key aim of this paper is to provide details on what product ion(s) should be monitored and under what operational conditions for maximum sensitivity for detecting an inhalation anaesthetic in exhaled breath. Hence, following the identification of the product ions for all four anaesthetics using the MCC-PTR-TOF 8000, for each anaesthetic the intensities (counts per second) of the product ions were then monitored over a range of reduced electric fields without the MCC, under "normal" and "humid" drift tube operating conditions.

"Humid" measurements are crucial, because these are closer to breath samples, and it is known that humidity in the drift tube can affect the product ion distributions. This is highlighted in two recent studies, which investigated the product ion distributions for nine deuterated compounds [165] and a series of ketones [3] in the PTR-TOF 8000. For the deuterated study, with the exception of acetone-d6, the key effect of the higher drift tube humidity was an increase of the deuterium/hydrogen isotope exchange reactions of the primary product ions with the ever present water in the drift tube. This led to the generation of various isotopologue product ions. For the ketones, the effect of humidity was not observed to be so dramatic, with the general outcome of the higher humidity in the drift tube resulting in a need for higher E/N (approximately 20 Td higher) to obtain similar product ion intensities to those found under the "normal" drift tube operating conditions.

In comparison to the two earlier studies [3, 165], investigating the consequences of humidity

Table 7.1: Product ion distributions (PID) determined using the MCC PTR-TOF 8000 resulting from the reactions of the $H_3O^+.(H_2O)_n$ ($n = 0$ and 1) reagent ions in the drift tube with the four halogenated ethers at three reduced electric field (E/N) values measured under "normal" drift tube conditions. Only product ions which contribute at least a branching percentage of 3% at any given reduced electric field over the range of 80-210 Td have been included. The m/z–values given for the neutral species and the product ions are for the lightest isotopomer, but the percentages provided have taken into account the contributions to the total ion signal of all isotopic variants (^{13}C and where relevant ^{37}Cl) to provide a more accurate branching percentage.

Anaesthetic	**Product ions**	**PID (%)**		
Stochiometric Formula	Formula, m/z (lightest isotopomer)	***E/N* (Td)**		
Monoisotopic mass		**80**	**140**	**180**
Desflurane	$C_3H_2F_5O^+$, 149.00	87	56	25
$CF_3CHFOCHF_2$	$C_3F_5O^+$, 146.99	8	20	6
168.00	C_2F_4H+, 101.00	-	2	8
	CHF_2^+, 51.00	5	22	61
Sevoflurane	$C_4H_3F_6O^+.H_2O$, 199.02	7	1	1
$(CF_3)_2CHOCH_2F$	$C_4H_3F_6O^+$, 181.01	68	97	81
200.01	CF_3^+, 69.00	-	-	3
	CHF_2^+, 51.00	-	2	15
	CH_2FO^+, 49.01	25	-	-
Isoflurane	$C_3F_4ClO^+.H_2O$, 180.97	3	-	-
$CF_3CHClOCHF_2$	$C_3H_2F_4ClO^+$, 164.97	74	5	2
183.97	$C_3F_4ClO^+$, 162.96	8	6	1
	$C_3HF_3ClO^+$, 144.97	5	1	-
	$C_2HF_3Cl^+$, 116.97	-	27	19
	$C_2H_2F_2ClO^+$, 114.98	6	1	-
	$CHFCl^+$, 66.98	3	42	63
	CHF_2^+, 51.00	1	18	15
Enflurane	$C_3F_4ClO^+$, 162.96	4	1	-
CHF_2OCF_2CHFCl	$C_3HF_3ClO^+$, 144.97	7	1	-
183.97	$C_2HF_3ClO^+$, 132.97	4	1	-
	$C_3H_3F_3Cl^+$, 130.99	31	-	-
	$C_2HF_3Cl^+$, 116.97	1	12	9
	$C_2H_2F_2ClO^+$, 114.98	3	2	1
	$C_2F_2ClO^+$, 112.96	9	7	1
	$CHFCl^+$, 66.98	31	62	78
	CHF_2^+, 51.00	9	14	11

on the product ion distributions, effects caused by differing humidity conditions in the drift (reaction) tube of a PTR-MS are found to be more dramatic on the production of the product ions for the anaesthetics studied in this investigation. Figures 7.2-7.5 provides the intensity curves (intensities of product ions in terms of counts per second (cps) as a function of the reduced electric field) for the product ions identified for (a) desflurane, (b) sevoflurane, (c) isoflurane and (d) enflurane over the range of reduced electric fields investigated under both "normal" and "humid" drift tube conditions. What is noticeable from this plot immediately is the dramatic decrease in signal intensity under the "humid" compared to the "normal" drift tube conditions for low reduced electric fields (*i.e.* approximately < 110 Td), and this is particularly so for isoflurane and enflurane.

7.4.1.3.1 Product ions resulting from desflurane and sevoflurane

For desflurane and sevoflurane the dominant product ion observed for the majority or all of the reduced electric field values investigated, respectively, results from the loss of HF following proton transfer from H_3O^+ to the anaesthetic. The difference in the E/N intensity profiles of this dominant product ion for desflurane and sevoflurane, Figure 7.2 and Figure 7.3, respectively, is surprising given that the same reaction pathway is followed with similar energetics. We have confirmed that this difference in intensity profiles is real by repeating the E/N intensity profile measurements with a dry and humid nitrogen sample containing a mixture of both desflurane (at approximately 500 ppbv) and sevoflurane (at approximately 400 ppbv).

For desflurane, above about 170 Td, the product ion at m/z 51.00 (assigned to be CHF_2^+) becomes the dominant product ion. Other product ions originating from desflurane are at m/z–values of 146.99 and 101.00, assigned to be $C_3F_5O^+$ and $C_2F_4H^+$, respectively, with their intensities being much less than the maximum reached by $C_3H_2F_5O^+$ at a lower reduced electric field.

In addition to the dominant product ion, four other product ions have been assigned to result from the reaction of H_3O^+ with sevoflurane. One, at m/z 199.02, is considered to result from the association of water to the dominant product ion $C_4F_6H_2OH^+$. As found for desflurane, CHF_2^+, at m/z 51.00, is also a product ion with a significant branching percentage, but with a relatively low intensity, at high reduced electric fields. The two other product ions observed are at m/z 69.00 (CF_3^+) and m/z 49.03 (CH_2FO^+), but with insignificant intensities compared to

(a)

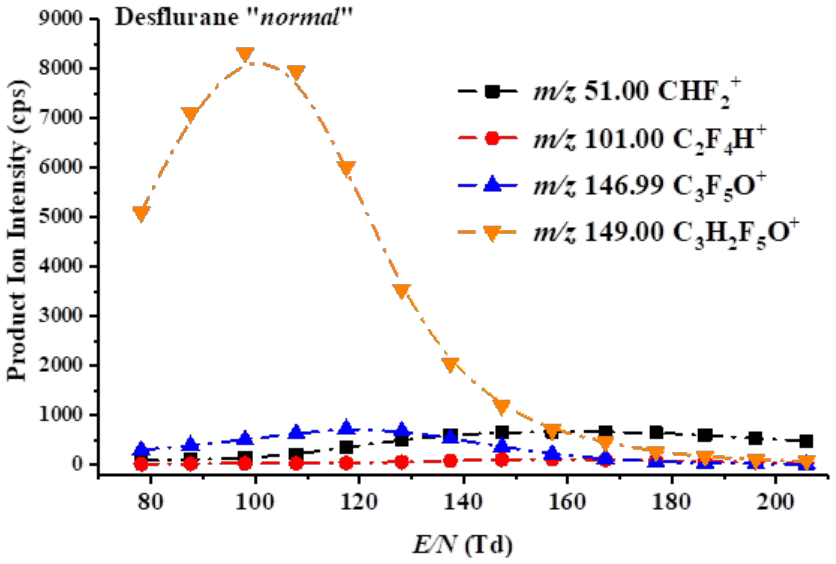

(b)

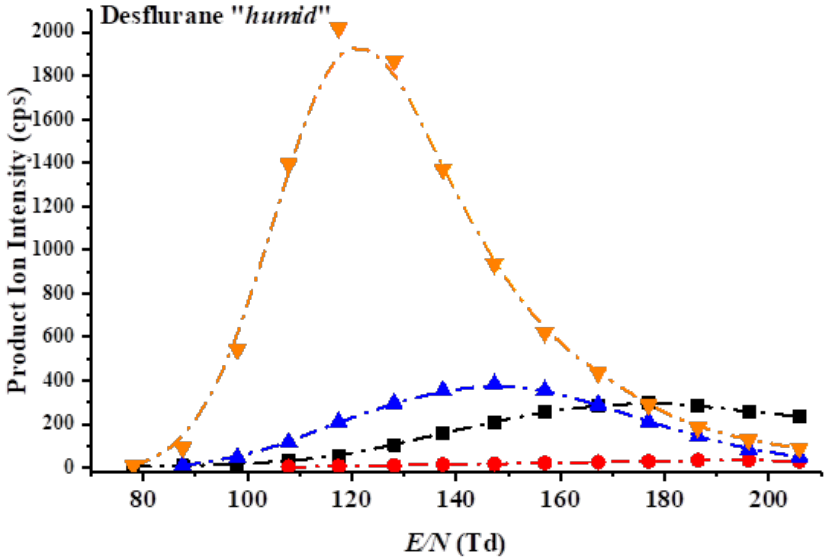

Figure 7.2: Signal intensities in terms of raw counts per second of the product ions resulting from reactions of the $H_3O^+.(H_2O)_n$ (predominantly $n = 0$ and 1 – see Figure 7.1) with desflurane as a function of the reduced electric field under (a) "normal" and (b) "humid" drift tube operating conditions. The m/z–values given for the product ions are for the lightest isotopomer, but the intensities have taken into account all isotopic variants, namely contributions from the ^{13}C.

(a)

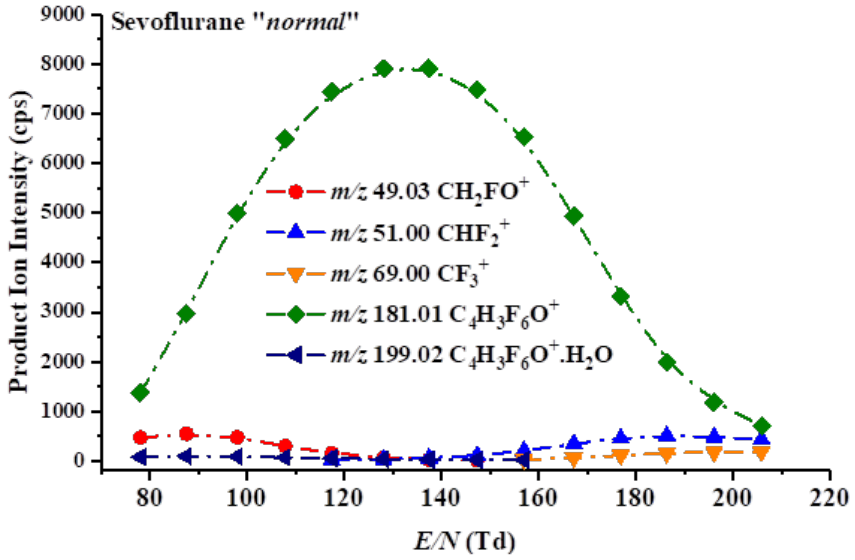

(b)

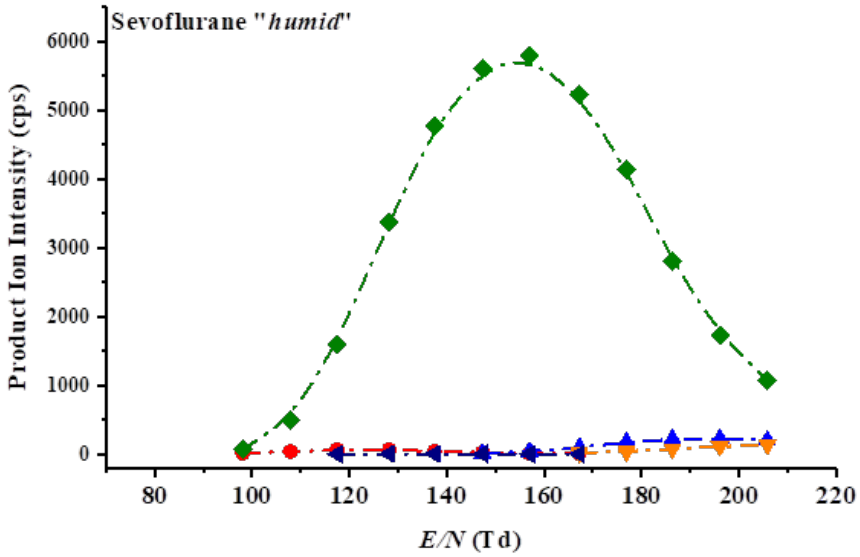

Figure 7.3: Signal intensities in terms of raw counts per second of the product ions resulting from reactions of the $H_3O^+.(H_2O)_n$ (predominantly $n = 0$ and 1 – see Figure 7.1) with sevoflurane as a function of the reduced electric field under (a) "normal" and (b) "humid" drift tube operating conditions. The m/z–values given for the product ions are for the lightest isotopomer, but the intensities have taken into account all isotopic variants, namely contributions from the ^{13}C–containing product ions.

(a)

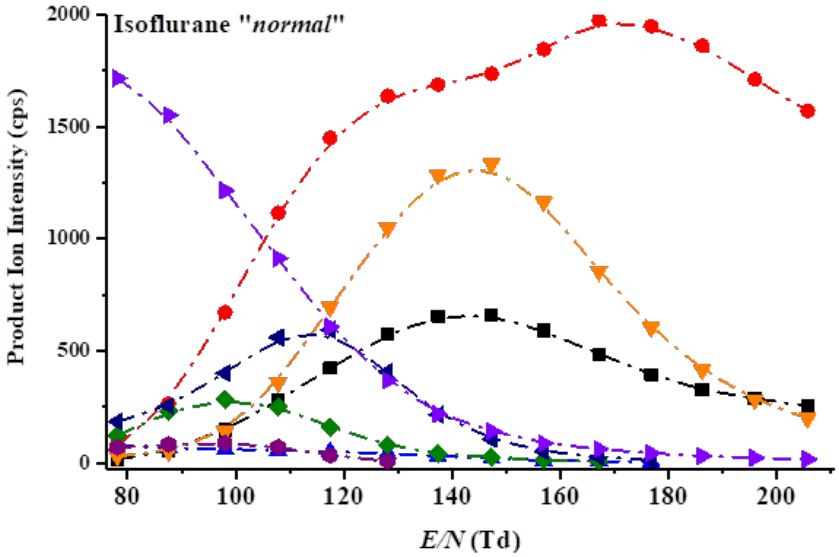

(b)

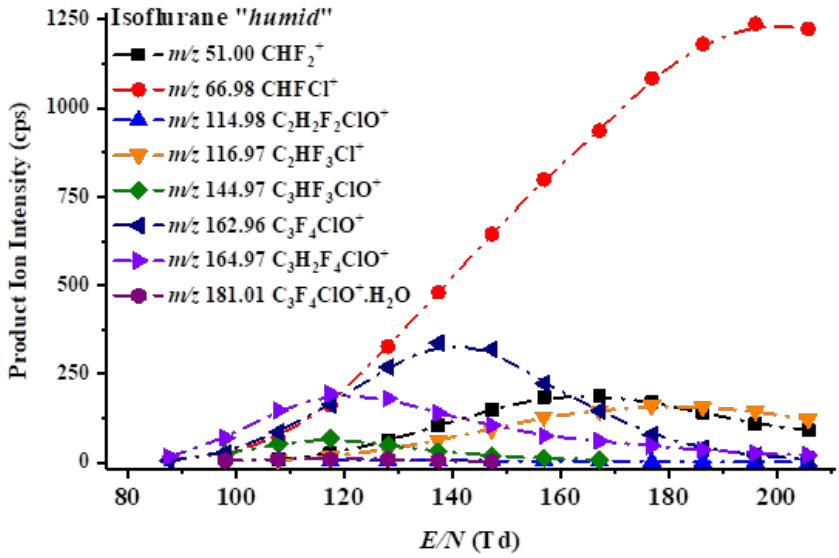

Figure 7.4: Signal intensities in terms of raw counts per second of the product ions resulting from reactions of the $H_3O^+.(H_2O)_n$ (predominantly $n = 0$ and 1 – see Figure 7.1) with isoflurane as a function of the reduced electric field under (a) "normal" and (b) "humid" drift tube operating conditions. The m/z–values given for the product ions are for the lightest isotopomer, but the intensities have taken into account all isotopic variants, namely contributions from the ^{13}C–containing product ions and the ^{37}Cl–containing product ions.

(a)

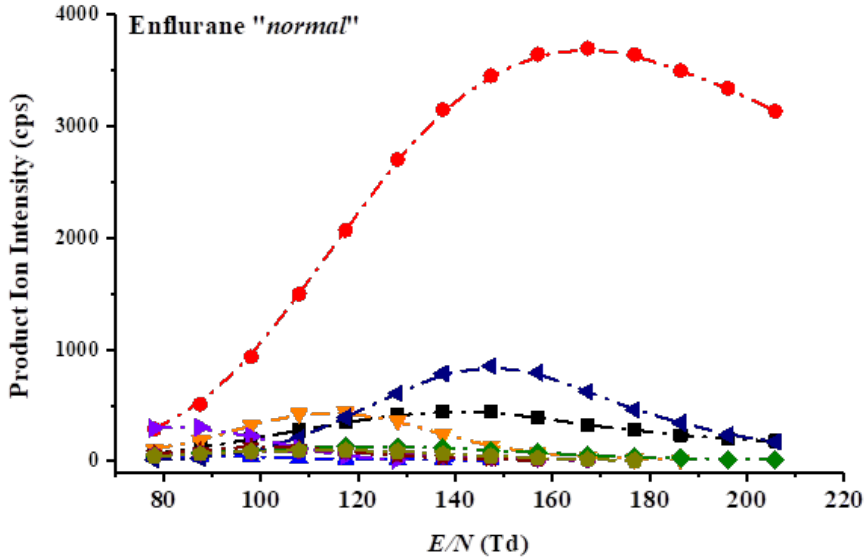

(b)

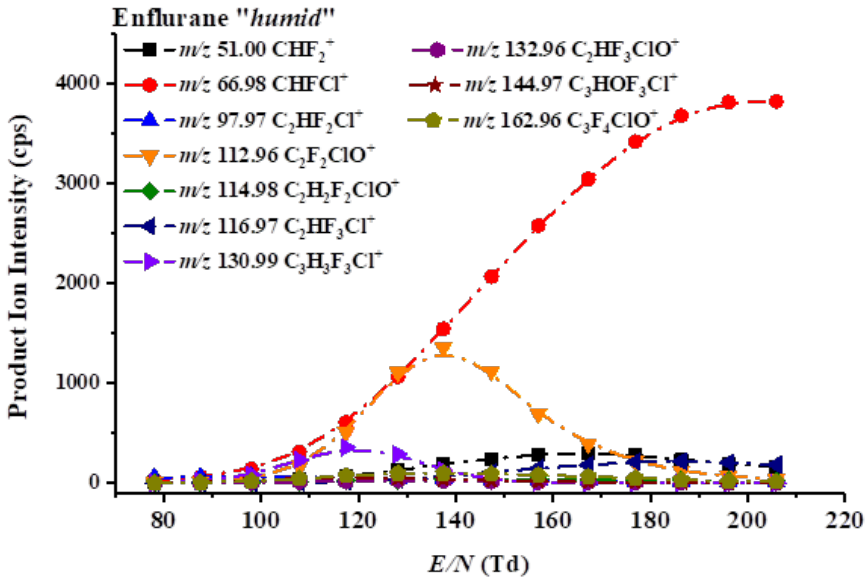

Figure 7.5: Signal intensities in terms of raw counts per second of the product ions resulting from reactions of the $H_3O^+.(H_2O)_n$ (predominantly $n = 0$ and 1 – see Figure 7.1) with enflurane as a function of the reduced electric field under (a) "normal" and (b) "humid" drift tube operating conditions. The m/z–values given for the product ions are for the lightest isotopomer, but the intensities have taken into account all isotopic variants, namely contributions from the ^{13}C–containing product ions and the ^{37}Cl–containing product ions.

the maximum achieved by $C_4H_3F_6O^+$.

Using a reduced electric field of 140 Td, a product ion resulting from the reaction of H_3O^+ with sevoflurane was identified with a nominal value of *m/z* 199 by Critchley *et al.* [114]. This was detected with a higher accuracy at *m/z* 198.999 by Trefz *et al.* [157]. As mentioned in the introduction, both studies assigned the product ion to be $C_4F_7OH_2^+$. In our measurements, at 80 Td the peak position in this mass range is at *m/z* 199.02, which is more consistent with the product ion $C_4F_6H_2OH^+.H_2O$. It is possible that at higher reduced electric fields the product ion we observe at *m/z* 199 is indeed $C_4F_7OH_2^+$, but its intensity is too low in our study for us to accurately measure its peak position. Given that, in agreement with this study, the two other PTR-MS studies that identify a product ion at a nominal *m/z* value of 199 show that the signal intensity relative to the other product ions is extremely low, it is of no relevance for determining breath concentrations of sevoflurane. Thus, given the low intensity involved, whether the ion at *m/z* 199 is either $C_4F_6H_2OH^+.H_2O$ and/or $C_4F_7OH_2^+$ is irrelevant to the current aim of this work, and hence we will not discuss it further in this paper.

7.4.1.3.2 Product ions resulting from isoflurane and enflurane

In comparison to desflurane and sevoflurane, for isoflurane and enflurane, the dominant product ion selected for monitoring purposes is at a much lower *m/z* value of 67, assigned to be $CHFCl^+$, which can only occur via significant fragmentation. This is discussed further in section 7.4.2, which deals with the interpretation of reaction pathways with the aid of DFT calculations leading to the product ions to be monitored for the breath analysis programme. Given the number and complexity of the product ions observed for these two anaesthetics, a full discussion of the reaction pathways and the energetics involved will be the subject of another paper for which the full energetics will be provided. We will just comment here on the product ions observed for enflurane at *m/z* 130.99 and at *m/z* 132.99 (with an intensity one third of that at *m/z* 130.99), which is consistent with a product ion having a molecular formula $C_3H_3F_3Cl^+$. It is difficult to provide an explanation as to how this product ion can be formed, because it requires the elimination of F_2O from the protonated parent.

7.4.1.3.3 Detection Sensitivities of the Anaesthetics

The "humid" intensity curves provide the results needed to fulfil a key objective of this invest-

Table 7.2: Best operating reduced electric fields values (highest sensitivity) and product ion to monitor for the anaesthetics desflurane, sevoflurane, isoflurane and enflurane in breath ("humid" drift tube conditions) and in closed environments (*e.g.* operating theatres) ("normal" drift tube conditions), determined using an Ionicon Analytik GmbH PTR-TOF 8000 instrument. The sensitivity of detection in terms of ncps/ppbv (total product ion cps normalised to 10^6 H_3O^+ reagent ions) under the "normal" drift tube operating conditions are provided.

Anaesthetic	***E/N* (Td) for highest sensitivity**		**Sensitivity (ncps/ppbv)**	**Product ion Formula, *m/z***
	"humid"	**"normal"**	**"normal"**	
desflurane	120	100	18	$C_3H_2F_5O^+$, 149.00
sevoflurane	150	130	20	$C_4H_3F_6O^+$, 181.01
isoflurane	200	150	11	$CHFCl^+$, 66.98 + 68.98
enflurane	200	130	9	$CHFCl^+$, 66.98 + 68.98

igation, namely to determine the appropriate PTR-TOF 8000 operational parameters and the product ion(s) in order to monitor the four inhalation anaesthetics in exhaled breath with the highest sensitivity. The key results are summarised in Table 7.2, which also provides details of the best sensitivity for "normal" conditions for comparison. Table 7.2 and figures 7.2-7.5 show that under the "normal" operating conditions, the best sensitivities are at lower reduced electric fields than required for a "humid" drift tube.

The total product ion intensities at the reduced electric fields for which the maximum signal is obtained to determine the sensitivity of detection, in terms of normalised counts per second (ncps) (normalised to 10^6 H_3O^+ reagent ions) for 1 ppbv of an anaesthetic, are also presented in Table 7.2.

We find that the sensitivity of detection for isoflurane and enflurane is less than that for desflurane and sevoflurane. Differences in reaction time will play a role, but also m/z–dependent transmission factors will have an effect. In a TOF-MS there is a discrimination against lower m/z ions. Given these factors and measurement errors associated with the calculation of the concentrations, the sensitivities obtained for all the anaesthetics are comparable, being between 10 and 20 ncps/ppbv.

For comparison, we investigated the instrument's sensitivity for detecting limonene, because it is known that limonene reacts with H_3O^+ with unit efficiency [166], and, given the proton affinity of $(H_2O)2$, we can expect $H_3O^+.H_2O$ will react with limonene via a proton transfer process also

at the collisional rate. For this compound the product ions to monitor are a fragment product ion at m/z 81.07, corresponding to $C_6H_9^+$, and the protonated parent, $C_{10}H_{17}^+$, at m/z 137.13. Given that the proton affinity of limonene is higher than that of water and the water dimer, the sum of the counts per second for the two product ions was normalised to 10^6 (H_3O^+ $H_3O^+.H_2O$). We find that we have maximum sensitivity for the detection of limonene at a reduced electric field of 80 Td, with a value of approximately 20 ncps/ppbv, *i.e.* similar to the sensitivities obtained for the anaesthetics.

7.4.2 DFT calculations

The experimental results show that for all four of the anaesthetics investigated in this study, a significant number of product ions are observed, and that all product ions are a result of dissociative processes, *i.e.* no protonated anaesthetic is observed. An objective of the computational calculations is to aid in interpreting this observation and to improve our understanding of the pathways leading to these product ions. These calculations have shown that many of the reaction pathways require significant increases in the free energy from that calculated at 298 K (up to several eVs in some instances) to deliver some of the product ions. The energy required to do this must be supplied to the ions through the translational energy gained in the electric field, which is in part converted to internal energy through collisions with the buffer gas. Within the drift tube thermodynamic equilibrium does not apply, because the reagent and product ions will have effective translational temperatures much higher than thermal owing to the drift velocities they obtain, which are dependent on ion mobility coefficients and the strength of the applied electric field. This results in collisional energies in the centre-of-mass frame between the reagent ions and the analytes that can drive reaction pathways, and once the primary product ions are produced resulting from the initial dissociative proton transfer reaction, these product ions can undergo further collisional induced dissociation.

Key to any analysis of product ions resulting from proton transfer are the values for the proton affinities (PA) and gas phase basicities (GB) for the analytes. Table 7.3 presents the calculated PA and GB for water, the water dimer and for the four anaesthetics (various protonation sites are provided). To our knowledge, for the four anaesthetics investigated in this study, this is first time these thermodynamic quantities have been calculated and presented. The quoted energies for the key (dominant) reaction pathways are referenced to the flurane and H_3O^+ at 298 K.

Table 7.3: Calculated proton affinities (PA) and gas-phase basicities (GB) for water, the water dimer and for the four halogenated ethers. Calculations were performed using the B3LYP Functional and the 6-31+G(d,p) basis set at 298 K. Values are given for various protonation sites (see text).

Compound	***PA*** **(kJ mol^{-1})**	***GB*** **(kJ mol^{-1})**
Water	684	653
Water dimer	842	777
Desflurane		
site 1	652	638
site 2	623	621
site 3	636	619
site 4	565	539
Sevoflurane		
site 1	587	572
site 2	653	625
site 3	678	660
Isoflurane		
site 1	670	655
site 2	642	622
site 3	637	608
site 4	573	552
Enflurane		
site 1	657	638
site 2	662	646
site 3	625	596
site 4	594	574

Of note is that none of the anaesthetics has proton affinities greater than water. An often–stated phrase in PTR-MS research papers is that for a compound to be detected with any sensitivity it needs to have a proton affinity greater than that of water. This is not strictly true, because, and as mentioned earlier, proton transfer can be driven by the translational energy gained by the reagent ions in the electric field and through a reagent ion's internal energy, which may have been gained during its formation in the ion source or through collisional processes in the drift tube. Furthermore, the key quantity is not the difference in the proton affinities (ΔH), but changes in the free energy (ΔG), and proton transfer from protonated water to a volatile will be thermodynamically spontaneous if ΔG is negative. What is crucial is that once formed the protonated parent must spontaneously dissociate, otherwise it will react with the far more abundant water in the drift tube, dramatically reducing the sensitivity for detection of the parent molecule in PTR-MS analysis. Thus dissociation of a protonated parent, which can thermodynamically donate its proton to water, must occur on a time scale less than the average time for a collision between the protonated analyte and water in the drift tube. If this is not the case any protonated analyte will donate its proton to water in the drift tube with unit efficiency in a reverse reaction, and, given that water is in far higher concentrations than the analyte in the drift tube, the chemical equilibrium will be in favour of H_3O^+ production. Here the former is happening leading to copious amounts of product ions resulting from dissociative proton transfer, and this explains why they can be detected with high sensitivity with PTR-MS when using H_3O^+ at the reagent ion.

7.4.2.1 Desflurane

The four protonation sites are schematically represented below:

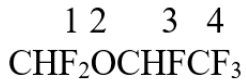

At 298 K proton transfer from H_3O^+ to desflurane is endothermic for all of the sites, with that to site 1 resulting in the lowest enthalpy (ΔH_{298} = + 32 kJ mol^{-1}) and free energy (ΔG_{298} = + 15 kJ mol^{-1}) changes.

Following proton transfer, the protonated desflurane fragments. The dominant fragment product ion observed in the experimental measurements, up to about a reduced electric field of

150 Td under "normal" drift tube conditions and 170 Td under "humid" drift tube conditions, is *m/z* 149.00 corresponding to loss of HF. This could occur from sites 1, 3, and 4, but loss from site 1 is the most likely as DFT investigations suggest that whilst loss from sites 3 and 4 is possible, further fragmentation is probable. Loss of HF from protonated desflurane does not involve a transition state (*i.e.* it is a barrierless process). The loss of HF from the other protonated anaesthetics does not involve a transition state either. The associated energetics with the loss of HF are ΔH_{298} = +81 kJ mol^{-1} and ΔG_{298} = +43 kJ mol^{-1}, which are easily accessible in the drift tube.

7.4.2.2 Sevoflurane

The protonation sites for sevoflurane are defined below:

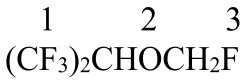

Protonation to site 3 is essentially thermoneutral at 298 K (ΔH_{298} = +6 kJ mol^{-1} and ΔG_{298} = -7 kJ mol^{-1}). Given the small enthalpy and free energy changes, proton transfer from H_3O^+ to sevoflurane is likely to be efficient, meaning that the reaction rate coefficient must be at the collisional value. This agrees with the results obtained from a selected ion flow tube study of the reaction of H_3O^+ with sevoflurane [163], for which the experimentally determined room temperature reaction rate coefficient of 3.4×10^{-9} cm^3 s^{-1} is equal to the calculated collisional rate coefficient.

The dominant product ion is again formed by loss of HF from the protonated parent, and whilst loss from both sites 1 and 3 is possible with both leading to stable product ions, loss from site 3 is most likely and has the energetics ΔH_{298} = +50 kJ mol^{-1} and ΔG_{298} = +4 kJ mol^{-1}.

7.4.2.3 Isoflurane

The four sites for protonation on the isoflurane molecule are schematically represented below:

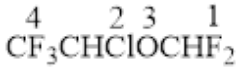

Protonation to site 1 is essentially thermoneutral at 298 K (ΔH_{298} = +14 kJ mol^{-1} and ΔG_{298} = -2 kJ mol^{-1}). A SIFT study reports that, as found for sevoflurane, the reaction with

H_3O^+ occurs at the collisional rate [163]. The dominant product ion recommended for monitoring purposes is at m/z 67, $CHFCl^+$, which can only occur via significant fragmentation. Extensive DFT investigations show that the only route to this ion is protonation at site 1 followed by the loss of HF. The resulting ion at m/z 165 has three possible further fragmentation routes but the one of interest here is fragmentation into the $CHFCl^+$ ions and the CF_3CHO neutral. This fragmentation involves a Transition State and a migration of the Cl atom. The energetics for the initial loss of HF are ΔH_{298} = +54 kJ mol^{-1} and ΔG_{298} = +8 kJ mol^{-1}. The further fragmentation into $CHFCl^+$ and associated Transition State have the energetics ΔH_{298} = +174 kJ mol^{-1} and ΔG_{298} = +77 kJ mol^{-1} and ΔH_{298} = +182 kJ mol^{-1} and ΔG_{298} = +77 kJ mol^{-1}, respectively.

7.4.2.4 Enflurane

The four sites for protonation on the enflurane molecule are defined as shown below:

$$\overset{1}{F_2}\overset{3}{C}H\overset{2}{O}\overset{}{C}\overset{4}{F_2}CHFCl$$

As mentioned earlier, the dominant product ion that can be used for exhaled breath monitoring purposes is at m/z 67, $CHFCl^+$, as found for isoflurane. The most plausible fragmentation pathway to this ion is loss of HF following protonation at site 1 (ΔH_{298} = +27 kJ mol^{-1} and ΔG_{298} = +15 kJ mol^{-1}) followed by further fragmentations to CHFO plus CF_2 and $CHFCl^+$, which appears to be barrierless. Whether this final fragmentation pathway is sequential or concerted is the subject of further theoretical investigations. The overall energetics are ΔH_{298} = +347 kJ mol^{-1} and ΔG_{298} = +203 kJ mol^{-1}.

7.5 Discussion and Concluding Remarks

The calculated proton affinities of the anaesthetics are significantly less than any of the water clusters. This explains the low product ion signal intensities observed for all of the anaesthetics under the "humid" drift tube conditions for low E/N (< 100 Td) when the protonated water dimer is the dominant reagent ion species.

In the selected ion flow tube study of isoflurane and sevoflurane by Wang *et al.*, the reaction rate coefficients for their reactions with H_3O^+ were determined from the relative decay rates of

H_3O^+ and O_2^+ reagent ions, and the assumption that O_2^+ reacts at the collisional rate [163]. This assumption is based on their observation that all other O_2^+/ether reactions they had studied proceed at their collisional rates [167], although care has to be taken with this, because even highly exothermic charge transfer reactions may proceed with reaction rate coefficients substantially below the collisional value [123, 168, 169]. Nevertheless, Wang *et al.* find that the relative decay rates of H_3O^+ and O_2^+ following their reaction with sevoflurane are in the ratio expected if both reactions proceed at their respective collisional rates. Wang *et al.* also find that their experimentally determined reaction rate coefficient of 3.4×10^{-9} cm^3 s^{-1} for the reaction of H_3O^+ with isoflurane is only slightly less than their calculated collisional rate value (k_c = 3.5×10^{-9} cm^3 s^{-1}) implying, they claim, that the proton affinity of isoflurane must be slightly less than that of water. Although the measured reaction rate coefficient is within experimental error identical to the collisional value, the accuracy of the collisional rate coefficient is compromised because the polarizability and dipole moment of isoflurane had to be estimated. Nonetheless, the calculations presented in this paper confirm that their claim is correct for the reaction pathway leading to protonation on site 1 (ΔH_{298} = +14 kJ mol^{-1}), with the reaction pathway being driven by entropic effects (ΔG_{298} = -2 kJ mol^{-1}), and hence the reaction should proceed at the collisional rate, as experimentally observed.

As expected from the calculated *PA*s and *GB*s of the four halogenated ethers, the intensities of the product ions (counts per second) are diminished at low reduced electric fields under both "normal" and "humid" tube conditions, but significantly much more under the "humid" conditions. This is because proton transfer from the reagent ion $H_3O^+.(H_2O)$ to any of the anaesthetics is highly endothermic, and even translational energy gained in the electric field and increases in internal energies of the reagent ions through collisions with the buffer gas are unable to drive proton transfer. Therefore, only H_3O^+ has a significant role to play in the ionisation of the halogenated ethers in our PTR-MS investigations.

No protonated fluranes are observed, rather following proton transfer substantial fragmentation is observed through reaction pathways leading to product ions which often require substantial energy input. This in part may be coming from any internal energy that the H_3O^+ may contain when it is either generated in the ion source or through that gained in collisions with the buffer gas in the drift tube. Product ions also gain energy from the field, which leads to collisional dissociation. For the majority of product ion fragmentation channels, this energy input is sub-

stantial. We comment that extensive fragmentation is also reported in the selected ion flow tube mass spectrometric (SIFT-MS) study by Wang *et al.*, with the dominant product ion being *m/z* 117 (CF_3CHCl^+). This is difficult to explain given that the ion/molecule reaction processes in a SIFT are considered to be thermal [170].

Although substantial fragmentation is observed both in this PTR-MS and the SIFT-MS studies following proton transfer from H_3O^+ to isoflurane, and as expected more so in the PTR-MS study, there are major differences in the product ions. The SIFT study by Wang *et al.* [163] reports a number of product ions that we have not observed, namely *m/z* 99 (assigned to be $CF_3CH_2O^+$), *m/z* 119 (assigned to be $CF_3CFHOH_2^+$), and *m/z* 147 (incorrectly assigned in the Wang *et al.* paper to be $CF_2HOCHClCH^+$ which has a *m/z* value of 128 and is in any case a radical cation). The following product ions recorded in this PTR-MS study: *m/z* 51 (assigned to be CHF_2^+), *m/z* 115 (assigned to be $C_2H_2F_2ClO^+$), *m/z* 145 (assigned to be $C_3HF_3ClO^+$), and *m/z* 163 (assigned to be $C_3F_4ClO^+$) are not reported in the SIFT paper. The only common product ion recorded in both studies is at *m/z* 117 ($C_2HF_3Cl^+$). An ion observed at *m/z* 67 in the SIFT study and assigned to be CF_2HO^+, is observed in our data, but because an ion signal is also observed in our mass spectrum at *m/z* 69 with an intensity to imply that that is associated with the ^{37}Cl isotope (*m/z* 69 is not observed in the SIFT mass spectrum) we have assigned *m/z* 67 to be $CHFCl^+$.

It is clear from this study, and others we have undertaken (for example see the paper by Malásková *et al.* [20]), that a meaningful interpretation of the ion-chemistry occurring in the PTR-MS is challenging, and headway is only possible when the experimental observations are in combination with quantum mechanical computational calculations of the ion/molecule reaction pathways leading to the product ions.

Finally, we comment that the major objective of this study has been successfully accomplished, namely the identification of which product ion(s) should be monitored at a defined reduced electric field value for a given anaesthetic with high specificity under the conditions similar to those for breath samples for the PTR-TOF 8000 instrument we are using. In summary, these product ions and reduced electric fields to be used are as follow: desflurane, $C_3H_2F_5O^+$ (*m/z* 149.00), at an *E/N* of 120 Td; sevoflurane, $C_4H_3F_6O^+$ (*m/z* 181.01), at an *E/N* of 150 Td; and for both isoflurane and enflurane, $CHFCl^+$ (*m/z* 66.98 and *m/z* 68.98), at an *E/N* of 200 Td. This provides us with the method to monitor the "washout" characteristics of any one of

the four inhalation anaesthetic present in a person following surgery, with the excretion from the body predominantly resulting via exhalation, because they are not efficiently metabolised. It is our intention that the washout measurements will be modelled using a simulation based on one developed for anaesthetics by King *et al.* [171], and since breath concentrations of VOCs with low blood:air partition coefficients ($\lambda_{b:air} \leq 5$, *e.g.* isoflurane has $\lambda_{b:air} = 1.4$ and sevoflurane has $\lambda_{b:air} = 0.6$) are very sensitive to breath flow $\dot{V}$ and blood flow $\dot{Q}$, ideally to aid the modelling the measured breath concentrations ($C_{measured}$) of the anaesthetics should be normalised according to the Farhi equation $C_{normalised} = C_{measured}\left(\lambda_{b:air} + \frac{\dot{V}}{\dot{Q}}\right)$, with no anaesthetic in the room air being breathed.

Chapter 8

Investigation of Phthalate Esters in Proton Transfer Reaction Mass Spectrometry via Direct Headspace Sampling

In this chapter, details of an unpublished PTR-MS study of the reactions of phthalic acid and ten phthalate esters with H_3O^+ as a function of the drift voltage and the reduced electric field is presented.

8.1 Introduction

Phthalate esters, or simply phthalates, form a family of chemicals that are commonly used as plasticisers, mainly to soften polyvinyl chloride (PVC), and which are present in products of everyday use like clothing, food packaging, toys, building materials, pharmaceuticals and personal care products [172–174]. Plasticised products have become ubiquitous in homes, schools and workplaces, and the exposure to phthalates has been proved to be higher than the tolerable daily intake (TDI), being up to twenty times higher than this limit for children [175, 176].

Phthalates are some of the pollutants that humans are most exposed to. The main routes of exposure to phthalates are through ingestion, inhalation and dermal absorption. An extens-

ive study of the sources of exposure for Europeans is that published by Wormuth *et al.* [177]. Ingestion of phthalates occurs mainly through food contamination in adults and through toys mouthing in children [178, 179]. Xu *et al.* reported the presence of 23 phthalate esters in food samples (*e.g.* dairy, meat, oil and canned products) [180]. Inhalation of phthalates can occur in enclosed spaces where plasticised products are present and these contaminants have migrated to the dust and the air. Geiss *et al.* found variable concentrations between summer and winter of phthalates, particularly diethyl phthalate (DEP), dibutyl phthalate (DBP) and bis(2-ethylhexyl) phthalate (DEHP), inside used car cabins [181]. These pollutants come predominantly from the car plastic parts and they can be present inside buildings as well, as PVC is a material often used in construction, for instance in vinyl flooring [182]. Regarding dermal absorption, the extended use of personal care products, like make up and contact lenses, are the main source of contamination, but dermal absorption can also occur through the use of medical equipment like plastic tubing and vinyl gloves [183–185].

Some studies relate phthalates to development and male reproductive (*i.e.* reduced sperm concentration). Other studies suggest that they are not harmful to the female reproductive system [186–190]. Experiments of DEHP exposure in mice suggest that it cannot be ruled out as a human carcinogen [191]. In children, the presence of phthalate metabolites in urine has been linked to attention deficit and hyperactivity disorder as well as asthma [192, 193]. Phthalates traces have been found in human blood and faeces and even in breastfeeding human milk [134, 194]. Duty *et al.* linked the presence of phthalates monoesters in urine to the use of personal care products [184]. An extensive discussion of the metabolism of phthalates is that published from Frederiksen *et al.*, and Wittassek *et al.* showed that the metabolism of DEHP consists mainly on oxidised phthalate products in urine while mono(2-ethylhexyl) phthalate (MEHP) is the primary metabolite in blood [195, 196].

Owing to the health risks they present, the use of phthalates has recently started to be controlled by the enforcing authorities in several countries. Since 2005, the EU has restricted the use of phthalates as plasticisers in toys for kids, and has banned toys and childcare articles carrying more than 0.1% mass of DBP, benzyl butyl phthalate (BBP) and DEHP [197]. A similar ban is imposed to diisononyl phthalate, diisodecyl phthalate and dioctyl phthalate, although scientific information is either lacking or conflictual. US and China implemented comparable regulations in 2008 and 2016 [198, 199]. The EU added more phthalates to the list of controlled

substances in later regulations, classified some of them as very toxic to aquatic organisms and included them in the REACH Candidate List as Substances of Very High Concern [200, 201].

Health and environmental hazards arising from phthalates exposure and contamination has led to the application of several analytical techniques to the detection and quantification of these plasticisers. Some of these techniques are LC-MS/MS, GC-MS, EI-MS, IMS, IMS-MS, ESI-HCD-MS and UHPLC-MS/MS [39, 178, 180, 202–205]. There are, however, no extensive studies of phthalates in PTR-MS as of today. Also, the main agreement so far within the scientific community with respect to phthalates is that further investigation is needed [206]. These two reasons are the main motivation for the study presented here.

In this chapter a study of the reactions of phthalic acid (PAcid*), dimethyl phthalate (DMP), diethyl phthalate (DEP), diallyl phthalate (DAP), dipropyl phthalate (DPP), dibutyl phthalate (DBP), monoethylhexyl phthalate (MEHP, also known as mono(2-ethylhexyl) phthalate), diisobutyl phthalate (DiBP), benzyl butyl phthalate (BBP), dibenzyl phthalate (DBeP) and bis(2-ethylhexyl) phthalate (DEHP, also known as di(2-ethylhexyl) phthalate) with H_3O^+ in the reaction region of a PTR-MS instrument as a function of the drift voltage and the reduced electric field is presented.

8.2 Methodology

8.2.1 Chemicals

The samples used for this study are PAcid (Sigma Aldrich, Gillingham, United Kingdom, 99.5%), DMP (Acros Organics, Thermo Fisher Scientific, Schwerte, Germany, 99%), DEP (Sigma Aldrich, 99.5%), DAP (Sigma Aldrich, 97%), DPP (Sigma Aldrich, 98%), DBP (Sigma Aldrich, 99%), MEHP (Sigma Aldrich, 97%), DiBP (Sigma Aldrich, 99%), BBP (Sigma Aldrich, 98%), DBeP (Alfa Aesar, Thermo Fisher Scientific (Kandel) GmbH, Kandel, Germany, 97%) and DEHP (Sigma Aldrich, 96%). They were used without further purification. The structure of these substances is provided in Table 8.1. The vapour pressure data at 25°C was taken from the U.S. Environmental Protection Agency database [91]. The vapour pressure values for DAP, MEHP, DiBP and DBeP are the predicted ones while the ones for the rest of compounds were experimentally measured.

*Phthalic acid is called PAcid instead of *PA* to avoid confusion with the abbreviation for proton affinity.

Table 8.1: Vapour pressure at 25°C and structure of phthalic acid, dimethyl phthalate, diethyl phthalate, diallyl phthalate, dipropyl phthalate, dibutyl phthalate, monoethylhexyl phthalate, diisobutyl phthalate, benzyl butyl phthalate, dibenzyl phthalate and diethylhexyl phthalate.

Compound	**VP (mbar)**	**Structure**
PAcid	8.48×10^{-7}	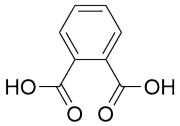
DMP	4.11×10^{-3}	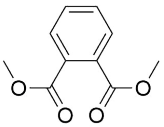
DEP	2.80×10^{-3}	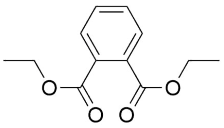
DAP	2.68×10^{-4}	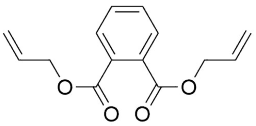
DPP	1.76×10^{-4}	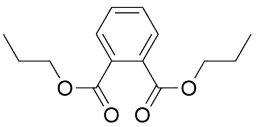
DBP	2.68×10^{-5}	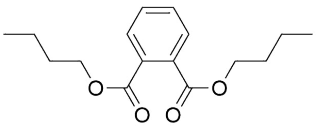
MEHP	1.08×10^{-6}	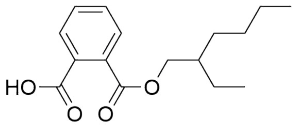
DiBP	5.41×10^{-4}	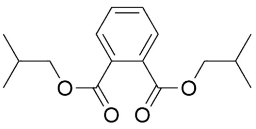
BBP	1.10×10^{-5}	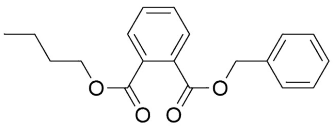
DBeP	1.59×10^{-6}	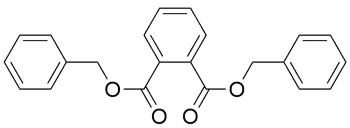
DEHP	1.89×10^{-7}	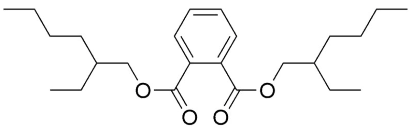

8.2.2 Experimental details

The analytical tool used for this study was the KORE Technology Ltd PTR-ToF-MS instrument described in chapter 2. The hollow cathode was set at a pressure of 1.15 mbar while the drift tube pressure was at 1.10 mbar. This was found to give the driest conditions in the reactor. Figure 8.1 shows that the branching percentage of H_3O^+ is 97% or higher at any reduced electric field, so that the contribution of $(H_2O)H_3O^+$ to the total reagent ion signal is 3% or less. The inlet line and the oven were both maintained at 100 °C. The experimental data for each phthalate was obtained by averaging two 10-second measurements for each E/N value, which was manipulated by keeping constant both the drift tube pressure and temperature, and only changing the drift voltage from approximately 160 V to 410 V to give a reduced electric field range of roughly 80 to 205 Td.

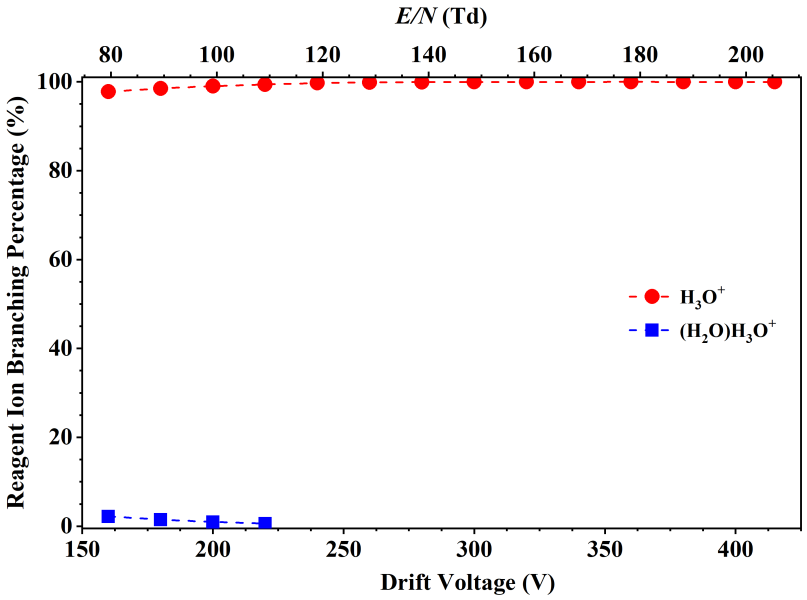

Figure 8.1: Reagent ion distribution plot as a function of the drift voltage and the E/N. Note that here the reagent ion signals are plotted as percentages while those in other chapters (*e.g.* Figure 3.2) are given in counts per second.

The phthalates were analysed via headspace sampling. 40 mL amber vials containing 1 - 5 mL of phthalate samples were connected to the inlet pipe of the PTR-ToF-MS to sample the headspace of the compound in the vial using oxygen-free nitrogen (99.998% purity, BOC Gases, Manchester, UK) as carrier gas. The vial was heated for the substances with the lowest vapour

pressure to reach an ion intensity of at least 1000 cps in total for the main product ions at an E/N of 120 Td.

The data acquisition was started only after approximately 30 minutes of preparing the experimental set up to avoid contamination. Even though the purity of the samples was of at least 95%, some volatile impurities were observed when the vials were first connected to the inlet line. The product ions arising from these substances were found to steadily decrease and disappear in approximately 10 - 15 minutes while the signals assigned to phthalate product ions showed a stable behaviour throughout. Also, the presence of impurities with similar or higher volatilities than the phthalates cannot be discarded either. For this reason, only the ions that are identified as phthalate products and that represent more than 3% of the total product ion signal are included here. Owing to the lack of comparable studies in the literature, the mzCloud mass spectral database proved to be very useful to aid in the ion identification process [205]. This database contains, among others, electrospray ionisation (ESI) higher-energy collisional dissociation (HCD) MS^n results of tens of thousands of chemicals, which, at the lower-energy end, are qualitatively comparable to PTR-MS and therefore mzCloud references[†] are given for many compounds in this chapter to support and/or argue the findings of this study.

8.3 Results and discussion

The reaction of the phthalate esters with $(H_2O)_nH_3O^+$ for $n > 0$ is negligible in the present PTR-MS results because of the low abundance of these reagent ions (see Figure 8.1) and hence only reactions with H_3O^+ are considered here (except for phthalic acid). Furthermore, only the proton affinity of DMP (ca. 940 kJ mol^{-1}) is known, with Hunter *et al.* only having reported the proton affinity for two DMP isomers: dimethyl isophthalate (843.5 kJ mol^{-1}) and dimethyl terephthalate (843.2 kJ mol^{-1}), which are not included in this study [32, 39]. The *PA*s are hence unknown for the rest of the studied substances.

Table 8.2 shows a summary of the observed product ions and their associated percentage product ion distributions at E/N values of 100, 140 and 180 Td resulting from the reactions of H_3O^+ with each of the studied phthalate samples. The most common fragmentation pathway observed in the present study is the loss of the two ester branches and an oxygen atom, as

[†]Note that the url in these references must be opened using Internet Explorer or the mzCloud desktop app [205].

indicated in Figure 8.2, to form protonated phthalic anhydride (*i.e.* m/z 149). Nevertheless, this ion is not observed from all the phthalates (*e.g.* dimethyl and diallyl phthalate). Another common product ion is the one arising from the loss of a formate ester group. A more complete diagram of the possible fragmentation pathways for the phthalates is given by Yin *et al.* for electron impact ionisation experiments [207].

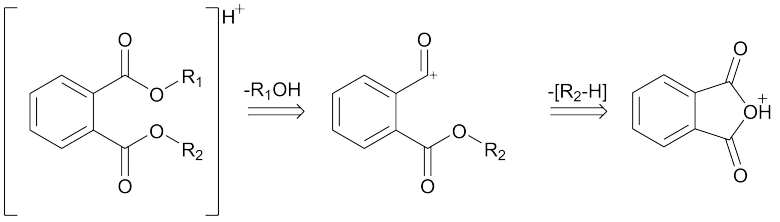

Figure 8.2: General fragmentation pathway from the protonated parent to protonated phthalic anhydride at m/z 149. Note that the neutral molecules are omitted.

Table 8.2: Product ions identified and their associated percentage product ion distributions measured at reduced electric fields of 100, 140, and 180 Td resulting from the reactions of H_3O^+ with several phthalate esters in order of increasing monoisotopic mass.

Phthalate	**Product ion**	**Product ion**	**PID (%)**		
Molecular formula	***m/z***	**formula**	***E/N* (Td)**		
Monoisotopic mass (g/mol)			**100**	**140**	**180**
PAcid	149.02	$C_8H_5O_3^+$	98	100	100
$C_8H_6O_4$	167.03	$(C_8H_6O_4)H^+$	2	0	0
166.03					
DMP	163.04	$C_9H_7O_3^+$	77	93	99
$C_{10}H_{10}O_4$	195.07	$(C_{10}H_{10}O_4)H^+$	23	7	1
194.06					
DEP	75.04	$C_3H_7O_2^+$	7	1	0
$C_{12}H_{14}O_4$	149.02	$C_8H_5O_3^+$	1	7	76
222.09	177.05	$C_{10}H_9O_3^+$	36	57	21
	223.10	$(C_{12}H_{14}O_4)H^+$	56	35	3
DAP	39.02	$C_3H_3^+$	0	0	15
$C_{14}H_{14}O_4$	41.04	$C_3H_5^+$	2	3	24
246.09	81.07	$C_6H_9^+$	4	10	19

(Continues on next page.)

Phthalate	**Product ion**	**Product ion**	**PID (%)**		
Molecular formula	***m/z***	**formula**	***E/N* (Td)**		
Monoisotopic mass (g/mol)			**100**	**140**	**180**
	189.06	$C_{11}H_9O_3^+$	10	27	29
	247.10	$(C_{14}H_{14}O_4)H^+$	84	60	13
DPP	79.05	$C_6H_7^+$	1	1	5
$C_{14}H_{18}O_4$	105.03	$C_7H_5O^+$	4	5	5
250.12	123.04	$C_7H_7O_2^+$	3	19	25
	149.02	$C_8H_5O_3^+$	3	21	54
	165.09	$C_{10}H_{13}O_2^+$	31	15	2
	191.03	$C_{11}H_{11}O_3^+$	15	6	2
	251.13	$(C_{14}H_{18}O_4)H^+$	43	33	7
DBP	79.05	$C_6H_7^+$	0	0	3
$C_{16}H_{22}O_4$	105.03	$C_7H_5O^+$	4	5	5
278.15	123.04	$C_7H_7O_2^+$	8	15	13
	149.02	$C_8H_5O_3^+$	15	41	68
	179.10	$C_{11}H_{15}O_2^+$	14	5	1
	205.09	$C_{12}H_{13}O_3^+$	19	4	2
	279.16	$(C_{16}H_{22}O_4)H^+$	40	30	8
MEHP	39.02	$C_3H_3^+$	0	1	15
$C_{16}H_{22}O_4$	41.04	$C_3H_5^+$	0	5	12
278.15	43.05	$C_3H_7^+$	1	7	4
	57.07	$C_4H_9^+$	17	18	6
	69.07	$C_5H_9^+$	2	7	3
	71.09	$C_5H_{11}^+$	17	7	2
	111.12	$C_8H_{15}^+$	6	3	0
	113.13	$C_8H_{17}^+$	6	1	0
	129.13	$C_8H_{17}O^+$	10	5	2
	149.02	$C_8H_5O_3^+$	41	46	56
DiBP	57.07	$C_4H_9^+$	2	3	5
$C_{16}H_{22}O_4$	149.02	$C_8H_5O_3^+$	7	17	65
278.15	205.09	$C_{12}H_{13}O_3^+$	3	1	1
	279.16	$(C_{16}H_{22}O_4)H^+$	88	79	29
BBP	79.05	$C_6H_7^+$	11	13	18

(Continues on next page.)

Phthalate	**Product ion**	**Product ion**	**PID (%)**		
Molecular formula	***m/z***	**formula**	***E/N* (Td)**		
Monoisotopic mass (g/mol)			**100**	**140**	**180**
$C_{19}H_{20}O_4$	91.05	$C_7H_7^+$	72	71	71
312.13	107.05	$C_7H_7O^+$	17	16	11
DBeP	79.05	$C_6H_7^+$	10	11	15
$C_{22}H_{18}O_4$	91.05	$C_7H_7^+$	75	76	75
346.12	107.05	$C_7H_7O^+$	15	13	10
DEHP	39.02	$C_3H_3^+$	1	1	12
$C_{24}H_{38}O_4$	41.04	$C_3H_5^+$	0	3	24
390.28	43.05	$C_3H_7^+$	0	12	9
	57.07	$C_4H_9^+$	15	26	16
	69.07	$C_5H_9^+$	0	5	5
	71.09	$C_5H_{11}^+$	26	22	6
	111.12	$C_8H_{15}^+$	6	6	2
	113.13	$C_8H_{17}^+$	25	5	3
	123.04	$C_7H_7O_2^+$	9	10	10
	129.13	$C_8H_{17}O^+$	10	5	3
	149.02	$C_8H_5O_3^+$	2	4	10
	235.17	$C_{15}H_{23}O_2^+$	6	1	0

8.3.1 Phthalic acid

Figure 8.3 shows the PID plot for the reaction of phthalic acid with the reagent ions as a function of the drift voltage and the reduced electric field. Only two product ions were observed: the protonated parent molecule ($(C_8H_6O_4)H^+$) at *m/z* 167 and protonated phthalic anhydride ($C_8H_5O_3^+$) at *m/z* 149. The latter is a characteristic phthalate product ion and is observed with many of these compounds.

The fact that these product ions resemble the reagent ions in Figure 8.1 hints that the protonated parent ion is a product of the non-dissociative reaction of phthalic acid with $(H_2O)H_3O^+$, which is only found at trace levels at low *E/N*. Proton transfer from $(H_2O)H_3O^+$ is softer than that from H_3O^+, with a difference in gas basicity of 124 kJ mol^{-1} or 1.285 eV. Even though there are no DFT calculations available, the loss of H_2O from protonated phthalic acid to give

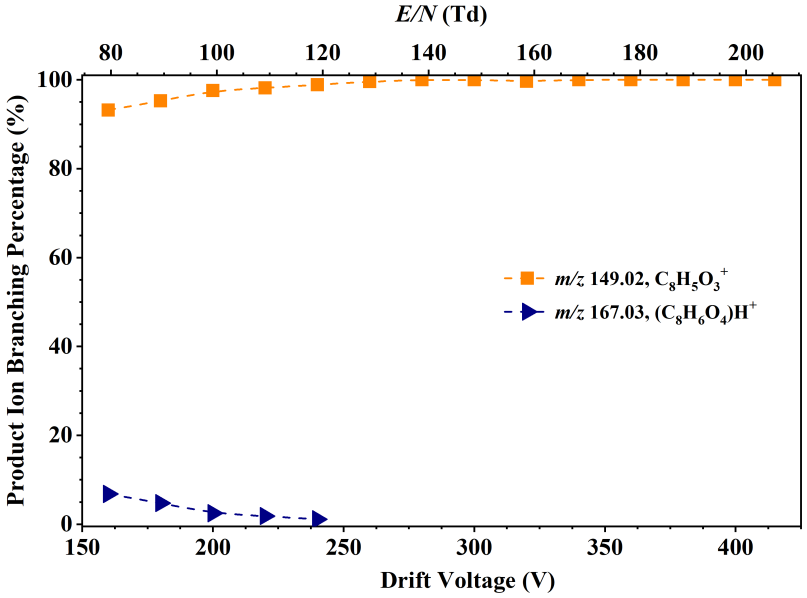

Figure 8.3: Percentage product ion distribution resulting from the reaction of phthalic acid with $(H_2O)_nH_3O^+$ (n = 0, 1) as a function of the drift voltage and the reduced electric field in the range from 80 to 205 Td.

protonated phthalic anhydride must be energetically favourable because the ion at m/z 149 is observed for all E/N values. The formation of this ion needs protonation of one of the hydroxy oxygen atoms, which is a similar pathway to that of benzoic acid to yield benzoyl$^+$ (see section 3.3.4.4).

8.3.2 Dimethyl phthalate

Dissociative proton transfer to yield $C_9H_7O_3^+$ at m/z 163 after the loss of methanol from the protonated parent is the dominant channel for the reaction of DMP with H_3O^+ (Figure 8.4). The protonated parent ion, $(C_{10}H_{10}O_4)H^+$ at m/z 195, only represents ca. 25% of the total product ion signal at around 80 Td and its intensity steadily decreases as the E/N increases.

Interestingly, it was found that DMP is the only one of the alkyl diester phthalates studied here in which protonated phthalic anhydride is not a product ion, which agrees with the results from other studies using GC-MS and ESI-HCD-MS^2 [207, 208]. The formation of protonated phthalic anhydride would require the further loss of the remaining methyl group in the ion observed at m/z 163. This finding is comparable to m/z 123 being observed with all the benzoates except with methyl benzoate (see section 3.3.4.1).

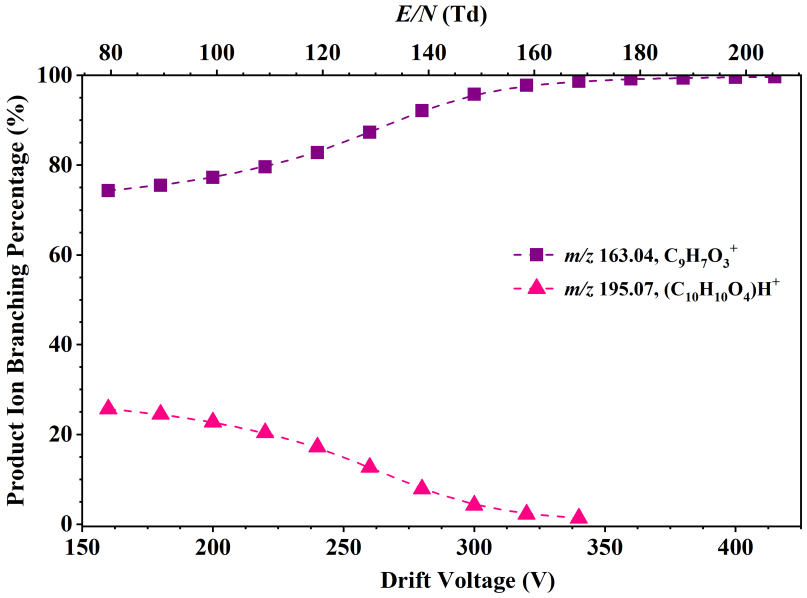

Figure 8.4: Percentage product ion distribution resulting from the reaction of DMP with H_3O^+ as a function of the drift voltage and the reduced electric field in the range from 80 to 205 Td.

8.3.3 Diethyl phthalate

Figure 8.5 shows the PID plot for the reaction of DEP with H_3O^+ as a function of the drift voltage and the reduced electric field. At low E/N, the most abundant ion at ca. 60% is the protonated parent, $(C_{12}H_{14}O_4)H^+$ at m/z 223, whose intensity steadily decreases as the reduced electric field increases. Another product ion is found at low E/N at m/z 75, tentatively assigned to protonated ethyl formate ($C_3H_7O_2^+$). The ion at m/z 177, assigned to $C_{10}H_9O_3^+$, results from the loss of ethanol from the protonated parent molecule and it peaks at around 150 Td with ca. 65% of the total product ion signal. At high E/N, the dominant ion is protonated phthalic anhydride ($C_8H_5O_3^+$), formed through collision-induced dissociation, going up to 95%. The mzCloud database results for diethyl phthalate agree with PTR-MS for E/N values higher than approximately 160 Td, although the protonated parent is not reported there while in the present PTR-MS experiments this ion at 160 Td represents ca. 10% of the total ion signal [209].

8.3.4 Diallyl phthalate

Non-dissociative proton transfer to yield the protonated parent molecule, $(C_{14}H_{14}O_4)H^+$, at m/z 247 is the dominant product ion for the reaction of DAP with H_3O^+ from low reduced electric

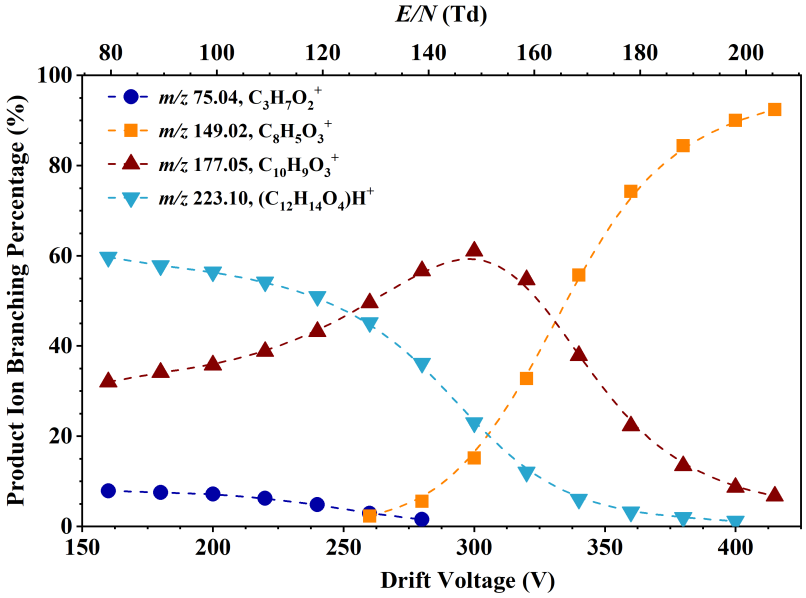

Figure 8.5: Percentage product ion distribution resulting from the reaction of DEP with H_3O^+ as a function of the drift voltage and the reduced electric field in the range from 80 to 205 Td.

field up to around 150 Td (Figure 8.6). Then the ion resulting from the loss of allyl alcohol ($C_{11}H_9O_3^+$ at m/z 189) becomes dominant. Other product ions observed at high E/N are $C_3H_5^+$, tentatively assigned to the allyl radical, and $C_3H_3^+$. These ions are produced in a cascade-like fragmentation pathway as the collisional energy increases. However, another ion (*i.e.* $C_6H_9^+$ at m/z 81) is observed over all the studied E/N range. Although its formation and structure are not clear yet, it has been reported at trace levels in the mzCloud database [210]. One of its possible structures is protonated cyclohexadiene arising from the benzene core of the molecule, but this is hardly the correct one because this is not observed with any other of the studied phthalates. Another possibility would be that it comes from the two allyl (*i.e.* -$CH_2CH{=}CH_2$) branches but this is highly unlikely as in the most stable DAP conformer these branches are not close to each other. Similarly to DMP, protonated phthalic anhydride was not observed in the DAP measurements.

8.3.5 Dipropyl phthalate

Figure 8.7 shows the PID for the reaction of H_3O^+ with DPP as a function of the reduced electric field in the range from 80 to 205 Td. At low E/N, the dominant ion is the protonated parent, $(C_{14}H_{18}O_4)H^+$, followed by the loss of one of the propyl formate (*i.e.* $C_4H_6O_2$) branches from

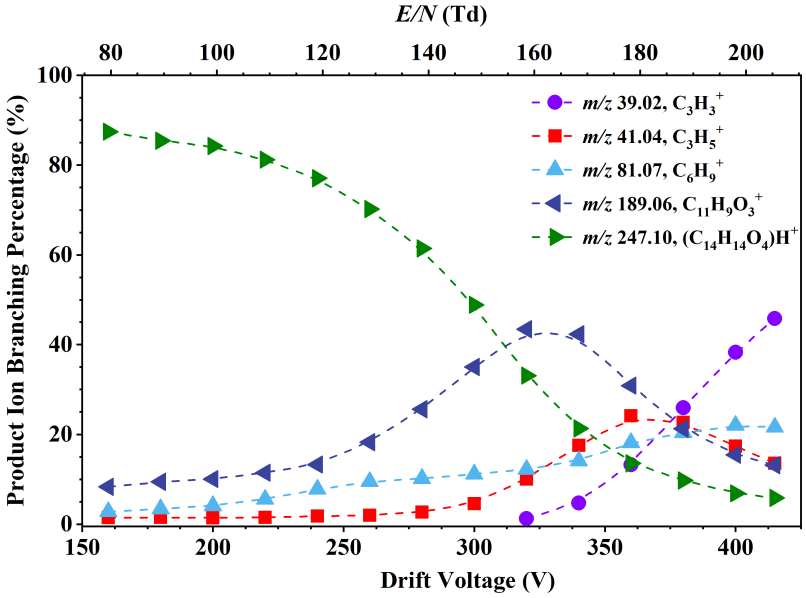

Figure 8.6: Percentage product ion distribution resulting from the reaction of DAP with H_3O^+ as a function of the drift voltage and the reduced electric field in the range from 80 to 205 Td.

the protonated parent, yielding $C_{10}H_{13}O_2^+$, tentatively assigned to protonated propyl benzoate, and the loss of propanol from the protonated parent, yielding $C_{11}H_{11}O_3^+$. The abundance of these three ions decrease with increasing reduced electric field and at ca. 150 Td protonated phthalic anhydride becomes dominant. The ions found at high E/N are protonated benzoic acid ($C_7H_7O_2^+$) and protonated benzene ($C_6H_7^+$). A minor contribution is observed for the whole E/N range from benzoyl$^+$ ($C_7H_5O^+$).

8.3.6 Dibutyl phthalate

The protonated parent ion $(C_{16}H_{22}O_4)H^+$ at m/z 279 is the most abundant ion from low E/N up to around 130 Td, after which protonated phthalic anhydride becomes the most abundant ion for the rest of the reduced electric field range (see Figure 8.8). At low E/N we also found the ion resulting from the loss of butanol from the protonated parent, $C_{12}H_{13}O_3^+$ at m/z 205, and the loss of butyl formate (*i.e.* $C_5H_8O_2$) to yield $C_{11}H_{15}O_2^+$ at m/z 179, which is tentatively assigned to protonated butyl benzoate. At high E/N some minor ions are protonated benzoic acid ($C_7H_7O_2^+$), benzoyl$^+$ ($C_7H_5O^+$) and protonated benzene ($C_6H_7^+$) at m/z 123, m/z 105 and m/z 79, respectively.

Tandem MS^3 spectra from the mzCloud database acquired by subsequently fragmenting the

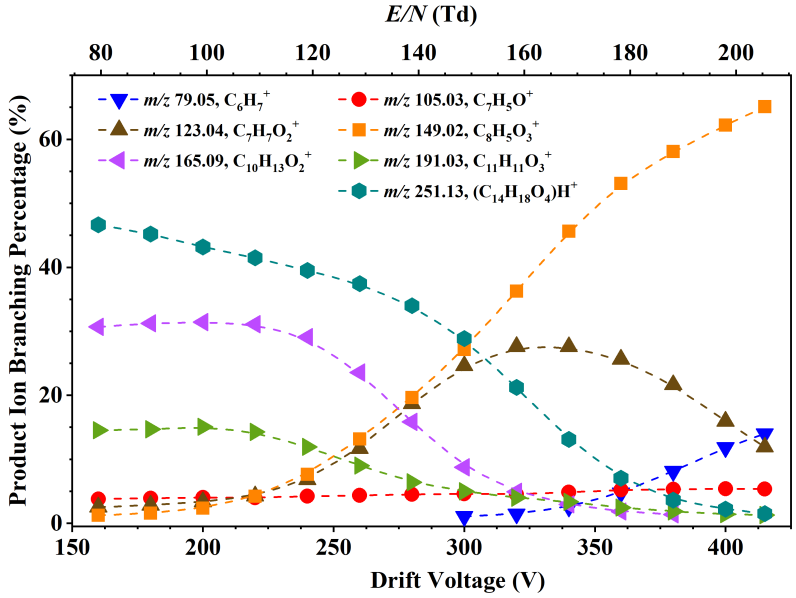

Figure 8.7: Percentage product ion distribution resulting from the reaction of DPP with H_3O^+ as a function of the drift voltage and the reduced electric field in the range from 80 to 205 Td.

protonated parent at m/z 279 and $C_{12}H_{13}O_3^+$ at m/z 205 proves that the formation of protonated phthalic anhydride from protonated DBP can occur following the pathway described in Figure 8.2 with m/z 205 being the intermediate [M - R_1OH]H^+ ion [211].

8.3.7 Monoethylhexyl phthalate

Protonated phthalic anhydride is the dominant product ion for all the E/N range for the reaction of MEHP with H_3O^+ (Figure 8.9). The protonated parent (*i.e.* m/z 279) was not observed for any reduced electric field value. $C_8H_{17}O^+$ at m/z 129 is tentatively assigned to protonated 2-ethylhexanal (structure shown in Figure 8.10) and all the other product ions potentially come from the successive fragmentation: $C_8H_{17}^+$ at m/z 113, $C_8H_{15}^+$ at m/z 111, $C_5H_{11}^+$ at m/z 71, $C_5H_9^+$ at m/z 69, $C_4H_9^+$ at m/z 57, $C_3H_7^+$ at m/z 43, $C_3H_5^+$ at m/z 41 and $C_3H_3^+$ at m/z 39. The ions at m/z 39, m/z 41, m/z 43 and m/z 57 are reported for EI-MS of 2-ethylhexanal [212].

The protonated parent was also not observed in the positive ESI-HCD-MS^2 spectra in the mzCloud database for MEHP [213].

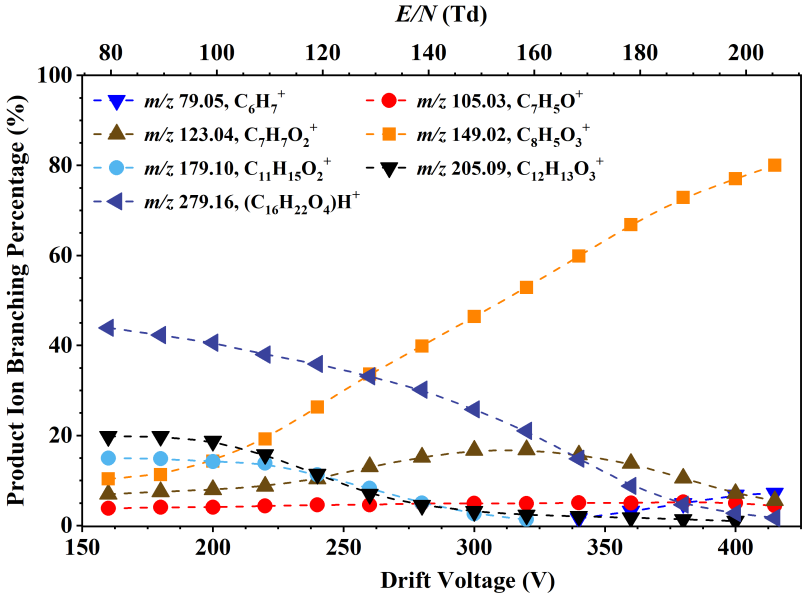

Figure 8.8: Percentage product ion distribution resulting from the reaction of DBP with H_3O^+ as a function of the drift voltage and the reduced electric field in the range from 80 to 205 Td.

8.3.8 Diisobutyl phthalate

The PID of the reaction of DiBP with H_3O^+ (Figure 8.11) is comparable to that of its isomer DBP (Figure 8.8), because the most relevant ions are the same but they appear at different percentages. The two dominant ions are the protonated parent ($(C_{16}H_{22}O_4)H^+$ at m/z 279) predominantly observed at lower E/N and protonated phthalic anhydride at higher E/N, but for DiBP the crossover point is at ca. 170 Td, instead of at ca. 130 Td for DBP. Another two product ions are observed: $C_4H_9^+$ at m/z 57 is tentatively assigned to isobutyl$^+$ and at low E/N there are traces of the loss of isobutanol from the protonated parent molecule ($C_{12}H_{13}O_3^+$ at m/z 205).

8.3.9 Benzyl butyl phthalate and dibenzyl phthalate

BBP and DBeP have a benzyl ester group in common and this seems to be crucial in the proton transfer and fragmentation processes as they show very similar product ion distributions (Figure 8.12). These plots suggest that the protonation sites in the benzyl branch are more basic than in the butyl branch of BBP. The ion $C_7H_7^+$ at m/z 91 is the dominant ion throughout the whole E/N range and this agrees with the mzCloud database [214]. This product ion

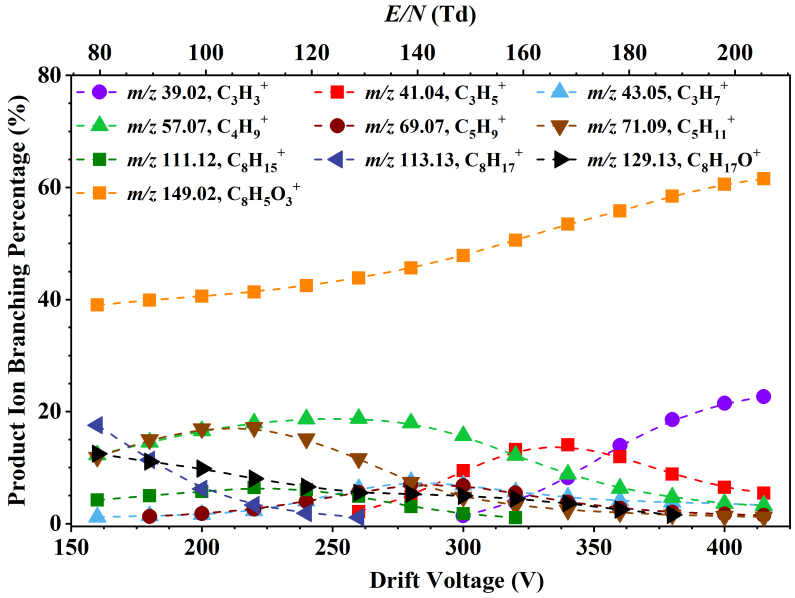

Figure 8.9: Percentage product ion distribution resulting from the reaction of MEHP with H_3O^+ as a function of the drift voltage and the reduced electric field in the range from 80 to 205 Td.

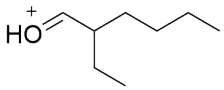

Figure 8.10: Tentative structure of protonated 2-ethylhexanal (*i.e.* $C_8H_{17}O^+$ at m/z 129).

could be mistakenly assigned to the benzyl ion, with structure $C_6H_5CH_2^+$. It is more likely that the ion being formed is the tropylium cation ($C_7H_7^+$), which is a stable cyclic aromatic ion [215, 216]. It is frequently observed in other mass spectrometry techniques from compounds containing a benzyl group and it is often the dominant product ion. It is energetically more stable than the benzyl ion, which rearranges to tropylium [217]. mzCloud also reports protonated phthalic anhydride (*i.e.* m/z 149) and the loss of benzyl alcohol from the protonated parent (*i.e.* $C_{12}H_{13}O_3^+$ at m/z 205) at the lower collisional energies, but these were not observed in PTR-MS. Furthermore, protonated phthalic anhydride has been reported a major ion for BBP in the literature. For instance, Earls *et al.* monitored protonated phthalic anhydride in GC-MS to quantify the migration of BBP from PVC toys and childcare products [179]. Two other product ions were observed in PTR-MS for both BBP and DBeP with a lower branching percentage than $C_7H_7^+$ are $C_6H_7^+$ at m/z 79, which is tentatively assigned to protonated benzene, and $C_7H_7O^+$,

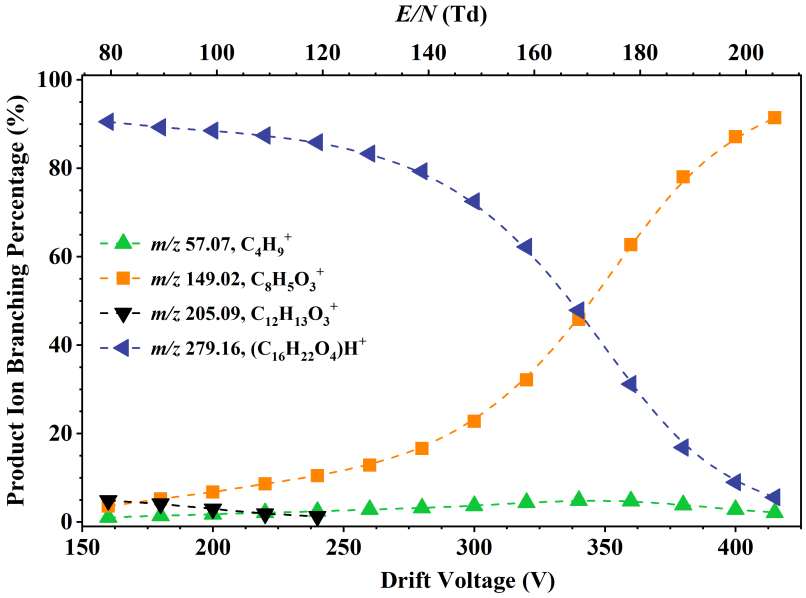

Figure 8.11: Percentage product ion distribution resulting from the reaction of DiBP with H_3O^+ as a function of the drift voltage and the reduced electric field in the range from 80 to 205 Td.

tentatively assigned to protonated benzaldehyde.

8.3.10 Bis(2-ethylhexyl) phthalate

Figure 8.13 shows that the reaction of DEHP with H_3O^+ yield similar PID results to those of MEHP (Figure 8.9), but the main difference is that here protonated phthalic anhydride is not the dominant ion for DEHP for any E/N value. Instead, there are many ions that become dominant throughout the studied E/N range. Furthermore, the only two product ions observed with DEHP that were not found with MEHP are $C_{15}H_{23}O_2^+$ at m/z 235 and $C_7H_7O_2^+$ at m/z 123, tentatively assigned to loss of 2-ethylhexyl formate from the protonated parent and protonated benzoic acid, respectively.

Similarly to MEHP, the ion at m/z 279, corresponding to the loss of C_8H_{16} from protonated DEHP, and the protonated parent $(C_{24}H_{38}O_4)H^+$ at m/z 391 were not observed, although these are reported at low collisional energies in the mzCloud database for ESI-HCD-MS^2 analysis of DEHP [218]. From the mzCloud results, protonated phthalic anhydride is reported and it is the dominant ion at low collisional energies. Likewise, the hydrocarbon ions at m/z 57, m/z 71 and m/z 113 are also reported in this database but not the ones at m/z 39, m/z 41 and m/z

(a)

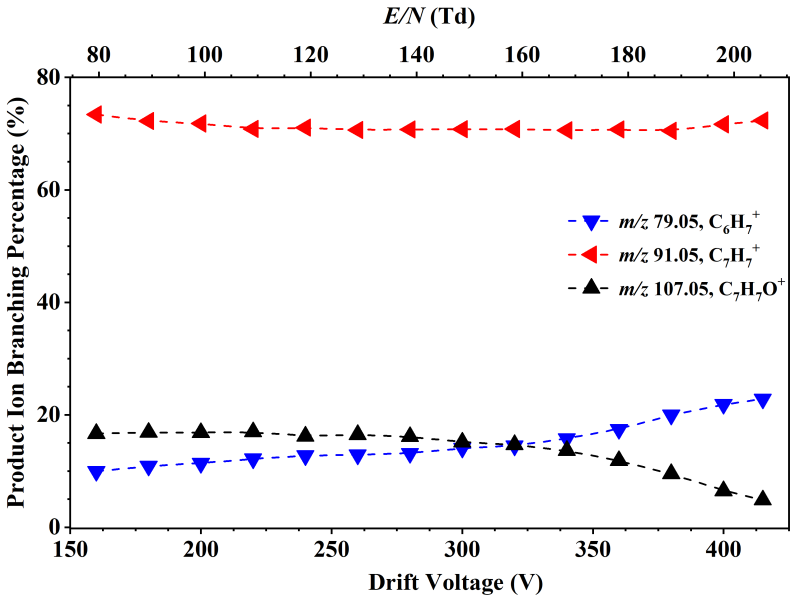

(b)

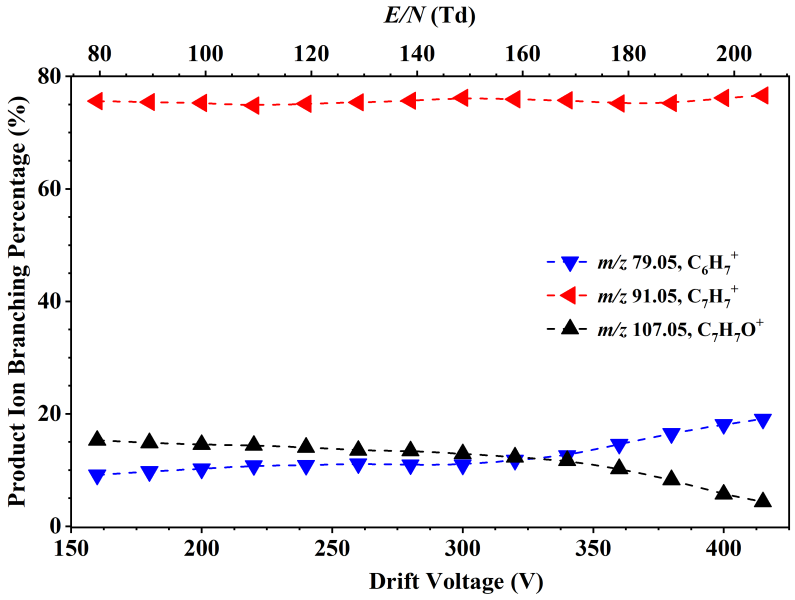

Figure 8.12: Percentage product ion distribution resulting from the reaction of (a) BBP and (b) DBeP with H_3O^+ as a function of the drift voltage and the reduced electric field in the range from 80 to 205 Td.

43 because of the cut-off at m/z 50 for mzCloud spectra. Furthermore, $C_8H_7O_4^+$ at m/z 167, which has the same structure as protonated phthalic acid, was not observed in PTR-MS but was reported in mzCloud.

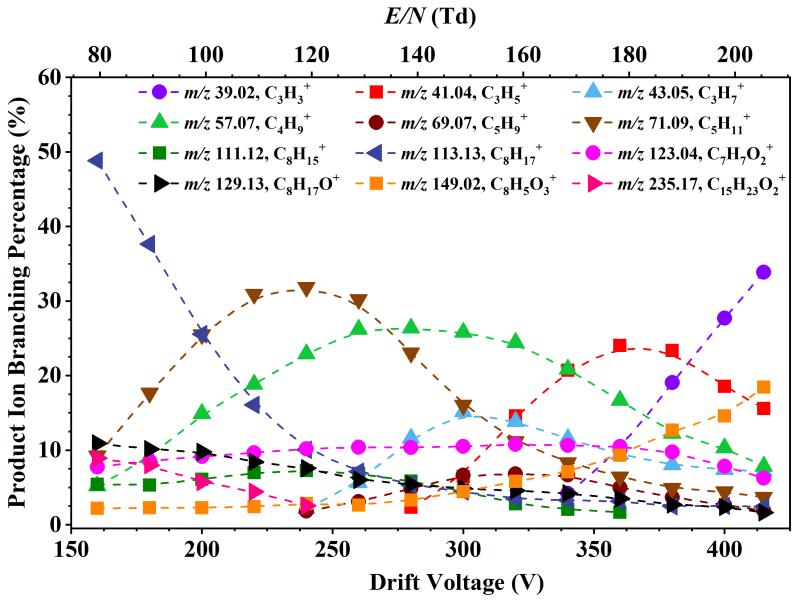

Figure 8.13: Percentage product ion distribution resulting from the reaction of DEHP with H_3O^+ as a function of the drift voltage and the reduced electric field in the range from 80 to 205 Td.

8.3.11 Separation of isomers: DBP vs DiBP vs MEHP

DBP, DiBP and MEHP are isomers, and thus the protonated parent for these molecules is at the identical m/z–value ($(C_{16}H_{22}O_4)H^+$, m/z 279). However, it is found that the reactions of these phthalates with H_3O^+ yield different product ion distributions at different reduced electric fields, providing a method to differentiate between them without needing any initial pre-separation. The difference between MEHP and the butyl-containing isomers (*i.e.* DBP and DiBP) is the presence of the protonated parent ion at low E/N for DBP and DiBP, which is not found for MEHP. To distinguish between DBP and DiBP it is necessary to compare other minor ions. The main differences between these two isomers is the higher signal of $C_{12}H_{13}O_3^+$ (m/z 205) from DBP at low E/N (*i.e.* around 20%) and $C_7H_7O_2^+$ (m/z 123) at high E/N, while in the case of DiBP the presence of the former is very little (only ca. 5%) and the latter is less than 3% (for this reason it is not included in plots and tables).

8.4 Conclusions

This unpublished study provides details on the reactions of a series of phthalates occurring within the drift tube of a PTR-MS. The product ion distributions as a function of the drift voltage and reduced electric field are presented for ten phthalate esters and a phthalic acid, including those phthalates that are banned and/or controlled within the EU, USA and China, namely DBP, BBP and DEHP. Different product ion distributions were found for DBP, DiBP and MEHP, which can be used to distinguish between these three phthalate ester isomers. The range of collisional energies provided by a PTR-MS instrument has proved to be suitable to manipulate the ion/molecule reactions to yield interesting and distinguishing fragmentation pathways. Many of the fragmentation channels were only observed at an E/N higher than a certain value, which indicates that they result from field-activated collision-induced dissociation. This can be either a pathway that is not thermodynamically allowed or a pathway that, whilst thermodynamically feasible, is kinetically rather thermodynamically driven.

A characteristic product ion observed for many of the phthalates is protonated phthalic anhydride (m/z 149, $C_8H_5O_3^+$), which is not a surprise as this ion has been widely reported as a phthalate indicator with different mass spectrometric techniques. For example, McLafferty analysed ca. 140000 EI mass spectra and found that 150 of the 700 spectra where the peak at m/z 149 was present corresponded to a phthalate. It is thus a fairly good indicator of the presence of a compound from this family [219, 220]. However, phthalates do not always fragment to produce this ion in PTR-MS and, when m/z 149 is observed, its abundance depends on the reduced electric field. For the alkyl diester phthalates the abundance of protonated phthalic anhydride increases with the alkyl chain length and with the reduced electric field. Furthermore, looking at the three more strictly regulated phthalates, protonated phthalic anhydride is only the dominant ion for reduced electric field values higher than approx. 130 Td for DBP, while for DEHP it only reaches 20% of the total ion signal and for BBP it is not a product ion found in PTR-MS. Therefore, caution must be taken before discarding the presence of phthalate esters when m/z 149 is not a product ion.

Moreover, all of the studied alkyl diester phthalates lose the corresponding alcohol (*i.e.* methanol for DMP, ethanol for DEP, propanol for DPP and butanol for DBP), whose abundance decreases with the alkyl chain length. For example, for DMP the loss of methanol (m/z 163) is

the dominant ion throughout all the E/N range, while for DBP the loss of butanol (m/z 205) is only ca. 20% at 80 Td and it steadily decreases with the reduced electric field. Protonated benzoate esters are also product ions observed with phthalates after losing a formate group (*e.g.* propyl benzoate for DPP, butyl benzoate for DBP and 2-ethylhexyl benzoate for DEHP).

Part III

CONCLUSIONS AND FURTHER REMARKS

Chapter 9

Conclusions and Further Remarks

The final conclusions and closing remarks are summarised in this chapter.

9.1 Summary of research findings

9.1.1 Theoretical and experimental investigations of cocaine and related compounds in PTR-MS

Detailed PTR-MS and theoretical (DFT) investigations of the reactions of cocaine and related compounds with $(H_2O)_nH_3O^+$ have been presented. A thermal desorption unit was used to vaporise the less volatile substances so that they could be transported to the drift tube of the PTR-MS instrument, while the investigations of benzoates and isobutyrates were done through headspace analysis. The product ion signal intensities obtained from the reaction of the compounds are given as a function of the reduced electric and the drift voltage for experiments in two different conditions of humidity (although for some compounds only the data under normal drift tube operating conditions were acquired).

The dominant reaction channel is non-dissociative proton transfer for cocaine, cocaethylene, methyl ecgonine, ethyl ecgonine, norcocaine, methyl ecgonidine, o-hydroxycocaine and methyl isobutyrate for the range of E/N investigated. With the exception of the isobutyrate esters, the most common dissociative pathway is the loss of an alcohol (*i.e.* MeOH, EtOH or iPrOH)). This is supported by the DFT results, which showed that the loss of an alcohol is a barrierless process once the proton is attached to the ester oxygen. A higher abundance of these dissociative product ions compared to the protonated parent was expected, because the fragmentation

pathway is exergonic and the proton is mobile between the main protonation sites. However, the low fragmentation observed in PTR-MS hints that the proton stays in the pyrolidine nitrogen, which is the most basic site, inhibiting any thermodynamically allowed dissociation.

9.1.2 Enhancement of Compound Selectivity Using a Radio Frequency Ion Funnel Proton Transfer Reaction Mass Spectrometer: Improved Specificity for Explosive Compounds

Selectivity enhancements in the detection of TNT have been achieved through the implementation of a radio frequency ion funnel in the drift tube of a PTR-ToF-MS. The ion funnel upgrade was originally conceived to funnel ions in the second half of the reactor to enhance sensitivity. However, we discovered that it can also be used to induce fragmentation of the product ions and improve compound specificity through the extra collisional energy delivered by the RF field in the so-called "RF mode".

The crucial aspect of this work is that it is a simple and cost-efficient alternative to other major and costly changes in instrumental design to improve the chemical specificity, such as having a high resolution time-of-flight mass spectrometer or adding a pre-separation technique.

9.1.3 Selective Reagent Ion Mass Spectrometric Investigations of the Nitroanilines

This research demonstrates the selectivity enhancement for the identification of three nitroaniline isomers through the use of SRI-MS techniques. The product ion distributions arising from the reaction of the nitroaniline isomers with H_3O^+ and O_2^+ as a function of the reduced electric field are illustrated with quantum chemical (DFT) calculations.

The protonated parent is dominant for the three isomers for a wide reduced electric field range. However, protonated 3-nitroaniline solvates more than the protonated 2- and 4- isomers at low *E/N*, with the $MH^+.H_2O$ ion reaching ca. 50% of the PID at 60 Td. This it is supported by the DFT calculations, which predicts that protonated 3-nitroaniline binds to water ca. 10 better than to protonated 2- and 4-nitroaniline. This provides a method to differentiate the 3- isomer from the 2- and 4- isomers. The parent ion was also dominant using charge transfer reactions, but $C_6H_6NO^+$ becomes the dominant ion for 4-nitroaniline above approximately 190 Td, which allows the identification of the 4- isomer, as the ion intensity for 2- or 3-nitroaniline

is never higher than ca. 15%.

9.1.4 Compendium of the Reactions of H_3O^+ With Selected Ketones of Relevance to Breath Analysis Using Proton Transfer Reaction Mass Spectrometry

This study has resulted in a large database of product ions and their relative intensities as a function of the E/N for the reactions of H_3O^+ and $H_3O^+.(H_2O)$ with a variety of ketones. The observed product ion distributions can vary when using different instruments with different operating conditions, and therefore the results are only indicative. The manipulation of the collisional energy did not enhance the selectivity and hence a pre-separation stage, such as the fastGC add-on used in this investigation, is needed to separate isomeric compounds.

Following this study, the investigation of aldehydes in PTR-MS at different values of the reduced electric field should be carried out. There are two motivations for this: (i) aldehydes are isomers of ketones, and (ii) both ketones and aldehydes are present in breath samples. However, previous PTR-MS studies have already demonstrated that aldehydes fragment considerably more than ketones, and therefore the contribution to the protonated parent ion signal coming from aldehydes will be a small part of that of the ketones at low and mid values of the E/N [142, 148].

9.1.5 Studies Pertaining to the Monitoring of Volatile Halogenated Anaesthetics in Breath by Proton Transfer Reaction Mass Spectrometry

The main goal of this study was identifying the product ions that should be monitored with PTR-MS at a defined E/N for a particular anaesthetic when the operating conditions resemble the breath samples analysed. This allows to follow the "washout" characteristics of any one of the four inhalation anaesthetic after surgery, which are mainly exhaled out.

Given the lower proton affinities and gas phase basicities compared to water, proton transfer to the fluranes is only occurring from H_3O^+, as proton transfer from the reagent ion $H_3O^+.(H_2O)$ to any of the anaesthetics is highly endothermic. This explains the reduction on the product ion signals at low E/N, which is much more acute in the so-called "humid" operating conditions. The protonated parent molecule was not observed for any of the fluranes and abundant fragmentation was found instead. This is however difficult to understand, given the little energy available upon proton transfer, and it is tentatively explained by electric field heating of both the reagent and

the product ions.

9.1.6 Investigation of Phthalate Esters in Proton Transfer Reaction Mass Spectrometry via Direct Headspace Sampling

These results demonstrate the feasibility for the detection of phthalic acid and ten phthalate esters using PTR-MS by means of headspace analysis. The product ion distributions arising from the reaction of the phthalates with H_3O^+ were provided as a function of the reduced electric range from 80 to 205 Td. Distinguishing three isomers, namely DBP, DiBP and MEHP, was proven possible without the need for pre-separation by solely comparing the product ion distributions at different E/N values. Protonated phthalic anhydride ($C_8H_5O_3^+$, m/z 149) is a common product ion observed, but it was not observed with dimethyl or diallyl phthalate. For the alkyl diester phthalates the abundance of protonated phthalic anhydride increases with the alkyl chain length and with the reduced electric field. The loss of the corresponding alcohol (*i.e.* methanol for DMP, ethanol for DEP, propanol for DPP and butanol for DBP) from the protonated parent was also observed for all the studied alkyl diester phthalates. In contrast to m/z 149, the abundance of the loss of an alcohol decreases with the alkyl chain length.

9.2 Conclusions and closing remarks

The work presented in this thesis aims to extend the knowledge of the ion/molecule processes taking place in SCI-MS techniques, mainly PTR-MS, through both experimental and theoretical studies. To accomplish this, several molecules of importance within the fields of homeland security and medicine have been investigated to generate a compendium of results, including the product ions and their abundances at different values of the reduced electric field. These substances of interest include illicit drugs and related compounds (chapter 3 and appendix A); explosive compounds: TNT and related mono- and di- nitrotoluenes (chapter 4) and nitroaniline isomers (chapter 5); linear, cyclic and branched ketones (chapter 6); anaesthetics (chapter 7); and phthalates (chapter 8). Most of the experimental work was done at the Molecular Physics group laboratory of the School of Physics and Astronomy at the University of Birmingham, Birmingham (UK), but part of it was done in collaboration with both industrial and academic institutions: Kore Technology, Ltd., Ely (UK); IONICON Analytik GmbH, Innsbruck (Austria); and the

Institute for Breath Research, Leopold-Franzens-Universität Innsbruck, Dornbirn (Austria). The theoretical work included in the present thesis consists of DFT calculations to obtain the key thermodynamic data of the neutral molecules as well as the energies of the proton transfer and fragmentation reaction pathways.

The different investigations contained in the present thesis have been carried out using a number of novel developments in the field. These are the RFIF, the TDU, the fastGC and the LCU. The implementation of these add-ons transformed the PTR-MS into a multidimensional device capable of performing quick chromatographic analysis (fastGC), analysing liquid (LCU) or solid (TDU) samples, and manipulating the ion/molecule chemistry (RFIF).

The DFT results are calculated at a temperature of 298 K, and they should therefore considered as indicative of the thermodynamically available fragmentation pathways, as the effective temperature of the ions in the reactor is considered to be higher. Note that the fact that a reaction is thermodynamically allowed does not imply that it occurs fast. With this in mind, these theoretical results were able to predict and support most of the ion/molecule processes experimentally observed. However, there exist some disagreement between the experimental and theoretical results that should be further investigated. For example, the loss of C_2H_4 from ethyl benzoate and ethyl isobutyrate and the loss of C_3H_6 from isopropyl benzoate are exergonic according to the DFT calculations, and these fragmentation pathways should therefore occur spontaneously. But they are only observed at E/N values higher than a certain threshold, in contrast with what is predicted by the DFT results. Moreover, the case of the anaesthetics is the opposite. Even though the proton transfer reaction from H_3O^+ to most of the main protonation sites of these compounds is predicted to be exergonic, product ions arising from this reaction where observed. The tentative explanation for this observations is that proton transfer is achieved due to the kinetic energy gained by the ions within the reduced electric field, followed by fragmentation, as the protonated parent molecules are not observed. Furthermore, the transition state needed for the loss of benzoic acid from protonated cocaine is still to be found.

PTR-MS has been widely proved to be a suitable tool for the detection of different families of compounds, but not all organic compounds that were meant to be part of this thesis could be detected and analysed. For instance, an unsuccessful attempt was made to detect glyphosate ($C_3H_8NO_5P$), a well known pesticide [221]. The reason behind this is thought to be the high melting point of glyphosate (189.5 °C) [222], as it is the case as well with benzoylecgonine (195

°C). The PTR-MS is not directly to blame for this but the sampling method. Also, inlet lines in PTR-MS instruments rarely reach more than 150 °C and therefore memory effects (*i.e.* adherence and slower desorption of less volatile compounds to surfaces) are present.

A key shortcoming of using the E/N parameter in PTR-MS is that it cannot be unambiguously defined with different combinations of pressure, temperature and drift voltage. To be able to repeat a set of experiments in the same conditions, more than one parameter must be therefore provided. For this reason, and although the use of the E/N parameter is very extended in the community, it would be necessary to move to another parameter that would uniquely define the collisional energy. An attempt to define such a parameter is being made by Renaud R. Dassonville, who was, as myself, part of the EU funded Innovative Training Network IMPACT*.

9.3 Future work

The following research lines would continue and/or expand the work presented in this thesis:

(i) The improvements in selectivity provided by the implementation of an RF ion funnel in the drift tube should be further exploited. It was demonstrated by the results shown in chapter 4 that this feature can be used to manipulate the ion/molecule chemistry of TNT. This should be therefore extended to other substances, for example to other explosive compounds (*e.g.* RDX, HMTD and nitroanilines) or to drugs (*e.g.* cocaine and heroin). There are different configurations of the RFIF available in the market, being noteworthy the recent developments achieved by KORE Technology Ltd in this regard. Furthermore, the RF ion funnel can be used in conjunction with fast switching capabilities, as it was demonstrated by González-Méndez *et al.* [14].

(ii) The feasibility of the deployment of the PTR-MS technology for the field detection of the substances investigated in this thesis is yet to be demonstrated. Some analytical techniques (*e.g.* LC-MS, GC-MS and UHPLC-MS) have been able to detect and quantify phthalates in complex mixtures and matrices (*e.g.* water, soil and some foods) [178, 180, 202]. However, the only PTR-MS study available so far is the one presented in this thesis, which consists on a preliminary study to characterise each of the substances by identifying their product

*Ion/Molecule Processes for Analytical Chemistry Technologies (IMPACT) was an Innovative Training Network funded by the European Commission's HORIZON 2020 Programme under Grant Agreement Number 674911 (http://impact-h2020itn.com).

ions. It is still to be proved if PTR-MS is a suitable tool to be deployed for the detection of phthalates in phthalate-containing systems. It would also be helpful to investigate the limits of detection achievable in PTR-MS for phthalates before a field deployment is attempted. On the other hand, an *open–label* study (which is in this case a kind of field deployment) is meant to be the continuation of the anaesthetics results presented in chapter 7. A similar study is that from Fernández del Río *et al.* for the elimination of isoflurane in post-operation conditions [158].

(iii) Further developing a soft chemical ionisation mass spectrometry technique that uses more than one reagent ion species simultaneously. The results presented in chapter 5 are an example of many of how the ion/molecule chemistry can be manipulated by using different reagent ions to differentiate between isomeric compounds [2, 70]. This could ideally be done instantaneously by generating more than one reagent ion species (typically H_3O^+, O_2^+ and NO^+) in the ion source at the same time and injecting them together into the drift tube for them to simultaneously react with the analyte. This would provide a more complete set of product ions than that obtained when only one reagent ion specie is present, easing the identification of the analyte(s) and reducing the number of false positives. It is obvious that, when studying a complex mixture, having so many reaction pathways occuring in parallel might not be advantageous, as it would yield very congested spectra. But this issue could be overcome by developing the proper software to perform a deconvolution of the contribution from each product ion to the intensities of the mass spectral peaks. Efforts on the development of a multiple-reagent ion source have been carried out by industrial partners within the IMPACT project. For instance, IONICON Analytik GmbH (Austria) has reported the triple off-axis ion source *TRION* that allows quick switching between different reagent ion species [44].

(iv) Development and implementation of high-temperature inlet systems suitable for very sticky substances or for substances with a melting point of ≥200 °C. Inlet lines in PTR-MS are usually heated, but not enough to completely avoid memory effects of sticky compounds. There exist desorption systems that can reach even ≥300 °C, like Tenax® tubes. However, most inlet lines cannot be heated at more than 120–150 °C for extended periods of time, which helps in the surface deposition and absorption of sticky substances.

References

1. González-Méndez, R., Watts, P., Olivenza-León, D., Reich, D. F., Mullock, S. J., Corlett, C. A., Cairns, S., Hickey, P., Brookes, M. & Mayhew, C. A. Enhancement of Compound Selectivity Using a Radio Frequency Ion-Funnel Proton Transfer Reaction Mass Spectrometer: Improved Specificity for Explosive Compounds. *Analytical Chemistry* **88,** 10624–10630 (2016). DOI: 10.1021/acs.analchem.6b02982.

2. Olivenza-León, D., Mayhew, C. A. & González-Méndez, R. Selective Reagent Ion Mass Spectrometric Investigations of the Nitroanilines. *Journal of the American Society for Mass Spectrometry,* 1–8 (2019). DOI: 10.1007/s13361-019-02325-0.

3. Malásková, M., Olivenza-León, D., Piel, F., Mochalski, P., Sulzer, P., Jürschik, S., Mayhew, C. & Maerk, T. Compendium of the reactions of H_3O^+ with selected ketones of relevance to breath analysis using proton transfer reaction mass spectrometry. *Frontiers in Chemistry* **7,** 401 (2019). DOI: 10.1021/acs.analchem.6b02982.

4. Malásková, M., Olivenza-León, D., Chellayah, P. D., Martini, J., Lederer, W., Ruzsanyi, V., Unterkofler, K., Mochalski, P., Märk, T. D., Watts, P. & Mayhew, C. A. Studies pertaining to the monitoring of volatile halogenated anaesthetics in breath by proton transfer reaction mass spectrometry. *Journal of Breath Research* **14,** 026004 (2020). DOI: 10.1088/1752-7163/ab5e30.

5. Barber, S., Blake, R. S., White, I. R., Monks, P. S., Reich, F., Mullock, S. & Ellis, A. M. Increased sensitivity in proton transfer reaction mass spectrometry by incorporation of a radio frequency ion funnel. *Analytical Chemistry* **84,** 5387–5391 (2012).

6. Sulzer, P., Petersson, F., Agarwal, B., Becker, K. H., Jürschik, S., Märk, T. D., Perry, D., Watts, P. & Mayhew, C. A. Proton transfer reaction mass spectrometry and the

unambiguous real-time detection of 2, 4, 6 trinitrotoluene. *Analytical Chemistry* **84,** 4161–4166 (2012).

7. Lindinger, W., Hansel, A. & Jordan, A. On-line monitoring of volatile organic compounds at pptv levels by means of proton-transfer-reaction mass spectrometry (PTR-MS). Medical applications, food control and environmental research. *International Journal of Mass Spectrometry and Ion Processes* **173,** 191–241 (1998). DOI: 10.1016/S0168-1176(97)00281-4.

8. De Gouw, J. A., Goldan, P. D., Warneke, C., Kuster, W. C., Roberts, J. M., Marchewka, M., Bertman, S. B., Pszenny, A. A. P. & Keene, W. C. Validation of proton transfer reaction-mass spectrometry (PTR-MS) measurements of gas-phase organic compounds in the atmosphere during the New England Air Quality Study (NEAQS) in 2002. *Journal of Geophysical Research: Atmospheres* **108** (2003).

9. Rogers, T., Grimsrud, E., Herndon, S., Jayne, J., Kolb, C., Allwine, E., Westberg, H., Lamb, B., Zavala, M., Molina, L., Molina, M. & Knighton, W. On-road measurements of volatile organic compounds in the Mexico City metropolitan area using proton transfer reaction mass spectrometry. *International Journal of Mass Spectrometry* **252,** 26–37 (2006). DOI: https://doi.org/10.1016/j.ijms.2006.01.027.

10. Piel, F., Müller, M., Mikoviny, T., Pusede, S. E. & Wisthaler, A. Airborne measurements of particulate organic matter by PTR-MS: a pilot study. *Atmospheric Measurement Techniques Discussions,* 1–20 (2019).

11. Lacko, M., Wang, N., Sovová, K., Pásztor, P. & Španěl, P. Addition of a fast GC to SIFT-MS for analyses of individual monoterpenes in mixtures. *Atmos Meas Tech Discuss* **2019,** 1–23 (2019).

12. González-Méndez, R., Reich, D. F., Mullock, S. J., Corlett, C. A. & Mayhew, C. A. Development and use of a thermal desorption unit and proton transfer reaction mass spectrometry for trace explosive detection: Determination of the instrumental limits of detection and an investigation of memory effects. *International Journal of Mass Spectrometry* **385,** 13–18 (2015). DOI: 10.1016/j.ijms.2015.05.003.

13. Sulzer, P., Agarwal, B., Jürschik, S., Lanza, M., Jordan, A., Hartungen, E., Hanel, G., Mark, L., Mark, T. D., González-Méndez, R., Watts, P. & Mayhew, C. A. Applications of switching reagent ions in proton transfer reaction mass spectrometric instruments for the improved selectivity of explosive compounds. *International Journal of Mass Spectrometry* **354,** 123–128 (2013). DOI: 10.1016/j.ijms.2013.05.004.

14. González-Méndez, R., Watts, P., Reich, D. F., Mullock, S. J., Cairns, S., Hickey, P., Brookes, M. & Mayhew, C. A. Use of Rapid Reduced Electric Field Switching to Enhance Compound Specificity for Proton Transfer Reaction-Mass Spectrometry. *Analytical Chemistry* **90,** 5664–5670 (2018). DOI: 10.1021/acs.analchem.7b05211.

15. Jürschik, S., Agarwal, B., Kassebacher, T., Sulzer, P., Mayhew, C. A. & Märk, T. D. Rapid and facile detection of four date rape drugs in different beverages utilizing proton transfer reaction mass spectrometry (PTR-MS). *Journal of Mass Spectrometry* **47,** 1092–1097 (2012).

16. Agarwal, B., Petersson, F., Jürschik, S., Sulzer, P., Jordan, A., Märk, T. D., Watts, P. & Mayhew, C. A. Use of proton transfer reaction time-of-flight mass spectrometry for the analytical detection of illicit and controlled prescription drugs at room temperature via direct headspace sampling. *Analytical and Bioanalytical Chemistry* **400,** 2631–2639 (2011). DOI: 10.1007/s00216-011-4892-8.

17. Fernández del Río, R., O'Hara, M., Holt, A., Pemberton, P., Shah, T., Whitehouse, T. & Mayhew, C. Volatile Biomarkers in Breath Associated With Liver Cirrhosis – Comparisons of Pre- and Post-liver Transplant Breath Samples. *EBioMedicine* **2,** 1243–1250 (2015). DOI: https://doi.org/10.1016/j.ebiom.2015.07.027.

18. Karl, T., Prazeller, P., Mayr, D., Jordan, A., Rieder, J., Fall, R. & Lindinger, W. Human breath isoprene and its relation to blood cholesterol levels: new measurements and modeling. *Journal of Applied Physiology* **91,** 762–770 (2001). DOI: 10.1152/jappl.2001.91.2.762.

19. Amann, A., Mochalski, P., Ruzsanyi, V., Broza, Y. Y. & Haick, H. Assessment of the exhalation kinetics of volatile cancer biomarkers based on their physicochemical properties. *Journal of Breath Research* **8,** 016003 (2014).

20. Malásková, M., Henderson, B., Chellayah, P. D., Ruzsanyi, V., Mochalski, P., Cristescu, S. M. & Mayhew, C. A. Proton transfer reaction time-of-flight mass spectrometric measurements of volatile compounds contained in peppermint oil capsules of relevance to real-time pharmacokinetic breath studies. *Journal of Breath Research* **13,** 046009 (2019).

21. Boscaini, E., van Ruth, S., Biasioli, F., Gasperi, F. & Märk, T. D. Gas Chromatography-Olfactometry (GC-O) and Proton Transfer Reaction-Mass Spectrometry (PTR-MS) Analysis of the Flavor Profile of Grana Padano, Parmigiano Reggiano, and Grana Trentino Cheeses. *Journal of Agricultural and Food Chemistry* **51,** 1782–1790 (2003). DOI: 10.1021/jf020922g.

22. Aprea, E., Biasioli, F., Carlin, S., Endrizzi, I. & Gasperi, F. Investigation of Volatile Compounds in Two Raspberry Cultivars by Two Headspace Techniques: Solid-Phase Microextraction/Gas Chromatography-Mass Spectrometry (SPME/GC-MS) and Proton-Transfer Reaction-Mass Spectrometry (PTR-MS). *Journal of Agricultural and Food Chemistry* **57,** 4011–4018 (2009). DOI: 10.1021/jf803998c.

23. Fabris, A., Biasioli, F., Granitto, P. M., Aprea, E., Cappellin, L., Schuhfried, E., Soukoulis, C., Märk, T. D., Gasperi, F. & Endrizzi, I. PTR-TOF-MS and data-mining methods for rapid characterisation of agro-industrial samples: influence of milk storage conditions on the volatile compounds profile of Trentingrana cheese. *Journal of Mass Spectrometry* **45,** 1065–1074. DOI: 10.1002/jms.1797.

24. Grob, R. L. & Barry, E. F. *Modern practice of gas chromatography* (Wiley Online Library, 1977).

25. Eiceman, G. A., Karpas, Z. & Hill Jr, H. H. *Ion mobility spectrometry* (CRC press, 2013).

26. Borsdorf, H. & Eiceman, G. A. Ion mobility spectrometry: principles and applications. *Applied Spectroscopy Reviews* **41,** 323–375 (2006).

27. Ewing, R. G., Atkinson, D. A., Eiceman, G. & Ewing, G. A critical review of ion mobility spectrometry for the detection of explosives and explosive related compounds. *Talanta* **54,** 515–529 (2001).

28. Smith, D. & Španěl, P. Selected ion flow tube mass spectrometry (SIFT-MS) for on-line trace gas analysis. *Mass Spectrometry Reviews* **24,** 661–700 (2005).

29. Španěl, P. & Smith, D. Progress in SIFT-MS: Breath analysis and other applications. *Mass Spectrometry Reviews* **30,** 236–267 (2011).

30. Munson, M. S. & Field, F.-H. Chemical ionization mass spectrometry. I. General introduction. *Journal of the American Chemical Society* **88,** 2621–2630 (1966).

31. Ellis, A. M. & Mayhew, C. A. *Proton Transfer Reaction Mass Spectrometry: Principles and Applications* (John Wiley & Sons, 2013).

32. Hunter, E. P. L. & Lias, S. G. Evaluated Gas Phase Basicities and Proton Affinities of Molecules: An Update. *Journal of Physical and Chemical Reference Data* **27,** 413–656 (1998). DOI: 10.1063/1.556018.

33. Goebbert, D. J. & Wenthold, P. G. Water Dimer Proton Affinity from the Kinetic Method: Dissociation Energy of the Water Dimer. *European Journal of Mass Spectrometry* **10,** 837–845 (2004). DOI: 10.1255/ejms.684.

34. IUPAC. *Compendium of chemical terminology* (Blackwell Scientific Publications Oxford, 1997).

35. NIST chemistry webbook. NIST standard reference database 69. National Institute of Standards and Technology (Eds P.J. Linstrom and W.G. Mallard).

36. Carrasco, E., Jiménez-Redondo, M., Tanarro, I. & Herrero, V. J. Neutral and ion chemistry in low pressure dc plasmas of H2/N2 mixtures: routes for the efficient production of NH_3 and NH_4^+. *Phys. Chem. Chem. Phys.* **13,** 19561–19572 (43 2011). DOI: 10.1039/C1CP22284H.

37. Müller, M., Piel, F., Gutmann, R., Sulzer, P., Hartungen, E. & Wisthaler, A. A novel method for producing $NH4^+$ reagent ions in the hollow cathode glow discharge ion source of PTR-MS instruments. *International Journal of Mass Spectrometry,* 116254 (2019).

38. González-Méndez, R., Watts, P., Howse, D., Procino, I., McIntyre, H. & Mayhew, C. Ion Mobility Studies on the Negative Ion-Molecule Chemistry of Isoflurane and Enflurane. *Journal of the American Society for Mass Spectrometry* **28,** 939–946 (2017). DOI: 10.1007/s13361-017-1616-0.

39. Michalczuk, B., Moravsky, L., Papp, P., Mach, P., Sabo, M. & Matejcik, S. Isomer and Conformer Selective Atmospheric Pressure Chemical Ionisation of dimethyl phthalate. *Physical Chemistry Chemical Physics* **21,** 13679–13685 (2019).

40. Guharay, S. K., Dwivedi, P. & Hill, H. H. Ion mobility spectrometry: Ion source development and applications in physical and biological sciences. *IEEE Transactions on Plasma Science* **36,** 1458–1470 (2008).

41. Wannier, G. H. Motion of gaseous ions in a strong electric field. *Physical Review* **83,** 281–289 (1951).

42. Wannier, G. H. Motion of gaseous ions in a strong electric field. II. *Physical Review* **87,** 795–798 (1952).

43. Turner, C., Španěl, P. & Smith, D. A longitudinal study of ammonia, acetone and propanol in the exhaled breath of 30 subjects using selected ion flow tube mass spectrometry, SIFT-MS. *Physiological Measurement* **27,** 321 (2006).

44. Jordan, A., Feil, S., Hanel, G., Märk, L. & Sulzer, P. A new High Resolution PTR-TOFMS instrument with RF-Drift Tube, Ion Funnel and the novel TRION Source. *Proceedings of the 8th International Conference on Proton Transfer Reaction Mass Spectrometry and its Applications.* Obergurgl, Austria (ed Hansel, A. and Dunkl, J.) (Innsbruck University Press, Feb. 2019), 133–135.

45. Ikezoe, Y., Matsuoka, S., Takebe, M. & Viggiano, A. Gas Phase Ion - Molecule Reaction Rate Constants Through 1986. *Maruzen Company Ltd, Tokyo* (1987).

46. Price, P., Swofford, H. & Buttrill, S. New drift-tube source for use in chemical ionization mass spectrometry. *Analytical Chemistry* **49,** 1497–1500 (1977).

47. Price, P., Swofford, H. & Buttrill, S. Drift tube chemical ionization mass spectrometry of esters. *Analytical Chemistry* **50,** 1127–1130 (1978).

48. Hirschfelder, J. O., Curtiss, C. F., Bird, R. B. & Mayer, M. G. *Molecular Theory of Gases and Liquids* (Wiley New York, 1954).

49. Ismail, A. F., Khulbe, K. C. & Matsuura, T. *Gas Separation Membranes: Polymeric and Inorganic* 14 (Springer, 2015).

50. Warneke, C., Van der Veen, C., Luxembourg, S., De Gouw, J. & Kok, A. Measurements of benzene and toluene in ambient air using proton-transfer-reaction mass spectrometry: calibration, humidity dependence, and field intercomparison. *International Journal of Mass Spectrometry* **207,** 167–182 (2001).

51. Krechmer, J., Lopez-Hilfiker, F., Koss, A., Hutterli, M., Stoermer, C., Deming, B., Kimmel, J., Warneke, C., Holzinger, R., Jayne, J. *et al.* Evaluation of a new reagent-ion source and focusing ion–molecule reactor for use in proton-transfer-reaction mass spectrometry. *Analytical Chemistry* **90,** 12011–12018 (2018).

52. KORE Technology Ltd. *Manual Z-7182-M.*

53. NIST. *Atomic weights and isotopic compositions for oxygen.* URL: `https://physics.nist.gov/cgi-bin/Compositions/stand_alone.pl?ele=O&isotype=some` (visited on 22/07/2019).

54. NIST. *Atomic weights and isotopic compositions for carbon.* URL: `https://physics.nist.gov/cgi-bin/Compositions/stand_alone.pl?ele=C&isotype=some` (visited on 22/07/2019).

55. NIST. *Atomic weights and isotopic compositions for chlorine.* URL: `https://physics.nist.gov/cgi-bin/Compositions/stand_alone.pl?ele=Cl&isotype=some` (visited on 22/07/2019).

56. NIST. *Atomic weights and isotopic compositions for bromine.* URL: `https://physics.nist.gov/cgi-bin/Compositions/stand_alone.pl?ele=Br&isotype=some` (visited on 22/07/2019).

57. Frisch, M. J., Trucks, G., Schlegel, H., Scuseria, G., Robb, M., Cheeseman, J., Scalmani, G., Barone, V., Mennucci, B., Petersson, G. *et al.* Gaussian 09, Revision D. 01. Gaussian Inc., Wallingford (2009).

58. Müller, M., Eichler, P., D'Anna, B., Tan, W. & Wisthaler, A. Direct sampling and analysis of atmospheric particulate organic matter by proton-transfer-reaction mass spectrometry. *Analytical Chemistry* **89,** 10889–10897 (2017).

59. KORE Technology Ltd. *PREFICS - Pre concentrator with Fast Integrated Chromatographic Separation.* URL: `https://www.kore.co.uk/prefics.html` (visited on 12/07/2019).

60. Conrad, F. J. *Hand held explosives detection system.* U.S. Patent 5 138 889, Aug. 1992.

61. Carroll, A. L., Miskolczy, G., Fraim, F. W., Achter, E. K. & Lieb, D. P. *Hand-held sample gun for vapor collection.* U.S. Patent 5 123 274, June 1992.

62. Jjunju, F. P., Maher, S., Li, A., Syed, S. U., Smith, B., Heeren, R. M., Taylor, S. & Cooks, R. G. Hand-held portable desorption atmospheric pressure chemical ionization ion source for in situ analysis of nitroaromatic explosives. *Analytical Chemistry* **87,** 10047–10055 (2015).

63. Staymates, M. E., MacCrehan, W. A., Staymates, J. L., Kunz, R. R., Mendum, T., Ong, T.-H., Geurtsen, G., Gillen, G. J. & Craven, B. A. Biomimetic sniffing improves the detection performance of a 3D printed nose of a dog and a commercial trace vapor detector. *Scientific Reports* **6,** 36876 (2016).

64. Blenkhorn, D. J. *Novel approaches to the measurement of complex atmospheric VOC mixtures using proton transfer reaction mass spectrometry.* PhD thesis (University of Birmingham, 2019).

65. Ruzsanyi, V., Fischer, L., Herbig, J., Ager, C. & Amann, A. Multi-capillary-column proton-transfer-reaction time-of-flight mass spectrometry. *Journal of Chromatography A* **1316,** 112–118 (2013).

66. Romano, A., Fischer, L., Herbig, J., Campbell-Sills, H., Coulon, J., Lucas, P., Cappellin, L. & Biasioli, F. Wine analysis by FastGC proton-transfer reaction-time-of-flight-mass spectrometry. *International Journal of Mass Spectrometry* **369,** 81–86 (2014).

67. Fischer, L., Klinger, A., Herbig, J., Winkler, K., Gutmann, R. & Hansel, A. The LCU: Versatile Trace Gas Calibration. *Proceedings of the 6th International Conference on Proton Transfer Reaction Mass Spectrometry and its Applications.* Obergurgl, Austria (eds Hansel, A. & Dunkl, J.) (Innsbruck University Press, Feb. 2013), 192–195.

68. Mastroianni, N., López-García, E., Postigo, C., Barceló, D. & de Alda, M. L. Five-year monitoring of 19 illicit and legal substances of abuse at the inlet of a wastewater treatment plant in Barcelona (NE Spain) and estimation of drug consumption patterns and trends. *Science of The Total Environment* **609,** 916–926 (2017).

69. United Nations Office on Drugs and Crime. *World drug report 2019* (United Nations Publications, 2019).

70. Lanza, M., Acton, W. J., Jürschik, S., Sulzer, P., Breiev, K., Jordan, A., Hartungen, E., Hanel, G., Märk, L., Mayhew, C. A. *et al.* Distinguishing two isomeric mephedrone substitutes with selective reagent ionisation mass spectrometry (SRI-MS). *Journal of Mass Spectrometry* **48,** 1015–1018 (2013).

71. Cone, E. J., Yousefnejad, D., Darwin, W. D. & Maguire, T. Testing human hair for drugs of abuse. II. Identification of unique cocaine metabolites in hair of drug abusers and evaluation of decontamination procedures. *Journal of Analytical Toxicology* **15,** 250–255 (1991).

72. Shimomura, E. T., Jackson, G. F. & Paul, B. D. *Critical Issues in Alcohol and Drugs of Abuse Testing* 215–224 (Elsevier, 2019).

73. Ambre, J., Ruo, T. I., Nelson, J. & Belknap, S. Urinary excretion of cocaine, benzoylecgonine, and ecgonine methyl ester in humans. *Journal of Analytical Toxicology* **12,** 301–306 (1988).

74. Fleming, S. W., Dasgupta, A. & Garg, U. *Clinical Applications of Mass Spectrometry* 145–156 (Springer, 2010).

75. Hezinová, V., Aturki, Z., Klepárník, K., D'Orazio, G., Foret, F. & Fanali, S. Simultaneous analysis of cocaine and its metabolites in urine by capillary electrophoresis-electrospray mass spectrometry using a pressurized liquid junction nanoflow interface. *Electrophoresis* **33,** 653–660 (2012).

76. Antonilli, L., Suriano, C., Grassi, M. C. & Nencini, P. Analysis of cocaethylene, benzoylecgonine and cocaine in human urine by high-performance thin-layer chromatography with ultraviolet detection: a comparison with high-performance liquid chromatography. *Journal of Chromatography B: Biomedical Sciences and Applications* **751,** 19–27 (2001).

77. McCance-Katz, E. F., Price, L. H., McDougle, C. J., Kosten, T. R., Black, J. E. & Jatlow, P. I. Concurrent cocaine-ethanol ingestion in humans: pharmacology, physiology, behavior, and the role of cocaethylene. *Psychopharmacology* **111,** 39–46 (1993).

78. Pennings, E. J., Leccese, A. P. & Wolff, F. A. d. Effects of concurrent use of alcohol and cocaine. *Addiction* **97,** 773–783 (2002).

79. Jatlow, P., Elsworth, J., Bradberry, C., Winger, G., Taylor, J., Russell, R. & Roth, R. Cocaethylene: A neuropharmacologically active metabolite associated with concurrent cocaine-ethanol ingestion. *Life Sciences* **48,** 1787–1794 (1991).

80. Snozek, C. L., Bjergum, M. W. & Langman, L. J. *LC-MS in Drug Analysis* 91–103 (Springer, 2012).

81. Harris, D. S., Everhart, E. T., Mendelson, J. & Jones, R. T. The pharmacology of cocaethylene in humans following cocaine and ethanol administration. *Drug and Alcohol Dependence* **72,** 169–182 (2003).

82. Lange, R. A. & Hillis, L. D. Cardiovascular complications of cocaine use. *New England Journal of Medicine* **345,** 351–358 (2001).

83. Farré, M., De la Torre, R., Llorente, M., Lamas, X., Ugena, B., Segura, J. & Camí, J. Alcohol and cocaine interactions in humans. *Journal of Pharmacology and Experimental Therapeutics* **266,** 1364–1373 (1993).

84. Schaffer, M., Cheng, C.-C., Chao, O., Hill, V. & Matsui, P. Analysis of cocaine and metabolites in hair: validation and application of measurement of hydroxycocaine metabolites as evidence of cocaine ingestion. *Analytical and Bioanalytical Chemistry* **408,** 2043–2054 (2016).

85. Paul, B. D., Lalani, S., Bosy, T., Jacobs, A. J. & Huestis, M. A. Concentration profiles of cocaine, pyrolytic methyl ecgonidine and thirteen metabolites in human blood and urine: determination by gas chromatography–mass spectrometry. *Biomedical Chromatography* **19,** 677–688 (2005).

86. Robandt, P. P., Reda, L. J. & Klette, K. L. Complete automation of solid-phase extraction with subsequent liquid chromatography-tandem mass spectrometry for the quantification of benzoylecgonine, m-hydroxybenzoylecgonine, p-hydroxybenzoylecgonine, and norben-

zoylecgonine in urine—application to a high-throughput urine analysis laboratory. *Journal of Analytical Toxicology* **32,** 577–585 (2008).

87. Klette, K. L., Poch, G. K., Czarny, R. & Lau, C. O. Simultaneous GC-MS analysis of meta-and para-hydroxybenzoylecgonine and norbenzoylecgonine: a secondary method to corroborate cocaine ingestion using nonhydrolytic metabolites. *Journal of Analytical Toxicology* **24,** 482–488 (2000).

88. Furton, K. G., Hong, Y.-c., Hsu, Y.-L., Luo, T., Rose, S. & Walton, J. Identification of odor signature chemicals in cocaine using solid-phase microextraction-gas chromatography and detector-dog response to isolated compounds spiked on US paper currency. *Journal of Chromatographic Science* **40,** 147–155 (2002).

89. Waggoner, L. P., Johnston, J. M., Williams, M., Jackson, J., Jones, M. H., Boussom, T. & Petrousky, J. A. Canine olfactory sensitivity to cocaine hydrochloride and methyl benzoate. *Chemistry-and Biology-Based Technologies for Contraband Detection* **2937** (1997), 216–226.

90. U.S. Environmental Protection Agency. *Chemistry Dashboard: Properties of cocaine.* URL: `https://comptox.epa.gov/dashboard/DTXSID2038443#properties` (visited on 14/10/2019).

91. U.S. Environmental Protection Agency. *Chemistry Dashboard.* URL: `https://comptox.epa.gov/dashboard/` (visited on 14/10/2019).

92. Wang, P. & Bartlett, M. G. Collision-induced dissociation mass spectra of cocaine, and its metabolites and pyrolysis products. *Journal of Mass Spectrometry* **33,** 961–967 (1998).

93. Moore, C., Coulter, C. & Crompton, K. Determination of cocaine, benzoylecgonine, cocaethylene and norcocaine in human hair using solid-phase extraction and liquid chromatography with tandem mass spectrometric detection. *Journal of Chromatography B* **859,** 208–212 (2007).

94. mzCloud - Advanced Mass Spectral Database. HighChem LLC, Slovakia. *Norcocaine.* URL: `www.mzcloud.org/dataviewer.aspx#Creference845` (visited on 28/10/2019).

95. Musshoff, F., Thieme, D., Schwarz, G., Sachs, H., Skopp, G. & Franz, T. Determination of hydroxy metabolites of cocaine in hair samples for proof of consumption. *Drug Testing and Analysis* **10,** 681–688 (2018).

96. Minoli, M., Casati, S., Angeli, I., Ravelli, A., Rota, P., Allevi, P. & Orioli, M. Analysis of hydroxy-cocaine metabolites as evidence of cocaine consumption: Identification by parent ion search and quantitation by UHPLC-MS/MS in hair. *Journal of Pharmaceutical and Biomedical Analysis* **172,** 167–174 (2019).

97. Haynes, W. M. *CRC Handbook of Chemistry and Physics* (CRC press, 2014).

98. mzCloud - Advanced Mass Spectral Database. HighChem LLC, Slovakia. *Cocaine.* URL: `www.mzcloud.org/dataviewer.aspx#Creference1016` (visited on 28/10/2019).

99. Shaffer, S. A., Tang, K., Anderson, G. A., Prior, D. C., Udseth, H. R. & Smith, R. D. A novel ion funnel for focusing ions at elevated pressure using electrospray ionization mass spectrometry. *Rapid Communications in Mass Spectrometry* **11,** 1813–1817 (1997).

100. Kelly, R. T., Tolmachev, A. V., Page, J. S., Tang, K. & Smith, R. D. The ion funnel: theory, implementations, and applications. *Mass Spectrometry Reviews* **29,** 294–312 (2010).

101. Blake, R. S., Whyte, C., Hughes, C. O., Ellis, A. M. & Monks, P. S. Demonstration of proton-transfer reaction time-of-flight mass spectrometry for real-time analysis of trace volatile organic compounds. *Analytical Chemistry* **76,** 3841–3845 (2004).

102. Ennis, C., Reynolds, J., Keely, B. & Carpenter, L. A hollow cathode proton transfer reaction time of flight mass spectrometer. *International Journal of Mass Spectrometry* **247,** 72–80 (2005). DOI: `10.1016/j.ijms.2005.09.008`.

103. Brown, P., Watts, P., Märk, T. & Mayhew, C. Proton transfer reaction mass spectrometry investigations on the effects of reduced electric field and reagent ion internal energy on product ion branching ratios for a series of saturated alcohols. *International Journal of Mass Spectrometry* **294,** 103–111 (2010).

104. Kassebacher, T., Sulzer, P., Jürschik, S., Hartungen, E., Jordan, A., Edtbauer, A., Feil, S., Hanel, G., Jaksch, S., Märk, L. *et al.* Investigations of chemical warfare agents and toxic industrial compounds with proton-transfer-reaction mass spectrometry for a real-time threat monitoring scenario. *Rapid Communications in Mass Spectrometry* **27,** 325–332 (2013).

105. Sulzer, P., Agarwal, B., Jürschik, S., Lanza, M., Jordan, A., Hartungen, E., Hanel, G., Märk, L., Märk, T. D., González-Méndez, R. *et al.* Applications of switching reagent ions in proton transfer reaction mass spectrometric instruments for the improved selectivity of explosive compounds. *International Journal of Mass Spectrometry* **354,** 123–128 (2013).

106. Agarwal, B., González-Méndez, R., Lanza, M., Sulzer, P., Märk, T. D., Thomas, N. & Mayhew, C. A. Sensitivity and selectivity of switchable reagent ion soft chemical ionization mass spectrometry for the detection of picric acid. *The Journal of Physical Chemistry A* **118,** 8229–8236 (2014).

107. Acton, W. J., Lanza, M., Agarwal, B., Jürschik, S., Sulzer, P., Breiev, K., Jordan, A., Hartungen, E., Hanel, G., Märk, L. *et al.* Headspace analysis of new psychoactive substances using a Selective Reagent Ionisation-Time of Flight-Mass Spectrometer. *International Journal of Mass Spectrometry* **360,** 28–38 (2014).

108. Lanza, M., Acton, W. J., Sulzer, P., Breiev, K., Jürschik, S., Jordan, A., Hartungen, E., Hanel, G., Märk, L., Märk, T. D. *et al.* Selective reagent ionisation-time of flight-mass spectrometry: a rapid technology for the novel analysis of blends of new psychoactive substances. *Journal of Mass Spectrometry* **50,** 427–431 (2015).

109. Mayhew, C., Sulzer, P., Petersson, F., Haidacher, S., Jordan, A., Märk, L., Watts, P. & Märk, T. Applications of proton transfer reaction time-of-flight mass spectrometry for the sensitive and rapid real-time detection of solid high explosives. *International Journal of Mass Spectrometry* **289,** 58–63 (2010).

110. Biasioli, F., Yeretzian, C., Märk, T. D., Dewulf, J. & Van Langenhove, H. Direct-injection mass spectrometry adds the time dimension to (B) VOC analysis. *TrAC Trends in Analytical Chemistry* **30,** 1003–1017 (2011).

111. Trefz, P., Schubert, J. K. & Miekisch, W. Effects of humidity, CO_2 and O_2 on real-time quantitation of breath biomarkers by means of PTR-ToF-MS. *Journal of Breath Research* **12,** 026016 (2018).

112. Herbig, J. & Beauchamp, J. Towards standardization in the analysis of breath gas volatiles. *Journal of Breath Research* **8,** 037101 (2014).

113. Ruzsányi, V., Kalapos, M. P., Schmidl, C., Karall, D., Scholl-Bürgi, S. & Baumann, M. Breath profiles of children on ketogenic therapy. *Journal of Breath Research* **12,** 036021 (2018).

114. Critchley, A., Elliott, T., Harrison, G., Mayhew, C., Thompson, J. & Worthington, T. The proton transfer reaction mass spectrometer and its use in medical science: applications to drug assays and the monitoring of bacteria. *International Journal of Mass Spectrometry* **239,** 235–241 (2004).

115. Shen, C., Li, J., Han, H., Wang, H., Jiang, H. & Chu, Y. Triacetone triperoxide detection using low reduced-field proton transfer reaction mass spectrometer. *International Journal of Mass Spectrometry* **285,** 100–103 (2009).

116. Jürschik, S., Sulzer, P., Petersson, F., Mayhew, C., Jordan, A., Agarwal, B., Haidacher, S., Seehauser, H., Becker, K. & Märk, T. Proton transfer reaction mass spectrometry for the sensitive and rapid real-time detection of solid high explosives in air and water. *Analytical and Bioanalytical Chemistry* **398,** 2813–2820 (2010).

117. González-Méndez, R. *Development and applications of proton transfer reaction-mass spectrometry for homeland security: trace detection of explosives* PhD thesis (University of Birmingham, 2017).

118. Petersson, F., Sulzer, P., Mayhew, C. A., Watts, P., Jordan, A., Märk, L. & Märk, T. D. Real-time trace detection and identification of chemical warfare agent simulants using recent advances in proton transfer reaction time-of-flight mass spectrometry. *Rapid Communications in Mass Spectrometry* **23,** 3875–3880 (2009). DOI: 10.1002/rcm.4334.

119. González-Méndez, R. & Mayhew, C. A. Applications of direct injection soft chemical ionisation-mass spectrometry for the detection of pre-blast smokeless powder organic additives. *Journal of the American Society for Mass Spectrometry* **30,** 615–624 (2019).

120. S., C. S. *Ullmann's Encyclopedia of Industrial Chemistry* **4,** 31–34. DOI: 10.1108/eb049034 (MCB UP Ltd, Jan. 1988).

121. Yuan, H., Li, D., Liu, Y., Xu, X. & Xiong, C. Nitrogen-doped carbon dots from plant cytoplasm as selective and sensitive fluorescent probes for detecting p-nitroaniline in both aqueous and soil systems. *Analyst* **140,** 1428–1431 (2015).

122. Lu, X., Yang, Y., Zeng, Y., Li, L. & Wu, X. Rapid and reliable determination of p-nitroaniline in wastewater by molecularly imprinted fluorescent polymeric ionic liquid microspheres. *Biosensors and Bioelectronics* **99,** 47–55 (2018).

123. Jarvis, G., Kennedy, R., Mayhew, C. & Tuckett, R. Charge transfer from neutral perfluorocarbons to various cations: long-range versus short-range reaction mechanisms. *International Journal of Mass Spectrometry* **202,** 323–343 (2000).

124. U.S. Environmental Protection Agency. *Chemistry Dashboard: Properties of 2-nitroaniline.* URL: `https://comptox.epa.gov/dashboard/dsstoxdb/results?search=DTXSID1025726#properties` (visited on 14/10/2019).

125. U.S. Environmental Protection Agency. *Chemistry Dashboard: Properties of 3-nitroaniline.* URL: `https://comptox.epa.gov/dashboard/dsstoxdb/results?search=DTXSID8020961#properties` (visited on 14/10/2019).

126. U.S. Environmental Protection Agency. *Chemistry Dashboard: Properties of 4-nitroaniline.* URL: `https://comptox.epa.gov/dashboard/dsstoxdb/results?search=DTXSID8020961#properties` (visited on 14/10/2019).

127. González-Méndez, R., Watts, P., Howse, D. C., Procino, I., McIntyre, H. & Mayhew, C. A. Ion mobility studies on the negative ion-molecule chemistry of pentachloroethane. *International Journal of Mass Spectrometry* **417,** 16–21 (2017).

128. Tonkyn, R. G., Winniczek, J. W. & White, M. G. Rotationally resolved photoionization of O_2^+ near threshold. *Chemical Physics Letters* **164,** 137–142 (1989).

129. Harrison, A. G. & Kallury, R. K. M. R. Chemical ionization mass spectra of mononitroarenes. *Organic Mass Spectrometry* **15,** 284–288 (1980).

130. Beynon, J., Lester, G. & Williams, A. Some specific molecular rearrangements in the mass spectra of organic compounds. *The Journal of Physical Chemistry* **63,** 1861–1868 (1959).

131. Petersson, F., Sulzer, P., Mayhew, C. A., Watts, P., Jordan, A., Märk, L. & Märk, T. D. Real-time trace detection and identification of chemical warfare agent simulants using recent advances in proton transfer reaction time-of-flight mass spectrometry. *Rapid Communications in Mass Spectrometry: An International Journal Devoted to the Rapid Dissemination of Up-to-the-Minute Research in Mass Spectrometry* **23,** 3875–3880 (2009).

132. Materić, D., Lanza, M., Sulzer, P., Herbig, J., Bruhn, D., Gauci, V., Mason, N. & Turner, C. Selective reagent ion-time of flight-mass spectrometry study of six common monoterpenes. *International Journal of Mass Spectrometry* **421,** 40–50 (2017).

133. Anderson, J. C. Measuring breath acetone for monitoring fat loss. *Obesity* **23,** 2327–2334 (2015).

134. De Lacy Costello, B., Amann, A., Al-Kateb, H., Flynn, C., Filipiak, W., Khalid, T., Osborne, D. & Ratcliffe, N. M. A review of the volatiles from the healthy human body. *Journal of Breath Research* **8,** 014001 (2014).

135. Tani, A., Hayward, S. & Hewitt, C. Measurement of monoterpenes and related compounds by proton transfer reaction-mass spectrometry (PTR-MS). *International Journal of Mass Spectrometry* **223,** 561–578 (2003).

136. Tani, A., Hayward, S., Hansel, A. & Hewitt, C. N. Effect of water vapour pressure on monoterpene measurements using proton transfer reaction-mass spectrometry (PTR-MS). *International Journal of Mass Spectrometry* **239,** 161–169 (2004).

137. De Gouw, J. & Warneke, C. Measurements of volatile organic compounds in the earth's atmosphere using proton-transfer-reaction mass spectrometry. *Mass Spectrometry Reviews* **26,** 223–257 (2007).

138. Demarcke, M., Amelynck, C., Schoon, N., Dhooghe, F., Van Langenhove, H. & Dewulf, J. Laboratory studies in support of the detection of sesquiterpenes by proton-transfer-reaction-mass-spectrometry. *International Journal of Mass Spectrometry* **279,** 156–162 (2009).

139. Kari, E., Miettinen, P., Yli-Pirilä, P., Virtanen, A. & Faiola, C. L. PTR-ToF-MS product ion distributions and humidity-dependence of biogenic volatile organic compounds. *International Journal of Mass Spectrometry* **430,** 87–97 (2018).

140. Graus, M., Müller, M. & Hansel, A. High Resolution PTR-TOF: Quantification and Formula Confirmation of VOC in Real Time. *Journal of the American Society for Mass Spectrometry* **21,** 1037–1044 (2010). DOI: 10.1016/j.jasms.2010.02.006.

141. Jordan, A., Haidacher, S., Hanel, G., Hartungen, E., Herbig, J., Märk, L., Schottkowsky, R., Seehauser, H., Sulzer, P. & Märk, T. An online ultra-high sensitivity Proton-transfer-reaction mass-spectrometer combined with switchable reagent ion capability (PTR+ SRI-MS). *International Journal of Mass Spectrometry* **286,** 32–38 (2009).

142. Buhr, K., van Ruth, S. & Delahunty, C. Analysis of volatile flavour compounds by Proton Transfer Reaction-Mass Spectrometry: fragmentation patterns and discrimination between isobaric and isomeric compounds. *International Journal of Mass Spectrometry* **221,** 1–7 (2002).

143. Španěl, P., Ji, Y. & Smith, D. SIFT studies of the reactions of H_3O^+, NO^+ and $O_2{}^+$ with a series of aldehydes and ketones. *International Journal of Mass Spectrometry and Ion Processes* **165,** 25–37 (1997).

144. Smith, D., Wang, T. & Španěl, P. Analysis of ketones by selected ion flow tube mass spectrometry. *Rapid Communications in Mass Spectrometry* **17,** 2655–2660 (2003).

145. Smith, D., Španěl, P. & Dryahina, K. H_3O^+, NO^+ and $O_2{}^+$ reactions with saturated and unsaturated monoketones and diones; focus on hydration of product ions. *International Journal of Mass Spectrometry* **435,** 173–180 (2019).

146. Spesyvyi, A., Smith, D. & Španěl, P. Ion chemistry at elevated ion–molecule interaction energies in a selected ion flow-drift tube: reactions of H_3O^+, NO^+ and $O_2{}^+$ with saturated aliphatic ketones. *Physical Chemistry Chemical Physics* **19,** 31714–31723 (2017).

147. Pan, Y., Zhang, Q., Zhou, W., Zou, X., Wang, H., Huang, C., Shen, C. & Chu, Y. Detection of ketones by a novel technology: dipolar proton transfer reaction mass spectrometry (DP-PTR-MS). *Journal of The American Society for Mass Spectrometry* **28,** 873–879 (2017).

148. Schwarz, K., Filipiak, W. & Amann, A. Determining concentration patterns of volatile compounds in exhaled breath by PTR-MS. *Journal of Breath Research* **3,** 027002 (2009).

149. Harrison, G., Critchley, A., Mayhew, C. & Thompson, J. Real-time breath monitoring of propofol and its volatile metabolites during surgery using a novel mass spectrometric technique: a feasibility study. *British Journal of Anaesthesia* **91,** 797–799 (2003).

150. Hornuss, C., Praun, S., Villinger, J., Dornauer, A., Moehnle, P., Dolch, M., Weninger, E., Chouker, A., Feil, C., Briegel, J. *et al.* Real-time monitoring of propofol in expired air in humans undergoing total intravenous anesthesia. *Anesthesiology: The Journal of the American Society of Anesthesiologists* **106,** 665–674 (2007).

151. Takita, A., Masui, K. & Kazama, T. On-line monitoring of end-tidal propofol concentration in anesthetized patients. *Anesthesiology: The Journal of the American Society of Anesthesiologists* **106,** 659–664 (2007).

152. Perl, T., Carstens, E., Hirn, A., Quintel, M., Vautz, W., Nolte, J. & Jünger, M. Determination of serum propofol concentrations by breath analysis using ion mobility spectrometry. *British Journal of Anaesthesia* **103,** 822–827 (2009).

153. Lorenz, D., Maurer, F., Trautner, K., Fink, T., Hüppe, T., Sessler, D. I., Baumbach, J. I., Volk, T. & Kreuer, S. Adhesion of volatile propofol to breathing circuit tubing. *Journal of Breath Research* **11,** 036005 (2017).

154. Rieder, J., Prazeller, P., Boehler, M., Lirk, P., Lindinger, W. & Amann, A. Online monitoring of air quality at the postanesthetic care unit by proton-transfer-reaction mass spectrometry. *Anesthesia & Analgesia* **92,** 389–392 (2001).

155. Rieder, J., Keller, C., Brimacombe, J., Gruber, G., Lirk, P., Summer, G. & Amann, A. Monitoring pollution by proton-transfer-reaction mass spectrometry during paediatric anaesthesia with positive pressure ventilation via the laryngeal mask airway or uncuffed tracheal tube. *Anaesthesia* **57,** 663–666 (2002).

156. Summer, G., Lirk, P., Hoerauf, K., Riccabona, U., Bodrogi, F., Raifer, H., Deibl, M., Rieder, J. & Schobersberger, W. Sevoflurane in exhaled air of operating room personnel. *Anesthesia & Analgesia* **97,** 1070–1073 (2003).

157. Trefz, P., Schmidt, M., Oertel, P., Obermeier, J., Brock, B., Kamysek, S., Dunkl, J., Zimmermann, R., Schubert, J. K. & Miekisch, W. Continuous real time breath gas monitoring in the clinical environment by proton-transfer-reaction-time-of-flight-mass spectrometry. *Analytical Chemistry* **85,** 10321–10329 (2013).

158. Fernández del Río, R., O'Hara, M., Pemberton, P., Whitehouse, T. & Mayhew, C. Elimination characteristics of post-operative isoflurane levels in alveolar exhaled breath via PTR-MS analysis. *Journal of Breath Research* **10,** 046006 (2016).

159. URL: `www.bbraun.com/en/%20products/b1/edmon.html` (visited on 30/07/2019).

160. Sakai, E. M., Connolly, L. A. & Klauck, J. A. Inhalation anesthesiology and volatile liquid anesthetics: focus on isoflurane, desflurane, and sevoflurane. *Pharmacotherapy: The Journal of Human Pharmacology and Drug Therapy* **25,** 1773–1788 (2005).

161. Yasuda, N., Lockhart, S. H., Weiskopf, R., Liu, J., Laster, M., Taheri, S., Peterson, N. *et al.* Comparison of kinetics of sevoflurane and isoflurane in humans. *Anesthesia & Analgesia* **72,** 316–324 (1991).

162. Haynes, S. & Lawler, P. An assessment of the consistency of ASA physical status classification allocation. *Anaesthesia* **50,** 195–199 (1995).

163. Wang, T., Smith, D. & Španěl, P. Selected ion flow tube studies of the reactions of H_3O^+, NO^+ and O_2^+ with the anaesthetic gases halothane, isoflurane and sevoflurane. *Rapid Communications in Mass Spectrometry* **16,** 1860–1870 (2002).

164. Bell, A., Ferrante, F., Hall, S., Mikhailov, V., Mitchell, D., Timperley, C., Watts, P. & Williams, N. Fragmentations and reactions of protonated O, O-dimethyl ethylphosphonate and some isotopomers produced by electrospray ionisation in an ion trap mass spectrometer. *International Journal of Mass Spectrometry* **269,** 46–54 (2008).

165. Mochalski, P., Mirmigkou, S., Unterkofler, K., Sulzer, P., Mayhew, C. A. & Märk, T. D. PTR-MS studies of the reactions of H_3O^+ with a number of deuterated volatile organic compounds and the subsequent sequential reactions of the primary product ions with water under normal and humid drift tube conditions: Implications for use of deuterated compounds for breath analysis. *International Journal of Mass Spectrometry* **436,** 65–70 (2019).

166. Wang, T., Španěl, P. & Smith, D. Selected ion flow tube, SIFT, studies of the reactions of H_3O^+, NO^+ and O_2^+ with eleven C10H16 monoterpenes. *International Journal of Mass Spectrometry* **228,** 117–126 (2003).

167. Španěl, P. & Smith, D. SIFT studies of the reactions of H_3O^+, NO^+ and O_2^+ with several ethers. *International Journal of Mass Spectrometry and Ion Processes* **172,** 239–247 (1998).

168. Mayhew, C. Reactions of Ne+ and Ne+ 2 ions with several molecular species at 300 K: the importance of energy resonance, Franck-Condon factors and electron correlation effects on reaction efficiencies. *Journal of Physics B: Atomic, Molecular and Optical Physics* **25,** 1865 (1992).

169. Jarvis, G. K., Mayhew, C. A. & Tuckett, R. P. Study of the gas phase reactions of several perfluorocarbons with positive ions of atmospheric interest. *The Journal of Physical Chemistry* **100,** 17166–17174 (1996).

170. Adams, N. & Smith, D. The selected ion flow tube (SIFT); a technique for studying ion-neutral reactions. *International Journal of Mass Spectrometry and Ion Physics* **21,** 349–359 (1976).

171. King, J., Unterkofler, K., Teschl, S., Amann, A. & Teschl, G. Breath gas analysis for estimating physiological processes using anesthetic monitoring as a prototypic example. *2011 Annual International Conference of the IEEE Engineering in Medicine and Biology Society* (2011), 1001–1004.

172. Graham, P. Phthalate ester plasticizers–why and how they are used. *Environmental Health Perspectives* **3,** 3–12 (1973).

173. Cao, X.-L. Phthalate esters in foods: sources, occurrence, and analytical methods. *Comprehensive Reviews in Food Science and Food Safety* **9,** 21–43 (2010).

174. Schettler, T. Human exposure to phthalates via consumer products. *International Journal of Andrology* **29,** 134–139 (2006).

175. Heudorf, U., Mersch-Sundermann, V. & Angerer, J. Phthalates: toxicology and exposure. *International Journal of Hygiene and Environmental Health* **210,** 623–634 (2007).

176. Lorz, P. M., Towae, F. K., Enke, W., Jäckh, R., Bhargava, N. & Hillesheim, W. Phthalic acid and derivatives. *Ullmann's Encyclopedia of Industrial Chemistry* (2000).

177. Wormuth, M., Scheringer, M., Vollenweider, M. & Hungerbühler, K. What are the sources of exposure to eight frequently used phthalic acid esters in Europeans? *Risk Analysis* **26,** 803–824 (2006).

178. Fan, J., Wu, L., Wang, X., Huang, X., Jin, Q. & Wang, S. Determination of the migration of 20 phthalate esters in fatty food packaged with different materials by solid-phase extraction and UHPLC–MS/MS. *Analytical Methods* **4,** 4168–4175 (2012).

179. Earls, A., Axford, I. & Braybrook, J. H. Gas chromatography–mass spectrometry determination of the migration of phthalate plasticisers from polyvinyl chloride toys and childcare articles. *Journal of Chromatography A* **983,** 237–246 (2003).

180. Xu, D., Deng, X., Fang, E., Zheng, X., Zhou, Y., Lin, L., Chen, L., Wu, M. & Huang, Z. Determination of 23 phthalic acid esters in food by liquid chromatography tandem mass spectrometry. *Journal of Chromatography A* **1324,** 49–56 (2014).

181. Geiss, O., Tirendi, S., Barrero-Moreno, J. & Kotzias, D. Investigation of volatile organic compounds and phthalates present in the cabin air of used private cars. *Environment International* **35,** 1188–1195 (2009).

182. Gong, M., Tripathi, H. & Poppendieck, D. G. *Letter Report: Emission of Bis (2-ethylhexyl) phthalate (DEHP) from Vinyl Flooring* tech. rep. (NIST, 2018).

183. Pérez-Feás, C., Barciela-Alonso, M. & Bermejo-Barrera, P. Presence of phthalates in contact lens and cleaning solutions. *Microchemical Journal* **99,** 108–113 (2011).

184. Duty, S. M., Ackerman, R. M., Calafat, A. M. & Hauser, R. Personal care product use predicts urinary concentrations of some phthalate monoesters. *Environmental Health Perspectives* **113,** 1530–1535 (2005).

185. Calafat, A. M., Needham, L. L., Silva, M. J. & Lambert, G. Exposure to di-(2-ethylhexyl) phthalate among premature neonates in a neonatal intensive care unit. *Pediatrics* **113,** e429–e434 (2004).

186. Rudel, R. A., Camann, D. E., Spengler, J. D., Korn, L. R. & Brody, J. G. Phthalates, alkylphenols, pesticides, polybrominated diphenyl ethers, and other endocrine-disrupting compounds in indoor air and dust. *Environmental Science & Technology* **37,** 4543–4553 (2003).

187. Foster, P., Cattley, R. & Mylchreest, E. Effects of di-n-butyl phthalate (DBP) on male reproductive development in the rat: implications for human risk assessment. *Food and Chemical Toxicology* **38,** S97–S99 (2000).

188. Benson, R. Hazard to the developing male reproductive system from cumulative exposure to phthalate esters—dibutyl phthalate, diisobutyl phthalate, butylbenzyl phthalate, diethylhexyl phthalate, dipentyl phthalate, and diisononyl phthalate. *Regulatory Toxicology and Pharmacology* **53,** 90–101 (2009).

189. Matsumoto, M., Hirata-Koizumi, M. & Ema, M. Potential adverse effects of phthalic acid esters on human health: a review of recent studies on reproduction. *Regulatory Toxicology and Pharmacology* **50,** 37–49 (2008).

190. Kay, V. R., Chambers, C. & Foster, W. G. Reproductive and developmental effects of phthalate diesters in females. *Critical Reviews in Toxicology* **43,** 200–219 (2013).

191. Rusyn, I. & Corton, J. C. Mechanistic considerations for human relevance of cancer hazard of di (2-ethylhexyl) phthalate. *Mutation Research/Reviews in Mutation Research* **750,** 141–158 (2012).

192. Kim, B., Cho, S., Kim, Y., Shin, M., Yoo, H., Kim, J., Yang, Y. H., Kim, H., Bhang, S. & Hong, Y. Phthalates exposure and attention-deficit/hyperactivity disorder in school-age children. *Biological Psychiatry* **66,** 958–963 (2009).

193. Bornehag, C. & Nanberg, E. Phthalate exposure and asthma in children. *International Journal of Andrology* **33,** 333–345 (2010).

194. Zhu, J., Phillips, S. P., Feng, Y.-L. & Yang, X. Phthalate esters in human milk: concentration variations over a 6-month postpartum time. *Environmental Science & Technology* **40,** 5276–5281 (2006).

195. Frederiksen, H., Skakkebaek, N. E. & Andersson, A.-M. Metabolism of phthalates in humans. *Molecular Nutrition & Food Research* **51,** 899–911 (2007).

196. Wittassek, M. & Angerer, J. Phthalates: metabolism and exposure. *International Journal of Andrology* **31,** 131–138 (2008).

197. European Parliament. Directive 2005/84/EC Of The European Parliament And The Council. *Official Journal of the European Union* **344,** 40–43 (2005).

198. Congress of the United States. Consumer Product Safety Improvement Act (CPSIA) of 2008. *Public Law 110–314* (2008).

199. Standardization Administration of the People's Republic of China. GB 6675-2014 Toy Safety Standard Updates. *Chinese Standard Publishing House, Beijing* (2014).

200. European Parliament. European Regulation No 1272/2008 of the European Parliament and of the Council. *Official Journal of the European Union* **20,** 1–1355 (2008).

201. Agency, E. C. *Candidate List of substances of very high concern for Authorisation.* URL: `https://echa.europa.eu/candidate-list-table` (visited on 12/12/2019).

202. Net, S., Delmont, A., Sempéré, R., Paluselli, A. & Ouddane, B. Reliable quantification of phthalates in environmental matrices (air, water, sludge, sediment and soil): A review. *Science of the Total Environment* **515,** 162–180 (2015).

203. Bergh, C., Torgrip, R. & Östman, C. Simultaneous selective detection of organophosphate and phthalate esters using gas chromatography with positive ion chemical ionization tandem mass spectrometry and its application to indoor air and dust. *Rapid Communications in Mass Spectrometry* **24,** 2859–2867 (2010). DOI: `10.1002/rcm.4690`.

204. Lacko, M., Papp, P. & Matejčík, Š. Dissociation of dicyclohexyl phthalate molecule induced by low-energy electron impact. *The Journal of Chemical Physics* **148,** 214305 (2018).

205. mzCloud - Advanced Mass Spectral Database. HighChem LLC, Slovakia. URL: `www.mzcloud.org` (visited on 28/10/2019).

206. Hauser, R. & Calafat, A. Phthalates and human health. *Occupational and Environmental Medicine* **62,** 806–818 (2005).

207. Yin, P., Chen, H., Liu, X., Wang, Q., Jiang, Y. & Pan, R. Mass spectral fragmentation pathways of phthalate esters by gas chromatography–tandem mass spectrometry. *Analytical Letters* **47,** 1579–1588 (2014).

208. mzCloud - Advanced Mass Spectral Database. HighChem LLC, Slovakia. *DMP.* URL: `www.mzcloud.org/dataviewer.aspx#Creference36` (visited on 11/12/2019).

209. mzCloud - Advanced Mass Spectral Database. HighChem LLC, Slovakia. *DEP.* URL: `www.mzcloud.org/dataviewer.aspx#Creference34#T87#c#452104` (visited on 11/11/2019).

210. mzCloud - Advanced Mass Spectral Database. HighChem LLC, Slovakia. *DAP.* URL: `www.mzcloud.org/dataviewer.aspx#Creference2659#T3697#c#371371` (visited on 11/11/2019).

211. mzCloud - Advanced Mass Spectral Database. HighChem LLC, Slovakia. *DBP.* URL: www.mzcloud.org/dataviewer.aspx#Creference32#T11463#c#2648091 (visited on 11/11/2019).

212. NIST. *Atomic weights and isotopic compositions for oxygen.* URL: https://webbook.nist.gov/cgi/cbook.cgi?ID=C123057&Mask=200#Mass-Spec (visited on 11/12/2019).

213. mzCloud - Advanced Mass Spectral Database. HighChem LLC, Slovakia. *MEHP.* URL: www.mzcloud.org/dataviewer.aspx#Creference2914 (visited on 20/11/2019).

214. mzCloud - Advanced Mass Spectral Database. HighChem LLC, Slovakia. *BBP.* URL: www.mzcloud.org/dataviewer.aspx#Creference29 (visited on 20/11/2019).

215. Rylander, P. N., Meyerson, S. & Grubb, H. M. Organic ions in the gas phase. II. The tropylium ion. *Journal of the American Chemical Society* **79,** 842–846 (1957).

216. Lifshitz, C. Tropylium ion formation from toluene: Solution of an old problem in organic mass spectrometry. *Accounts of Chemical Research* **27,** 138–144 (1994).

217. Cone, C., Dewar, M. J. & Landman, D. Gaseous ions. 1. MINDO/3 study of the rearrangement of benzyl cation to tropylium. *Journal of the American Chemical Society* **99,** 372–376 (1977).

218. mzCloud - Advanced Mass Spectral Database. HighChem LLC, Slovakia. *DEHP.* URL: www.mzcloud.org/dataviewer.aspx#Creference30 (visited on 20/11/2019).

219. McLafferty, F. W. *Registry of Mass Spectral Data: CD Rom with Structures* (John Wiley & Sons, Inc., 1989).

220. McLafferty, F. W. & Tureček, F. *Interpretation of Mass Spectra* (University Science Books, 1993).

221. Franz, J. E., Mao, M. K., Sikorski, J. A. *et al. Glyphosate: a unique global herbicide.* (American Chemical Society, 1997).

222. U.S. Environmental Protection Agency. *Chemistry Dashboard: Properties of glyphosate.* URL: https://comptox.epa.gov/dashboard/dsstoxdb/results?search=DTXSID1024122#properties (visited on 14/10/2019).

Appendices

Appendix A

Investigation of illicit drugs in PTR-MS

This appendix comprises a set of PTR-MS results are in a preliminary state due to time constraints and no proper analysis of the results has been done so far. These results include reduced electric field studies and fast switching investigations.

A.1 Reduced electric field study

The chemical composition, molecular weight and structure of 3,4-methylenedioxymethamphetamine (MDMA), morphine, codeine, heroin, cannabinol (CBN), delta-9-tetrahydrocannabinol (Δ-9-THC) and cannabidiol (CBD) are given in Table A.1. The product ion distributions as a function of the reduced electric field and the drift voltage for these substances are given in figures A.1 to A.7. All the measurements except those of the cannabinoids were acquired under the *normal* operating conditions explained in section 2.1.2.2.

Table A.1: Chemical composition, molecular weight and structure of MDMA, morphine, codeine, heroin, CBN, Δ-9-THC and CBD.

Compound	**Formula**	**MW (g/mol)**	**Structure**
MDMA	$C_{11}H_{15}NO_2$	193	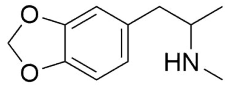
Morphine	$C_{17}H_{19}NO_3$	285	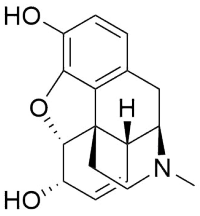
Codeine	$C_{18}H_{21}NO_3$	299	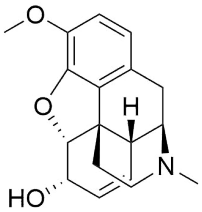
Heroin	$C_{21}H_{23}NO_5$	369	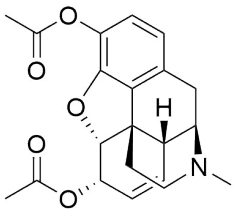
CBN	$C_{21}H_{26}O_2$	310	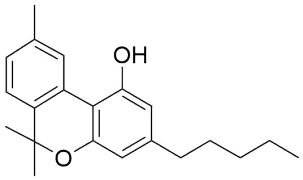
Δ-9-THC	$C_{21}H_{30}O_2$	314	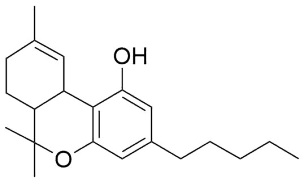
CBD	$C_{21}H_{30}O_2$	314	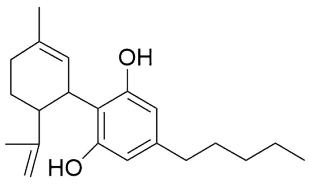

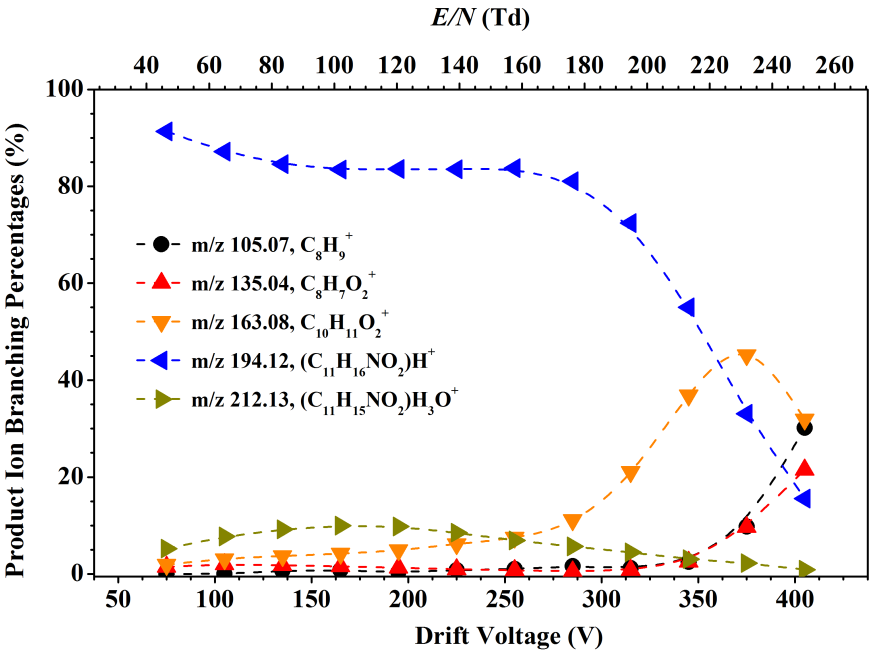

Figure A.1: Product ion distributions for MDMA as a function of the drift voltage and the reduced electric field.

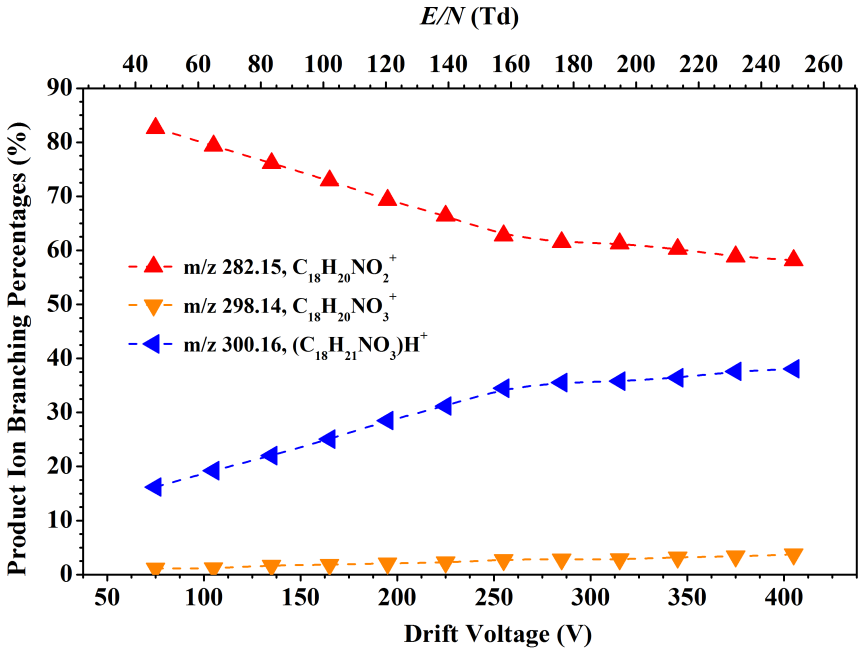

Figure A.2: Product ion distributions for codeine as a function of the drift voltage and the reduced electric field.

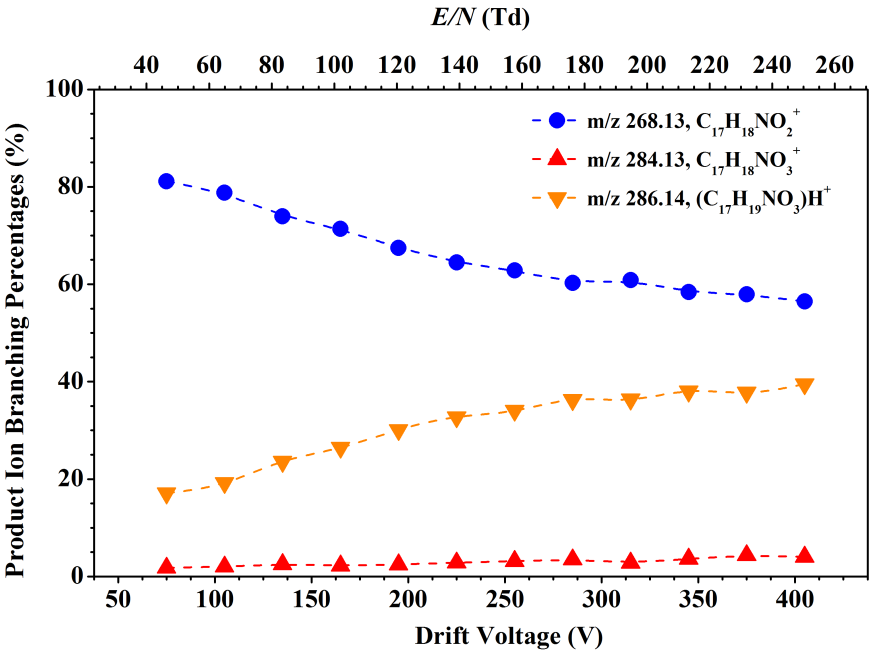

Figure A.3: Product ion distributions for morphine as a function of the drift voltage and the reduced electric field.

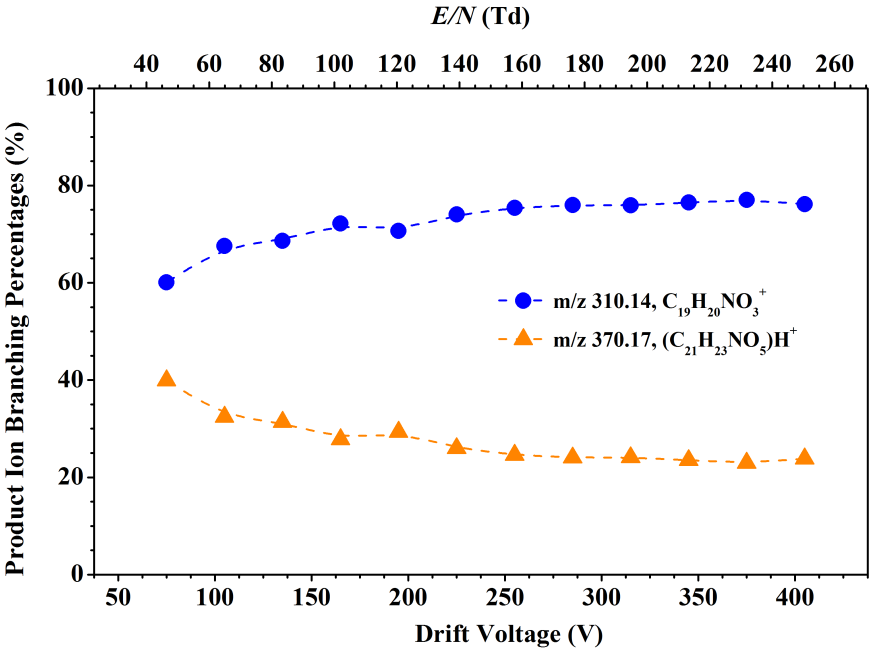

Figure A.4: Product ion distributions for heroin as a function of the drift voltage and the reduced electric field.

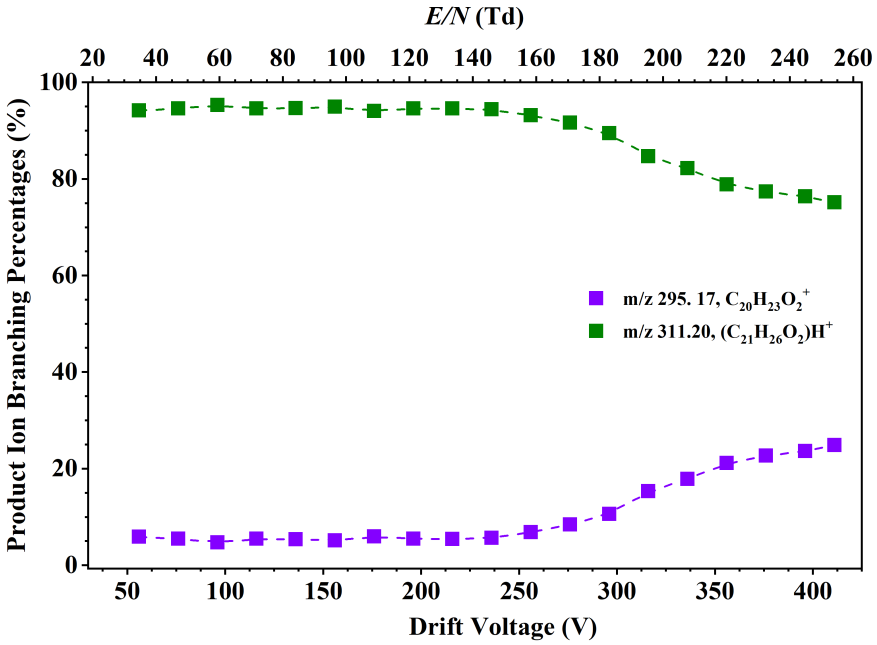

Figure A.5: Product ion distributions for CBN as a function of the drift voltage and the reduced electric field.

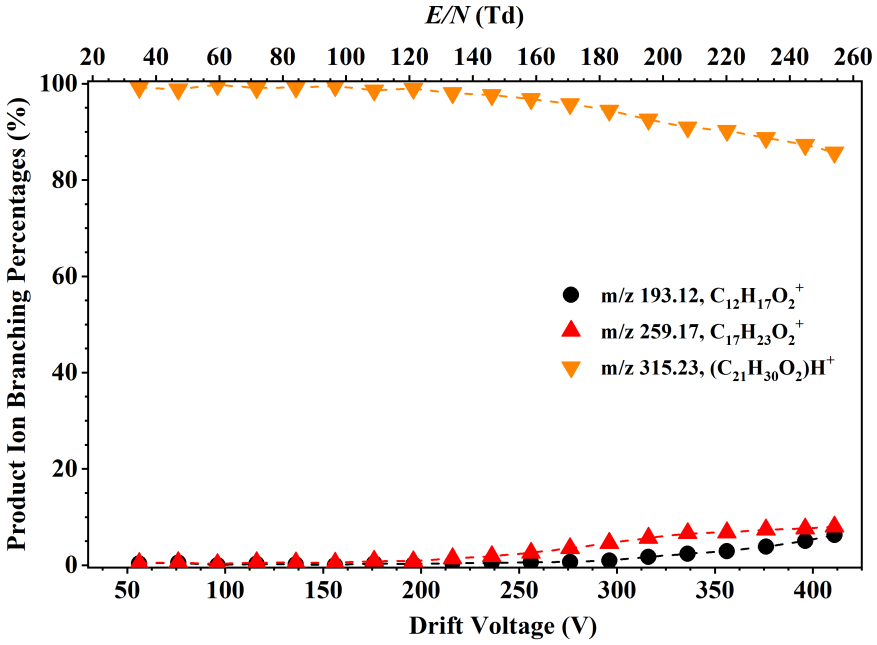

Figure A.6: Product ion distributions for Δ-9-THC as a function of the drift voltage and the reduced electric field.

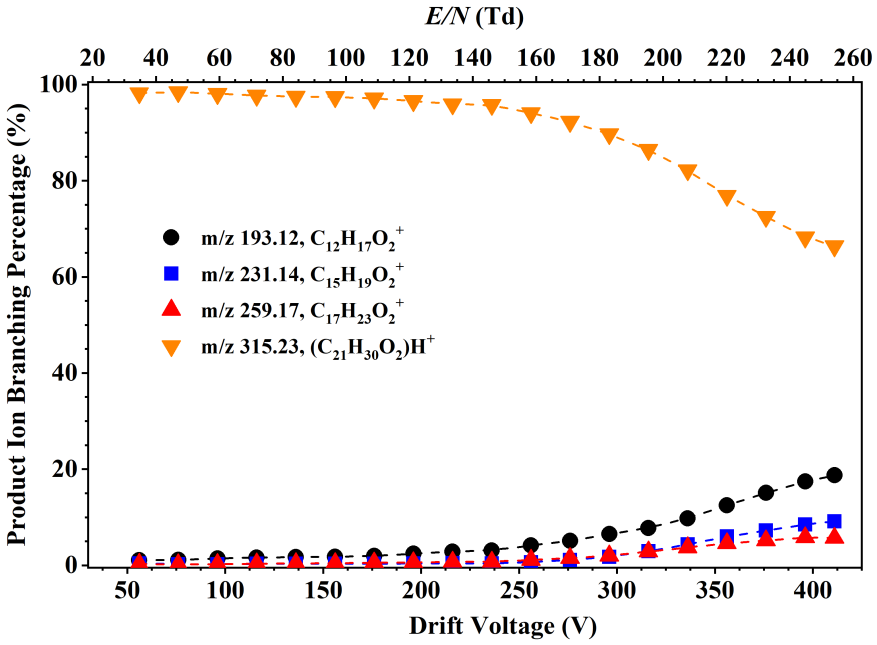

Figure A.7: Product ion distributions for CBD as a function of the drift voltage and the reduced electric field.

A.2 Reduced electric field fast switching results of drugs and related compounds

The E/N fast switching results presented here have been averaged over each cycle. The switching frequency is 1 Hz for all the experiments. This section includes fast switching results of $(H_2O)_nH_3O^+$ (n = 0, 1) (Figure A.8), cocaine (Figure A.9), methyl ecgonine (Figure A.10), ethyl ecgonine (Figure A.11), norcocaine (Figure A.12), o-hydroxycocaine (Figure A.13), CBN (Figure A.14), Δ-9-THC (Figure A.15) and CBD (Figure A.16).

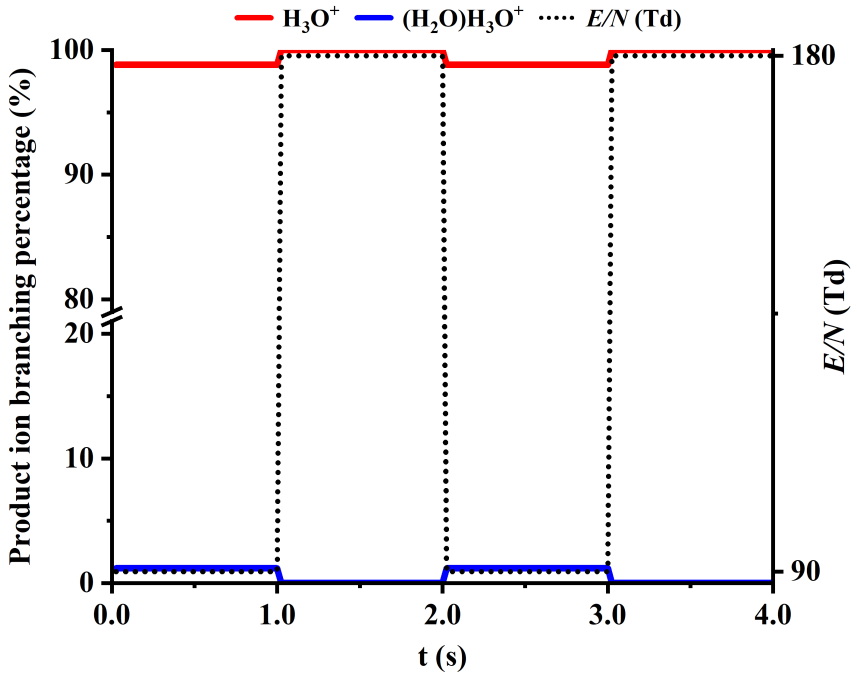

Figure A.8: Reagent ions reduced electric field fast switching plot.

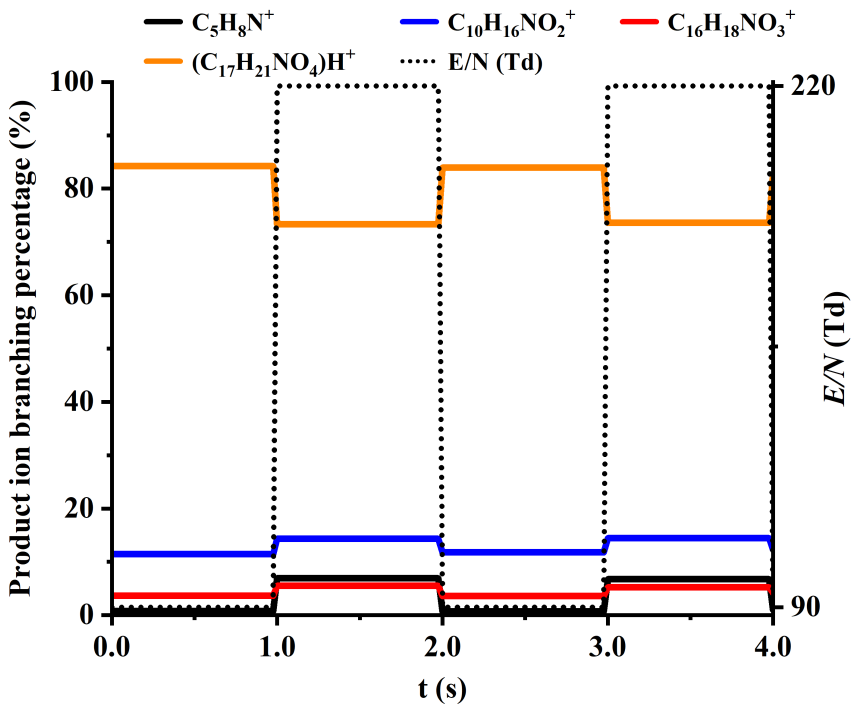

Figure A.9: Cocaine reduced electric field fast switching plot.

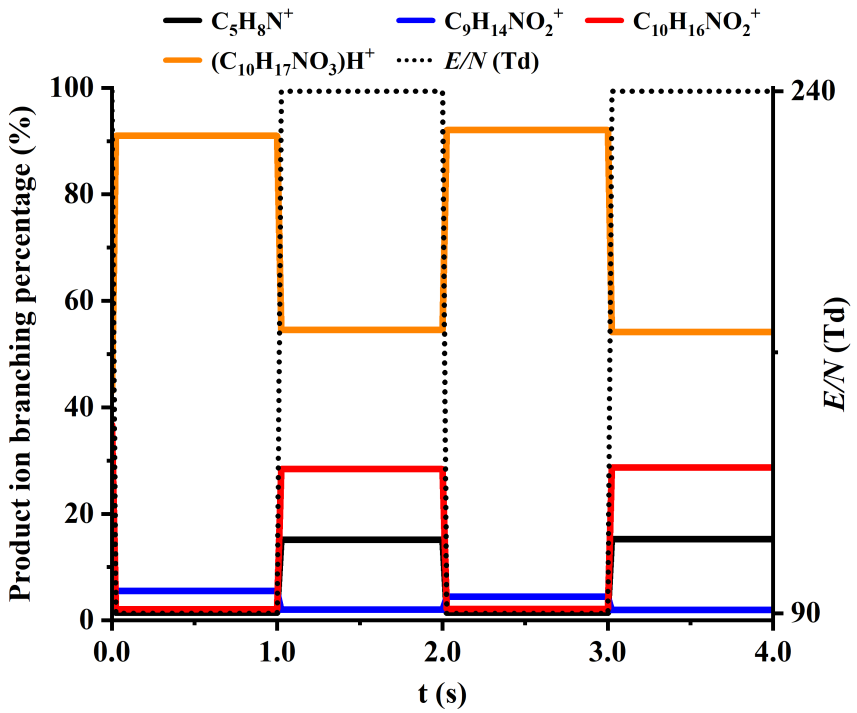

Figure A.10: Methyl ecgonine reduced electric field fast switching plot.

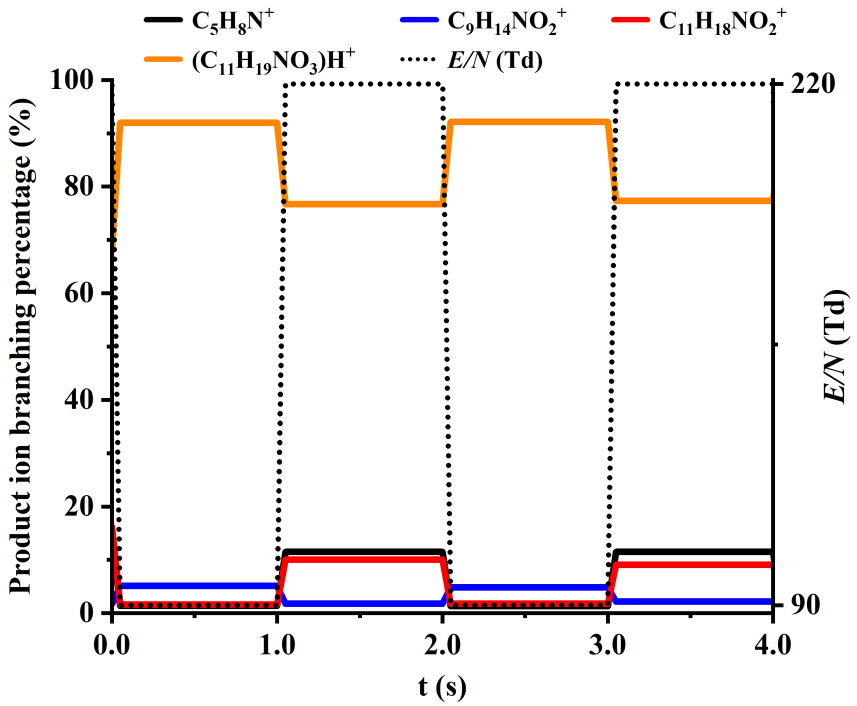

Figure A.11: Ethyl ecgonine reduced electric field fast switching plot.

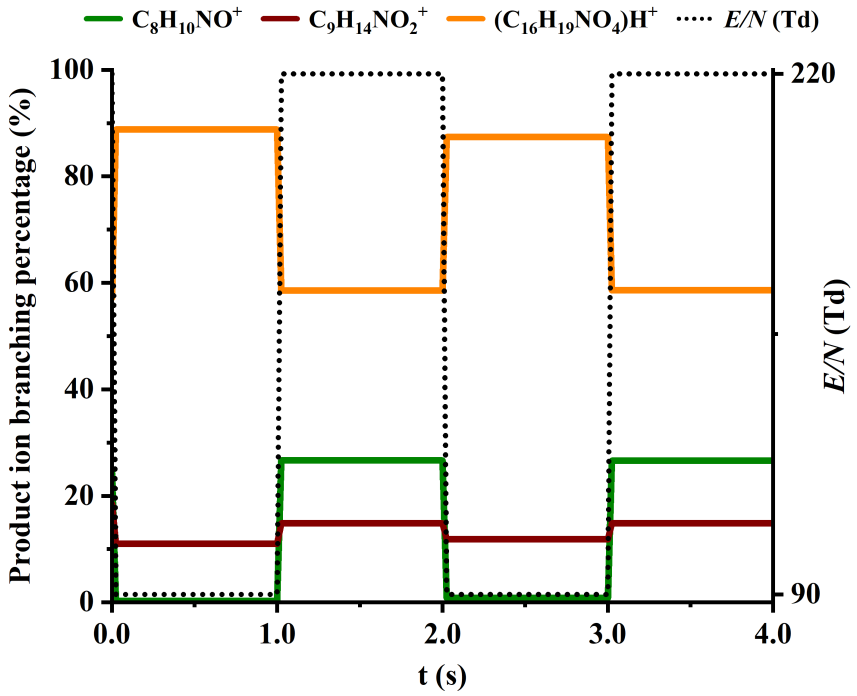

Figure A.12: Norcocaine reduced electric field fast switching plot.

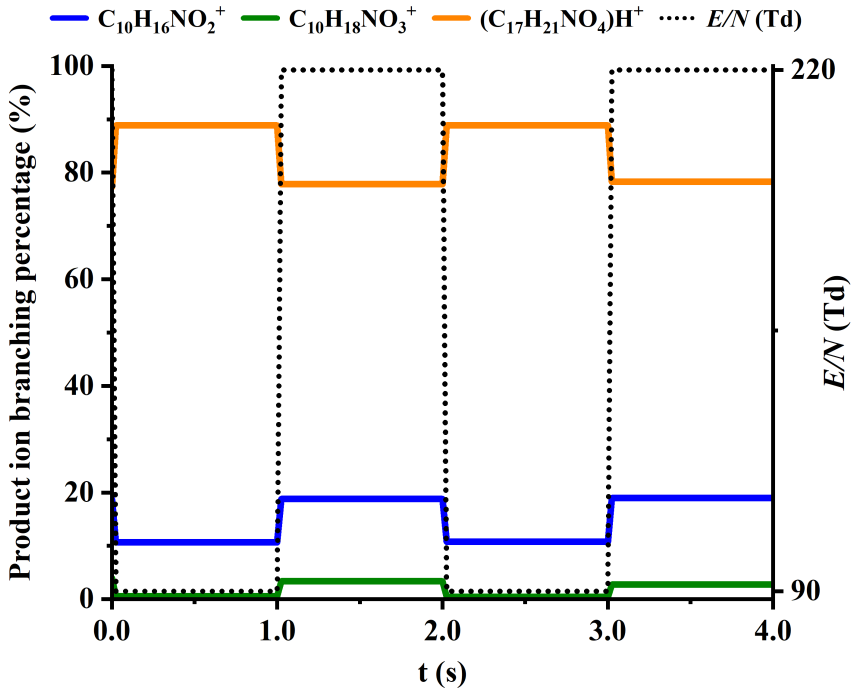

Figure A.13: o-Hydroxycocaine reduced electric field fast switching plot.

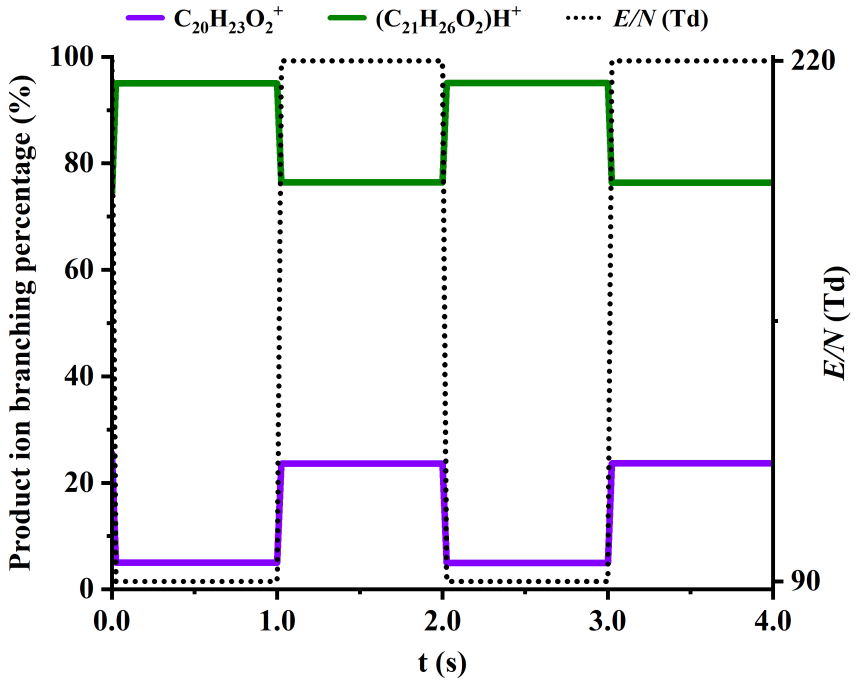

Figure A.14: CBN reduced electric field fast switching plot.

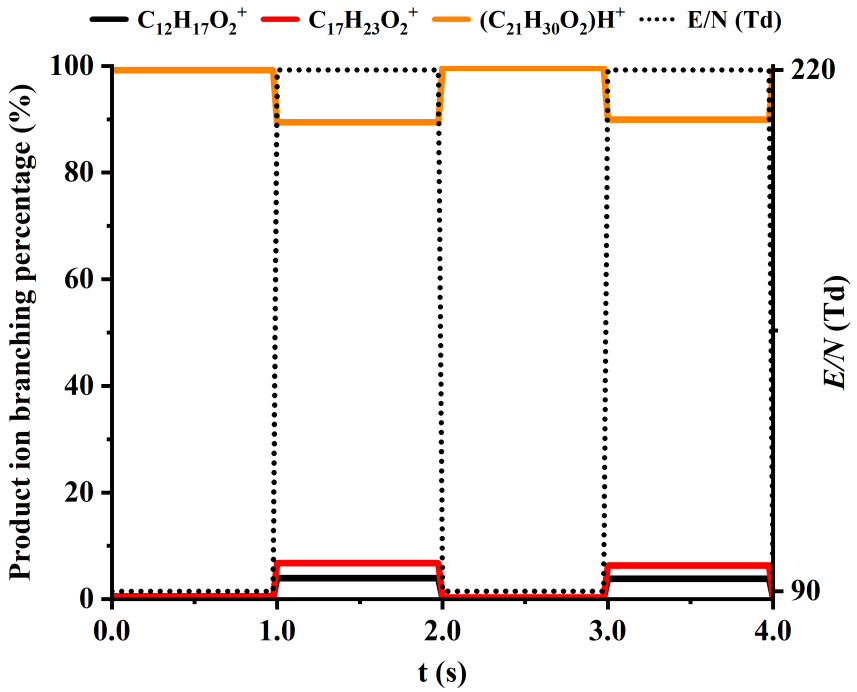

Figure A.15: Δ-9-THC reduced electric field fast switching plot.

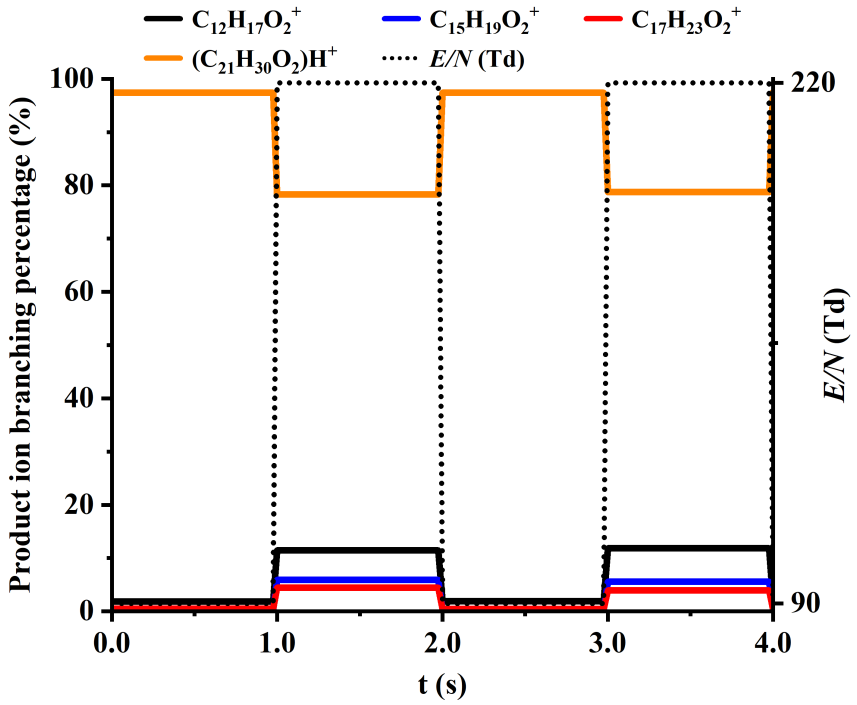

Figure A.16: CBD reduced electric field fast switching plot.

Appendix B

Articles in peer-reviewed journals

Published articles

1. González-Méndez, R., Watts, P., Olivenza-León, D., Reich, D. F., Mullock, S. J., Corlett, C. A., Cairns, S., Hickey, P., Brookes, M. & Mayhew, C. A. Enhancement of Compound Selectivity Using a Radio Frequency Ion-Funnel Proton Transfer Reaction Mass Spectrometer: Improved Specificity for Explosive Compounds. *Analytical Chemistry* **88,** 10624–10630 (2016). DOI: 10.1021/acs.analchem.6b02982.

2. Malásková, M., Olivenza-León, D., Piel, F., Mochalski, P., Sulzer, P., Jürschik, S., Mayhew, C. & Maerk, T. Compendium of the reactions of H_3O^+ with selected ketones of relevance to breath analysis using proton transfer reaction mass spectrometry. *Frontiers in Chemistry* **7,** 401 (2019). DOI: 10.1021/acs.analchem.6b02982*.

3. Olivenza-León, D., Mayhew, C. A. & González-Méndez, R. Selective Reagent Ion Mass Spectrometric Investigations of the Nitroanilines. *Journal of the American Society for Mass Spectrometry,* 1–8 (2019). DOI: 10.1007/s13361-019-02325-0.

4. Malásková, M., Olivenza-León, D., Chellayah, P. D., Martini, J., Lederer, W., Ruzsanyi, V., Unterkofler, K., Mochalski, P., Märk, T. D., Watts, P. & Mayhew, C. A. Studies pertaining to the monitoring of volatile halogenated anaesthetics in breath by proton transfer reaction mass spectrometry. *Journal of Breath Research* **14,** 026004 (2020). DOI: 10.1088/1752-7163/ab5e30†.

*MM, DOL and FP are Early Stage Researchers who have contributed equally to the measurements, data analyses and contribution to the completion of this paper.

†Ms Michaela Malásková and Mr David Olivenza-León are Early Stage Researchers attached to the IMPACT ITN. They contributed equally to the experimental investigations, and hence they should be considered as joint first authors.

analytical chemistry

Article

pubs.acs.org/ac

Enhancement of Compound Selectivity Using a Radio Frequency Ion-Funnel Proton Transfer Reaction Mass Spectrometer: Improved Specificity for Explosive Compounds

Ramón González-Méndez,*[,†] Peter Watts,[†] David Olivenza-León,[†] D. Fraser Reich,[‡] Stephen J. Mullock,[‡] Clive A. Corlett,[‡] Stuart Cairns,[§] Peter Hickey,[§] Matthew Brookes,[⊥] and Chris A. Mayhew[†,∥]

[†]Molecular Physics Group, School of Physics and Astronomy, University of Birmingham, Edgbaston, Birmingham B15 2TT, U.K.

[‡]Kore Technology Ltd, Cambridgeshire Business Park, Ely, Cambridgeshire CB7 4EA, U.K.

[§]Defence Science and Technology Laboratory, Fort Halstead, Sevenoaks, Kent TN14 7BP, U.K.

[⊥]Defence Science and Technology Laboratory, Porton Down, Salisbury, Wilshire SP4 0JQ, U.K.

[∥]Institut für Atemgasanalytik, Leopold-Franzens-Universitaet Innsbruck, Innsbruck 6020, Austria

ABSTRACT: A key issue with any analytical system based on mass spectrometry with no initial separation of compounds is to have a high level of confidence in chemical assignment. This is particularly true for areas of security, such as airports, and recent terrorist attacks have highlighted the need for reliable analytical instrumentation. Proton transfer reaction mass spectrometry is a useful technology for these purposes because the chances of false positives are small owing to the use of a mass spectrometric analysis. However, the detection of an ion at a given m/z for an explosive does not guarantee that that explosive is present. There is still some ambiguity associated with any chemical assignment owing to the presence of isobaric compounds and, depending on mass resolution, ions with the same nominal m/z. In this article we describe how for the first time the use of a radio frequency ion-funnel (RFIF) in the reaction region (drift tube) of a proton transfer reaction−time-of-flight−mass spectrometer (PTR-ToF-MS) can be used to enhance specificity by manipulating the ion−molecule chemistry through collisional induced processes. Results for trinitrotoluene, dinitrotoluenes, and nitrotoluenes are presented to demonstrate the advantages of this new RFIF-PTR-ToF-MS for analytical chemical purposes.

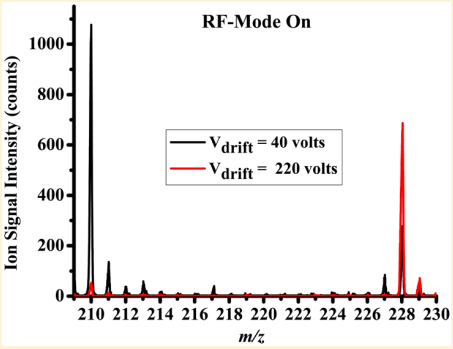

Ion funnels (IF) have been used since the late 1990s in conjunction with several ionization and mass spectrometric techniques with a key purpose of increasing ion transmission efficiency and hence instrumental sensitivity and dynamic range.[1,2] Of relevance to our study, Schaffer et al. developed a radio frequency (RF) IF for focusing and transmitting ions from relatively high pressure (>1 Torr) ion sources to mass spectrometers.[1] Given that the typical operating pressure of a drift tube used in proton transfer reaction mass spectrometry (PTR-MS) is close to the optimum pressure for the operation of a RFIF, Kore Technology Ltd. designed and developed a RFIF to be incorporated into drift tubes in order to increase the instruments sensitivity.[3] This compact drift tube can simultaneously operate as an ion funnel and a reaction region with a controllable reaction time (dependent on the voltage supplied across the tube). The funnel design and the supplied RF and DC fields act in such a way to channel reagent and product ions toward the exit orifice of the drift tube so that more ions leave the reaction region into the much lower pressure mass spectrometric region, thereby decreasing the loss of ions that occurs at the end of the drift tube. The proof-of principle study reported increases in sensitivity of this RFIF-PTR-ToF-MS system that were found to be dependent on the m/z of the product ions, but were typically between 1 and 2 orders of magnitude. For example enhancement factors of 45 and 200 were reported for protonated acetaldehyde and protonated acetone, respectively, at a reduced electric field of 120 Td (where this field refers to the DC voltage applied across the drift tube).[3]

Given that the RFIF forms part of the drift tube, we asked the question whether the high RF fields involved in the operation of an IF could be used to enhance collisions of the reagent and product ions with the buffer gas in the DT and hence change either the nature of the initial chemical ionization process or induce collisional induced dissociation, respectively, occurring within the DT? We hypothesized that changes would result from raising the internal energy of the product ions and the energy of the reactions between reagent ions and neutral species through collisional processes as a result of the applied RF field. The real question is whether the RF collisional induced dissociation would lead to substantial fragmentation, or be more selective resulting in unique product ions that can be

Received: August 2, 2016
Accepted: October 7, 2016
Published: October 7, 2016

DOI: 10.1021/acs.analchem.6b02982
Anal. Chem. 2016, 88, 10624−10630

used to identify a chemical compound of interest with a higher specificity than that achievable just by using a standard drift tube at a given reduced electric field. Here we report details on a collaborative project involving KORE Technology Ltd. and the University of Birmingham which investigated the application of a RFIF drift tube of a PTR-ToF-MS for improved selectivity using several explosives as illustrative compounds, namely 2,4,6-trinitrotoluene (TNT), 2,4-, 2,6-, and 3,4-dinitrotoluene (DNT) and 2-, 3-, and 4-nitrotoluene (NT). We will show how the application of a RFIF leads to a higher confidence in compound identification. We thus demonstrate for the first time that the addition of a RFIF to a PTR-ToF-MS results in a more multidimensional analytical instrument that improves the selectivity that can be achieved by operating a drift tube of a PTR-MS in DC mode only.

METHODS

Experimental Details. A KORE Technology Ltd. RFIF Series I PTR-ToF-MS was used. Details of KORE's PTR-ToF-MS system with no IF has been described in detail elsewhere,[4−6] and hence only the salient points of this instrument are provided here. Using a needle valve, water vapor is introduced into a hollow cathode discharge where, after ionization via electron impact and subsequent ion−molecule processes, the terminal reagent ion is H_3O^+.[7] These ions are transferred from the ion source into the drift tube (the reaction region) of the PTR-ToF-MS, which is typically at a pressure of 1 mbar and temperature 100 °C, where they encounter the analyte. H_3O^+ ions react with the analyte M by donating their protons at the collisional rate, providing M has a proton affinity greater than that of water ($PA(H_2O)$ = 691 kJ mol^{-1}). This process can be non-dissociative (resulting in the protonated molecule MH^+) and/or dissociative. Dissociative proton transfer results in product ions which may be useful in the identification of a compound. Fragmentation may be spontaneous upon proton transfer or may require additional energy which is supplied through collisions with the buffer gas resulting during the migration of ions under the influence of the electric field, *E*. The ratio of *E* to the buffer gas number density, *N*, is an important parameter (known as reduced electric field) which determines the mean collisional energy of ions with the neutral buffer gas. Hence it is the parameter often referred to and changed for investigating product ion branching ratios.[8−15]

The IF (schematically shown in Figure 1) consists of 29 stainless steel plates of 0.2 mm thickness, mounted on precision-machined ceramic rods at an even spacing of 3.2 mm per plate. Tabs on the electrodes permit a resistor chain on a ceramic strip to be connected in addition to two capacitor stacks which allow the RF to be applied to the second half of the reactor. The orifice diameters of the plates through the first half of the stack is 40 mm, as used in the standard drift tube reactor. In the second half of the drift tube the orifice diameter steadily decreases to 6 mm at the final plate before the exit orifice. Across the complete ion-funnel a DC voltage is applied driving ions axially. When just operating with this voltage we shall refer to the instrument as operating in DC-only mode. In addition to this, to the second part of the drift tube a RF field can applied. The resonant frequency of the system is ∼760 kHz and the amplitude selected for the majority of the studies (peak-to-peak) was 200 V, which is superimposed on the dc voltage gradient across the drift tube.

The main purpose of the RF field is to focus ions radially by creating repulsive effective potentials at the edges of the

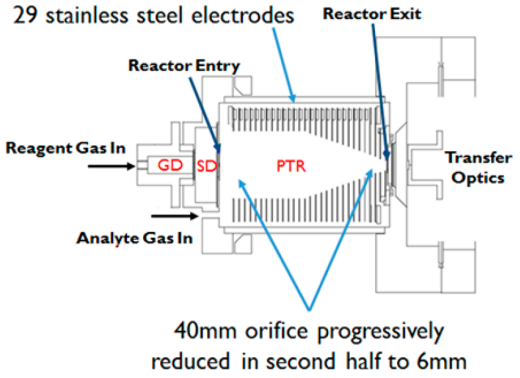

Figure 1. Schematic representation of the KORE Technology Ltd. radio frequency ion funnel drift tube (proton transfer reaction (PTR) region) used in this investigation. Also shown is the ion source region (glow discharge GD), and a source drift (SD) region which is used to extract ions from the GD, aid in breaking-up protonated water clusters and to enhance production of H_3O^+ via additional ion−molecule reactions involving ions that can react with water. After exiting the drift tube the transfer optics guide the ions into the ToF-MS region.

electrodes. However, in addition to this intended purpose, the RF results in ions oscillating between electrodes as they drift down the reactor. This gives ions higher collisional energies than those in the first half of the drift tube. We shall refer to operating the instrument with the RF on as RF-mode. At the end of the drift tube is a 400 μm orifice, through which ions enter the ion transfer region for ToF-MS.

The use of specifying a reduced electric field, *E*/*N*, is an appropriate parameter to use in DC-only mode, because it is well-defined. In RF-mode (ion funnel on) the presence of DC and RF electric fields complicates the situation, because the electric field strength varies with distance from the RF electrodes, so that specifying a reduced electric field is not appropriate. Barber et al.[3] simply adopted an empirical effective reduced electric field by finding operating conditions for the ion-funnel drift tube that matched the performance of the same drift tube when operated under DC-only mode. However, given that it is uncertain what the effective reduced electric field means, in this article we refer to the DC voltage (V_{drift}) applied across the drift tube.

A thermal desorption unit (TDU) connected to the inlet of the drift tube was used to introduce the explosive samples, details of which have been given elsewhere.[6] The TDU, connecting lines, and drift tube were operated at a temperature of 150 °C. PTFE swabs (ThermoFisher Scientific) onto which known quantities of explosives were deposited were placed into the TDU. The swabs came prepared from the manufacturer mounted on rectangular cardboard for easy insertion into the TDU. Once a seal was created, a carrier gas (in this study laboratory air) is heated to the temperature of the TDU before it flows through a series of holes in a heated metal plate. This heated air then passes through the swab and into the inlet system driving any desorbed material through to the drift tube creating a temporal concentration "pulse" of typically between 10−20 s of an explosive in the drift tube.[6] Each swab provided one measurement, which was replicated three times and then the results were averaged and any background signals were subtracted.

Explosive standards were purchased from AccuStandard Inc., New Haven, CT. Typically these standards contained 0.1 mg of the explosive compound in 1 mL of solvent. For TNT, 2,4- and

DOI: 10.1021/acs.analchem.6b02982
Anal. Chem. 2016, 88, 10624−10630

2,6-DNT, and the NTs this involved an acetonitrile:methanol (1:1) mix. 3,4-DNT was just mixed with methanol. These samples were diluted in the appropriate solvent(s) (HPLC grade) to provide the required quantity of an explosive. Typically 1 μL of a solvent containing the required mass of an explosive was spotted onto a PTFE swab.

Electronic Structure Calculations. To aid in the interpretation of the experimental results a series of electronic structure calculations have been undertaken at 298 K. These involve density functional theory calculations using the GAUSSIAN09 PROGRAM with the GaussView 5 interface.[16] The B3LYP functional with the 6-31+G(d,p) basis set was used throughout. Although it is appreciated that the drift tube temperature and the effective ion temperature are greater than 298 K, with the effective ion temperature being uncertain, the thermochemical calculations simply provide us with an indicator as to whether a reaction pathway is energetically possible or not.

RESULTS AND DISCUSSION

Reagent Ions. Before we begin discussing the results of the explosives, it is informative to present details on the reagent ion signal as a function of drift tube voltage, comparing intensities for DC-only mode (Figure 2a) and RF-mode (funnel-on) (Figure 2b) under identical operating conditions of hollow cathode and drift tube pressures and temperature. The observed decrease of H_3O^+ reagent ion signal with decreasing drift tube voltage is predominantly a result of the clustering with water molecules in the drift tube, which are not broken-up through collisions at lower drift tube voltages. The marked decrease in total reagent ion signal below about 50 Td is considered to be a result of the low SD potential, which scales with the DC drift tube potential. As the SD voltage decreases we can expect that fewer reagent ions reach the reactor entry.

Figure 2a shows that by 100 Td the H_3O^+ reagent ion signal has reduced significantly and that the protonated water clusters start to dominate at the lowest reduced electric field corresponding to a voltage drop across the drift tube of about 200 V under the operational temperature and pressure values used. (The actual percentage of protonated water clusters for fixed E/N is also strongly dependent on the humidity of the buffer gas in the drift tube, which is dependent on the amount of forward flow of H_2O from the ion source into the drift tube and the humidity of the laboratory air.) In RF-mode no protonated water clusters are observed, because they are broken-up through collisions in the RFIF region of the drift tube. Furthermore, at about 120 V the H_3O^+ intensity is approximately at its maximum value. As the drift voltage decreases, the reagent ion signal decreases. However, even at a drift tube voltage of only 20 V (which in DC-only mode would correspond to a reduced electric field of only about 10 Td) there is still a significant reagent ion count. This enhancement of reagent ion signal at low drift tube voltages can only be a result of the trapping that the RF field provides thereby reducing the diffusional loss that occurs in DC-only mode under low drift tube voltages.

2,4,6-Trinitrotoluene (TNT). Using both PTR-ToF-MS and PTR-Quad-MS systems Sulzer et al. have previously shown that there is an unusual dependence of the intensity of protonated TNT on the reduced electric field in that there is an increase in the sensitivity of detection with increasing E/N.[9,17] This increase continues until a maximum is reached at about 180 Td, after which the signal intensity shows the more usual

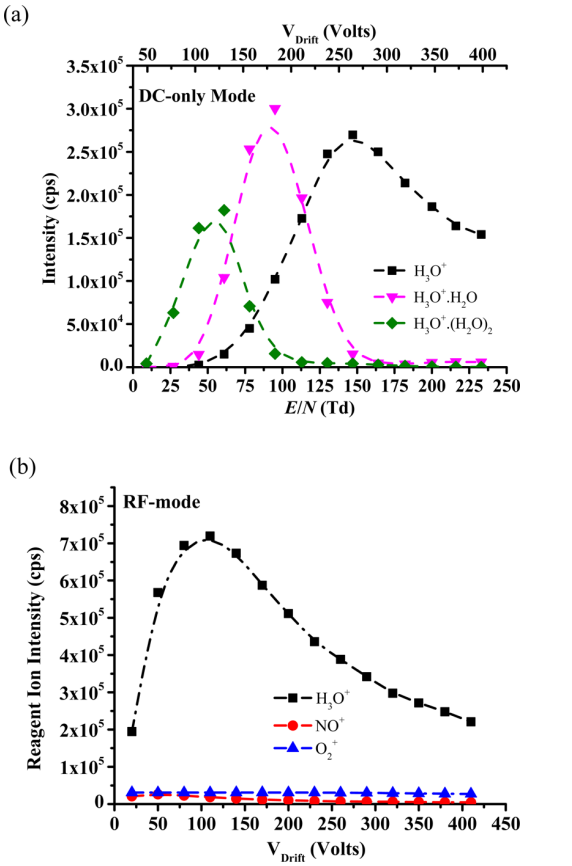

Figure 2. Ion intensities in counts per second (cps) of the water reagent ions present in the drift tube as a function of drift tube voltage (a) in DC-only mode and (b) in RF-mode (ion funnel on). For (b) the ion signals at m/z 30 (NO^+) and 32 (O_2^+) are presented because although low intensity they are still significant and are observed as a result of the improved ion transmission in RF-mode. In DC-mode the signal intensities of these ions are negligible and are therefore not presented.

behavior of decreasing with increasing E/N. This is opposite to what is commonly found in PTR-MS studies, because with reduced reaction times, fragmentation to non-specific product ions, and reduction in ion transmission the protonated molecule intensity reduces with increasing E/N. The explanation of this unusual intensity dependence for $TNTH^+$ has been described in detail.[9] In brief, it is a result of a secondary reaction of $TNTH^+{\cdot}H_2O$ (which is readily formed at low E/N) with H_2O leading to a terminal ion which does not contain TNT, namely $H_3O^+{\cdot}H_2O$.

In DC-only mode and when a product ion signal is detected, for all E/N values investigated only one product ion is observed that contains the explosive, namely protonated TNT at m/z 228. However, in RF mode, another fragment ion is found at m/z 210, the intensity of which increases with decreasing drift tube voltage (i.e., decreasing E/N in DC mode) down to values under which the PTR-ToF-MS does not perform in DC mode owing to a lack of sufficient transmission of ions to the mass spectrometer (Figure 2a). Typical results obtained for TNT are shown in Figure 3. That the fragment ion m/z 210 intensity increases with decreasing drift tube voltage (Figure 3) is perhaps not what is expected given that decreasing DC voltage means lower collisional energies. However, that only applies in

DOI: 10.1021/acs.analchem.6b02982
Anal. Chem. 2016, 88, 10624−10630

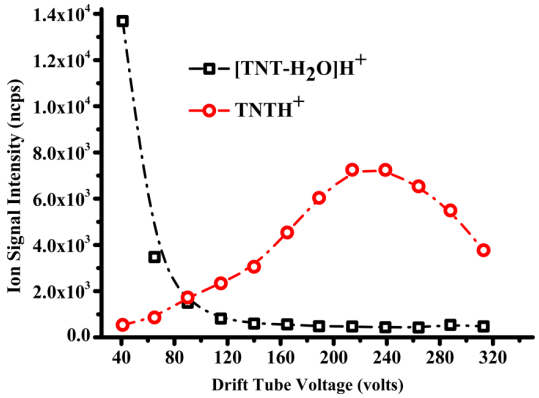

Figure 3. Product ion intensities as a function of drift tube voltage in RF mode. The data have been taken using 100 ng of TNT. The ion signals have been normalized to 10^6 H_3O^+ reagent ions and drift times. (The lines used in all graphs are just a guide to the eye.)

the first half of the drift tube. As the drift tube voltage is reduced more collisions in the RFIF region of the drift tube occur, which in turn enhances collisional induced dissociation.

Following proton transfer the protonated molecule gains sufficient internal energy through collisions in the RFIF section of the drift tube to eliminate H_2O:

$$H_3O^+ + TNT \rightarrow (TNTH^+)^* + H_2O \quad (1)$$

$$(TNTH^+)^* + M \rightarrow [TNT - H_2O]H^+ + H_2O + M \quad (2)$$

where M is a buffer gas molecule. Thus, specificity can be increased by either switching off and on the RFIF at a specific drift tube voltage or by switching the drift tube voltage. Note that a minor percentage of the observed m/z 210 results from the reaction of the O_2^+ (always present in low concentrations in the drift tube as an impurity ion) with TNT via a dissociative charge transfer process leading to the loss of OH from TNT^+.[12]

That the reaction pathway leading to the elimination of H_2O is overall energetically favorable (Table 1) but is only observed

Table 1. Energetics for the Proton Transfer from H_3O^+ to TNT Calculated Using the B3LYP Functional and the 6-31+G(d,p) Basis Set

products	ΔH_{298} kJ mol^{-1}	ΔG_{298} kJ mol^{-1}
$TNTH^+(2NO_2syn) + H_2O$	−46	−47
$TNTH^+(2NO_2anti) + H_2O$	−55	−55
$TNTH^+(4NO_2) + H_2O$	−68	−60
TS syn/anti + H_2O	−9	−5

in RF mode, is an indication that there must be an energy barrier for pathway (2). Evidence of this is provided from the results obtained when investigating the effects of changing the RF amplitude at fixed drift tube voltages and fixed frequency. Figure 4 provides a summary of these measurements, which shows that as the RF peak-to-peak voltage is decreased the intensity of the m/z 210 decreases for all drift tube voltages.

The initial step leading to m/z 228 is the transfer of a proton from H_3O^+ to TNT. Protonation of TNT can occur on the nitro groups at the 2 and 4 positions, both having similar proton affinities, although as elimination of water from $TNTH^+$ will presumably involve the methyl group only protonation of the nitro group in the 2 position is of relevance. However, protonation on the 4 nitro will occur (the PA and GB are

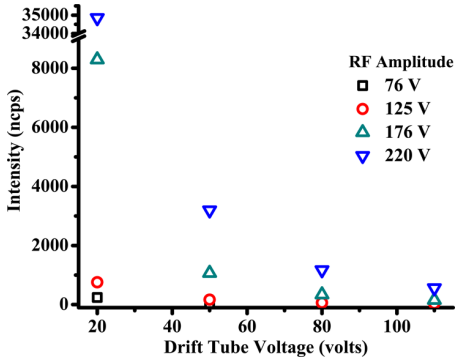

Figure 4. Intensities in ncps of the product ion $[TNT-H_2O]H^+$ as a function of drift tube voltage and RF amplitude (volts) with the frequency kept at 760 kHz (±3%).

slightly greater than the 2 nitro) and this will reduce the amount of $TNTH^+$ available to lose water. Two configurations are possible for protonation in the 2 position as illustrated in Figure 5, with the anti being slightly more stable by ca. 8 kJ

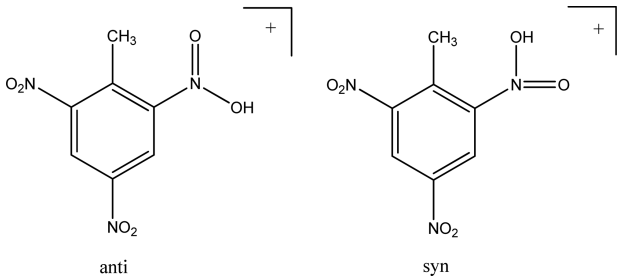

Figure 5. Two possible configurations resulting from protonation of TNT in the 2 position.

mol^{-1}. The transition state energetics for interconversion are $\Delta H^{\ddagger}_{298}$ + 46 kJ mol^{-1} and $\Delta G^{\ddagger}_{298}$ + 51 kJ mol^{-1} above the anti conformation, but whichever is formed there is sufficient energy in the initial protonation to allow rapid interconversion (Table 1).

There are three stable structures for the ion remaining after the elimination of water from $TNTH^+$ (Figure 6). A fourth structure, similar to $TNTH^+$–H_2O (b) with the hydrogens of the methylene group orthogonal to the ring, proved to be unstable and rearranged to $TNTH^+$–H_2O (a) . The energetics for the transformation of $TNTH^+$ to $TNTH^+$–H_2O (a–c) + H_2O are given in Table 2.

Various attempts using the QST3 approach were made to find transition states for these possible reactions but all lead to $TNTH^+$–H_2O (c), though interestingly the transition state had a close resemblance to $TNTH^+$–H_2O (b). The transition state was characterized by one imaginary frequency and the internal reaction coordinate leading to $TNTH^+$–H_2O (c) in the forward direction and $TNTH^+$ with the proton on the 2-nitro group in the syn conformation in the reverse direction. The activation energies relative to TNT + H_3O^+ are $\Delta H^{\ddagger}_{298}$ + 158 kJ mol^{-1} and $\Delta G^{\ddagger}_{298}$ + 162 kJ mol^{-1}.

The presumption that the elimination of water from protonated TNT can only occur when the methyl and nitro groups are adjacent to each other was readily tested by investigating isomers of DNT and NT. For those isomers that satisfy the condition of an adjacent nitro and methyl group,

DOI: 10.1021/acs.analchem.6b02982
Anal. Chem. 2016, 88, 10624–10630

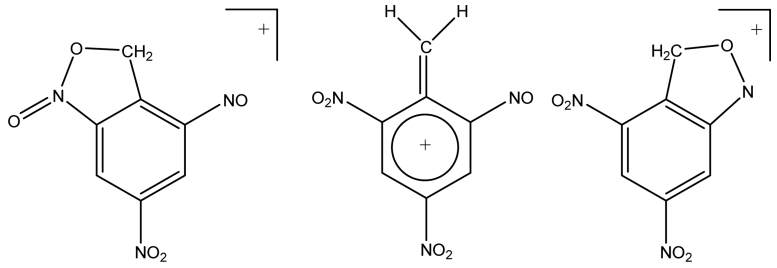

Figure 6. Stable structures of the $[TNT-H_2O]H^+$ ion.

Table 2. Energetics for the Elimination of Water from TNT Following Proton Transfer from H_3O^+ for the Three Stable Structures Shown in Figure 6

products	ΔH_{298} kJ mol^{-1}	ΔG_{298} kJ mol^{-1}
$TNTH^+$ - H_2O (a) + $2H_2O$	−104	−145
$TNTH^+$ - H_2O (b) + $2H_2O$	+47	−7
$TNTH^+$ - H_2O (c) + $2H_2O$	−128	−168

then $[DNT-H_2O]H^+$ and $[NT-H_2O]H^+$ fragement ions should be observed, otherwise not. Thus, we predicted to observe elimination of water from the 2,6-DNT, 2,4-DNT, and 2-NT but not from 3,4-DNT, 3-NT, or 4-NT following proton transfer in RF mode.

Dinitrotoluenes. In both RF-mode and DC-only mode for 3,4-DNT the only primary product ion that is observed with any significant intensity for all drift tube voltages is the protonated molecule. That no m/z 165 is observed, which would correspond to the elimination of water from the protonated molecule, is in agreement with our prediction, because neither nitro group are adjacent to the methyl group. With decreasing drift tube voltage the protonated 3,4-DNT clusters with H_2O, leading to a reduction in the $DNTH^+$ signal. While this is particularly significant in DC-only mode, with $DNTH^+\cdot(H_2O)_n$ (n = 1, 2 and 3) ions becoming the dominant product ions by about 100 Td, some water clustering is still observed in RF-mode. For example at a drift tube voltage of 20 V the percentage branching ratios are approximately 70, 20, and 10% for $DNTH^+$, $DNTH^+\cdot H_2O$, and $DNTH^+\cdot(H_2O)_2$, respectively.

For the 2,4- and 2,6-DNT isomers, at low drift tube voltages in addition to an observed ion at m/z 201 corresponding to the $DNTH^+\cdot H_2O$ in RF-mode a product ion is observed at m/z 165, which is $[DNT\text{-}H_2O]H^+$. Figure 7 illustrates this for 2,6-DNT, which shows that the probability for the elimination of water increases with decreasing drift tube voltage (the results for 2,4-DNT in RF-mode are similar, although the production for $[DNT\text{-}H_2O]H^+$ is less by about 10%). In DC-only mode, m/z 165 is also observed for 2,6-DNT, but its intensity only becomes significant when a high drift tube voltage is applied leading to reduced electric fields above about 180 Td, and even then the percentage ion product distribution is only approximately 10% (Figure 8). However, this can explain the slight increase in the production of m/z 165 in Figure 7 when the applied drift tube voltage is above about 275 V. With increasing drift tube voltage additional fragment ions are found at m/z 136 and 91, corresponding to an elimination of HONO and $2NO_2$, respectively, from the protonated molecule. These two ions are also found with significant intensities for 2,6-DNT when operating in DC-only mode when the reduced electric fields is greater than about 160 Td. That $DNTH^+\cdot H_2O$ is observed in RF-mode at low drift tube voltages, when no protonated water clusters are observed (Figure 2b), requires some explanation. We propose that following a collision the energy involved is distributed in more degrees of freedom for $DNTH^+\cdot H_2O$ than for $H_3O^+\cdot(H_2O)_n$ and hence it is less likely for energy to be concentrated into losing the water molecule.

Building on the comprehensive investigation of the TNT system we can go straight to the salient structures and energetics for the loss of water from 2,4-DNT and 2,6-DNT following proton transfer from H_3O^+. These calculations are given in Table 3a and b, respectively.

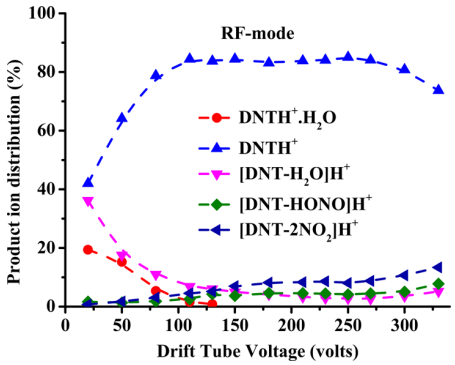

Figure 7. Percentage product ion distributions resulting from the reaction of H_3O^+ with 2,6-DNT in RF-mode including the secondary process resulting in the association of the protonated molecule with water as a function of supplied drift tube voltage.

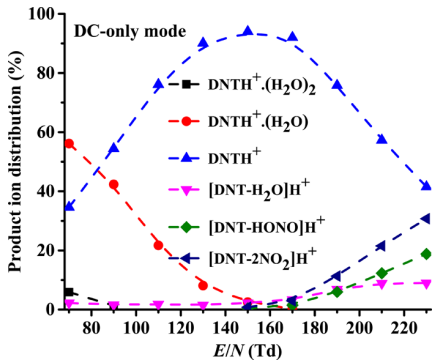

Figure 8. Percentage product ion distributions resulting from the reaction of H_3O^+ with 2,6-DNT in DC-only mode including the secondary process resulting in the association of the protonated molecule with water as a function reduced electric field.

DOI: 10.1021/acs.analchem.6b02982
Anal. Chem. 2016, 88, 10624−10630

Table 3. Energetics for the Elimination of Water from (a) 2,4-DNT and (b) 2,6-DNT Following Proton Transfer from H_3O^+

(a)		
products	ΔH_{298} kJ mol^{-1}	ΔG_{298} kJ mol^{-1}
2,4-DNTH$^+$(syn) + H_2O	−89	−87
2,4-DNTH$^+$(anti) + H_2O	−96	−95
TS syn/anti + H_2O	−21	−16
TS for loss of H_2O + H_2O	+126	+130
2,4-DNT-H_2O(c) + 2H_2O	−146	−187
(b)		
products	ΔH_{298} kJ mol^{-1}	ΔG_{298} kJ mol^{-1}
2,6-DNTH$^+$(syn) + H_2O	−87	−88
2,6-DNTH$^+$(anti) + H_2O	−95	−95
TS syn/anti + H_2O	−42	−38
TS for loss of H_2O + H_2O	+117	+120
2,6-DNT-H_2O(c) + 2H_2O	−177	−217

Nitrotoluenes. In order to further investigate the requirement of methyl and nitro functional groups to be adjacent in order to facilitate the elimination of water when using the RFIF, the three isomers of nitrotoluene have been investigated. We can expect in RF-mode that only 2-NT should have a reaction pathway which would lead to the elimination of water following proton transfer from H_3O^+. For 3-NT and 4-NT no such elimination should occur. A review of the resulting mass spectra for all three isomers shows that is the case. However, the nitrotoluenes are more complicated than TNT and the DNTs, because other product ions are observed even at the lowest drift tube voltage. The NT isomers show significant fragmentation following proton transfer. This is found to occur in not only RF-mode but also DC-only mode. In addition to the elimination of water, which is not the dominant product ion, channels corresponding to the elimination of C_2H_6, NO, CH_3NO, NO_2, and HONO are observed in both modes. This is illustrated in Figure 9 for 2-NT when operating (a) in RF-mode and (b) in DC-only mode. At low drift tube voltages NTH$^+$·H_2O is observed (Figure 4a) in RF mode, presumably for reasons described above for DNT.

Table 4 presents the DFT energetics calculations for the elimination of water for 2-NT following proton transfer from H_3O^+.

CONCLUSIONS

A PTR-ToF-MS equipped with a radio frequency ion funnel, originally designed to improve sensitivity, has been used in an unusual way to induce fragmentation of product ions through changes in collisional induced dissociation. We have illustrated how this can be used to improve compound specificity by monitoring the ion signal in RF-mode. We propose that the rapid switching between RF and DC modes would be the best method to enhance selectivity. We are currently developing the instrument to achieve this, and this will be the subject of another article. The key point of this work is that in place of major and costly changes in instrumental design to improve chemical specificity, such as having a high mass resolution time-of-flight mass spectrometer or adding a pre-separation technique, which also makes the instrument unacceptable for use in security areas, a new analytical method has been described which at its heart manipulates the ion chemistry.

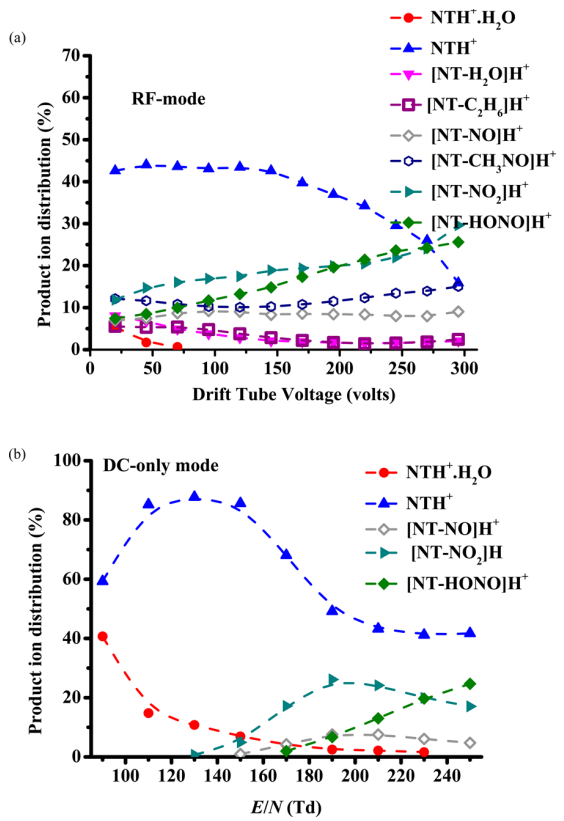

Figure 9. Percentage product ion distributions resulting from the reaction of H_3O^+ with 2-NT in (a) RF-mode and (b) DC-only mode as a function drift tube voltage. Included are the secondary ion−molecule processes resulting in the association of the protonated molecule with water.

Table 4. Energetics for the Elimination of Water from 2-NT Following Proton Transfer from H_3O^+

products	ΔH_{298} kJ mol^{-1}	ΔG_{298} kJ mol^{-1}
2-NTH$^+$(syn) + H_2O	−132	−138
2-NTH$^+$(anti) + H_2O	−105	−110
TS syn/anti + H_2O	−71	−76
TS for loss of H_2O + H_2O	+82	+78
2-NT-H_2O + 2H_2O	−93	−126

AUTHOR INFORMATION

Corresponding Author

*Tel.:+44 121 414 4668; E-mail: R.GonzalezMendez@bham.ac.uk.

Notes

The authors declare no competing financial interest.

ACKNOWLEDGMENTS

We thank the Defence Science and Technology Laboratory for funding R.G.M. This project was in part supported by the PIMMS and IMPACT ITNs which are in turn supported by the European Commission's seventh Framework Programme under Grant Agreement Numbers 287382 and 674911, respectively.

REFERENCES

(1) Schaffer, S. A.; Tang, K.; Anderson, G. A.; Prior, D. C.; Udseth, H. R.; Smith, R. D. *Rapid Commun. Mass Spectrom.* **1997**, *11*, 1813.

DOI: 10.1021/acs.analchem.6b02982
Anal. Chem. 2016, 88, 10624−10630

(2) Kelly, R. T.; Tolmachev, A. V.; Page, J. S.; Tang, K.; Smith, R. D.; et al. *Mass Spectrom. Rev.* **2010**, *29* (2), 294.
(3) Barber, S.; et al. *Anal. Chem.* **2012**, *84* (12), 5387.
(4) Blake, R. S.; Whyte, C.; Hughes, C. O.; Ellis, A. M.; Monks, P. S. *Anal. Chem.* **2004**, *76*, 3841.
(5) Ennis, C. J.; Reynolds, J. C.; Keely, B. J.; Carpenter, L. J. *Int. J. Mass Spectrom.* **2005**, *247* (1−3), 72.
(6) González-Méndez, R.; Reich, D. F.; Mullock, S. J.; Corlett, C. A.; Mayhew, C. A. *Int. J. Mass Spectrom.* **2015**, *385*, 13.
(7) Ellis, A.M.; Mayhew, C.A. *Proton Transfer Reaction Mass Spectrometry: Principles and Applications*, First ed., John Wiley and Sons, 2014.
(8) Brown, P.; Watts, P.; Märk, T. D.; Mayhew, C. A. *Int. J. Mass Spectrom.* **2010**, *294*, 103.
(9) Sulzer, P.; Petersson, F.; Agarwal, B.; Becker, K. H.; Jürschik, S.; Märk, T. D.; Perry, D.; Watts, P.; Mayhew, C. A. *Anal. Chem.* **2012**, *84*, 4161.
(10) Jürschik, S.; Agarwal, B.; Kassebacher, T.; Sulzer, P.; Mayhew, C. A.; Märk, T. D. *J. Mass Spectrom.* **2012**, *47*, 1092.
(11) Kassebacher, T.; Sulzer, P.; Jürschik, S.; Hartungen, E.; Jordan, A.; Edtbauer, A.; Feil, S.; Hanel, G.; Jaksch, S.; Märk, L.; Mayhew, C. A.; Märk, T. D. *Rapid Commun. Mass Spectrom.* **2013**, *27*, 325.
(12) Sulzer, P.; Agarwal, B.; Jürschik, S.; Lanza, M.; Jordan, A.; Hartungen, E.; Hanel, G.; Märk, L.; Märk, T. D.; González-Méndez, R.; Watts, P.; Mayhew, C. A. *Int. J. Mass Spectrom.* **2013**, *354*, 123.
(13) Agarwal, B.; González-Méndez, R.; Lanza, M.; Sulzer, P.; Märk, T. D.; Thomas, N.; Mayhew, C. A. *J. Phys. Chem. A* **2014**, *118*, 8229.
(14) Acton, W. J.; Lanza, M.; Agarwal, B.; Jurschik, S.; Sulzer, P.; Breiev, K.; Jordan, A.; Hartungen, E.; Hanel, G.; Märk, L.; Mayhew, C. A.; Märk, T. D. *Int. J. Mass Spectrom.* **2014**, *360*, 28.
(15) Lanza, M.; Acton, W. J.; Sulzer, P.; Breiev, K.; Jürschik, S.; Jordan, A.; Hartungen, E.; Hanel, G.; Märk, L.; Märk, T. D.; Mayhew, C. A. *J. Mass Spectrom.* **2015**, *50*, 427.
(16) DFT calculations were performed using the Gaussian 03 program with the GaussView interface. Frisch, M. J.; Trucks, G. W.; Schlegel, H. B.; Scuseria, G. E.; Robb, M. A.; Cheeseman, J. R.; Scalmani, G.; Barone, V.; Mennucci, B.; Petersson, G. A.; Nakatsuji, H.; Caricato, M.; Li, X.; Hratchian, H. P.; Izmaylov, A. F.; Bloino, J.; Zheng, G.; Sonnenberg, J. L.; Hada, M.; Ehara, M.; Toyota, K.; Fukuda, R.; Hasegawa, J.; Ishida, M.; Nakajima, T.; Honda, Y.; Kitao, O.; Nakai, H.; Vreven, T.; Montgomery, J. A., Jr., Peralta, J. E.; Ogliaro, F.; Bearpark, M.; Heyd, J. J.; Brothers, E.; Kudin, K. N.; Staroverov, V. N.; Kobayashi, R.; Normand, J.; Raghavachari, K.; Rendell, A.; Burant, J. C.; Iyengar, S. S.; Tomasi, J.; Cossi, M.; Rega, N.; Millam, J. M.; Klene, M.; Knox, J. E.; Cross, J. B.; Bakken, V.; Adamo, C.; Jaramillo, J.; Gomperts, R.; Stratmann, R. E.; Yazyev, O.; Austin, A. J.; Cammi, R.; Pomelli, C.; Ochterski, J. W.; Martin, R. L.; Morokuma, K.; Zakrzewski, V. G.; Voth, G. A.; Salvador, P.; Dannenberg, J. J.; Dapprich, S.; Daniels, A. D.; Farkas, O.; Foresman, J. B.; Ortiz, J. V.; Cioslowski, J.; Fox, D. J. *Gaussian 09*, Revision A.02;Gaussian, Inc.: Wallingford CT, 2009.
(17) Mayhew, C. A.; Sulzer, P.; Petersson, F.; Haidacher, S.; Jordan, A.; Märk, L.; Watts, P.; Märk, T. D. *Int. J. Mass Spectrom.* **2010**, *289*, 58.

DOI: 10.1021/acs.analchem.6b02982
Anal. Chem. 2016, 88, 10624−10630

frontiers in Chemistry

ORIGINAL RESEARCH
published: 13 June 2019
doi: 10.3389/fchem.2019.00401

Compendium of the Reactions of H_3O^+ With Selected Ketones of Relevance to Breath Analysis Using Proton Transfer Reaction Mass Spectrometry

Michaela Malásková[1†], David Olivenza-León[2†], Felix Piel[3,4†], Paweł Mochalski[1,5], Philipp Sulzer[3], Simone Jürschik[3], Chris A. Mayhew[1,2] and Tilmann D. Märk[3,4]*

[1] Institute for Breath Research, Fakultät für Chemie und Pharmazie, Leopold-Franzens-Universität Innsbruck, Dornbirn, Austria, [2] Molecular Physics Group, School of Physics and Astronomy, University of Birmingham, Birmingham, United Kingdom, [3] IONICON Analytik Gesellschaft m.b.H., Innsbruck, Austria, [4] Institut für Ionenphysik und Angewandte Physik, Universität Innsbruck, Innsbruck, Austria, [5] Institute of Chemistry, Faculty of Mathematics and Natural Sciences, Jan Kochanowski University, Kielce, Poland

OPEN ACCESS

Edited by:
Amala Dass, University of Mississippi, United States

Reviewed by:
Michael H. Nantz, University of Louisville, United States
Renato Zenobi, ETH Zürich, Switzerland

***Correspondence:**
Paweł Mochalski
pawel.mochalski@uibk.ac.at

†Early Stage Researchers who have contributed equally to the measurements, data analyses and contribution to the completion of this paper

Specialty section:
This article was submitted to Analytical Chemistry, a section of the journal Frontiers in Chemistry

Received: *08 March 2019*
Accepted: *17 May 2019*
Published: *13 June 2019*

Citation:
Malásková M, Olivenza-León D, Piel F, Mochalski P, Sulzer P, Jürschik S, Mayhew CA and Märk TD (2019) Compendium of the Reactions of H_3O^+ With Selected Ketones of Relevance to Breath Analysis Using Proton Transfer Reaction Mass Spectrometry. Front. Chem. 7:401. doi: 10.3389/fchem.2019.00401

Soft chemical ionization mass spectrometric techniques, such as proton transfer reaction mass spectrometry (PTR-MS), are often used in breath analysis, being particularly powerful for real-time measurements. To ascertain the type and concentration of volatiles in exhaled breath clearly assignable product ions resulting from these volatiles need to be determined. This is difficult for compounds where isomers are common, and one important class of breath volatiles where this occurs are ketones. Here we present a series of extensive measurements on the reactions of H_3O^+ with a selection of ketones using PTR-MS. Of particular interest is to determine if ketone isomers can be distinguished without the need for pre-separation by manipulating the ion chemistry through changes in the reduced electric field. An additional issue for breath analysis is that the product ion distributions for these breath volatiles are usually determined from direct PTR-MS measurements of the compounds under the normal operating conditions of the instruments. Generally, no account is made for the effects on the ion-molecule reactions by the introduction of humid air samples or increased CO_2 concentrations into the drift tubes of these analytical devices resulting from breath. Therefore, another motivation of this study is to determine the effects, if any, on the product ion distributions under the humid conditions associated with breath sampling. However, the ultimate objective for this study is to provide a valuable database of use to other researchers in the field of breath analysis to aid in analysis and quantification of trace amounts of ketones in human breath. Here we present a comprehensive compendium of the product ion distributions as a function of the reduced electric field for the reactions of H_3O^+. $(H_2O)_n$ (n = 0 and 1) with nineteen ketones under normal and humid (100% relative humidity for 37 °C) PTR-MS conditions. The ketones selected for inclusion in this compendium are (in order of increasing molecular weight): 2-butanone; 2-pentanone; 3-pentanone; 2-hexanone; 3-hexanone;

2-heptanone; 3-heptanone; 4-heptanone; 3-octanone; 2-nonanone; 3-nonanone; 2-decanone; 3-decanone; cyclohexanone; 3-methyl-2-butanone; 3-methyl-2-pentanone; 2-methyl-3-pentanone; 2-methyl-3-hexanone; and 2-methyl-3-heptanone.

Keywords: ketones, breath analysis, PTR-MS, reduced electric field, fastGC

INTRODUCTION

Depending on the actual mass resolution, current proton transfer reaction mass spectrometers (PTR-MS) are easily capable of separating many protonated isobaric compounds through a peak fitting procedure providing their mass separation is at least 0.01 Da. The selectivity of PTR-MS can be further improved by the manipulation of the ion-molecule chemistry that occurs between a reagent ion and a given isobar in the drift tube to produce different product ions. This can be achieved by (i) changing the reagent ion, examples for which have been presented in the literature for explosives (Sulzer et al., 2013; Agarwal et al., 2014), or psychoactive substances (Acton et al., 2014; Lanza et al., 2015), and/or (ii) the collisional processes in the drift tube through changing the reduced electric field. Changes in the reduced electric field (the ratio of the electric field strength, *E*, to the gas number density, *N*, in the drift tube) to alter the product ion distributions have been demonstrated in the areas of homeland security, e.g., detection of chemical warfare agents (Petersson et al., 2009), explosives (Mayhew et al., 2010; Sulzer et al., 2012, 2013), and rape drugs (Jürschik et al., 2012), and in environmental science, e.g., the identification of monoterpenes (Materić et al., 2017).

This application of changing collisional processes through changes in the reduced electric field to enhance compound selectivity has led to the development of a computer- controlled fast switching drift tube voltage (González-Méndez et al., 2018) and the adaptation of a radio frequency ion-funnel drift tube (González-Méndez et al., 2016).

Although today there are several ways to enhance the selectivity of PTR-MS for isobaric compounds, distinguishing isomeric compounds is still more of an issue. With no pre-separation of isomeric compounds, rarely can isomers be easily identified using PTR-MS through differences in product ion distributions, even if the ion-molecule chemistry occurring in the drift tube of PTR-MS is manipulated in a structured way. One study has demonstrated how reactions of O_2^+ and NO^+ can be used to distinguish two isomeric mephedrone substitutes (4-methylethcathinone and N-ethylbuphedrone) whereas reactions with H_3O^+ could not (Lanza et al., 2013). However, such examples in ion-isomer chemistry are usually the exception rather than the rule.

Isomers of ketones are so far difficult to identify unambiguously with a PTR-MS instrument. Pre-separation offered by standard gas chromatography (GC) techniques can be used, but they take away the main advantage of PTR-MS, namely its real-time analytical capabilities. The recent development of fast gas chromatography (fastGC) coupled to PTR-MS provides a compromise between real-time measurements, ensuring reasonably fast analysis (within approximately 90 s), whilst still taking advantage of limited pre-separation of compounds to improve the analytical specificity of PTR-MS (Ruzsanyi et al., 2013; Romano et al., 2014; Anderson, 2015).

In this paper we have used the fastGC PTR-MS technique in order to accurately determine the product ion distributions for a large selection of ketones as a function of reduced electric field so that we can unambiguously determine their product ions, without any concerns from impurities in the samples. Ketones have been selected for this study, because they form a common class of compounds found in breath, blood and urine (de Lacy Costello et al., 2014), and their detection holds many possibilities for non-invasive diagnostic and monitoring procedures in health services. One example is the diagnosis of ketosis, resulting from the elevation of ketone bodies in the blood. Detecting changes in ketone concentrations could thus be used to diagnose diabetic ketosis. A key ketone found in high concentrations in breath is acetone, the production of which (as for most ketones) is linked to fat metabolism, and hence its detection in breath could provide a window to predict fat loss (Anderson, 2015). Given the importance of acetone in the breath, it has been investigated numerous times with PTR-MS, and hence acetone does not form part of this current study. Less attention has been given to other ketones in PTR-MS studies. Hence this investigation has focused its attention on other important breath ketones, although generally found in much lower concentrations in the breath than for acetone. This has produced a wealth of new data, providing a useful database of the product ion distributions resulting from the reactions of H_3O^+ and H_3O^+. (H_2O) with ketones using PTR-MS.

Awareness of possible changes in the reaction processes occurring in the drift tube of a PTR-MS instrument resulting from changes in humidity have been known for some time (Warneke et al., 2001; Tani et al., 2003, 2004). Breath samples are humid, and thus product ion distributions determined under the "normal" operating conditions of PTR-MS (e.g., using purified air or nitrogen as the buffer gas in the drift tube) may not be a true reflection of those associated with a humid gas sample in the drift tube. This is because it can be expected that a higher humidity associated with breath samples (100% relative humidity at 32–34°C) will affect the product ion distributions through changes in the energy associated with the collisional processes. Furthermore, if protonated water clusters can react with a breath volatile via proton transfer, far less energy will be available in the reaction than for that associated with H_3O^+, and with higher humidity comes a greater production of protonated water clusters for a given reduced electric field. This effect will generally be more important at low reduced electric field values (i.e., $< \sim$120 Td, 1 Td $= 10^{-17}$ V cm^2) when collisions will lead to less break-up of the protonated water clusters to H_3O^+ and neutral water(s). Moreover, if the protonated water clusters cannot react with a volatile, then a reduction in the sensitivity of detection of that compound results. Finally, differences in product ion

distributions will arise if secondary processed occur, such as when primary product ions react with water.

A review of the literature shows that PTR-MS product ion distributions of compounds of interest to breath research are generally determined under the "normal" operating conditions, i.e., where the humidity in the drift tube is determined by the diffusion of water from the discharge region into the drift tube, which will be less than that associated with a breath sample. An objective of this work is to improve our knowledge on the effects of humidity on product ion distributions.

The first studies associated with investigating the effects of humidity on reaction processes in PTR-MS focused on sensitivity issues. For example, Warneke et al. (2001) showed how the sensitivity for the detection of benzene and toluene at fixed reduced electric fields decreased with increasing humidity, owing to unreactive $H_3O^+.(H_2O)_n$ clusters. Hence, de Gouw et al. (2003) suggested employing a humidity factor to determine the concentrations of a compound if it reacts with protonated water clusters, a factor which takes into account the efficiencies of the proton transfer reaction and the transmission of $H_3O^+.(H_2O)$ relative to that of H_3O^+. These factors were determined and used to correct for the influences of humidity on the detection sensitivity for methanol, acetonitrile, acetaldehyde, acetone, benzene and toluene by de Gouw and Warneke (2007). A PTR-MS investigation of the effects of humidity on the product ion distributions resulting from the reactions of H_3O^+ with two sesquiterpenes (α-cedrene and longifolene) was undertaken by Demarcke et al. (2009). In that study, no substantial influence of the humidity in the drift tube on the product ion yields was observed. More recently, the effects of humidity on product ion distributions have been investigated for α-pinene, δ-limonene, and longifolene by Kari et al. (2018) at two different *E/N* values (80 Td and 130 Td) (Kari et al., 2018), and for more than 20 volatile organic compounds (VOCs), including aldehydes, ketones, aromatic compounds and hydrocarbons by Trefz et al. (2018) at one fixed *E/N* (139 Td) (Trefz et al., 2018). In the former study, no significant changes in the product ion distributions were observed. However, Trefz et al. reported large differences in VOC intensities between "dry" and "humid" samples. Thus, the effect of humidity appears to depend very much on the volatile chemical compound.

In this paper we present details on the reactions of H_3O^+ and associated water clusters with a selected number of ketones over a large reduced electric field range of 100–220 Td, and compare product ions obtained under "normal" and "humid" operating conditions of the drift tube. This work demonstrates that changes in product ion distributions do occur for fixed *E/N* for different humidities, and hence it clearly demonstrates that humidity effects should be considered when relying on product ion distributions for undertaking breath research with a PTR-MS.

MATERIALS AND METHODS

Sample Preparation

Samples were prepared in two different ways depending on the humidity of the measurement.

For measurements under normal conditions, an open glass vial containing a ketone was purged with high purity N_2 (Alphagaz 1, Air Liquide GmbH., Austria), which had been previously passed through a P300-1 Filter (VICI AG, Switzerland) for purification (6.0). The vial was then covered with parafilm. Using a glass syringe a quantity of headspace was taken from the vial through the parafilm. This headspace containing the ketone and N_2 was then injected into a PTFE bag filled with 3L of dry 6.0 N_2, which was already connected to the inlet of the PTR-ToF-MS instrument. This injected volume into the bag varied from 5 μL to 10 mL, depending on the volatility of the ketone.

Humid samples were prepared using a Liquid Calibration Unit (LCU, IONICON Analytik GmbH, Austria). The LCU generates defined gaseous concentrations from aqueous solutions of volatile and semi-volatile organics. A description of the LCU has already been provided in detail by Fischer et al. (2013). Briefly, a homebuilt liquid flow controller injects a defined flow into a nebuliser (X175, Burgener Research Inc., United Kingdom). Vaporization of the aqueous solution produces micro droplets, which are evaporated in a heating chamber maintained at 100°C. The heating chamber is being constantly flushed by a buffer gas, e.g., zero air or N_2, diluting the organic sample and thus generating a continuous stream of a defined trace gas mixture.

For this study, to generate the humid samples, 16 mL glass vials, kept at a constant temperature of 30°C, were filled with a trace quantity of a ketone [1–10 μL (depending on the volatility of the ketone)] diluted in 100 mL of purified water. A sample flow of this ketone/water mixture at 35 μL/min was diluted in a N_2 flow of 950 mL/min to achieve a 5% absolute humidity. The combined flow was then directly connected to the fastGC inlet system of the PTR-ToF-MS instrument.

For both the dry and humid measurements, the dilution of the samples were prepared to yield a concentration of the ketone in the drift tube to be approximately 100 ppbv.

The experiments presented here were done through an automated measurement procedure. This consisted of background measurements for 5 min. For the dry mixtures, this involved the PTFE bag filled only with purified N_2. For the humid standards this step involved a vial containing only purified water. Next, the prepared samples were directed to the drift tube for a 2-min stabilization period, which was next followed by 2 min and 40 s of fastGC measurement at an *E/N* of 180 Td to help identify the product ions produced in the drift tube for a given ketone and a 26-min *E/N* set of measurements over the range 100–220 Td in steps of 10 Td (1 min each), in both directions, to provide two data sets.

FastGC PTR-ToF-MS

Details of PTR-ToF-MS and methods of operation have been reviewed extensively in the literature (Ellis and Mayhew, 2014), and therefore only brief details are required here. For this study, measurements were taken using a PTR-TOF 8000 with a fastGC add-on (IONICON Analytik GmbH, Austria) (Jordan et al., 2009; Graus et al., 2010). Briefly, water vapor is introduced into a hollow cathode discharge to generate $H_3O^+.(H_2O)_n$ ($n = 0, 1, 2, \ldots$), initially through electron ionization of water and subsequent ion-molecule reactions with water. These reagent ions are then

TABLE 1 | Product ions identified and their associated product ion branching ratios (percentages) measured at reduced electric fields of 100, 140, and 180 Td resulting from the reactions of H_3O^+ with several ketones.

Ketone **Molecular formula** **Nominal MW**	**Product ion *m/z* (Th)**	**Product ion formula**	**Product ion branching percentages**					
			Normal *E/N* (Td)			**Humid *E/N* (Td)**		
			100	**140**	**180**	**100**	**140**	**180**
2-butanone	73.07	$C_4H_8OH^+$	100	99	87	100	100	88
C_4H_8O	55.05	$C_4H_7^+$	0	1	10	0	0	10
72	39.02	$C_3H_3^+$	0	0	3	0	0	2
2-pentanone	87.08	$C_5H_{10}OH^+$	99	67	20	99	84	29
$C_5H_{10}O$	45.03	$C_2H_5O^+$	1	33	70	1	16	66
86	39.02	$C_3H_3^+$	0	0	10	0	0	5
3-pentanone	87.08	$C_5H_{10}OH^+$	98	72	23	99	91	43
$C_5H_{10}O$	69.07	$C_5H_9^+$	1	4	2	1	4	4
86	45.03	$C_2H_5O^+$	1	20	55	0	4	39
	41.04	$C_3H_5^+$	0	3	5	0	1	5
	39.02	$C_3H_3^+$	0	1	15	0	0	9
2-hexanone	101.10	$C_6H_{12}OH^+$	100	94	48	100	95	49
$C_6H_{12}O$	59.05	$C_3H_7O^+$	0	1	3	0	1	3
100	45.03	$C_2H_5O^+$	0	5	39	0	4	40
	39.02	$C_3H_3^+$	0	0	10	0	0	8
3-hexanone	101.10	$C_6H_{12}OH^+$	93	73	31	96	88	44
$C_6H_{12}O$	83.09	$C_6H_{11}^+$	1	4	4	1	4	5
100	59.05	$C_3H_7O^+$	3	9	15	3	7	17
	55.05	$C_4H_7^+$	0	3	5	0	0	12
	45.03	$C_2H_5O^+$	2	5	15	0	0	0
	41.04	$C_3H_5^+$	0	4	6	0	1	9
	39.02	$C_3H_3^+$	1	1	18	0	0	13
	31.02	CH_3O^+	0	1	6	0	0	0
2-heptanone	115.11	$C_7H_{14}OH^+$	94	76	31	96	86	52
$C_7H_{14}O$	97.10	$C_7H_{13}^+$	4	10	7	2	7	9
114	59.05	$C_3H_7O^+$	1	2	4	2	3	6
	55.05	$C_4H_7^+$	0	9	14	0	4	20
	45.03	$C_2H_5O^+$	1	3	15	0	0	0
	39.02	$C_3H_3^+$	0	0	29	0	0	13
3-heptanone	115.11	$C_7H_{14}OH^+$	98	89	35	99	95	57
$C_7H_{14}O$	97.10	$C_7H_{13}^+$	2	5	4	1	4	5
114	59.05	$C_3H_7O^+$	0	0	0	0	1	7
	55.05	$C_4H_7^+$	0	4	8	0	0	12
	41.04	$C_3H_5^+$	0	1	7	0	0	3
	39.02	$C_3H_3^+$	0	0	27	0	0	16
	31.02	CH_3O^+	0	1	19	0	0	0
4-heptanone	115.11	$C_7H_{14}OH^+$	98	90	52	99	95	70
$C_7H_{14}O$	73.07	$C_4H_9O^+$	0	1	2	0	0	0
114	59.05	$C_3H_7O^+$	1	2	6	1	1	4
	55.05	$C_4H_7^+$	0	6	15	0	4	16
	53.04	$C_4H_5^+$	0	0	5	0	0	3
	39.02	$C_3H_3^+$	1	1	20	0	0	7
3-octanone	129.13	$C_8H_{16}OH^+$	99	96	46	100	98	73
$C_8H_{16}O$	69.07	$C_5H_9^+$	0	3	5	0	1	6
128	59.05	$C_3H_7O^+$	1	1	3	0	1	4
	41.04	$C_3H_5^+$	0	0	11	0	0	10
	39.02	$C_3H_3^+$	0	0	35	0	0	7
2-nonanone	143.14	$C_9H_{18}OH^+$	100	93	34	100	97	62
$C_9H_{18}O$	83.09	$C_6H_{11}^+$	0	0	0	0	1	4

(Continued)

TABLE 1 | Continued

Ketone Molecular formula Nominal MW	Product ion *m/z* (Th)	Product ion formula	Product ion branching percentages					
			Normal *E/N* (Td)			Humid *E/N* (Td)		
			100	140	180	100	140	180
142	69.07	$C_5H_9^+$	0	4	4	0	2	6
	55.05	$C_4H_7^+$	0	1	4	0	0	7
	41.04	$C_3H_5^+$	0	1	10	0	0	10
	39.02	$C_3H_3^+$	0	1	48	0	0	11
3-nonanone	143.14	$C_9H_{18}OH^+$	100	87	48	100	100	79
$C_9H_{18}O$	55.05	$C_4H_7^+$	0	4	6	0	0	5
142	41.04	$C_3H_5^+$	0	8	11	0	0	6
	39.02	$C_3H_3^+$	0	1	35	0	0	10
2-decanone	157.16	$C_{10}H_{20}OH^+$	100	94	48	100	99	81
$C_{10}H_{20}O$	83.09	$C_6H_{11}^+$	0	2	3	0	1	6
156	55.05	$C_4H_7^+$	0	3	13	0	0	13
	39.02	$C_3H_3^+$	0	1	36	0	0	0
3-decanone	157.16	$C_{10}H_{20}OH^+$	99	95	48	100	100	86
$C_{10}H_{20}O$	55.05	$C_4H_7^+$	1	4	10	0	0	7
156	39.02	$C_3H_3^+$	0	1	42	0	0	7
cyclohexanone	99.08	$C_6H_{10}OH^+$	99	88	30	99	93	40
$C_6H_{10}O$	81.07	$C_6H_9^+$	1	12	65	1	7	56
98	79.05	$C_6H_7^+$	0	0	5	0	0	3
	39.02	$C_3H_3^+$	0	0	0	0	0	1
3-methyl-2-butanone	87.08	$C_5H_{10}OH^+$	100	98	63	99	96	66
$C_5H_{10}O$	69.07	$C_5H_9^+$	0	2	5	1	3	7
86	45.03	$C_2H_5O^+$	0	0	8	0	0	8
	41.04	$C_3H_5^+$	0	0	4	0	1	8
	39.02	$C_3H_3^+$	0	0	20	0	0	11
3-methyl-2-pentanone	101.10	$C_6H_{12}OH^+$	100	70	23	100	73	22
$C_6H_{12}O$	59.05	$C_3H_7O^+$	0	11	28	0	7	26
100	57.07	$C_4H_9^+$	0	4	3	0	5	4
	45.03	$C_2H_5O^+$	0	15	39	0	15	40
	39.02	$C_3H_3^+$	0	0	7	0	0	8
2-methyl-3-pentanone	101.10	$C_6H_{12}OH^+$	98	61	17	95	74	24
$C_6H_{12}O$	59.05	$C_3H_7O^+$	1	15	29	3	9	29
100	57.07	$C_4H_9^+$	0	4	2	0	3	3
	45.03	$C_2H_5O^+$	1	20	41	2	13	40
	39.02	$C_3H_3^+$	0	0	11	0	1	4
2-methyl-3-hexanone	115.11	$C_7H_{14}OH^+$	95	66	24	96	72	24
$C_7H_{14}O$	97.10	$C_7H_{13}^+$	5	14	8	4	10	7
114	59.05	$C_3H_7O^+$	0	8	17	0	4	17
	55.05	$C_4H_7^+$	0	4	5	0	2	7
	45.03	$C_2H_5O^+$	0	5	17	0	11	27
	41.04	$C_3H_5^+$	0	3	7	0	1	6
	39.02	$C_3H_3^+$	0	0	22	0	0	12
2-methyl-3-heptanone	129.13	$C_8H_{16}OH^+$	96	76	26	97	81	28
$C_8H_{16}O$	111.12	$C_8H_{15}^+$	3	5	3	2	5	3
128	69.07	$C_5H_9^+$	0	8	5	0	4	5
	59.05	$C_3H_7O^+$	0	0	0	0	3	14
	45.03	$C_2H_5O^+$	0	2	8	0	3	10
	43.05	$C_3H_7^+$	1	2	2	1	2	3
	41.04	$C_3H_5^+$	0	6	15	0	2	15
	39.02	$C_3H_3^+$	0	1	41	0	0	22

Values for the product ion branching percentages are given whilst operating the drift tube under "normal" conditions and under "humid" (breath humidity) conditions. Errors in the branching percentages are estimated to be <20%.

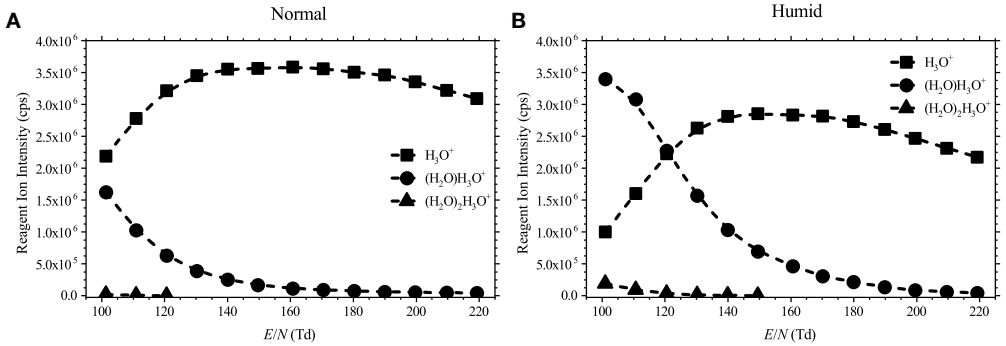

FIGURE 1 | Reagent ion intensities in counts per second (cps) as a function of the reduced electric field for **(A)** normal (dry buffer gas) and **(B)** humid (5% absolute humidity buffer gas) conditions.

transferred to the drift tube via a focusing lens. The distribution of the protonated water clusters in the reaction region depends on the *E/N* value and the humidity in the drift tube as shown in **Figure 1**.

These reagent ions are then transported down the drift tube under the influence of the uniform electric field. Analytes are injected into the drift tube through an inlet pipe. Proton transfer from hydronium to the analyte takes place within the drift tube if the proton affinity (PA) of the analyte is higher than that of water ($PA(H_2O) = 691$ kJ mol^{-1}). Proton transfer can be non-dissociative and dissociative. However, it should be stressed that fragmentation of the protonated molecule can be a barrierless process and occur spontaneously, or it can be induced by the collision of the reagent ions with analyte and/or charged analyte with the buffer gas.

For all measurements the drift tube was kept at a pressure of 2.3 mbar, with both the inlet system and drift tube being maintained at 100°C. The collisional energies of the reagent and product ions were controlled by the value of the reduced electric field. For this study we kept the drift tube at constant pressure and temperature (and hence constant *N*), and changed the drift tube voltage to alter the value of *E*/*N*. The drift voltage could be changed from 410 V up to a maximum of 890 V. For the applied values of the drift tube pressure and temperature these values correspond to an *E/N* range from 100 to 220 Td.

Using a dry buffer gas in the drift tube of a PTR-MS instrument does not mean that it is operated under dry conditions, since some amounts of water vapor diffuse from the hollow cathode. This condition will be denoted as "normal" operating condition later in this paper. When a water saturated buffer gas was used, this is referred in the text as operating the drift tube under "humid" conditions.

FastGC was used to separate analytes of interest from possible contaminants in the produced standards. The fastGC add-on used in this study is a modification of the setup used by Romano et al. (2014) and Ruzsanyi et al. (2013). Therefore, only the modifications relevant for this study will be provided here. An MXT-1 column (10 m × 0.53 mm, film thickness 0.25 μm, dimethyl polysiloxane phase, Restek, USA) was used. The samples were injected into a 0.5 ml sample loop made of passivated stainless steel. A custom-made valve block consisting of four three-way valves and a needle valve has been replaced by a 10-port passivated valve (VICI AG, Switzerland) and a three-way gas valve made from polyether ether ketone (PEEK) was used. All parts of the inlet system are installed within the oven that houses the drift tube to prevent cold spots. This revised setup enabled constant filling of the sample loop and constant back-flushing of the capillary column with the carrier gas. 8 ml/min and 20 ml/min of 6.0 N_2 were used as carrier gas and make-up gas, respectively. A voltage ramp of 0.5 V/s from 10 V up to 80 V was applied raising the temperature of the capillary column from room value up to 240°C.

Chemicals

The following liquid substances were purchased from Sigma-Aldrich: 2-pentanone (98%), 3-pentanone (99%), 2-hexanone (98%), 3-hexanone (98%), 3-heptanone (analytical standard), 4-heptanone (98%), 2-nonanone (99%), 3-nonanone (99%), 2-decanone (98%), cyclohexanone (99.8%), 3-methyl-2-pentanone (99%), 2-methyl-3-pentanone (97%), 2-methyl-3-hexanone (98%), and 2-methyl-3-heptanone (99%). 2-butanone (99.5%), 2-heptanone (98.5%), and 3-methyl-2-butanone (98.5%) were purchased from Honeywell. 3-octanone (99%) and 3-decanone (97%) were purchased from Acros Organics and SAFC, respectively. These were used with no further purification.

Data Analysis

The "PTR-MS Viewer" (IONICON Analytik GmbH, Austria) was used to identify peaks in the mass spectra and to extract peak data. Raw peak data, i.e., data not corrected for transmission factors, were normalized to 1 million reagent ions and had any backgrounds subtracted. By using the "raw" data, the product ion distributions we have determined here can be more easily compared with other measurements using different PTR-MS instruments. However, we emphasize that the product ion distributions that have been determined for the selection of ketones chosen for this study have to be taken with some caution if a PTR-TOF 8000 is not being used, and that researchers need to determine product ion distributions for their own instruments and conditions.

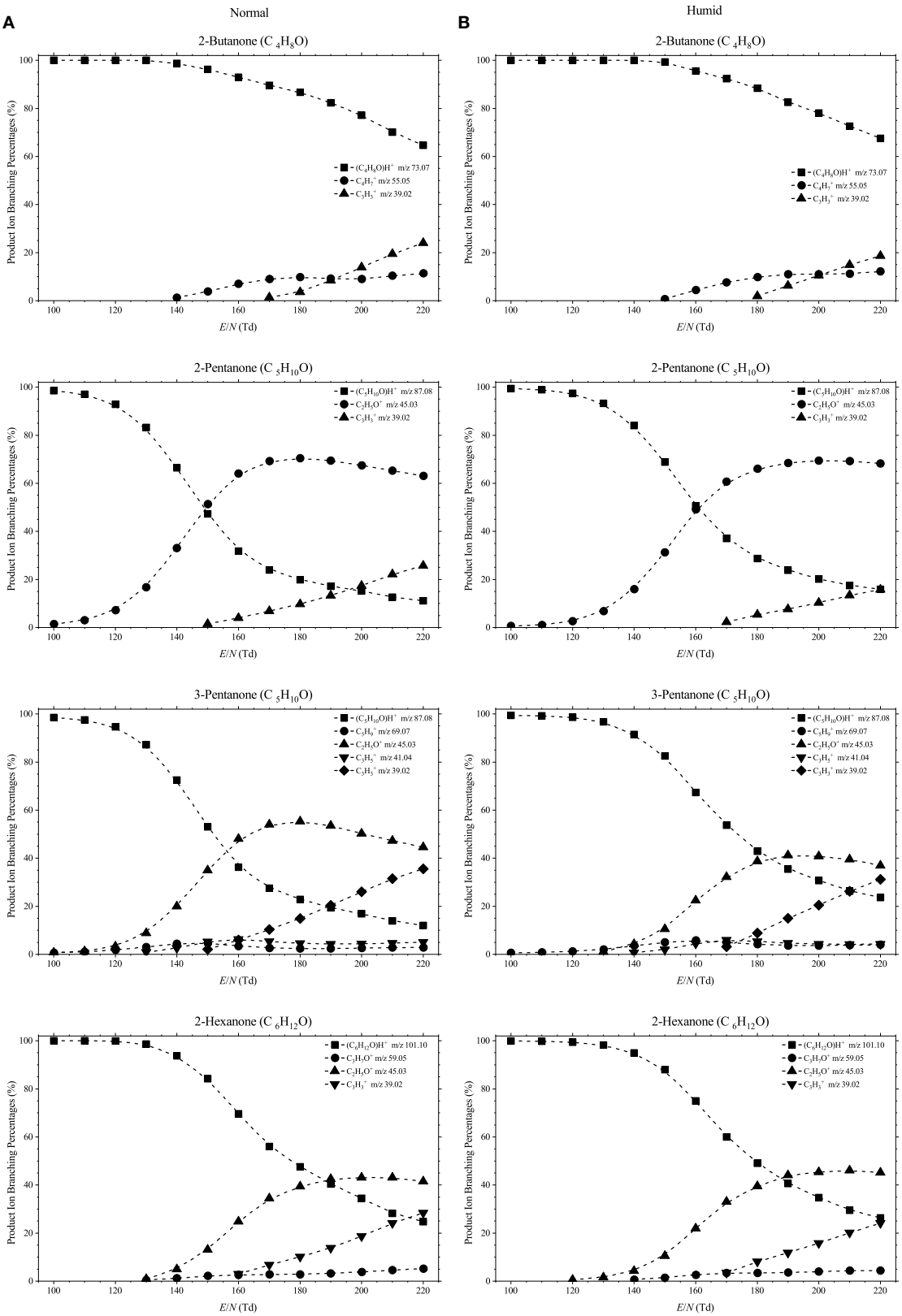

FIGURE 2 | Continued

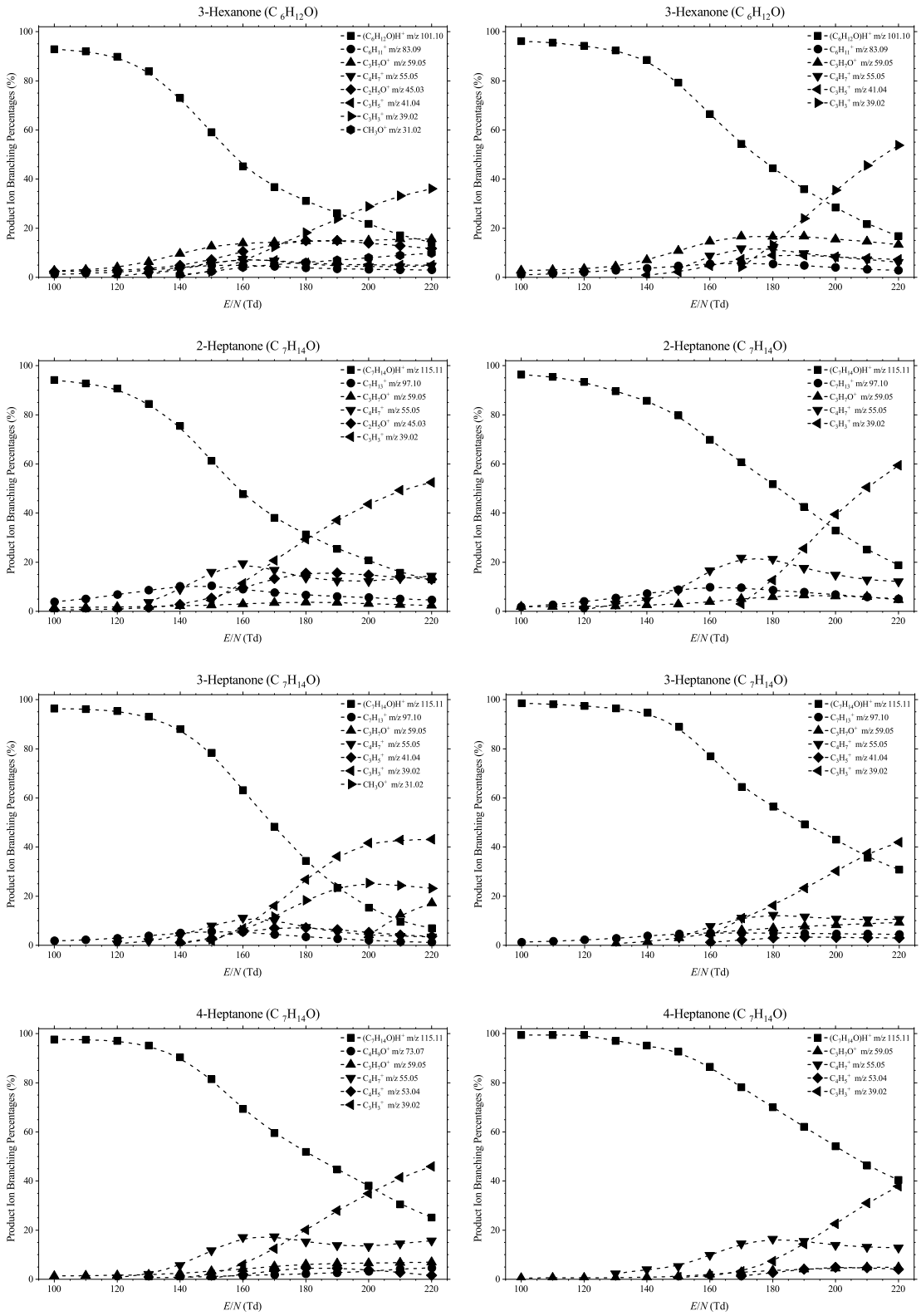

FIGURE 2 | Continued

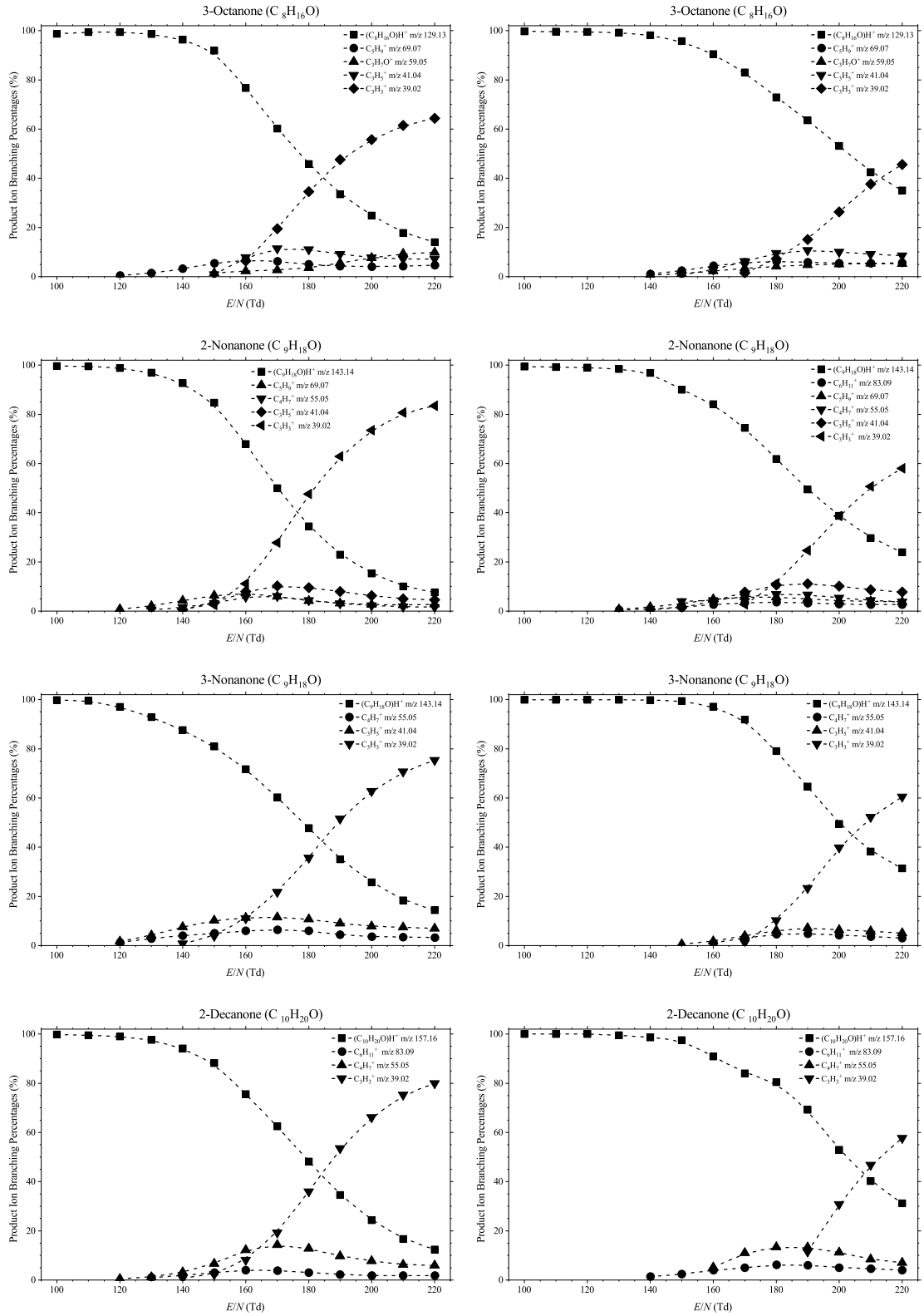

FIGURE 2 | Continued

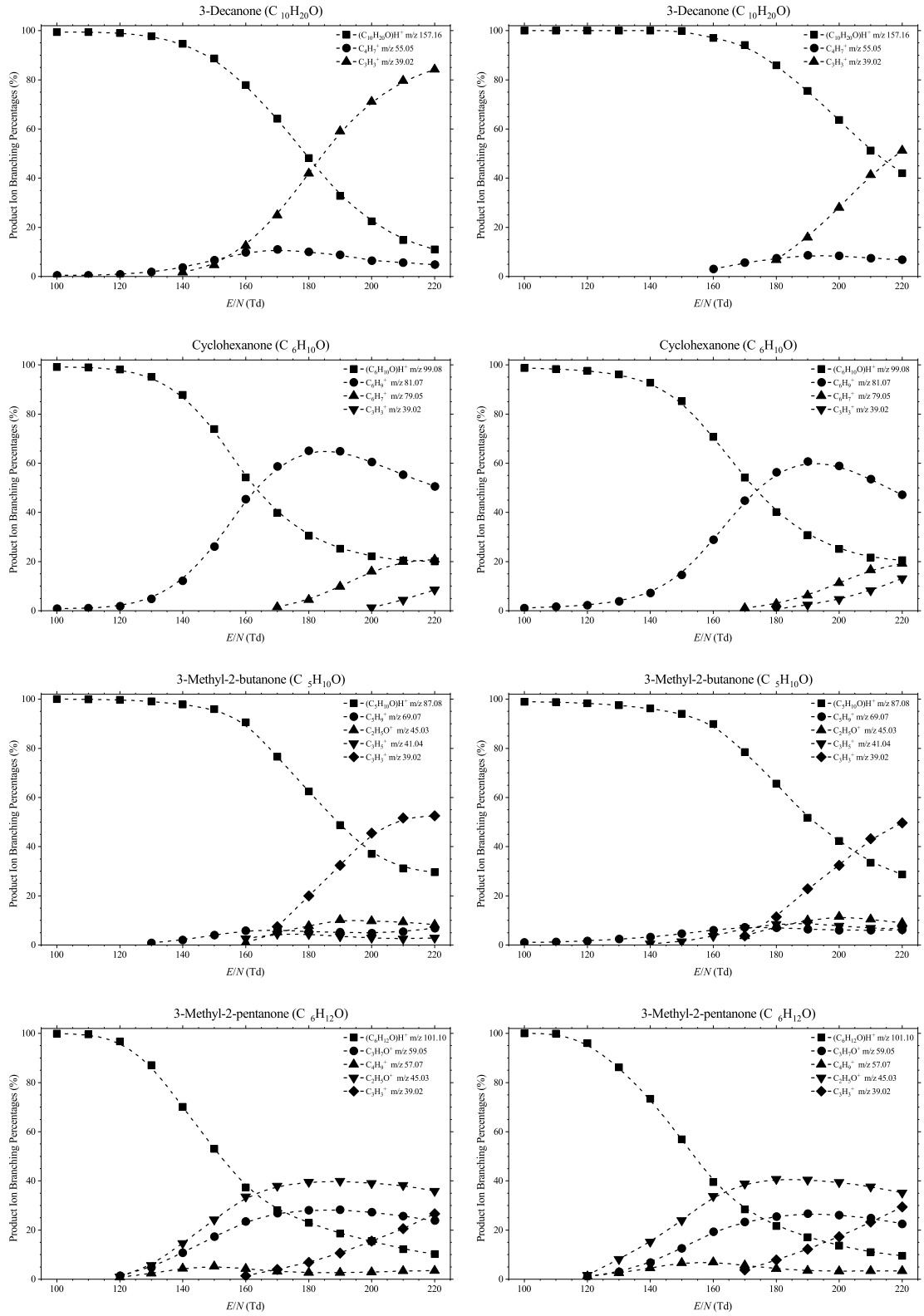

FIGURE 2 | Continued

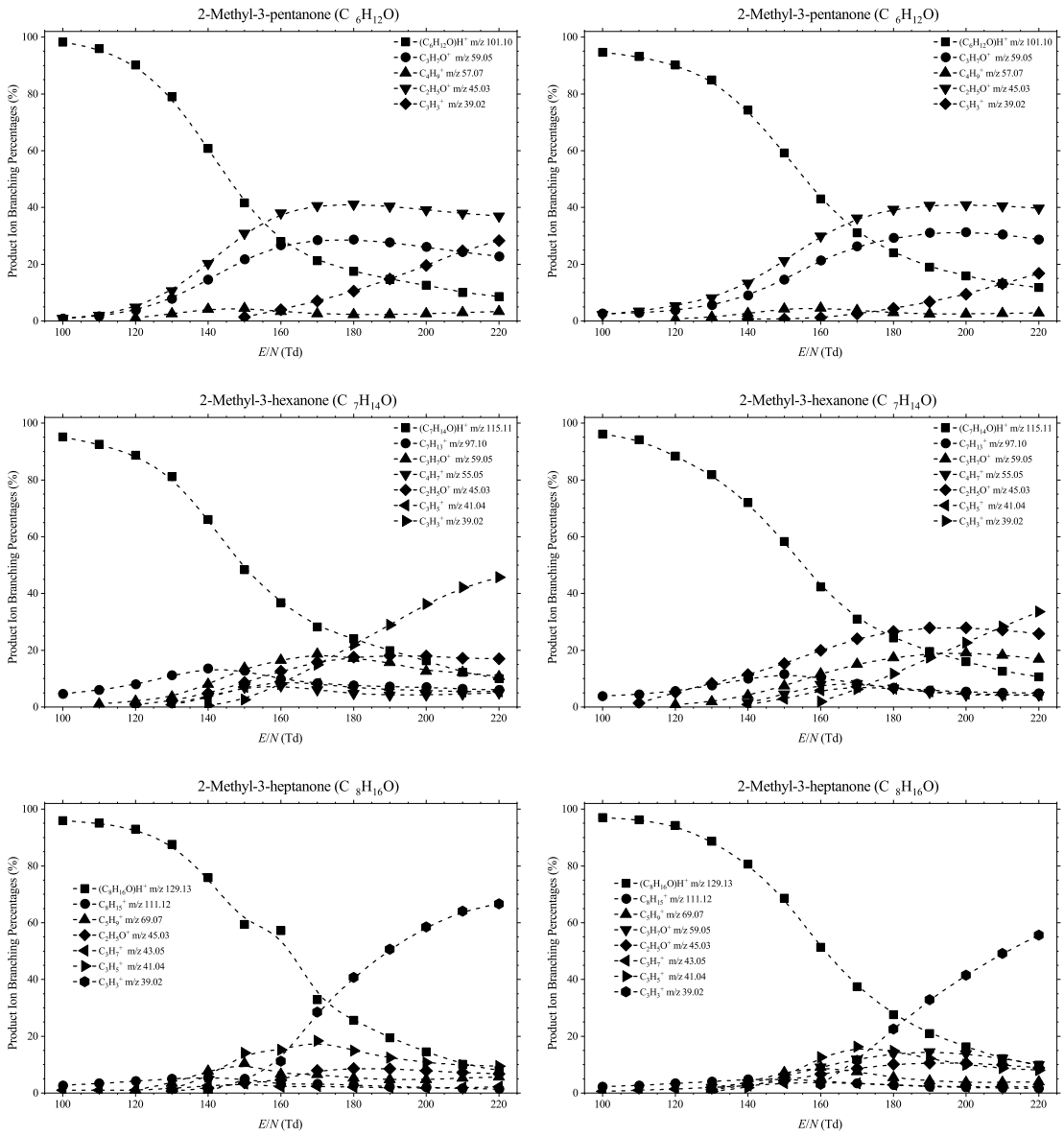

FIGURE 2 | Product ion distributions (branching percentages) as a function of *E/N* resulting from reaction with H_3O^+ (and potentially $H_3O^+.H_2O$ as stated above) under **(A)** normal and **(B)** high humidity drift tube conditions with several ketones.

RESULTS AND DISCUSSION

Table 1 presents a summary of the product ion distributions (percentages) for all the ketones investigated in this study at three selected reduced electric fields, namely 100 Td, 140 Td, and 180 Td under normal and humid conditions. These values give a good representation of all product ions observed and quickly illustrate the effects of humidity on the product ion distributions, if any. The table starts with the thirteen linear chained ketones in order of molecular weight (MW), followed by the one cyclic ketone (cyclohexanone), and finishing with five non-linear ketones, also presented in order of increasing nominal MW, and, for low *E/N* (see **Figure 1**), from reactions of $H_3O^+.H_2O$ with those ketones whose proton affinities are greater than that associated with $(H_2O)_2$ (808 kJ mol^{-1}), i.e., 2-butanone (827 kJ mol^{-1}), 2-pentanone (833 kJ mol^{-1}), 3-pentanone (837 kJ mol^{-1}), and 3-methyl-2-butanone (836 kJ mol^{-1}).

The dependence of the product ion branching percentages as a function of *E/N* are shown graphically in **Figure 2**. The chemical formulae of the product ions given in **Table 1** and **Figure 2** have been tentatively identified via the exact *m/z* (to 2 decimal places) and isotope (^{13}C) intensities. Only product ions who make a contribution to the branching percentage of at least 3% at any reduced electric field value are included in the table and figure.

Below approximately 140 Td, the protonated parent is the dominant product ion observed for all ketones. This is in reasonable agreement with other PTR-MS studies. For example, in the study by Buhr et al. (2002) at one reduced electric field of approximately 140 Td, the authors showed that proton transfer from H_3O^+ to ketones will predominantly be non-dissociative, regardless of chain length. This limited dissociation observed in PTR-MS for reduced electric fields below 140 Td also agrees with studies using the thermalized conditions in Selected Ion Flow Tube—Mass Spectrometry (SIFT-MS) (Spanel et al., 1997; Smith et al., 2003, 2019), and suprathermal Selected Ion Flow Drift Tube (SIFDT) investigations (Specyvyi et al., 2017).

Above 140 Td, fragmentation of the protonated parent is observed, a fact that was not reported by Buhr et al. for 2-butanone, 2-hexanone, 2-heptanone, 3-heptanone, 4-heptanone, 3-octanone, 2-nonanone, and 2-decanone, for which only the protonated parent is observed. Limited fragmentation is, however, reported by Buhr et al. at 140 Td for 2-pentanone, with a product ion being observed at *m/z* 45, which we also observe and assign it to be $C_2H_5O^+$ (protonated acetaldehyde) although it is found with a much higher relative intensity compared to the protonated parent in our study than found by Buhr et al. This difference in intensity is most probably associated with differences in the transmission of ions, because Buhr et al. used a quadrupole mass spectrometer.

In the present study, significant percentages of hydrocarbon ions, $C_nH_m^+$, are seen. This agrees with another *E/N* study of the ketones, 2-butanone, 2-pentanone, 2-hexanone, 2-heptanone, and cyclohexanone by Pan et al. (2017), who used a dipolar proton transfer reaction (quadrupole) mass spectrometer. Their study, which covered the reduced electric fields of approximately 50–110 Td, reported the *m/z* values of the product ions we have found, but observed substantially more fragmentation than we detected, even at their low *E/N* values. The amount of fragmentation reported at low *E/N* (as low as 50 Td) by Pan et al. is surprising, given that at these *E/N* values the reagent ion signal in our instruments would be protonated water clusters. This again illustrates that care must be taken when comparing results from different PTR-MS instruments.

In our study, typically 2–7 fragmentation channels have been observed. However, many of them were significant only at higher reduced electric field values. For instance, $C_3H_3^+$ and $C_3H_5^+$ ions occur only for *E/N* values higher than about 150 Td. Thus, for *E/N* values up to about 130 Td, the protonated molecules are dominant having well-above 80% branching percentages associated with that channel. Interestingly, the highest number of fragmentation channels was noted for 3-hexanone (7 channels) and C7 ketones; 2-heptanone (5 channels), 3-heptanone (6 channels), 4-heptanone (5 channels), and 2-methyl-3-hexanone (6 channels). As expected, heavier ketones are found to fragment considerably less.

For several ketones, the proton transfer process is followed by the elimination of an H_2O molecule leading to the observed hydrocarbon ions $C_nH_{2n-1}^+$. However, these channels have small associated branching percentages, and at higher values of the reduced electric field undergo further fragmentation.

The channel leading to the $C_2H_5O^+$ ion is very abundant in fragmentation patterns of C5 and C6 ketones. Interestingly, the mass spectra of C8 and C9 ketones do not have oxygen-containing fragmentation channels.

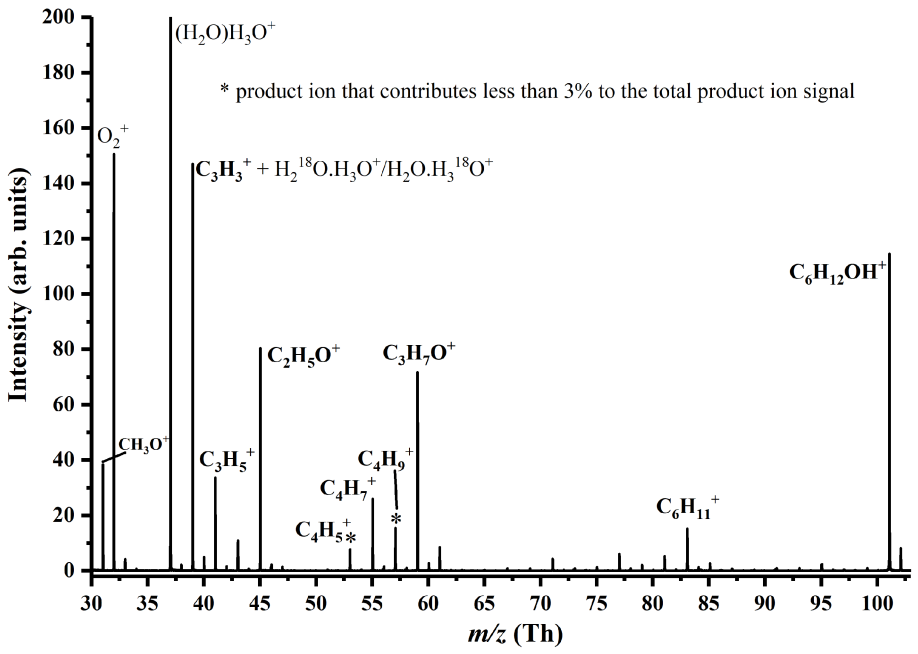

FIGURE 3 | Mass spectrum for 3-hexanone recorded at 180 Td. Product ions coming from the compound are identified. The product ions $C_4H_5^+$ and $C_4H_9^+$ each contribute <3% to the total product ion percentage even at the highest reduced electric field investigated.

High humidity reduces the fragmentation of ketones. Interestingly, this effect is most evident for the *E/N* values of 150–160 Td. For example, the abundance of the protonated parent ion of 2-pentanone under normal conditions for 150 Td is 47%; whereas, in humid air, it has a branching percentage of 69%. The analogous values for 3-nonanone are 48 and 79%, respectively. This interesting dependence can be attributed to the formation of considerable amounts of protonated water clusters, which can react with ketones of interest. Consequently, far less energy is available for fragmentation in such reactions than for those associated with H_3O^+. At the higher *E/N* values formation of water clusters is suppressed and, thereby, the positive effect of humidity on having reduced fragmentation is weakened. The general effect of the higher humidity is to shift the product ion branching percentage curves by approximately 20 Td to higher *E/N*.

To illustrate the quality of the data, a mass spectrum recorded at 180 Td for 3-hexanone is provided in **Figure 3**. This highlights some product ions which are associated with the volatile, but are not included in the tabulation or **Figure 2**, because their contributions to the total relative abundance are <3% for any reduced electric field value.

CONCLUSIONS

This work provides a large body of data and an extensive library of product ion distributions as a function of reduced electric field for the reactions of $H_3O^+.(H_2O)_n$ ($n = 0$ and 1) with a selection of ketones using the powerful analytical technique of PTR-ToF-MS. Although the study was originally conceived owing to the importance of ketones in the breath, and the need to determine what product ions should be monitored using PTR-MS, these results should be of interest to researchers working in other areas such as the environmental sciences and atmospheric chemistry.

A key outcome from this work is that product ion distributions at any specific reduced electric field can only be used to provide an indication of what ion-molecule channels are occurring. Detailed branching percentages are only specific to a given PTR-MS instrument and then under the specific operational conditions, not least the humidity present in the drift tube, as demonstrated in the results from this study.

Of the ketone isomers investigated in this study, it is apparent that it is not possible to provide any selectivity by manipulating the ion chemistry through changes in the reduced electric field. For this to be accomplished, the use fast gas chromatography coupled to PTR-MS is needed when analyzing gas samples that contain a mixture of ketone isomers, as often occurs in breath samples.

In the context of the ketones analyses in real breath samples by PTR-MS, the functional isomers of species from this chemical family (such as e.g., aldehydes) also need to be considered and investigated as their protonated forms cannot be separated from the respective protonated ketones. The ketones' PTR-MS analyses in the presence of their functional isomers require further studies. However, it is worth mentioning here, that aldehydes undergo significant fragmentation in the PTR-MS instruments and the abundance of their protonated parent ions is usually very small (<10%) (Buhr et al., 2002; Schwartz et al., 2009). Consequently, the presence of aldehydes in the breath sample can only have minor influence on the parent ions of the respective ketones.

DATA AVAILABILITY

The raw data supporting the conclusions of this manuscript will be made available by the authors, without undue reservation, to any qualified researcher.

AUTHOR CONTRIBUTIONS

MM, DOL, and FP are Early Stage Researchers employed on the EU IMPACT ITN. They contributed equally to the experimental measurements, data analyses and contribution to the completion of this paper. PM proposed the study. PM, PS, SJ, CAM, and TDM contributed equally to the writing of the paper.

ACKNOWLEDGMENTS

We thank the Marie Skłodowska-Curie Actions Innovative Training Network: Ion-Molecule Processes for Analytical Chemistry Technologies (IMPACT) (www.impact-h2020itn.com) which has supported this research through the European Commission's HORIZON 2020 Programme under Grant Agreement Number 674911. The first three authors of this paper, MM, DOL, and FP are Early Stage Researchers in this IMPACT network.

REFERENCES

Acton, J., Lanza, M., Agarwal, B., Jürschik, S., Sulzer, P., Breiev, K., et al. (2014). Headspace analysis of new psychoactive substances using a Selective Reagent Ionisation-Time of Flight-Mass Spectrometer. *Int. J. Mass Spectrom.* 360, 28–38. doi: 10.1016/j.ijms.2013.12.009

Agarwal, B., González-Méndez, R., Lanza, M., Sulzer, P., Märk, T. D., Thomas, N., et al. (2014). Sensitivity and selectivity of switchable reagent ion soft chemical ionization mass spectrometry for the detection of picric acid. *J. Phys. Chem. A* 118, 8229–8236. doi: 10.1021/jp5010192

Anderson, J. C. (2015). Measuring breath acetone for monitoring fat loss: review *Obesity* 23, 2327–2334. doi: 10.1002/oby.21242

Buhr, K., Van Ruth, S., and Delahunty, C. (2002). Analysis of volatile flavour compounds by Proton Transfer Reaction-Mass Spectrometry: fragmentation patterns and discrimination between isobaric and isomeric compounds. *Int. J. Mass Spectrometry* 221, 1–7. doi: 10.1016/S1387-3806(02)00896-5

de Gouw, J. A., Goldan, P. D., Warneke, C., Kuster, W. C., Roberts, J. M., Marchewka, M., et al. (2003). Validation of proton transfer reaction-mass spectrometry (PTR-MS) measurements of gas-phase organic compounds in the atmosphere during the New England Air Quality Study (NEAQS) in 2002 *J. Geophys. Res.* 108:D4682. doi: 10.1029/2003JD003863

de Gouw, J. A., and Warneke, C. (2007). Measurements of volatile organic compounds in the earth's atmosphere using proton-transfer-reaction mass spectrometry. *Mass Spectrom. Rev.* 26, 223–227. doi: 10.1002/mas.20119

de Lacy Costello, B., Amann, A., Al-Kateb, H., Flynn, C., Filipiak, W., Khalid, T., et al.. (2014). A review of the volatiles from the healthy human body. *J. Breath Res.* 8:014001. doi: 10.1088/1752-7155/8/1/014001

Demarcke, M., Amelynck, C., Schoon, N., Dhooghe, F., Van Langenhove, H., and Dewulf, J. (2009). Laboratory studies in support of the detection of sesquiterpenes by proton-transfer-reaction-mass-spectrometry. *Int. J. Mass Spectrom.* 279, 156–162. doi: 10.1016/j.ijms.2008.10.023

Ellis, A. M., and Mayhew, C. A. (2014). *Proton Transfer Reaction Mass Spectrometry: Principles and Applications.* Chichester: John Wiley & Sons.

Fischer, L., Klinger, A., Herbig, J., Winkler, K., Gutmann, R., and Hansel, A. (2013). In: Proceedings of the 6th International Conference on Proton Transfer Reaction Mass Spectrometry and its Applications) 192–194.

González-Méndez, R., Watts, P., Fraser Reich, D., Mullock, S. J., Cairns, S., Hickey, P., et al. (2018). Use of rapid reduced electric field switching to enhance compound specificity for proton transfer reaction-mass spectrometry. *Anal. Chem.* 90, 5664–5670. doi: 10.1021/acs.analchem.7b05211

González-Méndez, R., Watts, P., Olivenza Leon, D., Reich, D. F., and Mullock, S. J., Corlett, et al. (2016). Enhancement of compound selectivity using a radio frequency ion-funnel proton transfer reaction mass spectrometer: improved specificity for explosive compounds. *Anal. Chem.* 88, 10624–10630. doi: 10.1021/acs.analchem.6b02982

Graus, M., Müller, M., and Hansel, A. (2010). High resolution PTR-TOF: quantification and formula confirmation of VOC in real time. *J. Am. Soc. Mass Spectrom.* 21, 1037–1044. doi: 10.1016/j.jasms.2010.02.006

Jordan, A., Haidacher, S., Hanel, G., Hartungen, E., Märk, L., Seehauser, H., et al. (2009). An online ultra-high sensitivity Proton-transfer-reaction mass-spectrometer combined with switchable reagent ion capability (PTR + SRI – MS). *Int. J. Mass Spectrom.* 286, 32–38. doi: 10.1016/j.ijms.2009.06.006

Jürschik, S., Agarwal, B., Kassebacher, T., Sulzer, P., Mayhew, C. A., and Märk, T. D. (2012). Rapid and facile detection of four "date rape drugs" in different beverages utilizing Proton-Transfer-Reaction Mass Spectrometry (PTR-MS). *J. Mass Spectrom.* 47, 1092–1097. doi: 10.1002/jms.2993

Kari, E., Miettinen, P., Yli-Pirilä, P., Virtanen, A., and Faiol, C. L. (2018). PTR-ToF-MS product ion distributions and humidity-dependence of biogenic volatile organic compounds. *Int. J. Mass Spectrom.* 430, 87–97. doi: 10.1016/j.ijms.2018.05.003

Lanza, M., Acton, W. J., Jürschik, S., Sulzer, P., Breiev, K., Jordan, A., et al. (2013). Distinguishing two isomeric mephedrone substitutes with selective reagent ionisation mass spectrometry (SRI-MS). *J. Mass Spectrom.* 48, 1015–1018. doi: 10.1002/jms.3253

Lanza, M., Acton, W. J., Sulzer, P., Breiev, K., Jürschik, S., Jordan, A., et al. (2015). Selective reagent ionisation-time of flight-mass spectrometry: a rapid technology for the novel analysis of blends of new psychoactive substances. *J. Mass Spectrom.* 50, 427–431. doi: 10.1002/jms.3514

Materić, D., Lanza, M., Sulzer, P., Herbig, J., Bruhn, D., Gauci, V., et al. (2017). Selective reagent ion-time of flight-mass spectrometry study of six common monoterpenes. *Int. J. Mass Spectrom.* 421, 40–50. doi: 10.1016/j.ijms.2017.06.003

Mayhew, C. A., Sulzer, P., Petersson, F., Haidacher, S., Jordan, A., Märk, L., et al. (2010). Applications of proton transfer reaction time-of-flight mass spectrometry for the sensitive and rapid real-time detection of solid high explosives. *Int. J. Mass Spectrom.* 289, 58–63. doi: 10.1016/j.ijms.2009.09.006

Pan, Y., Zhang, Q., Zhou, W., Zou, X., Wang, H., Huang, C., et al. (2017). Detection of ketones by a novel technology: dipolar proton transfer reaction mass spectrometry (DP-PTR-MS). *J. Am. Soc. Mass Spectrom.* 28, 873–879. doi: 10.1007/s13361-017-1638-7

Petersson, F., Sulzer, P., Mayhew, C. A., Watts, P., Jordan, A., Märk, L., et al. (2009). Real-time trace detection and identification of chemical warfare agent simulants using recent advances in proton transfer reaction time-of-flight mass spectrometry. *Rapid Commun. Mass Spectrom.* 23, 3875–3880. doi: 10.1002/rcm.4334

Romano, A., Fischer, L., Herbig, J., Campbell-Sills, H., Coulon, J., Lucas, P., et al. (2014). Wine analysis by FastGC proton-transfer reaction-time-of-flight-mass spectrometry. *Int. J. Mass Spectrom.* 369, 81–86. doi: 10.1016/j.ijms.2014.06.006

Ruzsanyi, V., Fischer, L., Herbig, J., Ager, C., and Amann, A. (2013). Multi-capillary-column proton-transfer-reaction time-of-flight mass spectrometry. *J. Chromatogr. A* 1316, 112–118. doi: 10.1016/j.chroma.2013.09.072

Schwartz, K., Filipiak, W., and Amann, A. (2009). Determining concentration patterns of volatile compounds in exhaled breath by PTR-MS. *J. Breath Res.* 3:027002. doi: 10.1088/1752-7155/3/2/027002

Smith, D., Spanel, P., and Dryahina, K. (2019). H_3O^+, NO^+ and $O_2^{+\cdot}$ reactions with saturated and unsaturated monoketones and diones; focus on hydration of product ions. *Int. J. Mass Spectrom.* 435, 173–180. doi: 10.1016/j.ijms.2018.10.027

Smith, D., Wang, T., and Spanel, P. (2003). Analysis of ketones by selected ion flow tube mass spectrometry. *Rapid Comm. Mass Spectrom.* 17, 2655–2660. doi: 10.1002/rcm.1244

Spanel, P., Ji, Y., and Smith, D. (1997). SIFT studies of the reactions of H_3O^+, NO^+ and $O_2^{+\cdot}$ with a series of aldehydes and ketones. *Int. J. Mass Spectrom.* 165/166, 25–37. doi: 10.1016/S0168-1176(97)00166-3

Specyvyi, A., Smith, D., and Spanel, P. (2017). Ion chemistry at elevated ion–molecule interaction energies in a selected ion flow-drift tube: reactions of H_3O^+, NO^+ and $O_2^{+\cdot}$ with saturated aliphatic ketones. *Phys. Chem. Chem. Phys.* 19, 31714–31723. doi: 10.1039/C7CP05795D

Sulzer, P., Agarwal, B., Jürschik, S., Lanza, M., and Jordan, A., Hartungen, et al. (2013). Applications of switching reagent ions in proton transfer reaction mass spectrometric instruments for the improved selectivity of explosive compounds. *Int. J. Mass Spectrom.* 354–355, 123–128. doi: 10.1016/j.ijms.2013.05.004

Sulzer, P., Petersson, F., Agarwal, B., Becker, K. H., Jürschik, S., Märk, T. D., et al. (2012). Proton transfer reaction mass spectrometry and the unambiguous real-time detection of 2,4,6 TNT. *Anal. Chem.* 84, 4161–4166. doi: 10.1021/ac3004456

Tani, A., Hayward, S., Hansel, A., Hewitt, C. N. (2004). Effect of water vapour pressure on monoterpene measurements using proton transfer reaction-mass spectrometry (PTR-MS). *Int. J. Mass Spectrom.* 239, 161–169. doi: 10.1016/j.ijms.2004.07.020

Tani, A., Hayward, S., and Hewitt, C. N. (2003). Measurement of monoterpenes and related compounds by proton transfer reaction-mass spectrometry (PTR-MS). *Int. J. Mass Spectrom.* 223–224, 561–578. doi: 10.1016/S1387-3806(02)00880-1

Trefz, P., Schubert, J. K., and Miekisch, W. (2018). Effects of humidity, CO_2 and O_2 on real-time quantitation of breath biomarkers by means of PTR-ToF-MS. *J. Breath Res.* 12:026016. doi: 10.1088/1752-7163/aa9eea

Warneke, C., Van Der Veen, C., Luxembourg, S., De Gouw, J. A., and Kok, A. (2001). Measurements of benzene and toluene in ambient air using proton-transfer-reaction mass spectrometry: calibration, humidity dependence, and field intercomparison. *Int. J. Mass Spectrom.* 207:167. doi: 10.1016/S1387-3806(01)00366-9

Conflict of Interest Statement: FP and TDM was employed by company IONICON Analytik Gesellschaft m.b.H.

The remaining authors declare that the research was conducted in the absence of any commercial or financial relationships that could be construed as a potential conflict of interest.

J. Am. Soc. Mass Spectrom. (2019)
DOI: 10.1007/s13361-019-02325-0

RESEARCH ARTICLE

Selective Reagent Ion Mass Spectrometric Investigations of the Nitroanilines

David Olivenza-León,[1] Chris A. Mayhew,[1,2] Ramón González-Méndez[1,3]

[1]Molecular Physics Group, School of Physics and Astronomy, University of Birmingham, Edgbaston, Birmingham, B15 2TT, UK
[2]Institut für Atemgasanalytik, Leopold-Franzens-Universität Innsbruck, Rathausplatz 4, 6850, Dornbirn, Austria
[3]Centre for Agroecology, Water and Resilience, Coventry University, Coventry, CV1 5FB, UK

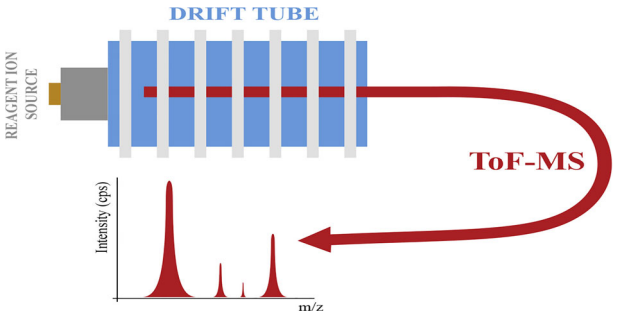

Abstract. This paper presents an investigation of proton and charge transfer reactions to 2-, 3- and 4-nitroanilines ($C_6H_6N_2O_2$) involving the reagent ions $H_3O^+ \cdot (H_2O)_n$ ($n = 0$, 1 and 2) and O_2^+, respectively, as a function of reduced electric field (60–240 Td), using Selective Reagent Ion–Time-of-Flight–Mass Spectrometry (SRI–ToF–MS). To aid in the interpretation of the $H_3O^+ \cdot (H_2O)_n$ experimental data, the proton affinities and gas-phase basicities for the three nitroaniline isomers have been determined using density functional theory. These calculations show that proton transfer from both the H_3O^+ and $H_3O^+ \cdot H_2O$ reagent ions to the nitroanilines will be exoergic and hence efficient, with the reactions proceeding at the collisional rate. For proton transfer from H_3O^+ to the NO_2 sites, the exoergicities are 171 kJ mol^{-1} (1.8 eV), 147 kJ mol^{-1} (1.5 eV) and 194 kJ mol^{-1} (2.0 eV) for 2-, 3- and 4-nitroanilines, respectively. Electron transfer from all three of the nitroanilines is also significantly exothermic by approximately 4 eV. Although a substantial transfer of energy occurs during the ion/molecule reactions, the processes are found to predominantly proceed via non-dissociative pathways over a large reduced electric field range. Only at relatively high reduced electric fields (> 180 Td) is dissociative proton and charge transfer observed. Differences in fragment product ions and their intensities provide a means to distinguish the isomers, with proton transfer distinguishing 2-nitroaniline (2–NA) from 3- and 4-NA, and charge transfer distinguishing 4-NA from 2- and 3-NA, thereby providing a means to enhance selectivity using SRI–ToF–MS.

Keywords: Soft chemical i-mass spectrometry, Proton transfer reaction mass spectrometry, Nitroanilines, Explosives, Charge transfer

Received: 22 June 2019/Revised: 14 August 2019/Accepted: 15 August 2019

Introduction

Selective Reagent Ion–Mass Spectrometry (SRI–MS) is a commonly used soft chemical ionisation technique used in a broad range of analytical fields and applications [1, 2]. These include environmental analysis, food science, atmospheric chemistry, health science, homeland security and breath analysis [3–12]. Its analytical technique is based on ion/molecule reactions in a controlled environment, namely a drift tube maintained at a constant pressure, temperature, humidity and fixed electric field. Commonly used reagent ions are H_3O^+ and O_2^+, which react with traces of neutral organic molecules, injected directly into the drift tube of the instrument, usually with no pre-separation step. This allows for real-time analysis with a time resolution of approx.

Research highlights
- First investigations on the use of selective reagent ion mass spectrometry for nitroaniline isomers involving proton transfer and charge transfer reactions as a function of reduced electric field
- DFT calculations of the proton affinities and gas-phase basicities of the nitroanilines
- Identification of individual isomers through the manipulation of the ion chemistry

Correspondence to: Ramón González–Méndez;
e-mail: R.GonzalezMendez@bham.ac.uk;
Ramon.Gonzalez-Mendez@coventry.ac.uk

Published online: 09 September 2019

100 ms. These attributes make SRI–MS an ideal technique for detecting compounds that are only transiently (seconds) present in the drift tube. When H_3O^+ is only used as the reagent ion, the technique is better known as Proton Transfer Reaction–Mass Spectrometry (PTR–MS) [1]. In this study, we investigated reactions involving both O_2^+ and H_3O^+, and hence, the term SRI–MS is more appropriate for the work presented here.

During the last 10 years, a large amount of work exploring the capabilities of SRI–MS for Homeland Security has been undertaken [3–5, 13–22]. Two key objectives of this work are the following: (i) instrumental development for enhancing SRI–MS analytical performance (such as use of different reagent ions [16], new sample inlet methods [13], use of ion funnel for either enhanced sensitivity or selectivity [18, 23] and fast reduced electric field switching for enhanced selectivity [20]) and (ii) improving our knowledge of the underlying ion/molecule chemistry occurring within the reagent region of the analytical device.

A limitation with the selectivity of SRI–MS is associated with its capability to distinguish isomers. This is particularly true for proton transfer reactions, where often only the protonated parent[1] is observed, but not necessarily so for other reaction processes such as charge transfer [24]. Here we present a SRI–MS study of the isomers of nitroanilines (2-, 3- and 4-nitroaniline) to ascertain whether they can be distinguished through the manipulation of the ion/chemistry. Another motivation for this study is that nitroanilines exhibit certain explosive characteristics, owing to their structure (aromatic ring with nitro functional group substituents). Therefore, these compounds represent a natural continuation of our SRI–MS studies of explosive compounds [3–5, 13, 15–22].

An additional interest is that nitroanilines are a family of chemical compounds used in the manufacture of dyes, pharmaceuticals and pesticides [25], so it is important to characterise them from a quality control need as different isomers have different properties and reactivities. They also exhibit a high toxicity, particularly the [1, 4] isomer [26], so it is relevant to develop analytical methods for quick, selective and reliable identification for environmental purposes.

Nitroanilines ($C_6H_6N_2O_2$, m/z 138.04 Da (lightest isotopologue)) are a derivative of aniline, a commonly used precursor in the polymer industry, and hence is widespread in the environment [27]. Here we investigate whether the position of the nitro group plays a role in the ion/molecule processes. We present details on the product ion distributions resulting from the reactions of H_3O^+ and O_2^+. To aid in the interpretation of the experimental measurements involving the reagent ions $H_3O^+(H_2O)_n$ ($n = 0$, 1 and 2), quantum mechanical calculations have been undertaken to determine proton affinities and gas-phase basicities.

[1]Although revised IUPAC recommendations for terminology in mass spectrometry (Pure Appl. Chem., 2013, Vol. 85, No. 7, pp. 1515–1609) suggest replacing the term "parent" with "precursor", since for this work, ions are not mass selected, the term "precursor" is not appropriate. We note that "protonated parent" is commonly used within the PTR–MS community [1].

Experimental Details

SRI–MS

For this investigation, a Kore Technology Ltd. Series I Selective Reagent Ion–Time of Flight–Mass Spectrometer (SRI–ToF–MS) instrument was used, details of which been given elsewhere [1, 28], and therefore only brief and pertinent details will be presented in this paper.

Proton Transfer Reaction Mode This mode exploits the proton transfer reaction of H_3O^+ and, depending on the reduced electric field (the ratio of the electric field strength (E) to the gas number density (N)) applied in the drift tube and the humidity, also protonated water clusters with molecules of interest M:

$$H_3O^+ \cdot (H_2O)_n + M \rightarrow MH^+ + (n+1)H_2O \quad (1)$$

where $n = 0$, 1 and 2 are the most important for our operational conditions (see Figure 1) but also (in low concentrations and only at low E/N (less than approximately 100 Td (1 Td = 10^{-17} V cm^2)) $n = 3$. Proton transfer can be either non-dissociative or spontaneously dissociative. Following non-dissociative proton transfer, collisional induced dissociation may occur, with the probability of this increasing with increasing reduced electric field.

To produce the reagent ions, a series of ion-molecule processes (including three-body association) take place in a hollow cathode glow discharge, initiated by an electric discharge in water vapour and associated drift tube buffer gas that has diffused back into the ionisation source. The reagent ions that are generated in the ion source region are transferred into the drift tube by an applied voltage gradient. The relative intensities of the water reagent ions in the drift tube of the KORE instrument used as a function of E/N are summarised in Figure 1, which illustrates that under our operating conditions,

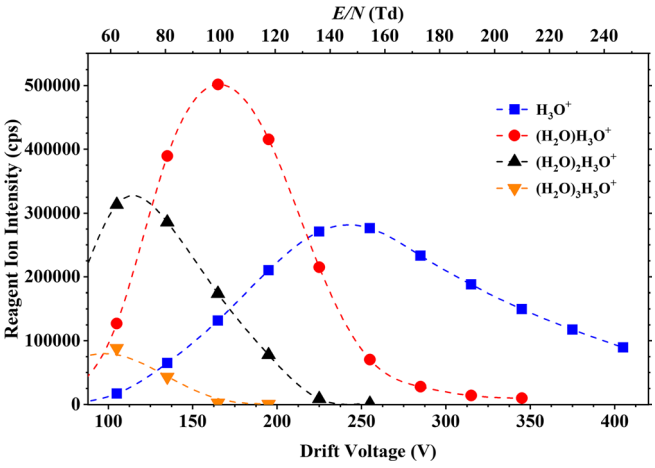

Figure 1. Ion intensities in counts per second (cps) of the water reagent ions ($H_3O^+ \cdot (H_2O)n$, n = 0, 1, 2 and 3) recorded at the detector of the KORE SRI–ToF–MS as a function of reduced electric field (approximately 60–250 Td)

only at relatively high *E/N* values (greater than 140 Td) does H_3O^+ become the dominant reagent ion.

Although H_3O^+ (and associated protonated water clusters—depending on the value of the reduced electric field) dominates the reagent ion signal, other reagent ions are always present in the drift tube. These "impurity" reagent ions result from back diffusion of the buffer gas in the drift tube into the ion source. These reagent ions are those that cannot react with water, such as O_2^+. However, these are at very low concentrations. Under our experimental conditions, the intensity of was O_2^+ was maintained below 0.5% of that of the H_3O^+ signal.

The signal intensity of $H_3{}^{16}O^+$ is generally too large to be measured directly. Therefore, the signal intensity for the spectral line peaking at *m/z* 21.02, corresponding to $H_3{}^{18}O^+$, was recorded. The *m/z* 19.02 intensity, corresponding to $H_3{}^{16}O^+$, was determined in the normal manner by multiplying the *m/z* 21.02 signal by 487. Similarly, the *m/z* 37.03 signal intensity, corresponding to $H_3{}^{16}O^+{\cdot}H_2{}^{16}O$, was not measured directly. Instead, the signal intensity at *m/z* 39.03 ($H_3{}^{18}O^+{\cdot}H_2{}^{16}O$ or $H_3{}^{16}O^+{\cdot}H_2{}^{18}O$) was recorded and multiplied by 243.

Charge Transfer Reaction Mode For the production of O_2^+, pure oxygen (99.998% purity, BOC Gases, Manchester, UK) was flowed into the ion source. This leads to the formation of mainly O_2^+ reagent ions (> 95%). Figure 2 shows the O_2^+ ion signal intensity in counts per second (cps) as a function of *E/N*. Once injected into the drift tube, O_2^+ may react with the analyte M via charge transfer, provided that the ionisation energy (IE) of M is less than that of O_2 (IE (O_2) = 12.07 eV). Unlike proton transfer, an exothermic reaction is a necessary but not sufficient criterion for charge transfer to occur, and hence, the reaction rate coefficient may not necessarily be collisional [29]. However, if charge transfer does occur, it may also be either non-dissociative (resulting in the singly charged parent ion (M^+)) or dissociative. Fragmentation might be spontaneous upon charge transfer or require additional energy through collisions in the drift tube. H_3O^+ is also observed when operating the ion source in oxygen mode. This is due to residual water vapour in the system. However, this can be ignored owing to its signal intensity being approximately 0.1% of the O_2^+ signal for the experimental conditions used throughout our measurements.

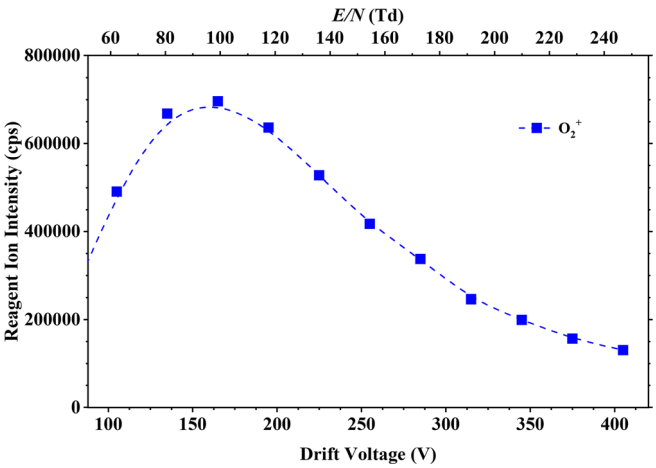

Figure 2. Ion intensities in counts per second (cps) of O_2^+ recorded at the detector of the KORE SRI–ToF–MS as a function of reduced electric field (approximately 60–250 Td)

Operational Procedures

Liquid samples were vapourised making use of a thermal desorption unit (TDU), connected to the inlet of the drift tube via passivated stainless steel (Silconert®). Details of the TDU have been given elsewhere [13]. The TDU, connecting lines and drift tube were operated at a temperature of 150 °C. For this study, oxygen-free nitrogen (99.998% purity, BOC Gases, Manchester, UK) was used as the carrier gas. PTFE swabs (Thermo Fisher Scientific, Cheshire, UK), onto which known quantities of the sample had been deposited, were manually placed into the TDU. Upon closure of the TDU unit, a high force annular "anvil" compressed the PTFE to plastically deform and convert it into a gas tight circular seal around the rim of the swab. At the same time, laboratory air heated to a specified temperature rapidly heats the PTFE and as it passes through carries any thermally desorbed material into the heated inlet line through to the drift (reaction) region. The temporal desorption profile is typically between 10 and 20 s [13]. For each measurement, one swab was used, which was replicated three times. The results were then averaged, and any background signals were subtracted.

The drift tube pressure was set at 1 mbar, and the glow discharge (for both water vapour and oxygen) was set at 1.4 mbar. The only variable was the operating drift tube voltage, which was adjusted over a range of approximately 100 to 400 V to provide an appropriate reduced electric field range of about 60–250 Td.

Chemicals

Individual nitroaniline (2-, 3- and 4-) isomers for this study were purchased from Sigma Aldrich (Cheshire, UK), all of which came with stated purities of at least 98%. At room temperature, nitroanilines are yellowish-orange granulated solids. For the measurements, granules were dissolved in a mixture of MeOH:AcN 1:1 (V/V) (analytical grade) to provide a concentration of approx. 100 µg/mL. A volume of 1 µL of this solution was deposited onto the swab and left the solvents to evaporate at room temperature for approximately 1 min before placing the swab into the TDU.

DFT Calculations

Density functional theory (DFT) calculations have been undertaken to determine the proton affinities and gas-phase basicities of the water monomer, dimer and trimer and the three nitroanilines. These calculations were conducted using Gaussian09W and GaussView05 for Windows [30]. The B3LYP functional with the 6-31+G(d,p) basis set was used throughout, a combination which has been found to be satisfactory based on our previous work [31, 32].

Results

For this section, only product ions with branching percentages greater than 1% for any given reduced electric field value are reported. The uncertainty in any branching percentage is approximately 10%. In all cases, only the mass to charge ratio of the lightest isotope is given. However, when calculating the product ion distributions, we considered all of the isotopologues. For the product ion distribution (PID) plots (branching percentages), the voltage applied to the drift tube is shown in the main *x*-axis, and the reduced electric field *E*/*N* achieved for that particular voltage is showed in the secondary *x*-axis.

DFT Calculations

Table 1 presents the calculated proton affinities (PA) and gas-phase basicities (GB) for the water monomer, the water dimer, the water trimer and the three nitroanilines. For the nitroaniline isomers, values are provided for the two possible protonation sites, namely on the amino and nitro groups. Aniline and nitrobenzene are also shown for comparison. Table 1 also provides for convenience the ionisation energies of oxygen and the nitroanilines [33].

The proton affinities of the water dimer and trimer are higher than that of the monomer, because of the added stability by sharing the proton with additional waters. The proton affinity of water clusters increases as the number of water molecules increases, but the incremental effect declines as the cluster grows as illustrated in the DFT calculations.

As shown in Table 1, whilst for simpler chemical structures as aniline and nitrobenzene, the aniline's NH_2 substituent is much more basic than the NO_2 of nitrobenzene, this is not the case in the nitroanilines where both groups are on the ring. The interaction of the nitro group (electron withdrawing effect from the aromatic ring) and the amine group (electron donating effect to the aromatic ring) reverse their basicities, in the order 4-nitroaniline (4-NA) > 2-NA > 3-NA. Based on this data, with the exception of the 2-NA where the groups are in close proximity, it is likely that the $NA{\cdot}H^+$ for the 3 and 4 isomers is a mixture of species.

The DFT calculations show that proton transfer from $H_3O^+{\cdot}(H_2O)_n$ ($n = 0$ and 1) to both sites of all three of the nitroanilines is exoergic. $H_3O^+{\cdot}(H_2O)_2$ can also proton transfer to the NO_2 site of 4-NA.

Fragmentation Patterns and Branching Ratios Studies for Reactions with H_3O^+

2-Nitroaniline Figure 3 shows the product ion distribution (PID) plot for 2-nitroaniline resulting reactions with $H_3O^+{\cdot}(H_2O)_n$ ($n = 0$ and 1) (see Figure 1) as a function of *E*/*N* over the range from 60 to 250 Td. The protonated parent, $[2\text{-}NA{\cdot}H]^+$, at *m*/*z* 139.05 is the most intense product ion until about 220 Td, after which fragment product ions dominate. Fragment product ions begin to appear at about 150 Td, starting with at *m*/*z* 121.04 (resulting from the loss of a water molecule from the protonated parent, $[2\text{-}NA\text{-}H_2O]H^+$), and which becomes dominant above about 220 Td. Other fragment product ions are observed with increasing *E*/*N*, namely *m*/*z* 93.06 (assigned to the loss of a nitro group from the protonated parent, leading to a $C_6H_7N^+$ ion) and *m*/*z* 91.04 (caused by the loss of a nitro group followed by the sequential loss of a hydrogen molecule, leading to a $C_6H_5N^+$ ion). At low reduced electric fields (less than about 120 Td), a product ion is observed at *m*/*z* 157.06, which is simply $2\text{-}NAH^+{\cdot}H_2O$, resulting from a third body association reaction of the protonated parent with water. Its intensity increases as the *E*/*N* decreases because of reduced collisional induced dissociation.

Figure 4 shows two overlaid mass spectra at two different *E*/*N* values for 2-nitroaniline, exemplifying the difference in performance for the instrument—similar plots (not shown) were found for the rest of the samples and for oxygen chemistry.

3-Nitroaniline Figure 5 shows the PID plot for 3-nitroaniline resulting from its reaction with $H_3O^+{\cdot}(H_2O)_n$

Table 1. Proton Affinities (PA), Gas-Phase Basicities (GB) and Ionisation Energies (IE) for Nitroaniline (NA) Isomers. The PA and GB Values Have Been Calculated Using the B3LYP Functional and the 6-31+G(d,p) Basis Set at 298 K. ΔH_{298} and ΔG_{298} Refer to the Enthalpies and Free Energies for the Addition of Water to the Protonated Species. For Convenience, the Ionisation Energies of O_2 and the Three Nitroanilines Are Also Provided

Chemical	Site	PA[a]	GB[a]	ΔH_{298}[a]	ΔG_{298}[a]	IE (eV)[b]
Water		684	653			
Water dimer		842	777			
Water trimer		937	841			
O_2						12.07 [34]
2-NA	NH_2	840	806	−69	−37	8.27
	NO_2	858	824	−76	−43	
3-NA	NH_2	824	796	−78	−43	8.31
	NO_2	830	800	−84	−51	
4-NA	NH_2	810	784	−78	−43	8.34
	NO_2	879	847	−73	−39	
Aniline	NH_2	874	846	−72	−40	
Nitrobenzene	NO_2	806	775	−90	−55	

[a]Thermochemical data expressed in kilojoules per mole
[b]Ionisation energies (in eV) have been taken from NIST database [33]

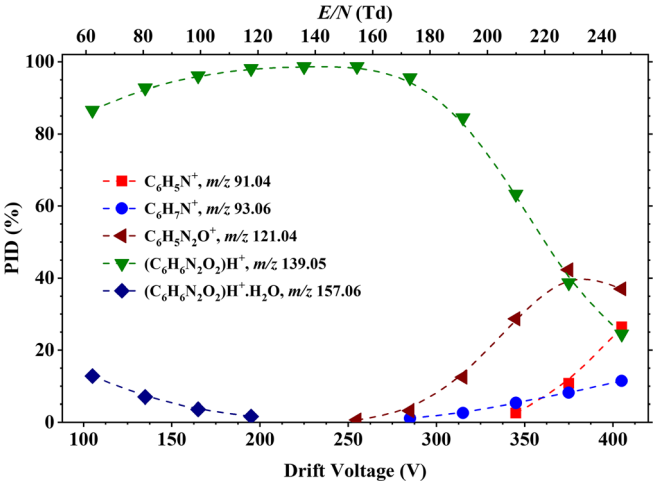

Figure 3. Percentage product ion distribution (PID in %) resulting from the reaction of 2-nitroaniline with $H_3O^+ \cdot (H_2O)_n$ ($n = 0$ and 1) as a function of the reduced electric field from 60 to 250 Td

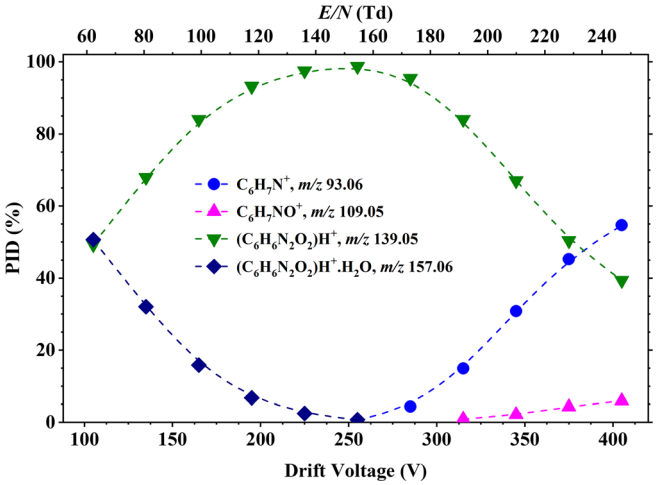

Figure 5. Percentage product ion distribution resulting from the reaction of 3-nitroaniline with $H_3O^+ \cdot (H_2O)_n$ ($n = 0$ and 1) as a function of the reduced electric field from 60 to 250 Td

($n = 0$ and 1) as a function of the reduced electric field E/N for the range from 20 to 250 Td. Similar to the results obtained for 2-NA, the protonated parent [3-NA·H]+ is the dominant product ion up to about 220 Td. However, unlike 2-NA, much more association of the protonated parent with water is observed at low reduced electric fields (< 140 Td), under identical operational (reduced electric field and humidity) conditions. At 60 Td, $3\text{-NAH}^+ \cdot H_2O$ has approximately the same branching percentage as the protonated parent.

Above ca. 230 Td, the fragment product ion $C_6H_7N^+$ dominates. Another product ion, starting at an E/N value of approximately 190 Td, is observed at m/z 109.05. This is considered to result from the loss of NO from the protonated parent leading to $C_6H_7NO^+$ [35]. This product ion was not observed for 2-nitroaniline.

4-Nitroaniline Figure 6 presents the PID for the reaction of 4-nitroaniline with $H_3O^+ \cdot (H_2O)_n$ ($n = 0$ and 1) as a function of the reduced electric field E/N for the range from 60 to 250 Td. For this isomer, the protonated parent, $[4\text{-NA}\cdot H]^+$, dominates throughout the whole E/N range. Little fragmentation occurs, with only one product ion being observed at m/z 93.06 (corresponding to the loss of a nitro group from the protonated parent molecule) above about 160 Td. Three-body association of the protonated parent with water is also observed at m/z 157.06, with a similar intensity to that found for 2-NA.

Thus, we find that protonated 3-NA solvates more readily than do protonated 2-NA and 4-NA, and this merits some discussion. Table 1 shows that the ΔG_{298} for the association of water to protonated 2 and 4-NA is 43 kJ mol^{-1}, whereas the ΔG_{298} for association of water to protonated 3-NA is 51 kJ mol^{-1}. Whilst 8 kJ mol^{-1} may not seem a great difference, when converted into equilibrium constants, at the operating

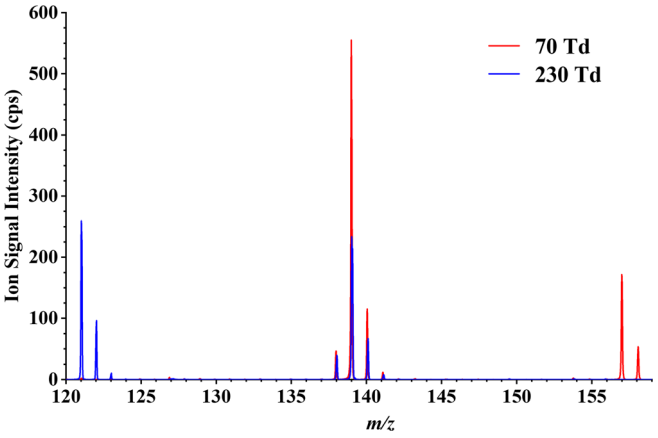

Figure 4. Overlaid mass spectra for 2-nitroaniline at 70 and 230 Td. This figure illustrates the clear difference in ion signal intensities for m/z 121.04, 139.05 and 157.06 upon the reduced electric field applied to the DT of the instrument

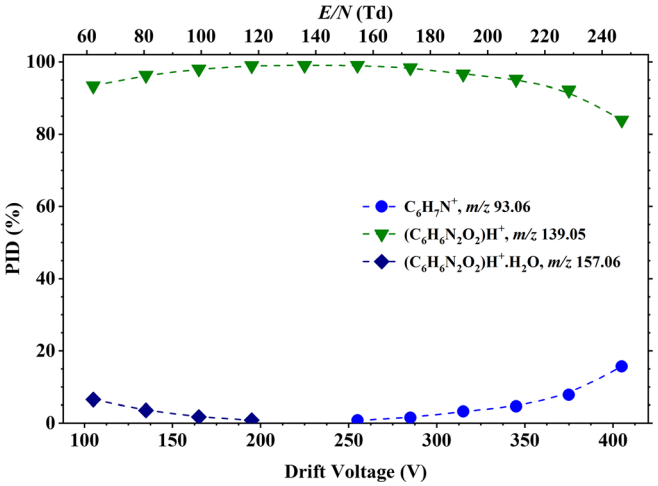

Figure 6. Percentage product ion distribution resulting from the reaction of 4-nitroaniline with $H_3O^+ \cdot (H_2O)_n$ ($n = 0$, 1 and 2) as a function of the reduced electric field from 60 to 250 Td

temperature of the drift tube (423 K), 3-NAH^+ binds water approximately ten times better than 2-NAH^+ and 4-NAH^+.

In comparison to the product ion fragmentation patterns found for 2- and 3-NA, the 4-NA isomer is quite different. This is a direct effect of the *para* position for the functional groups in the aromatic ring. The amine and nitro substituents are far off from each other, and therefore, there is no option for an intermediate transition state where a ring is formed prior to leading to the final product ion. This is consistent with chemical ionisation work reported for the nitroarenes with electron-releasing substituents [36].

Fragmentation Patterns and Branching Percentage Studies for Reactions with O_2^+

2-Nitroaniline Figure 7 presents a summary of the results for the reaction of O_2^+ with 2-NA as a function of reduced electric field. The parent ion at *m/z* 138.04, $[2\text{-NA}]^+$, resulting from non-dissociative charge transfer, dominates up to about 230 Td. Its abundance decreases as the reduced electric field increases, and at *E/N*, above ca. 230 Td, *m/z* 80.05 (assigned to the product ion $C_5H_6N^+$) becomes dominant. Other product ions, resulting from dissociative charge transfer, are observed at *m/z* 65.04 ($C_5H_5^+$), *m/z* 92.07 ($C_6H_6N^+$) (loss of NO_2), *m/z* 108.04 ($C_6H_6NO^+$) (loss of NO) and *m/z* 121.04 ($C_6H_5N_2O^+$) (loss of OH). $C_6H_5N_2O^+$ was not observed in any of the other isomers.

3-Nitroaniline For 3-NA, a very similar fragmentation product ion pattern found for that of 2-NA is observed, as shown in Figure 8. Products ions are observed at *m/z* 65.04 ($C_5H_5^+$), 80.05 ($C_5H_6N^+$), *m/z* 92.07 ($C_6H_6N^+$), *m/z* 108.04 ($C_6H_6NO^+$) and *m/z* 138.04, $[3\text{-NA}]^+$, but with slight differences in their intensities at very high *E/N* values. For 3-NA, the parent ion at *m/z* 138.04, $[3\text{-NA}]^+$ dominates for most of the reduced electric field investigated. But by about 240 *m/z*, 80.05 ($C_5H_6N^+$) becomes dominant. A clear difference is the intensity for the product ion at *m/z* 92.05 ($C_6H_6N^+$), going up to ca. 15% (compared to only ca. 5% for 2-NA) and at *m/z* 65.04 ($C_5H_5^+$) (ca. 12% for 3-NA compared to ca. 6% for 2-NA).

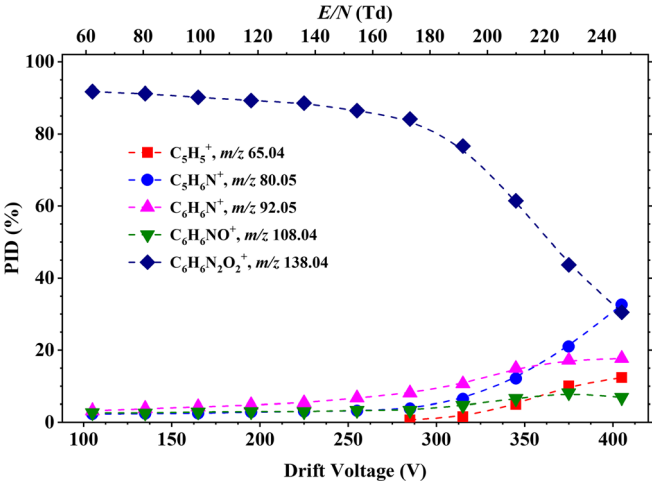

Figure 8. Percentage product ion distribution resulting from the reaction of 3-nitroaniline with O_2^+ as a function of the reduced electric field in the range from 60 to 250 Td

4-Nitroaniline The product ion fragmentation pattern for 4-NA, as shown in Figure 9, is very different from that observed for the other two isomers, with a simpler product ion distribution being observed, having only three product ions. This is a direct consequence of the *para* position for the substituents in the aromatic ring. The parent ion at *m/z* 138.04, $[4\text{-NA}]^+$, dominates from 60 Td up to ca. 190 Td, after which the product ion at *m/z* 108.04 ($C_6H_6NO^+$) becomes dominant. For *E/N* values above 190 Td, another fragment ion at *m/z* 80.05 ($C_5H_6N^+$) becomes relevant, having a maximum intensity of ca. 30% at an *E/N* value of 250 Td.

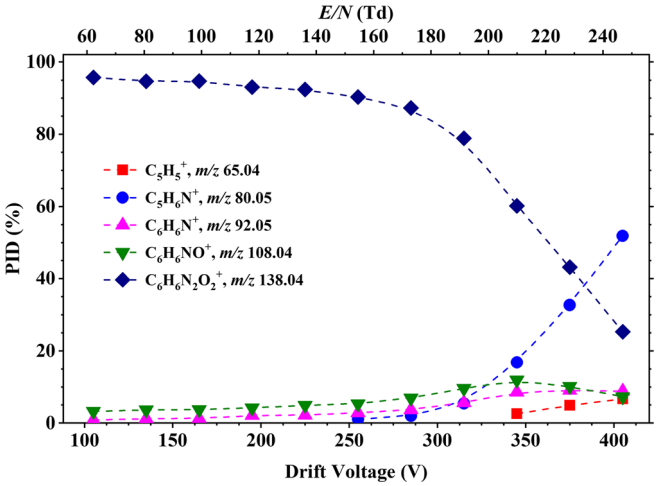

Figure 7. Percentage product ion distribution resulting from the reaction of 2-nitroaniline with O_2^+ as a function of the reduced electric field from 60 to 250 Td

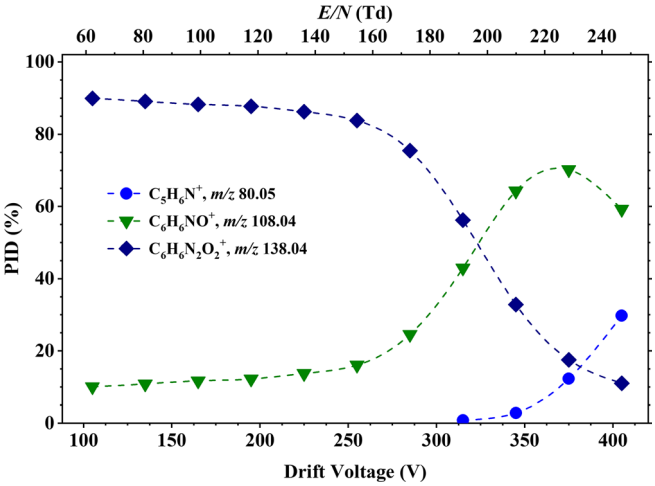

Figure 9. Percentage product ion distribution resulting from the reaction of 4-nitroaniline with O_2^+ as a function of the reduced electric field in the range from 60 to 250 Td

Conclusions

This work reports the product ions from the reaction of 2-, 3- and 4-nitroaniline isomers with H_3O^+ and O_2^+ as a function of the reduced electric field in a SRI–ToF–MS. We have shown that selective reagent ion mass spectrometry, using either water or oxygen as reagent gases, can be used to detect nitroaniline isomers with good selectivity. The most abundant product ion for all the isomers for the reactions with H_3O^+ is the protonated parent at *m/z* 139.05 over an extended reduced electric field range. For the reactions with O_2^+, non-dissociative charge transfer results in the parent ion at *m/z* 138.04 being the most abundant product ion. However, relative ion abundances are different for each reagent ion. 2- and 3-NA show very similar fragmentation patterns with O_2^+, whilst with H_3O^+, 2-NA shows smaller water clustering at low *E/N* and its fragment product ions become dominant at a lower *E/N* than found for 3-NA. 4-NA shows less fragmentation with H_3O^+, and for the reaction with O_2^+, a distinctive fragment ion is observed at *m/z* 108.04, which becomes dominant above about 190 Td. The presence or absence of this product ion at *m/z* 108.04 easily allows for reliable identification of the 4-NA isomer.

This study demonstrates how it is possible to distinguish isomers based on the manipulation of the ion/molecule chemistry and/or using different reagent ions that favour different ionisation mechanisms.

Acknowledgements

We thank the Marie Skłodowska-Curie Actions Innovative Training Network: Ion-Molecule Processes for Analytical Chemistry Technologies (IMPACT) (www.impact-h2020itn.com) which has supported this research through the European Commission's HORIZON 2020 Programme under Grant Agreement Number 674911. DOL is an Early Stage Researcher on IMPACT. We also thank Dr. Peter Watts (a member of the Molecular Physics Group, School of Physics and Astronomy, University of Birmingham, UK) for undertaking the DFT calculations presented in this paper. The authors also thank Mahroz Mirzahekmati for producing the graphical abstract.

Open Access

References

1. Ellis, A. M., Mayhew, C. A.: Proton Transfer Reaction Mass Spectrometry: Principles and Applications. 1st ed. Wiley, p 336 (2014)
2. Biasioli, F., Yeretzian, C., Märk, T.D., Dewulf, J., Van Langenhove, H.: Direct-injection mass spectrometry adds the time dimension to (B) VOC analysis. TrAC Trends Anal. Chem. **30**(7), 1003–1017 (2011)
3. Mayhew, C.A., Sulzer, P., Petersson, F., Haidacher, S., Jordan, A., Märk, L., Watts, P., Märk, T.D.: Applications of proton transfer reaction time-of-flight mass spectrometry for the sensitive and rapid real-time detection of solid high explosives. Int. J. Mass Spectrom. **289**(1), 58–63 (2010)
4. Sulzer, P., Petersson, F., Agarwal, B., Becker, K.H., Jürschik, S., Märk, T.D., Perry, D., Watts, P., Mayhew, C.A.: Proton transfer reaction mass spectrometry and the unambiguous real-time detection of 2,4,6 trinitrotoluene. Anal. Chem. **84**(9), 4161–4166 (2012)
5. Kassebacher, T., Sulzer, P., Jürschik, S., Hartungen, E., Jordan, A., Edtbauer, A., Feil, S., Hanel, G., Jaksch, S., Märk, L., Mayhew, C.A., Märk, T.D.: Investigations of chemical warfare agents and toxic industrial compounds with proton-transfer-reaction mass spectrometry for a real-time threat monitoring scenario. Rapid Commun. Mass Spectrom. **27**(2), 325–332 (2013)
6. Fernández del Río, R., O'Hara, M.E., Holt, A., Pemberton, P., Shah, T., Whitehouse, T., Mayhew, C.A.: Volatile biomarkers in breath associated with liver cirrhosis — comparisons of pre- and post-liver transplant breath samples. EBioMedicine. **2**(9), 1243–1250 (2015)
7. Trefz, P., Schubert, J.K., Miekisch, W.: Effects of humidity, CO2 and O2 on real-time quantitation of breath biomarkers by means of PTR-ToF-MS. J. Breath. Res. **12**(2), 026016 (2018)
8. Herbig, J., Beauchamp, J.: Towards standardization in the analysis of breath gas volatiles. J. Breath. Res. **8**(3), 037101 (2014)
9. Ruzsányi, V., Kalapos, M.P., Schmidl, C., Karall, D., Scholl-Bürgi, S., Baumann, M.: Breath profiles of children on ketogenic therapy. J. Breath. Res. **12**(3), 036021 (2018)
10. Agarwal, B., Petersson, F., Jürschik, S., Sulzer, P., Jordan, A., Märk, T.D., Watts, P., Mayhew, C.A.: Use of proton transfer reaction time-of-flight mass spectrometry for the analytical detection of illicit and controlled prescription drugs at room temperature via direct headspace sampling. Anal. Bioanal. Chem. **400**(8), 2631–2639 (2011)
11. Lanza, M., Acton, W.J., Sulzer, P., Breiev, K., Jürschik, S., Jordan, A., Hartungen, E., Hanel, G., Märk, L., Märk, T.D., Mayhew, C.A.: Selective reagent ionisation-time of flight-mass spectrometry: a rapid technology for the novel analysis of blends of new psychoactive substances. J. Mass Spectrom. **50**(2), 427–431 (2015)
12. Critchley, A., Elliott, T., Harrison, G., Mayhew, C., Thompson, J., Worthington, T.: The proton transfer reaction mass spectrometer and its use in medical science: applications to drug assays and the monitoring of bacteria. Int. J. Mass Spectrom. **239**(2–3), 235–241 (2004)
13. González-Méndez, R., Reich, D.F., Mullock, S.J., Corlett, C.A., Mayhew, C.A.: Development and use of a thermal desorption unit and proton transfer reaction mass spectrometry for trace explosive detection: determination of the instrumental limits of detection and an investigation of memory effects. Int. J. Mass Spectrom. **385**, 13–18 (2015)
14. Shen, C., Li, J., Han, H., Wang, H., Jiang, H., Chu, Y.: Triacetone triperoxide detection using low reduced-field proton transfer reaction mass spectrometer. Int. J. Mass Spectrom. **285**(1–2), 100–103 (2009)
15. Jürschik, S., Sulzer, P., Petersson, F., Mayhew, C.A., Jordan, A., Agarwal, B., Haidacher, S., Seehauser, H., Becker, K., Märk, T.D.: Proton transfer reaction mass spectrometry for the sensitive and rapid real-time detection of solid high explosives in air and water. Anal. Bioanal. Chem. **398**(7–8), 2813–2820 (2010)
16. Sulzer, P., Agarwal, B., Jürschik, S., Lanza, M., Jordan, A., Hartungen, E., Hanel, G., Märk, L., Märk, T.D., González-Méndez, R., Watts, P., Mayhew, C.A.: Applications of switching reagent ions in proton transfer reaction mass spectrometric instruments for the improved selectivity of explosive compounds. Int. J. Mass Spectrom. **354–355**(0), 123–128 (2013)
17. Agarwal, B., González-Méndez, R., Lanza, M., Sulzer, P., Märk, T.D., Thomas, N., Mayhew, C.A.: Sensitivity and selectivity of switchable reagent ion soft chemical ionization mass spectrometry for the detection of picric acid. J. Phys. Chem. A. **118**(37), 8229–8236 (2014)
18. González-Méndez, R., Watts, P., Olivenza-León, D., Reich, D.F., Mullock, S.J., Corlett, C.A., Cairns, S., Hickey, P., Brookes, M., Mayhew, C.A.: Enhancement of compound selectivity using a radio frequency ion-funnel proton transfer reaction mass spectrometer: improved specificity for explosive compounds. Anal. Chem. **88**(21), 10624–10630 (2016)

19. González-Méndez, R.: Development and Applications of Proton Transfer Reaction-Mass Spectrometry for Homeland Security: Trace Detection of Explosives. PhD, University of Birmingham, (2017)
20. González-Méndez, R., Watts, P., Reich, D.F., Mullock, S.J., Cairns, S., Hickey, P., Brookes, M., Mayhew, C.A.: Use of rapid reduced electric field switching to enhance compound specificity for proton transfer reaction-mass spectrometry. Anal. Chem. **90**(9), 5664–5670 (2018)
21. Petersson, F., Sulzer, P., Mayhew, C.A., Watts, P., Jordan, A., Märk, L., Märk, T.D.: Real-time trace detection and identification of chemical warfare agent simulants using recent advances in proton transfer reaction time-of-flight mass spectrometry. Rapid Commun. Mass Spectrom. **23**(23), 3875–3880 (2009)
22. González-Méndez, R., Mayhew, C.A.: Applications of direct injection soft chemical ionisation-mass spectrometry for the detection of pre-blast smokeless powder organic additives. J. Am. Soc. Mass Spectrom. **30**(4), 615–624 (2019)
23. Barber, S., Blake, R.S., White, I.R., Monks, P.S., Reich, F., Mullock, S., Ellis, A.M.: Increased sensitivity in proton transfer reaction mass spectrometry by incorporation of a radio frequency ion funnel. Anal. Chem. **84**(12), 5387–5391 (2012)
24. Lanza, M., Acton, W.J., Jürschik, S., Sulzer, P., Breiev, K., Jordan, A., Hartungen, E., Hanel, G., Märk, L., Mayhew, C.A., Märk, T.D.: Distinguishing two isomeric mephedrone substitutes with selective reagent ionisation mass spectrometry (SRI-MS). J. Mass Spectrom. **48**(9), 1015–1018 (2013)
25. Yuan, H.; Li, D.; Liu, Y.; Xu, X.; Xiong, C.: Nitrogen-doped carbon dots from plant cytoplasm as selective and sensitive fluorescent probes for detecting p-nitroaniline in both aqueous and soil systems. Analyst. **140**(5), 1428–1431 (2015**)**
26. Lu, X., Yang, Y., Zeng, Y., Li, L., Wu, X.: Rapid and reliable determination of p-nitroaniline in wastewater by molecularly imprinted fluorescent polymeric ionic liquid microspheres. Biosens. Bioelectron. **99**, 47–55 (2018)
27. Booth, G.: Ullmann's encyclopedia of industrial chemistry. Ref. Serv. Rev. **16**(4), 31–34 (2007)
28. Blake, R.S., Monks, P.S., Ellis, A.M.: Proton-transfer reaction mass spectrometry. Chem. Rev. **109**(3), 861–896 (2009)
29. Jarvis, G., Kennedy, R., Mayhew, C., Tuckett, R.P.: Charge transfer from neutral perfluorocarbons to various cations: long-range versus short-range reaction mechanisms. Int. J. Mass Spectrom. **202**(1–3), 323–343 (2000)
30. Frisch, M.; Trucks, G.; Schlegel, H.; Scuseria, G.; Robb, M.; Cheeseman, J.; Scalmani, G.; Barone, V.; Mennucci, B.; Petersson, G.: Gaussian 09, revision A. 1. Gaussian Inc., Wallingford (2009**)**
31. González-Méndez, R., Watts, P., Howse, D.C., Procino, I., McIntyre, H., Mayhew, C.A.: Ion mobility studies on the negative ion-molecule chemistry of isoflurane and enflurane. J. Am. Soc. Mass Spectrom. **28**(5), 939–946 (2017)
32. González-Méndez, R., Watts, P., Howse, D.C., Procino, I., McIntyre, H., Mayhew, C.A.: Ion mobility studies on the negative ion-molecule chemistry of pentachloroethane. Int. J. Mass Spectrom. **417**, 16–21 (2017)
33. P.J. Linstrom, W. G. M., Eds., NIST Chemistry WebBook. (2015)
34. Tonkyn, R.G., Winniczek, J.W., White, M.G.: Rotationally resolved photoionization of O2+ near threshold. Chem. Phys. Lett. **164**(2–3), 137–142 (1989)
35. Beynon, J., Lester, G., Williams, A.: Some specific molecular rearrangements in the mass spectra of organic compounds. J. Phys. Chem. **63**(11), 1861–1868 (1959)
36. Harrison, A.G., Kallury, R.K.M.R.: Chemical ionization mass spectra of mononitroarenes. Org. Mass Spectrom. **15**(6), 284–288 (1980)

Studies pertaining to the monitoring of volatile halogenated anaesthetics in breath by proton transfer reaction mass spectrometry

Journal of Breath Research

PAPER

Studies pertaining to the monitoring of volatile halogenated anaesthetics in breath by proton transfer reaction mass spectrometry

Michaela Malásková[1], David Olivenza-León[2], Prema D Chellayah[2], Judith Martini[3], Wolfgang Lederer[3], Veronika Ruzsanyi[1], Karl Unterkofler[1,4], Paweł Mochalski[1,5], Tilmann D Märk[6], Peter Watts[2] and Chris A Mayhew[1,2,7]

[1] Institute for Breath Research, Leopold-Franzens-Universität Innsbruck, Rathausplatz 4, A 6850, Dornbirn, Austria
[2] Molecular Physics Group, School of Physics and Astronomy, University of Birmingham, Edgbaston, Birmingham, B15 2TT, United Kingdom
[3] Univ. Klinik für Anästhesie und Intensivmedizin, Medizinische Universität Innsbruck, Anichstr. 35, A-6020 Innsbruck, Austria
[4] University of Applied Sciences Vorarlberg, Hochschulstr. 1, A-6850 Dornbirn, Austria
[5] Institute of Chemistry, Jan Kochanowski University, Świętokrzyska 15G, PL-25406 Kielce, Poland
[6] Institut für Ionenphysik und Angewandte Physik, Leopold-Franzens-Universit¨at Innsbruck, Technikerstr. 25, A-6020 Innsbruck, Austria
[7] Author to whom any correspondence should be addressed.

E-mail: christopher.mayhew@uibk.ac.at

Keywords: PTR-ToF-MS, anaesthetics, halogenated ethers, pharmacokinetics, isoflurane, proton affinities, gas-phase basicities

OPEN ACCESS

RECEIVED
1 October 2019

REVISED
28 November 2019

ACCEPTED FOR PUBLICATION
3 December 2019

PUBLISHED
14 February 2020

Abstract

Post-operative isoflurane has been observed to be present in the end-tidal breath of patients who have undergone major surgery, for several weeks after the surgical procedures. A major new non-controlled, non-randomized, and open-label approved study will recruit patients undergoing various surgeries under different inhalation anaesthetics, with two key objectives, namely (1) to record the washout characteristics following surgery, and (2) to investigate the influence of a patient's health and the duration and type of surgery on elimination. In preparation for this breath study using proton transfer reaction time-of-flight mass spectrometry (PTR-TOF-MS), it is important to identify first the analytical product ions that need to be monitored and under what operating conditions. In this first paper of this new research programme, we present extensive PTR-TOF-MS studies of three major anaesthetics used worldwide, desflurane ($CF_3CHFOCHF_2$), sevoflurane ($(CF_3)_2CHOCH_2F$), and isoflurane ($CF_3CHClOCHF_2$) and a fourth one, which is used less extensively, enflurane (CHF_2OCF_2CHFCl), but is of interest because it is an isomer of isoflurane. Product ions are identified as a function of reduced electric field (E/N) over the range of approximately 80 Td to 210 Td, and the effects of operating the drift tube under '*normal*' or '*humid*' conditions on the intensities of the product ions are presented. To aid in the analyses, density functional theory (DFT) calculations of the proton affinities and the gas-phase basicities of the anaesthetics have been determined. Calculated energies for the ion-molecule reaction pathways leading to key product ions, identified as ideal for monitoring the inhalation anaesthetics in breath with a high sensitivity and selectivity, are also presented.

1. Introduction

The monitoring of unlabelled drugs in the body in real-time offers an opportunity to determine their therapeutic effectiveness and washout characteristics in a continuous and non-invasive way. By way of illustration, several soft chemical ionisation studies have highlighted the use of breath analysis to detect intravenous anaesthetics, such as propofol during surgery [1–5], or to monitor the concentrations of inhaled anaesthetics post-surgery, either in the breath of patients or within operating and recovery rooms in hospitals [6–10]. The former has led to the development of a low cost analytical device to monitor

propofol levels in the breath of patients during anaesthesia or under sedation in real-time [11]. The latter provides interesting information on the length of time these anaesthetics remain in a patient's body so that the pharmacokinetics of these anaesthetics can be better understood. Within this context, the work presented in this paper explores some potential applications of breath gas analysis in inhalation anaesthesia, which are applicable to use in a clinical setting.

In a recent proton transfer reaction—quadrupole—mass spectrometric (PTR-Quad-MS) study, involving a number of severely ill patients who had undergone major surgery, it was found that the inhalation anaesthetic used, isoflurane, took several weeks to be fully eliminated [10]. This was a very limited study, involving a small number of extremely sick people, and hence a key aim of our new research programme is to extend this pilot isoflurane study to explore the elimination characteristics for a number of inhalation anaesthetics used in surgical procedures, and to investigate the dependence of the lifetime of an anaesthetic in the body on various factors that could influence the outcome, including the duration and type of surgery, the quantity of an anaesthetic inhaled, ventilation, and the health, body mass index (BMI), gender, and age of patients.

Once inhaled, an inhalation anaesthetic enters the blood stream through the alveoli where it is transported and delivered to the brain, but on its journey to the brain some of the anaesthetic becomes stored in tissues. Of the inhalation anaesthetics being investigated, desflurane and sevoflurane have the lower tissue solubility, and therefore we can expect those two anaesthetics to be eliminated from the body in shorter timescale than that for isoflurane. Nevertheless, their lifetime in the human body may still be long given that they are primarily eliminated from the body via exhalation, and are only minimally metabolised by the liver and kidneys [12]. The low solubility of sevoflurane in blood suggests that this agent should enter and leave the body more rapidly than isoflurane. The closeness of sevoflurane and isoflurane tissue/blood partition coefficients suggests that the rates of equilibration with and elimination from tissues should be similar [13]. Yet sevoflurane is eliminated faster than isoflurane, despite its greater blood/tissue partition coefficient, but slower than desflurane.

The Medical University of Innsbruck has recently granted us ethical approval to undertake long-term respiratory gas analyses of patients following scheduled surgery. For this, the patients will be classified according to their American Society of Anaesthesiologists (ASA) physical status classification, which is used for defining the pre-operative risk assessment of the physical conditions (fitness) of patients [14]. Our study is restricted to ASA 1–3, where ASA 1 refers to normal healthy individual, ASA 2 denotes pre-operative patients who have a mild systemic disease and ASA 3 is assigned to those patients who have a severe systemic disease. It will be of considerable interest to see how the physical fitness and physical status of our volunteers will affect the retention and exhalation of an inhalation anaesthetic.

For the analyses of breath samples, we will be using mass spectrometric analytical methods, with the key instruments being proton transfer reaction mass spectrometry (PTR-MS) and ion mobility spectrometry. Proton transfer reaction mass spectrometry is a popular analytical tool used for detecting volatile compounds in complex chemical environments for a wide range of applications, ranging from food sciences through to homeland security [15–20]. It is particularly ideal for real-time measurements, which is useful for tracking rapid changes of trace volatiles such as occurs in the atmosphere, industrial processing and in breath and for those studies for which pre-preparation and pre-concentration of the gas samples are not possible.

Before any detailed breath washout measurements on any analytical device are undertaken, it is important to ascertain how the various anaesthetics can be best detected (highest sensitivity with high selectivity) for a given analytical instrument. In the case of PTR-MS this is associated with determining the product ions (types and intensities) resulting from the reactions of reagent ions with the individual anaesthetics in the drift (reaction) tube over a range of reduced electric fields. (The reduced electric field is defined by the ratio E/N, where E is the electric field strength and N is the total molecular gas number density in the drift tube of a PTR-MS. The unit used for E/N is the Townsend (Td), where $1\ \mathrm{Td} = 1 \times 10^{-17}\ \mathrm{V\ cm^2}$.)

In the PTR-Quad-MS study of isoflurane ($C_3H_2ClF_5O$, monoisotopic mass (lightest isotopomer) 183.97 Da) by Fernández del Río *et al* [10], the product ion branching percentages over a small range of reduced electric fields (96–138 Td) were investigated. Prior to that study, PTR-Quad-MS studies of isoflurane were reported by Rieder *et al* [6] at one fixed E/N to determine the air quality in a post-anaesthetic care unit. In that study they claim to have monitored protonated isoflurane, but no such product ion was observed in the study by Fernández del Río *et al.* Only product ions resulting from dissociative proton transfer are reported in the paper by Fernández del Río *et al.* Therefore, a minor objective of the work presented in this paper is to resolve this discrepancy in the observed product ions between the two published isoflurane studies.

In addition to isoflurane, two other halogenated ether compounds are routinely used as modern inhalation anaesthetics for surgical procedures, namely desflurane ($C_3H_2F_6O$, 168.00 Da) and sevoflurane ($C_4H_3F_7O$, 200.01 Da). The choice of anaesthetic is determined by the anaesthetist on its pharmacological properties, a patient's underlying diseases and use of

medication, the type of breathing system being used, and duration and type of surgical procedure [12].

The first reported PTR-MS study of sevoflurane is by Critchley *et al* [21], using the same PTR-Quad-MS as used in the later isoflurane study of Fernández del Río *et al* but only at one fixed reduced electric field of approximately 140 Td. As found for isoflurane, proton transfer to sevoflurane is dissociative. Given the low mass resolution of PTR-Quad-MS systems, the reported product ions are only listed at nominal m/z values of m/z 199, tentatively identified as $C_4F_7OH_2^+$, which would result from the elimination of H_2 from the protonated parent, m/z 181, identified as $C_4F_6H_2OH^+$, which results from the loss of HF from the protonated parent, and m/z 49, ascribed to be $CHFOH^+$. The product ion at m/z of 181 was by far the dominant product ion observed by Critchley *et al.* In agreement to this, Summer *et al* [8], who also used a PTR-Quad-MS instrument, report using a product ion at m/z of 181 to monitor sevoflurane, although it is incorrectly identified in their work as the protonated parent. In a later study by Trefz *et al* [9], who used a Proton Transfer Reaction—Time-of-Flight—Mass Spectrometer (PTR-ToF-MS), which has a far higher mass resolution compared to a PTR-Quad-MS, they reported sevoflurane product ions at m/z ratios of 181.007 and 198.999, with the product ion at m/z 181.007 being by far the most intense, in agreement with the study by Critchley *et al.* Given the high mass accuracy achievable with a PTR-ToF-MS, the product ion reported by Trefz *et al* at m/z 198.999 is certainly consistent with the product ion assignment, $C_4F_7OH_2^+$, of Critchley *et al.*

In contrast to the PTR-MS results, two investigations of the reaction of H_3O^+ with sevoflurane by Selected Ion Flow Tube-Mass Spectrometry (SIFT-MS) (Critchley *et al* [21] and Wang *et al* [22]) observed the same three product ions. In the study by Critchley *et al* the product ion at the nominal m/z value of 199 was by far the most intense of the three product ions. The earlier SIFT-MS study by Wang *et al* found that the intensities of the product ions varied greatly with the experimental parameters and conditions, namely reaction length and the humidity in the flow tube, respectively, with the longer the reaction length resulting in $CHFOH^+$ being the dominant product ion. When using moist air in the flow tube, Wang *et al* observed that all of the product ions, other than $CHFOH^+$, react with water and are lost.

Although enflurane is rarely used in operations, it is included in this study because it is still commercially available, and furthermore being an isomer of isoflurane it is analytically challenging to distinguish from isoflurane and provides an interesting comparison to the ion chemistry for isoflurane. To our knowledge, there have been no other reported PTR-MS studies of desflurane and enflurane.

Details of the current PTR-ToF-MS studies of the four inhalation anaesthetics, desflurane, sevoflurane, isoflurane and enflurane as a function of reduced electric field and drift tube humidity will be presented in the following text. These provide a new or an improved understanding of the ion-molecule chemistry occurring in the drift (reaction) region of a PTR-MS for these anaesthetics. This study clearly establishes which product ions and drift tube conditions should be used in order to monitor these anaesthetics in breath following surgery with a high selectivity and sensitivity. Furthermore, and for the first time, we present in this paper density functional theory (DFT) calculations of the proton affinities, gas-phase basicities and changes in the enthalpy and free energy for the key reaction pathways leading to the product ions to be monitored for all four of the halogenated ethers. These are used in this paper to aid in the interpretation of the observed product ions.

2. Methods

2.1. Chemicals

For these present studies, surgical grade inhalation anaesthetics were obtained. Sevoflurane (CAS number: 28523-86-6) and isoflurane (CAS number: 26675-46-7) were purchased from the biopharmaceutical company AbbVie, enflurane (CAS number: 13838-16-9) was supplied by Abbott Products Operations AG, and desflurane (CAS number: 57041-67-5) was sourced from Baxter International. The chemicals were used directly without further purification for the PTR-MS headspace analyses reported in this paper. All of these chemicals are liquids at room temperature.

2.2. Proton transfer reaction-time-of-flight-mass spectrometry (PTR-ToF-MS)

Thorough descriptions of the instrument's operating principles and details of its applications are provided in depth by Ellis and Mayhew [15]. Hence only pertinent details will be provided here. All of the PTR-ToF-MS measurements presented in this paper were taken using an Ionicon Analytik GmbH (Innsbruck, Austria) PTR-TOF 8000, with or without the addition of a multicapillary column (MCC) for gas chromatographic pre-separation. The MCC was used under '*normal*' drift tube conditions to help in identifying the product ions coming from an anaesthetic of interest through limited pre-separation, thereby providing us with a higher confidence in product ion assignment to an anaesthetic. However, MCC separation capabilities are less than can be obtained with conventional (single capillary column) GC. For MCC, temporal resolution is sacrificed for smaller size and shorter cycle times, and therefore we cannot completely rule out an impurity that may be present in the sample being investigated contributing to the observed product ions.

The PTR-TOF 8000 and the MCC have been described elsewhere by Ruzsanyi *et al* [23], and

therefore only a brief overview of settings is given here. The ion source was operated at a current of 3.5 mA and a voltage of 160 V, with the source-out voltage maintained at 140 V. The source valve opening was set at 40%. The drift tube's pressure and temperature were maintained at 2.3 mbar and 60 °C, respectively. The voltage drop across the drift tube was varied from 365 V up to 965 V at the fixed drift tube pressure, resulting in a range of reduced electric field values ranging from approximately 80 Td up to about 210 Td. The MCC was used at a temperature of 40 °C with a N_2 (99.9999% purity) flow of 10 ml min^{-1}. For the MCC measurements, resulting products ions under three reduced electric field values of 80 Td, 140 Td and 180 Td were investigated.

The mass spectra, obtained by converting the drift times of the ions in the ToF-MS analyser, ranged from approximately m/z 3 to m/z 230, and were acquired in a time of 1 s by co-adding 25 000 single 40 μs extraction periods recorded at a sampling frequency of 10 GHz. The mass resolution in the present experiment obtained from the detected peaks was ≈2400 at m/z 100. The total duration of a complete reduced electric field experimental run was approximately 14 min, which corresponds to the acquisition of 60 mass spectra per single E/N value. The averages of the ion signal levels at each m/z value identified to be associated with a given anaesthetic from these 60 spectra were used to calculate the intensities and branching percentages of the product ions.

Data were analysed using the PTR-MS Viewer 3.2.8, which also performed mass calibration and peak identification. Raw product ion signal intensities (counts per second) were used and, where needed for determining the sensitivity of detection, these were normalised to a constant reagent ion signal of 10^6 $H_3{}^{16}O^+$ per second for each reduced electric field measurement. The $H_3{}^{16}O^+$ signal intensity cannot be measured directly, owing to its high intensity, which saturates the detector. Instead the signal intensity for the spectral line peaking at m/z 21.02, corresponding to $H_3{}^{18}O^+$, was recorded, from which the intensity of $H_3{}^{16}O^+$ was calculated.

Two humidity conditions in the drift tube were investigated, which will be referred to as '*normal*' or '*humid*', with the latter approximately corresponding to that of exhaled breath. '*Normal*' corresponds to the case where a dry buffer gas (absolute humidity <0.1%) is being flowed into the drift tube, but note that owing to diffusion of water vapour from the ion source into the drift tube, the buffer gas in the drift tube is not dry and hence is at a higher absolute humidity. '*Humid*' refers to the situation when water saturated buffer gas is used (absolute humidity 5%).

Although H_3O^+ (or the protonated water dimer—depending on the value of the reduced electric field applied) dominates the reagent ion signal, other reagent ions are always present in the drift tube, with the dominant ones being NO^+ and $O_2{}^+$, which are at levels of 1%–2% and 2%–6% relative to H_3O^+, respectively, with the value depending on the reduced electric field value and under '*normal*' operating conditions. Generally, at such low percentages they can be ignored, but care must be taken that product ions are not coming from reactions with these reagent ions if proton transfer from H_3O^+ or $H_3O^+.H_2O$ is not efficient or at values of E/N where the reagent ion signal intensities are low.

2.3. Sampling procedures

The samples were prepared as follows: A Tedlar® bag (SKC Inc., USA) of 3 l capacity was flushed with N_2 (99.9999% purity) multiple times in order reduce any possible background volatile contamination. Then the bag was filled with 2 l of dry N_2 (for the so-called '*normal*' measurements) or with 2 l of N_2 bubbled through water at room temperature (for the so-called '*humid*' measurements). Background mass spectra were recorded for each reduced electric field from approximately 80 to about 210 Td in steps of 10 Td, first ascending and then descending.

To prepare the anaesthetic samples, a 1 l gas bulb (Supelco, Canada) was maintained at 60 °C while evacuating. The gas bulb was then closed, and 0.5 μl of an anaesthetic was injected into it through a septum. Dry N_2 was then introduced into the bulb to bring it to atmospheric pressure. Finally, a 5 ml sample of the gas was taken from the bulb and introduced into the bag containing either dry or humid N_2. This bag was then connected to the heated inlet of the PTR-TOF 8000 for direct measurement.

The anaesthetic concentrations entering the drift tube were in the range of approximately 400–500 parts per billion by volume (ppbv). These concentrations are sufficiently low to ensure there was not any detectable loss of the reagent ion signal, but sufficiently high to give good product ion signal intensities.

2.4. Density functional theory calculations

Density functional theory (DFT) calculations have been undertaken to determine the proton affinities (PA) and gas-phase basicities (GB) of water, the water dimer, desflurane, sevoflurane, isoflurane and enflurane. These calculations were conducted using the Gaussian09W program with the GaussView05 for Windows interface and the B3LYP functional with 6–31 + G(d,p) basis set [24] at 298 K. It should be noted that using 298 K is arbitrary as the temperature of the drift tube bath (buffer) gas is greater than this (in this study it is at 333 K) and that the translational temperature of the ions even higher due to the electric field (see later). But this is not considered too important as the energetics (particularly ΔGs rather than ΔHs) are being used to assist in determining the likely fragmentation pathways to the observed ions [25].

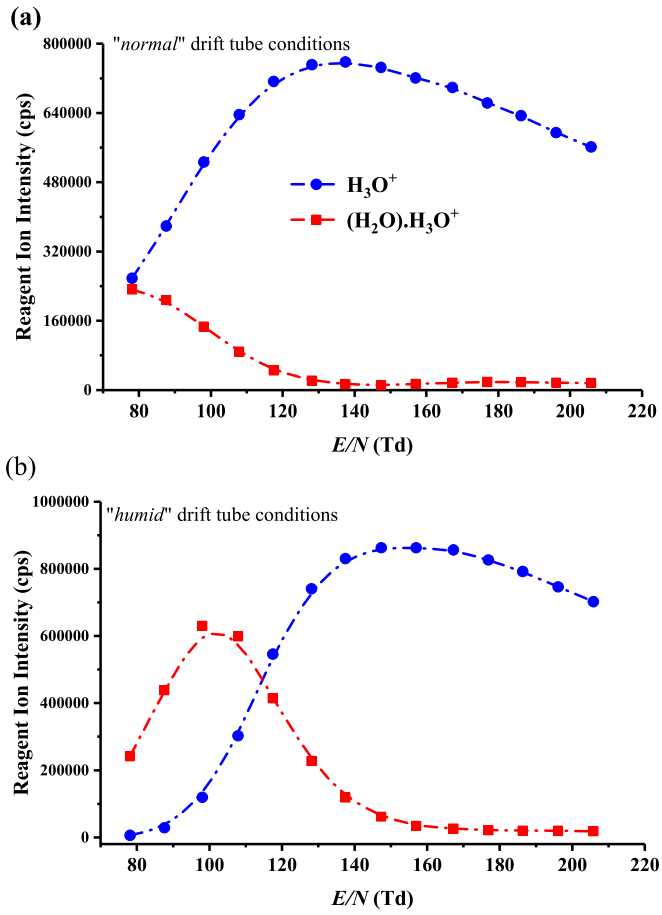

Figure 1. Reagent ion intensities in counts per second (cps) for $H_3O^+.(H_2O)_n$, where n = 0 and 1, recorded at the detector of the PTR-TOF 8000 used in this investigation under (a) '*normal*' and (b) '*humid*' operating conditions as a function of the reduced electric field (*E*/*N*).

A full account of the DFT results and their interpretation for the four anaesthetics is on-going, and are too extensive to be given with any detail in this experimentally focused paper. Furthermore, given that the main focus of this paper is to provide details on which product ion(s) should be monitored to determine the concentrations of these four volatile anaesthetics in breath with the best sensitivity, we only present sufficient DFT information to provide details on the pathways leading the key product ions that are to be recommended for monitoring purposes in the breath analysis research programme. A more detailed report on the DFT calculations will be the subject of another paper.

3. Results

3.1. PTR-ToF-MS results

3.1.1. $H_3O^+.(H_2O)_n$ (n = 0 and 1) reagent ions

The intensities (counts per second) of the reagent ions $H_3O^+.(H_2O)_n$ (n = 0 and 1) in the PTR-ToF-MS experiments, as measured at the detector as a function of reduced electric field (obtained by changing the drift tube voltage at constant drift tube pressure) under the '*normal*' and the '*humid*' drift tube conditions already defined [26, 27] are illustrated in figures 1(a) and (b), respectively. It can be seen that under '*normal*' operating conditions, H_3O^+ remains the dominant reagent ion for the complete range of the reduced electric fields investigated. This is not the case under '*humid*' conditions, for which the dominant reagent ion becomes $H_3O^+.(H_2O)$ for reduced electric fields below about 110 Td, and by about 80 Td it is the only reagent ion with any significant intensity.

Under both '*normal*' and '*humid*' operating conditions we find that the reagent ions $H_3O^+.(H_2O)_n$ (n = 2 and 3) make negligible contributions to the total reagent ion signal at any reduced electric field. For example, at the lowest reduced electric field applied (80 Td), under '*normal*' and '*humid*' conditions, combined they contribute less than 3% and 10%, respectively, to the total reagent ion signal, with their intensities significantly declining with increasing reduced electric field, as is expected. Although it should be appreciated that these intensities correspond to those measured at the detector and hence they may not be a completely true reflection of the distributions present in the drift tube, we have found that changes in voltage supplied to the ion extraction lens, which is situated behind the skimmer cone just after

Table 1. Product ion distributions (percentages) determined using the MCC PTR-TOF 8000 resulting from the reactions of the $H_3O^+.(H_2O)_n$ (n = 0 and 1) reagent ions in the drift tube with the four halogenated ethers at three reduced electric field (E/N) values measured under '*normal*' drift tube conditions. Only product ions which contribute at least a branching percentage of 3% at any given reduced electric field over the range of 80–210 Td have been included. The m/z values given for the neutral species and the product ions are for the lightest isotopomer, but the percentages provided have taken into account the contributions to the total ion signal of all isotopic variants (^{13}C and where relevant ^{37}Cl) to provide a more accurate branching percentage.

Anaesthetic Stochiometric Formula m/z (lightest isotopomer)	Product Ions formula, m/z (lightest isotopomer)	E/N (Td) 80	140	180%
Desflurane	$C_3H_2F_5O^+$, 149.00	87	56	25
$CF_3CHFOCHF_2$	$C_3F_5O^+$, 146.99	8	20	6
168.00	$C_2F_4H^+$, 101.00	—	2	8
	CHF_2^+, 51.00	5	22	61
Sevoflurane	$C_4H_3F_6O^+.H_2O$, 199.02	7	1	1
$(CF_3)_2CHOCH_2F$	$C_4H_3F_6O^+$, 181.01	68	97	81
200.01	CF_3^+, 69.00	—	—	3
	CHF_2^+, 51.00	—	2	15
	CH_2FO^+, 49.01	25	—	—
Isoflurane	$C_3F_4ClO^+.H_2O$, 180.97	3	—	—
$CF_3CHClOCHF_2$	$C_3H_2F_4ClO^+$, 164.97	74	5	2
183.97	$C_3F_4ClO^+$, 162.96	8	6	1
	$C_3HF_3ClO^+$, 144.97	5	1	—
	$C_2HF_3Cl^+$, 116.97	—	27	19
	$C_2H_2F_2ClO^+$, 114.98	6	1	—
	$CHFCl^+$, 66.98	3	42	63
	CHF_2^+, 51.00	1	18	15
Enflurane	$C_3F_4ClO^+$, 162.96	4	1	—
CHF_2OCF_2CHFCl	$C_3HF_3ClO^+$, 144.97	7	1	—
183.97	$C_2HF_3ClO^+$, 132.97	4	1	—
	$C_3H_3F_3Cl^+$, 130.99	31	—	—
	$C_2HF_3Cl^+$, 116.97	1	12	9
	$C_2H_2F_2ClO^+$, 114.98	3	2	1
	$C_2F_2ClO^+$, 112.96	9	7	1
	$CHFCl^+$, 66.98	31	62	78
	CHF_2^+, 51.00	9	14	11

the exit of orifice of the drift tube does not significantly alter the relative intensities. Therefore, we will assume that the measurements at the detector provide a reasonable indication of the protonated water and protonated water cluster distributions within the drift tube. Given their low intensities under any operating conditions, the reagent ions $H_3O^+.(H_2O)_n$ (n = 2 and 3) have been neglected in any analysis of the measurements obtained.

3.1.2. MCC-PTR-ToF-MS results

The m/z values (lightest isotopomer), the molecular ion formulae (the identification of which is greatly aided by the accurate measurement of the mass spectral peak owing to the high mass resolution of the PTR-TOF 8000) and distributions of the product ions (percentages) at three E/N values selected determined using the MCC-PTR-TOF 8000 are provided in table 1. The molecular formulae of the product ions have been identified via the exact m/z (to 2 decimal places) and isotopic (^{13}C and where relevant ^{37}Cl) intensities. This section only presents the product ions that have been identified to derive from a given anaesthetic and which result in a branching percentage of 3% or above at any given reduced electric field value investigated in this study. It should, however, be noted that there are difficulties associated with the accurate determination of the branching percentages owing to m/z discrimination in PTR-MS. There are several factors influencing this, including diffusional and Coulombic losses of the product ions in the drift tube, and m/z discrimination in the transfer optics, mass analyser and the ion detector. Collectively, they cannot be easily quantified with a reliable accuracy over a wide range of reduced electric fields, and thus reported branching percentages are only indicative rather than quantitative, and are rather specific for the PTR-MS and its settings being used.

Details of the various product ions follow in the next section. Here we comment that the proton transfer reaction of H_3O^+ with all four anaesthetics is found to be completely dissociative, with a substantial number of product ions resulting from the reaction, and this is particularly so for isoflurane and enflurane.

3.1.3. Reduced electric field (E/N) investigations of the product ion intensities resulting from the individual anaesthetics

The key aim of this paper is to provide details on what product ion(s) should be monitored and under what

operational conditions for maximum sensitivity for detecting an inhalation anaesthetic in exhaled breath. Hence, following the identification of the product ions for all four anaesthetics using the MCC-PTR-TOF 8000, for each anaesthetic the intensities (counts per second) of the product ions were then monitored over a range of reduced electric fields without the MCC, under '*normal*' and '*humid*' drift tube operating conditions.

'*Humid*' measurements are crucial, because these are closer to breath samples, and it is known that humidity in the drift tube can affect the product ion distributions. This is highlighted in two recent studies, which investigated the product ion distributions for nine deuterated compounds [27] and a series of ketones [28] in the PTR-TOF 8000. For the deuterated study, with the exception of acetone-d_6, the key effect of the higher drift tube humidity was an increase of the deuterium/hydrogen isotope exchange reactions of the primary product ions with the ever present water in the drift tube. This led to the generation of various isotopologue product ions. For the ketones, the effect of humidity was not observed to be so dramatic, with the general outcome of the higher humidity in the drift tube resulting in a need for higher E/N (approximately 20 Td higher) to obtain similar product ion intensities to those found under the '*normal*' drift tube operating conditions

In comparison to the two earlier studies [27, 28], investigating the consequences of humidity on the product ion distributions, effects caused by differing humidity conditions in the drift (reaction) tube of a PTR-MS are found to be more dramatic on the production of the product ions for the anaesthetics studied in this investigation. Figure 2 provides the intensity curves (intensities of product ions in terms of counts per second (cps) as a function of the reduced electric field) for the product ions identified for (a) desflurane, (b) sevoflurane, (c) isoflurane and (d) enflurane over the range of reduced electric fields investigated under both (i) '*normal*' and (ii) '*humid*' drift tube conditions. What is noticeable from this figure immediately is the dramatic decrease in signal intensity under the '*humid*' compared to the '*normal*' drift tube conditions for low reduced electric fields (i.e. approximately $<$110 Td), and this is particularly so for isoflurane and enflurane.

3.1.3.1. Product ions resulting from desflurane and sevoflurane

For desflurane and sevoflurane the dominant product ion observed for the majority or all of the reduced electric field values investigated, respectively, results from the loss of HF following proton transfer from H_3O^+ to the anaesthetic. The difference in the E/N intensity profiles of this dominant product ion for desflurane and sevoflurane, figures 2(a) and (b), respectively, is surprising given that the same reaction pathway is followed with similar energetics. We have confirmed that this difference in intensity profiles is real by repeating the E/N intensity profile measurements with a dry and humid nitrogen sample containing a mixture of both desflurane (at approximately 500 ppbv) and sevoflurane (at approximately 400 ppbv).

For desflurane, above about 170 Td, the product ion at m/z 51.00 (assigned to be CHF_2^+) becomes the dominant product ion. Other product ions originating from desflurane are at m/z values of 146.99 and 101.00, assigned to be $C_3F_5O^+$ and $C_2F_4H^+$, respectively, with their intensities being much less than the maximum reached by $C_3H_2F_5O^+$ at a lower reduced electric field.

In addition to the dominant product ion, four other product ions have been assigned to result from the reaction of H_3O^+ with sevoflurane. One, at m/z 199.02, is considered to result from the association of water to the dominant product ion $C_4F_6H_2OH^+$. As found for desflurane, CHF_2^+, at m/z 51.00, is also a product ion with a significant branching percentage, but with a relatively low intensity, at high reduced electric fields. The two other product ions observed are at m/z 69.00 (CF_3^+) and m/z 49.03 (CH_2FO^+), but with insignificant intensities compared to the maximum achieved by $C_4H_3F_6O^+$.

Using a reduced electric field of 140 Td, a product ion resulting from the reaction of H_3O^+ with sevoflurane was identified with a nominal value of m/z 199 by Critchley *et al* [21]. This was detected with a higher accuracy at m/z 198.999 by Trefz *et al* [9]. As mentioned in the introduction, both studies assigned the product ion to be $C_4F_7OH_2^+$. In our measurements, at 80 Td the peak position in this mass range is at m/z 199.02, which is more consistent with the product ion $C_4F_6H_2OH^+.H_2O$. It is possible that at higher reduced electric fields the product ion we observe at m/z 199 is indeed $C_4F_7OH_2^+$, but its intensity is too low in our study for us to accurately measure its peak position. Given that, in agreement with this study, the two other PTR-MS studies that identify a product ion at a nominal m/z value of 199 show that the signal intensity relative to the other product ions is extremely low, it is of no relevance for determining breath concentrations of sevoflurane. Thus, given the low intensity involved, whether the ion at m/z 199 is either $C_4F_6H_2OH^+.H_2O$ and/or $C_4F_7OH_2^+$ is irrelevant to the current aim of this work, and hence we will not discuss it further in this paper.

3.1.3.2. Product ions resulting from isoflurane and enflurane

In comparison to desflurane and sevoflurane, for isoflurane and enflurane, the dominant product ion selected for monitoring purposes is at a much lower m/z value of 67, assigned to be $CHFCl^+$, which can only occur via significant fragmentation. This is discussed further in section 3.2, which deals with the interpretation of reaction pathways with the aid of

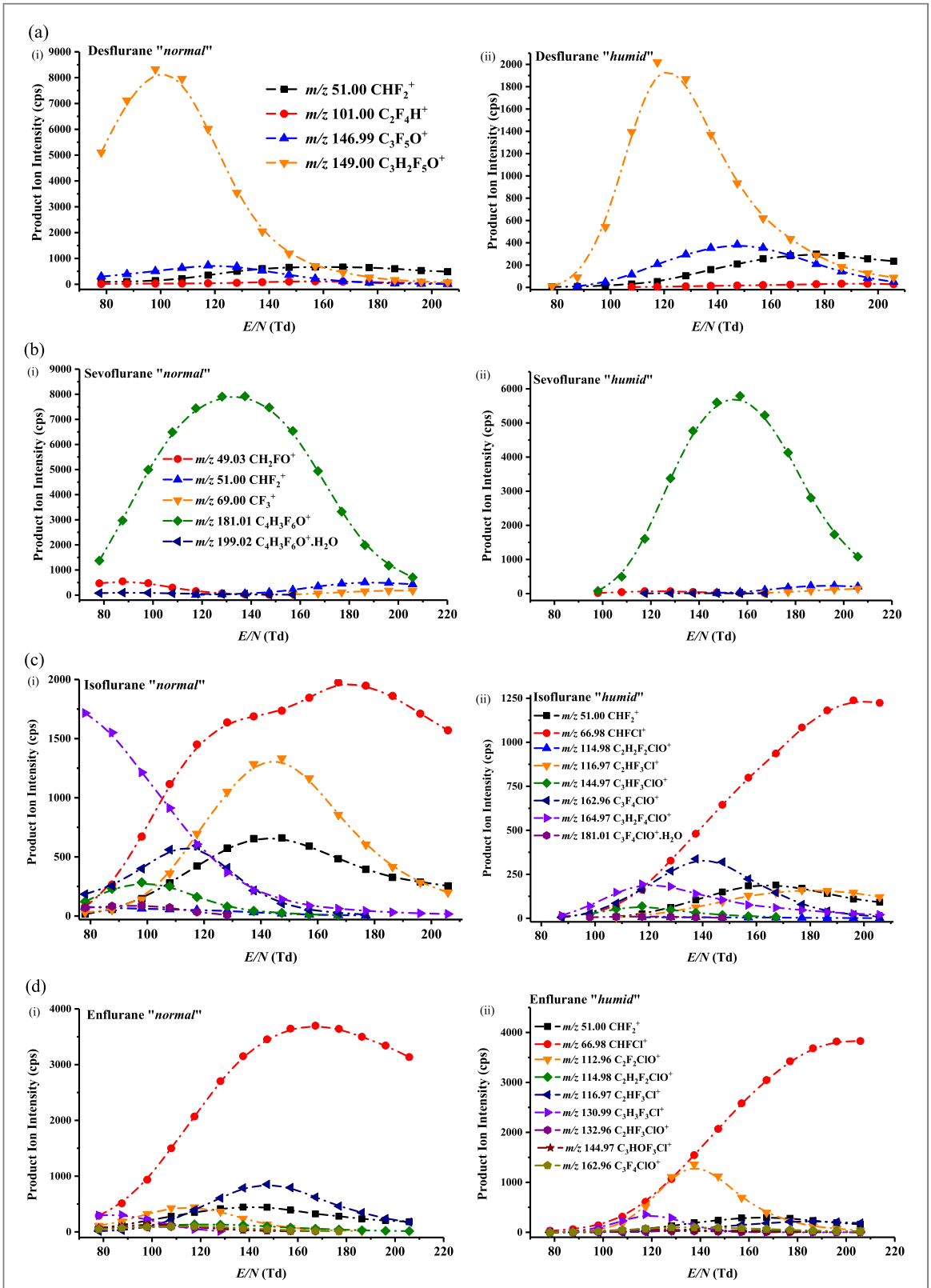

Figure 2. Signal intensities in terms of raw counts per second of the product ions resulting from reactions of the $H_3O^+.(H_2O)_n$ (predominantly n = 0 and 1—see figure 1 and text) with (a) desflurane, (b) sevoflurane, (c) isoflurane and (d) enflurane as a function of the reduced electric field (E/N) under (i) '*normal*' and (ii) '*humid*' drift tube operating conditions. The m/z values given for the product ions are for the lightest isotopomer, but the intensities have taken into account all isotopic variants, namely contributions from the ^{13}C containing product ions and in addition, for isoflurane and enflurane, the ^{37}Cl containing product ions.

DFT calculations leading to the product ions to be monitored for the breath analysis programme. Given the number and complexity of the product ions observed for these two anaesthetics, a full discussion of the reaction pathways and the energetics involved will be the subject of another paper for which the full energetics will be provided. We will just comment here on one product ion observed for enflurane at m/z

Table 2. Best operating reduced electric fields values (highest sensitivity) and product ion to monitor for the anaesthetics desflurane, sevoflurane, isoflurane and enflurane in breath (‘*humid*’ drift tube conditions) and in closed environments (e.g. operating theatres) (‘*normal*’ drift tube conditions), determined using an Ionicon Analytik GmbH PTR-TOF 8000 instrument. The sensitivity of detection in terms of ncps/ppbv (total product ion cps normalised to 10^6 H_3O^+ reagent ions) under the ‘*normal*’ drift tube operating conditions are provided.

Inhalation Anaesthetic	Required E/N (Td) for highest sensitivity ‘*humid*’	‘*normal*’	Sensitivity ncps/ppbv ‘*normal*’	Key product ion(s) for monitoring an anaesthetic chemical formula m/z
desflurane	120	100	18	$C_3H_2F_5O^+$ 149.00
sevoflurane	150	130	20	$C_4H_3F_6O^+$ 181.01
isoflurane	200	150	11	$CHFCl^+$ 66.98 + 68.98
enflurane	200	130	9	$CHFCl^+$ 66.98 + 68.98

130.99 (and at m/z 132.99 with an intensity one third of that at m/z 130.99), which is consistent with a product ion having a molecular formula $C_3H_3F_3Cl^+$. It is difficult to provide an explanation as to how this product ion can be formed, because it requires the elimination of F_2O from the protonated parent.

3.1.3.3. Detection sensitivities of the anaesthetics

The ‘*humid*’ intensity curves provide the results needed to fulfil a key objective of this investigation, namely to determine the appropriate PTR-TOF 8000 operational parameters and the product ion(s) to monitor the four inhalation anaesthetics in exhaled breath with the highest sensitivity. The key results are summarised in table 2, which also provides details of the best sensitivity for ‘normal’ conditions for comparison. Table 2 and figure 2 show that under the ‘*normal*’ operating conditions, the best sensitivities are at lower reduced electric fields than required for a ‘*humid*’ drift tube.

The total product ion intensity at the reduced electric fields for which the maximum signal is obtained to determine the sensitivity of detection in terms of normalised counts per second (ncps) (normalised to 10^6 H_3O^+ reagent ions) for 1 ppbv of an anaesthetic. The results for this are also presented in table 2.

We find that the sensitivity of detection for isoflurane and enflurane is less than that for desflurane and sevoflurane. Differences in reaction time will play a role, but also m/z dependent transmission factors will have an effect. In a TOF-MS there is a discrimination against lower m/z ions. Given these factors and measurement errors associated with the calculation of the concentrations, the sensitivities obtained are comparable, being between 10 and 20 ncps/ppbv.

For comparison, we investigated the instrument’s sensitivity for detecting limonene, because it is known that limonene reacts with H_3O^+ with unit efficiency [29], and, given the proton affinity of $(H_2O)_2$, we can expect $H_3O^+{\cdot}H_2O$ will react with limonene via a proton transfer process also at the collisional rate. For this compound the product ions to monitor are a fragment product ion at m/z 81.07, corresponding to $C_6H_9^+$, and the protonated parent, $C_{10}H_{17}^+$, at m/z 137.13. Given that the proton affinity of limonene is higher than that of water and the water dimer, the sum of the counts per second for the two product ions was normalised to 10^6 (H_3O^+ + $H_3O^+.H_2O$). We find that we have maximum sensitivity for the detection of limonene at a reduced electric field of 80 Td, with a value of approximately 20 ncps/ppbv, i.e. similar to the sensitivities obtained for the anaesthetics.

3.2. DFT calculations

The experimental results show that for all four of the anaesthetics investigated in this study, a significant number of product ions are observed, and that all product ions are a result of dissociative processes, i.e. no protonated anaesthetic is observed. An objective of the computational calculations is to aid in interpreting this observation and to improve our understanding of the pathways leading to these product ions. These calculations have shown that many of the reaction pathways require significant increases in the free energy from that calculated at 298 K (up to several eVs in some instances) to deliver some of the product ions. The energy required to do this must be supplied to the ions through the translational energy gained in the electric field, which is in part converted to internal energy through collisions with the buffer gas. Within the drift tube thermodynamic equilibrium does not apply, because the reagent and product ions will have effective translational temperatures much higher than thermal owing to the drift velocities they obtain, which are dependent on ion mobility coefficients and the strength of the applied electric field. This results in collisional energies in the centre-of-mass frame between the reagent ions and the analytes that can drive reaction pathways, and once the primary product ions are produced resulting from the initial dissociative proton transfer reaction, these product ions can undergo further collisional induced dissociation.

Key to any analysis of product ions resulting from proton transfer are the values for the proton affinities (PAs) and gas-phase basicities (GBs) for the analytes. Table 3 presents the calculated PAs and GBs for water, the water dimer and for the four anaesthetics (various protonation sites are provided). To our knowledge, for the four anaesthetics investigated in this study, this is first time these thermodynamic quantities have been calculated and presented. The quoted energies for the

Table 3. Calculated proton affinities (PA) and gas-phase basicities (GB) for water, the water dimer and for the four halogenated ethers in units of kJ mol^{-1}. Calculations were performed using the B3LYP Functional and the 6–31 + G (d,p) basis set at 298 K. Values for a given anaesthetic are given for various protonation sites (see text).

Compound	PA (kJ mol^{-1})	GB (kJ mol^{-1})
water	684	653
water dimer	842	777
desflurane		
site 1	652	638
site 2	623	621
site 3	636	619
site 4	565	539
sevoflurane		
site 1	587	572
site 2	653	625
site 3	678	660
isoflurane		
site 1	670	655
site 2	642	622
site 3	637	608
site 4	573	552
enflurane		
site 1	657	638
site 2	662	646
site 3	625	596
site 4	594	574

key (dominant) reaction pathways are referenced to the flurane and H_3O^+ at 298 K.

Of note is that none of the anaesthetics has proton affinities greater than water. An often stated phrase in PTR-MS research papers is that for a compound to be detected with any sensitivity it needs to have a proton affinity greater than that of water. This is not strictly true, because, and as mentioned earlier, proton transfer can be driven by the translational energy gained by the reagent ions in the electric field and through a reagent ion's internal energy, which may have been gained during its formation in the ion source or through collisional processes in the drift tube. Furthermore, the key quantity is not the difference in the proton affinities (ΔH), but changes in the free energy (ΔG), and proton transfer from protonated water to a volatile will be thermodynamically spontaneous if ΔG is negative. What is crucial is that once formed the protonated parent must spontaneously dissociate, otherwise it will react with the far more abundant water in the drift tube, dramatically reducing the sensitivity for detection of the parent molecule in PTR-MS analysis. Thus dissociation of a protonated parent, which can thermodynamically donate its proton to water, must occur on a timescale less than the average time for a collision between the protonated analyte and water in the drift tube. If this is not the case any protonated analyte will donate its proton to water in the drift tube with unit efficiency in a reverse reaction, and, given that water is in far higher concentrations than the analyte in the drift tube, the chemical equilibrium will be in favour of H_3O^+ production. Here the former is happening leading to copious amounts of product ions resulting from dissociative proton transfer, and this explains why they can be detected with high sensitivity with PTR-MS when using H_3O^+ at the reagent ion.

3.2.1. Desflurane

The four protonation sites are schematically represented below:

$$\overset{1}{\mathrm{C}}\mathrm{HF}_2\overset{2}{\mathrm{O}}\mathrm{C}\overset{3}{\mathrm{H}}\mathrm{F}\overset{4}{\mathrm{C}}\mathrm{F}_3$$

At 298 K proton transfer from H_3O^+ to desflurane is endothermic for all of the sites, with that to site 1 resulting in the lowest enthalpy ($\Delta H_{298} = +32$ kJ mol^{-1}) and free energy ($\Delta G_{298} = +15$ kJ mol^{-1}) changes.

Following proton transfer, the protonated desflurane fragments. The dominant fragment product ion observed in the experimental measurements, up to about a reduced electric field of 150 Td under '*normal*' drift tube conditions and 170 Td under '*humid*' drift tube conditions, is m/z 149.00 corresponding to loss of HF. This could occur from sites 1, 3, and 4, but loss from site 1 is the most likely as DFT investigations suggest that whilst loss from sites 3 and 4 is possible, further fragmentation is probable. Loss of HF does not involve a transition state, i.e. it is a barrierless process and this is so for loss of HF from the other three flurranes. The associated energetics are with $\Delta H_{298} = +81$ kJ mol^{-1} and $\Delta G_{298} = +43$ kJ mol^{-1}, which are easily accessible in the drift tube.

3.2.2. Sevoflurane

The protonation sites for sevoflurane are defined below:

$$(\overset{1}{\mathrm{C}}\mathrm{F}_3)_2\mathrm{C}\overset{2}{\mathrm{H}}\mathrm{O}\mathrm{C}\overset{3}{\mathrm{H}}_2\mathrm{F},$$

with protonation to site 3 being essentially thermoneutral at 298 K ($\Delta H_{298} = +6$ kJ mol^{-1} and $\Delta G_{298} = -7$ kJ mol^{-1}). Given the small enthalpy and free energy changes, proton transfer from H_3O^+ to sevoflurane is likely to be efficient, meaning that the reaction rate coefficient must be at the collisional value. This agrees with the results obtained from a selected ion flow tube study of the reaction of H_3O^+ with sevoflurane [23], for which the experimentally determined room-temperature reaction rate coefficient of 3.4×10^{-9} cm^3 s^{-1} is equal to the calculated collisional rate coefficient.

The dominant product ion is again formed by loss of HF from the protonated parent, and whilst loss from both sites 1 and 3 is possible with both leading to stable product ions, loss from site 3 is most likely and has the energetics $\Delta H_{298} = +50$ kJ mol^{-1} and $\Delta G_{298} = +4$ kJ mol^{-1}.

3.2.3. Isoflurane

The four sites for protonation on the isoflurane molecule are schematically represented below:

$$\overset{4}{C}F_3\overset{2}{C}H\overset{3}{C}l\overset{1}{O}CHF_2.$$

Protonation to site 1 is essentially thermoneutral at 298 K ($\Delta H_{298} = +14$ kJ mol^{-1} and $\Delta G_{298} = -2$ kJ mol^{-1}). A SIFT study reports that, as found for sevoflurane, the reaction with H_3O^+ occurs at the collisional rate. The dominant product ion recommended for monitoring purposes is at m/z 67, $CHFCl^+$, which can only occur via significant fragmentation. Extensive DFT investigations show that the only route to this ion is protonation at site 1 followed by the loss of HF. The resulting ion at m/z 165 has three possible further fragmentation routes but the one of interest here is fragmentation into $CHFCl^+$ and CF_3CHO. This fragmentation involves a Transition State and a migration of the Cl atom. The energetics for the initial loss of HF are $\Delta H_{298} = +54$ kJ mol^{-1} and $\Delta G_{298} = +8$ kJ mol^{-1}. The further fragmentation and associated Transition State have the energetics $\Delta H_{298} = +174$ kJ mol^{-1} and $\Delta G_{298} = +77$ kJ mol^{-1} and $\Delta H^{\ddagger}_{298} = +182$ kJ mol^{-1} and $\Delta G^{\ddagger}_{298} = +77$ kJ mol^{-1}, respectively.

3.2.4. Enflurane

The four sites for protonation on the enflurane molecule are defined as shown below:

$$\overset{1}{F}_2CH\overset{3}{O}C\overset{2}{F}_2CH\overset{4}{F}Cl$$

As mentioned earlier, the dominant product ion that can be used for exhaled breath monitoring purposes is at m/z 67, $CHFCl^+$, as found for isoflurane. The most plausible fragmentation pathway to this ion is loss of HF following protonation at site 1 ($\Delta H_{298} = +27$ kJ mol^{-1} and $\Delta G_{298} = +15$ kJ mol^{-1}) followed by further fragmentations to CHFO plus CF_2 and $CHFCl^+$, which appears to be barrierless. Whether this final fragmentation pathway is sequential or concerted is the subject of further theoretical investigations. The overall energetics are $\Delta H_{298} = +347$ kJ mol^{-1} and $\Delta G_{298} = +203$ kJ mol^{-1}.

4. Discussion and concluding remarks

The calculated proton affinities of the anaesthetics are significantly less than any of the water clusters. This explains the low product ion signal intensities observed for all of the anaesthetics under the '*humid*' drift tube conditions for low E/N (<100 Td) when the protonated water dimer is the dominant reagent ion species.

In the selected ion flow tube study of isoflurane and sevoflurane by Wang *et al* the reaction rate coefficients for their reactions with H_3O^+ were determined from the relative decay rates of H_3O^+ and O_2^+ reagent ions, and the assumption that O_2^+ reacts at the collisional rate [22]. This assumption is based on their observation that all other O_2^+/ether reactions they had studied proceed at their collisional rates [30], although care has to be taken with this, because even highly exothermic charge transfer reactions may proceed with reaction rate coefficients substantially below the collisional value [31–33]. Nevertheless, Wang *et al* find that the relative decay rates of H_3O^+ and O_2^+ following their reaction with sevoflurane are in the ratio expected if both reactions proceed at their respective collisional rates. Wang *et al* also find that their experimentally determined reaction rate coefficient of 3.4×10^{-9} cm^3 s^{-1} for the reaction of H_3O^+ with isoflurane is only slightly less than their calculated collisional rate value ($k_c = 3.5 \times 10^{-9}$ cm^3 s^{-1}) implying, they claim, that the proton affinity of isoflurane must be slightly less than that of water. Although the measured reaction rate coefficient is within experimental error identical to the collisional value, the accuracy of the collisional rate coefficient is compromised because the polarizability and dipole moment of isoflurane had to be estimated. Nonetheless, the calculations presented in this paper confirm that their claim is correct for the reaction pathway leading to protonation on site 1 ($\Delta H_{298} = +14$ kJ mol^{-1}), with the reaction pathway being driven by entropic effects ($\Delta G_{298} = -2$ kJ mol^{-1}), and hence the reaction should proceed at the collisional rate, as experimentally observed.

As expected from the calculated PAs and GBs of the four halogenated ethers, the intensities of the product ions (counts per second) are diminished at low reduced electric fields under both '*normal*' and '*humid*' tube conditions, but significantly much more under the '*humid*' conditions. This is because proton transfer from the reagent ion $H_3O^+.(H_2O)$ to any of the anaesthetics is highly endothermic, and even translational energy gained in the electric field and increases in internal energies of the reagent ions through collisions with the buffer gas are unable to drive proton transfer. Therefore, only H_3O^+ has a significant role to play in the ionisation of the halogenated ethers in our PTR-MS investigations.

No protonated fluranes are observed, rather following proton transfer substantial fragmentation is observed through reaction pathways leading to product ions which often require substantial energy input. This in part may be coming from any internal energy that the H_3O^+ may contain when it is either generated in the ion source or through that gained in collisions with the buffer gas in the drift tube. Product ions also gain energy from the field, which leads to collisional dissociation. For the majority of product ion fragmentation channels, this energy input is substantial. We comment that extensive fragmentation is also reported in the selected ion flow tube mass spectrometric (SIFT-MS) study by Wang *et al* with the dominant product ion being m/z 117 (CF_3CHCl^+). This is

difficult to explain given that the ion/molecule reaction processes in a SIFT are considered to be thermal [34].

Although substantial fragmentation is observed both in this PTR-MS and the SIFT-MS studies following proton transfer from H_3O^+ to isoflurane, and as expected more so in the PTR-MS study, there are major differences in the product ions. The SIFT study by Wang *et al* [22] reports a number of product ions that we have not observed, namely m/z 99 (assigned to be $CF_3CH_2O^+$), m/z 119 (assigned to be CF_3CFHO H_2^+), and m/z 147 (incorrectly assigned in the Wang *et al* paper to be $CF_2HOCHClCH^+$ which has a m/z value of 128 and is in any case a radical cation). The following product ions recorded in this PTR-MS study: m/z 51 (assigned to be CHF_2^+), m/z 115 (assigned to be $C_2H_2F_2ClO^+$), m/z 145 (assigned to be $C_3HF_3ClO^+$), and m/z 163 (assigned to be $C_3F_4ClO^+$) are not reported in the SIFT paper. The only common product ion recorded in both studies is at m/z 117 ($C_2HF_3Cl^+$). An ion observed at m/z 67 in the SIFT study and assigned to be CF_2HO^+, is observed in our data, but because an ion signal is also observed in our mass spectrum at m/z 69 with an intensity to imply that that is associated with the ^{37}Cl isotope (m/z 69 is not observed in the SIFT mass spectrum) we have assigned m/z 67 to be $CHFCl^+$.

It is clear from this study, and others we have undertaken (for example see the paper by Malásková *et al* [26]), that a meaningful interpretation of the ion-chemistry occurring in the PTR-MS is challenging, and headway is only possible when the experimental observations are in combination with quantum mechanical computational calculations of the ion-molecule reaction pathways leading to the product ions.

Finally, we comment that the major objective of this study has been successfully accomplished, namely the identification of what product ion(s) should be monitored at a defined reduced electric field value for a given anaesthetic with high specificity under the conditions similar to those for breath samples for the PTR-TOF 8000 instrument we are using. In summary, these product ions and reduced electric fields to be used are as follow: desflurane, $C_3H_2F_5O^+$ (m/z 149.00), at an E/N of 120 Td; sevoflurane, $C_4H_3F_6O^+$ (m/z 181.01), at an E/N of 150 Td; and for both isoflurane and enflurane, $CHFCl^+$ (m/z 66.98 and m/z 68.98), at an E/N of 200 Td. This provides us with the method to monitor the 'washout' characteristics of any one of the four inhalation anaesthetic present in a person following surgery, with the excretion from the body predominantly resulting via exhalation, because they are not efficiently metabolised. It is our intention that the washout measurements will be modelled using a simulation based on one developed for anaesthetics by King *et al* [35], and since breath concentrations of VOCs with low blood:air partition coefficients ($\lambda_{b:air} \leqslant 5$, e.g. isoflurane has $\lambda_{b:air} = 1.4$ and sevoflurane has $\lambda_{b:air} = 0.6$) are very sensitive to breath flow $\dot{V}$ and blood flow $\dot{Q}$, ideally to aid the modelling the measured breath concentrations ($C_{measured}$) of the anaesthetics should be normalised according to the Farhi equation $C_{normalised} = C_{measured}\left(\lambda_{b:air} + \frac{\dot{V}}{\dot{Q}}\right)$, with no anaesthetic in the room air being breathed.

Acknowledgments

We thank the Marie Skłodowska-Curie Actions Innovative Training Network: Ion-Molecule Processes for Analytical Chemistry Technologies (IMPACT) (www.impact-h2020itn.com), which has supported this research through the European Commission's HORIZON 2020 Programme under Grant Agreement Number 674911. Ms Michaela Malásková and Mr David Olivenza-León are Early Stage Researchers attached to the IMPACT ITN. They contributed equally to the experimental investigations, and hence they should be considered as joint first authors. Dr Prema Chellayah acknowledges the financial support of the Ministry of Health Malaysia for her PhD programme in the Molecular Physics Group, School of Physics and Astronomy, at the University of Birmingham, UK.

ORCID iDs

Michaela Malásková https://orcid.org/0000-0002-4681-2376
David Olivenza-León https://orcid.org/0000-0002-2922-7722
Wolfgang Lederer https://orcid.org/0000-0002-8486-1988
Veronika Ruzsanyi https://orcid.org/0000-0001-9631-364X
Karl Unterkofler https://orcid.org/0000-0002-1078-9645
Paweł Mochalski https://orcid.org/0000-0002-6934-1562
Chris A Mayhew https://orcid.org/0000-0002-5014-7241

References

[1] Harrison G R, Critchley A D, Mayhew C A and Thompson J M 2003 Real-time breath monitoring of propofol and its volatile metabolites during surgery using a novel mass spectrometric technique: a feasibility study *Br. J. Anaesth.* **91** 797–9
[2] Hornuss C *et al* 2007 Real-time monitoring of propofol in expired air in humans undergoing total intravenous anesthesia *Anesthesiology* **106** 665–74
[3] Takita A, Masui K and Kazama T 2007 On-line monitoring of end-tidal propofol concentration in anesthetized patients *Anesthesiology* **106** 659–64
[4] Perl T, Carstens E, Hirn A, Quintel M, Vautz W, Nolte J and Jünger M 2009 Determination of serum propofol concentrations by breath analysis using ion mobility spectrometry *Br. J. Anaesth.* **103** 822–7

[5] Lorenz D, Maurer F, Trautner K, Fink T, Hüppe T, Sessler D I, Baumbach J I, Volk T and Kreuer S 2017 Adhesion of volatile propofol to breathing circuit tubing *J. Breath Res.* **11** 036005
[6] Rieder J, Prazeller P, Boehler M, Lirk P, Lindinger W and Amann A 2001 Online monitoring of air quality at the post-anaesthetic care unit by proton-transfer-reaction mass spectrometry *Anesth. Analg.* **92** 389–92
[7] Rieder J, Keller C, Brimacombe J, Gruber G, Lirk P, Summer G and Amann A 2002 Monitoring pollution by proton-transfer-reaction mass spectrometry during paediatric anaesthesia with positive pressure ventilation via the laryngeal mask airway or uncuffed tracheal tube *Anaesthesia* **57** 663–6
[8] Summer G, Lirk P, Hoerauf K, Riccabona U, Bodrogi F, Raifer H, Deibl M, Rieder J and Schobersberger W 2003 Sevoflurane in exhaled air of operating room personnel *Anesth. Analg.* **97** 1070–3
[9] Trefz P, Schmidt M, Oertel P, Obermeier J, Brock B, Kamysek S, Dunkl J, Zimmermann R, Schubert J K and Miekisch W 2013 Continuous real time breath gas monitoring in the clinical environment by proton-transfer-reaction-time-of-flight-mass spectrometry *Anal. Chem.* **85** 10321–9
[10] Fernández del Río R, O'Hara M E, Pemberton P, Whitehouse T and Mayhew C A 2016 Elimination characteristics of post-operative isoflurane levels in alveolar exhaled breath via PTR-MS analysis *J. Breath Res.* **10** 046006
[11] Propofol Monitor (accessed 30th July 2019)https://.bbraun.com/en/products/b1/edmon.html
[12] Sakai E M, Connolly L A and Klauck J A 2005 Inhalation anesthesiology and volatile liquid anaesthetics: focus on isoflurane, desflurane, and sevoflurane *Pharmacotherapy* **25** 1773–88
[13] Yasuda N, Lockhart S H, Eger E I, Weiskopf R B, Liu J, Laster M, Taheri S and Peterson N A 1991 Comparison of kinetics of sevoflurane and isoflurane in humans *Anesth. Analg.* **72** 316–24
[14] Haynes S R and Lawler P G P 1995 An assessment of the consistency of ASA physical status classification allocation *Anaesthesia* **50** 195–9
[15] Ellis A M and Mayhew C A 2014 *Proton Transfer Reaction Mass Spectrometry Principles and Applications* (New York: Wiley)
[16] Agarwal B, Petersson F, Jurschik S, Sulzer P, Jordan A, Mark T D, Watts P and Mayhew C A 2011 Use of proton transfer reaction time-of-flight mass spectrometry for the analytical detection of illicit and controlled prescription drugs at room temperature via direct headspace sampling *Anal. Bioanal. Chem.* **400** 2631–9
[17] Lanza M *et al* 2015 Selective reagent ionisation-time of flight-mass spectrometry: a rapid technology for the novel analysis of blends of new psychoactive substance *J. Mass Spectrom.* **50** 427–31
[18] Kassebacher T *et al* 2013 Investigations of chemical warfare agents and toxic industrial compounds with proton-transfer-reaction mass spectrometry for a real-time threat monitoring scenario *Rapid Commun. Mass Spectrom.* **27** 325–32
[19] Mayhew C A, Sulzer P, Petersson F, Haidacher S, Jordan A, Mark L, Watts P and Mark T D 2010 Applications of proton transfer reaction time-of-flight mass spectrometry for the sensitive and rapid real-time detection of solid high explosives *Int. J. Mass spectrom.* **289** 58–63
[20] Sulzer P, Petersson F, Agarwal B, Becker K H, Jurschik S, Mark T D, Perry D, Watts P and Mayhew C A 2012 Proton transfer reaction mass spectrometry and the unambiguous real-time detection of 2,4,6 trinitrotoluene *Anal. Chem.* **84** 4161–6
[21] Critchley A D J, Elliott T S, Harrison G, Mayhew C A, Thompson J M and Worthington T 2004 The proton transfer reaction mass spectrometer and its use in medical science: applications to drug assays and the monitoring of bacteria *Int. J. Mass spectrom.* **239** 235–41
[22] Wang T, Smith D and Spanel P 2002 Selected ion flow tube studies of the reactions of H_3O^+, NO^+ and O_2^+ with the anaesthetic gases halothane, isoflurane and sevoflurane *Rapid Commun. Mass Spectrom.* **16** 1860–70
[23] Ruzsanyi V, Fischer L, Herbig J, Ager C and Amann A 2013 Multi-capillary-column proton-transfer-reaction time-of-flight mass spectrometry *J. Chromatogr.* A **1316** 112–8
[24] Frisch M J *et al* 2009 *Gaussian 09, Revision A.1* (Wallingford, CT: Gaussian, Inc.)
[25] Bell A J, Ferrante F, Hall S E, Mikhailov V, Mitchell D, Timperley C M, Watts P and Williams N 2009 Fragmentations and reactions of protonated *O,O*-dimethyl ethylphosphonate and some isotopomers produced by electrospray ionisation in an ion trap mass spectrometer *Int. J. Mass Spec.* **269** 46–54
[26] Malásková M, Henderson B, Chellayah P D, Ruzsanyi V, Mochalski P, Cristescu S M and Mayhew C A 2019 Proton transfer reaction time-of-flight mass spectrometric measurements of volatile compounds contained in peppermint oil capsules of relevance to real-time pharmacokinetic breath studies *J. Breath Res.* **13** 046009
[27] Mochalski P, Mirmigkou S, Unterkofler K, Sulzer P, Mayhew C A and Märk T D 2019 PTR-MS studies of the reactions of H_3O^+ with a number of deuterated volatile organic compounds and the subsequent sequential reactions of the primary product ions with water under normal and humid drift tube conditions: implications for use of deuterated compounds for breath analysis *Int. J. Mass spectrom.* **436** 65–70
[28] Malásková M, Olivenza-León D, Piel F, Mochalski P, Sulzer P, Jürschik S, Mayhew C A and Märk T D 2019 Compendium of the reactions of H_3O^+ with selected ketones of relevance to breath analysis using proton transfer reaction mass spectrometry *Frontiers in Chemistry* **7** 401
[29] Wang T, Spanel P and Smith D 2003 Selected ion flow tube, SIFT, studies of the reactions of H_3O^+, NO^+ and O_2^+ with eleven $C_{10}H_{16}$ monoterpenes *Int. J. Mass spectrom.* **228** 117–26
[30] Spanel P and Smith D 1998 SIFT studies of the reactions of H_3O^+, NO^+ and O_2^+ with several ethers *Int. J. Mass Spec. Ion Processes* **172** 239–47
[31] Mayhew C A 1992 Reactions of Ne^+ and Ne_2^+ ions with several molecular species at 300 K: the importance of energy resonance, Franck-Condon factors and electron correlation effects on reaction efficiencies *J. Phys. B: At. Mol. Opt. Phys.* **25** 1865–81
[32] Jarvis G K, Mayhew C A and Tuckett R P 1996 Study of the gas phase reactions of several perfluorocarbons with positive ions of atmospheric interest *J. Phys. Chem.* **100** 17166–74
[33] Jarvis G K, Kennedy R A, Mayhew C A and Tuckett R P 2000 Charge transfer from neutral perfluorocarbons to various cations: long-range versus short-range reaction mechanisms *Int. J. Mass Spectrom. and Ion Processes* **202** 323–43
[34] Adams N G and Smith D 1976 The selected ion flow tube (SIFT); a technique for studying ion-neutral reactions *Int. J. Mass Spectrom. and Ion Physics* **21** 349–59
[35] King J, Unterkofler K, Teschl S, Amann A and Teschl G 2011 Breath gas analysis for estimating physiological processes using anesthetic monitoring as a prototypic example *33rd Annual Int. Conf. of the IEEE Eng. Med. Biol. Soc. (Boston, MA, August 30th–September 3rd)* pp 1001–4